

UNIVERSITY OF OKLAHOMA
GRADUATE COLLEGE

BIOTIC AND ABIOTIC CHEMICAL WEATHERING OF SILICICLASTIC SEDIMENTS IN
COLD ENVIRONMENTS

A DISSERTATION
SUBMITTED TO THE GRADUATE FACULTY
in partial fulfillment of the requirements for the
Degree of
DOCTOR OF PHILOSOPHY

By
CANSU DEMIREL-FLOYD

Norman, Oklahoma

2022

BIOTIC AND ABIOTIC CHEMICAL WEATHERING OF SILICICLASTIC SEDIMENTS IN
COLD ENVIRONMENTS

A DISSERTATION APPROVED FOR THE
SCHOOL OF GEOSCIENCES

BY THE COMMITTEE CONSISTING OF

Dr. Megan E. Elwood Madden, Chair

Dr. Gerilyn S. Soreghan, Co-Chair

Dr. Andrew S. Elwood Madden

Dr. Elizabeth Karr

Dr. Kristen R. Marra

© Copyright by Cansu Demirel-Floyd 2022

All Rights Reserved.

TABLE OF CONTENTS

Acknowledgements.....	vi
Dissertation Summary.....	ix
Chapter 1. Investigating weathering signatures in terrestrial muds: Can we separate climatic signatures from provenance?	1
Abstract.....	2
Introduction.....	3
Geological Setting.....	5
Methods	3
Results.....	12
Discussion.....	23
Conclusions.....	36
Acknowledgements.....	38
References.....	38
Tables.....	50
Figures	52
Chapter 2. Cyanobacterial weathering in warming periglacial sediments: Implications for nutrient cycling and potential biosignatures	66
Abstract.....	67
Introduction.....	67
Materials And Methods.....	71
Results.....	77
Discussion.....	81
Conclusions.....	87
Acknowledgements.....	88
References.....	88
Tables.....	95
Figures	96
Chapter 3. Limited bioweathering by cyanobacteria in cold, nutrient-limited conditions: Implications for microbe-mineral interactions and aquatic chemistry in cold environments.....	106

Abstract.....	107
Introduction.....	107
Methods	110
Results.....	117
Discussion.....	121
Conclusions.....	129
Acknowledgements.....	129
References.....	130
Tables.....	136
Figures	138
SUPPLEMENTARY MATERIALS FOR CHAPTER 1	154
Supplementary Text for Chapter 1.....	154
Supplementary Figures for Chapter 1	171
Supplementary Tables for Chapter 1	173
SUPPLEMENTARY MATERIALS FOR CHAPTER 2	229
Supplementary Figures for Chapter 2.....	229
Supplementary Tables for Chapter 2	234
SUPPLEMENTARY MATERIALS FOR CHAPTER 3	247
Supplementary Tables for Chapter 3	247

Acknowledgements

Graduate education is one of those periods of life that, no matter how much of things you think you are, you will need intellectual and even emotional guidance. Many life-changing events happened during my doctoral degree that made me think that I was blessed have my advisor, Dr. Megan Elwood Madden, to guide me through both exciting and challenging times, as well as in the processes of shaping my career. She always understood that life happened, was (still is) extremely patient and still managed to keep me going when I thought I couldn't work at all. I could have not thought of a better advisor, both in academia and real life, and I am grateful. Many thanks to my co-chair, Dr. Lynn Soreghan, who was always there to help and support me, and who always guided me and included me in the events within her own research group. In other words, she was my co-chair on paper, but really was another great advisor that I was lucky to have. Thanks to my committee members Drs. Andy Elwood Madden, Liz Karr and Kristen Marra. They always kept their doors open to me when I had questions and challenged me when needed. Dr. Andy Elwood Madden always was there the numerous times I had instrumental challenges, as well as always finding time to answer my questions even if not scheduled. Dr. Liz Karr helped me through my experimental design process, as well as making sure I was okay during one of the most challenging times of my life, to the extent of arranging meals for my significant other during his chemotherapy. I can never find the right words to thank her. And Dr. Kristen Marra guided me with her extensive knowledge on the topic of my dissertation. Though she was a remote member, she was always approachable and ready to help.

I have a long list of people I have to thank that got me through today. Outside of my committee, there was one other person that was always in my academic family, and even went to the extent of getting ordained for me and my significant other's wedding. Dr. Bradley Stevenson

was always there from the day I stepped in the US for the first for a summer course to helping me find perfect PhD advisor for me, which is how I ended up in OU School of Geosciences. Though Dr. Stevenson was my husband James's advisor, he never treated me any different, helped me with my questions and opened his lab for me to carry out my work. His door was never closed for a random question or guide me and James through tough times. We both will always be grateful. In addition, I also thank his lab group and the whole Microbiology Department for their support and for always treating me as their own. Special thanks additionally to Drs. Paul Lawson, Amy Callaghan, Boris Wavrick and Anne Dunn for providing access to microbiology lab equipment and facilities.

I am grateful for Dr. Charity Lander for guiding me through my career development, even exposing me to NASA mission proposals. I thank Dr. Preston Larson for the numerous times and countless hours he helped me with scanning electron microscopy. Thanks to Dr. Claire Curry for even helping me out with last minute statistics related questions. Thanks to Dr. Mike Soreghan for allowing access to his lab, and always including me in his research group events. Thanks to Dr. Paul Schroeder and his family for always supporting my scientific endeavors. Many thanks to my geochemistry and sedimentology lab group professors and friends that always had the time to give a hand. Thanks to Autumn Roche for her long hours of work helping me with sample processing and grain size analysis. Thanks to Dan Mason and Andrew Rodriguez for their help with Raman Spectroscopy. Special thanks to Nina Webb, Lily Pfeifer, Steven Adams and Alicia Bonar for their continuous help in both in the lab and life, being such great colleagues and great friends. Another special thanks to Chelsey Gallagher who was my remote working accountability body that helped me keep on working at home during COVID-19

closures. I thank the whole School of Geosciences staff, professors and colleagues for their support through the good and bad, and providing an inclusive environment.

Finally, I thank my whole family and friends I haven't mentioned here. I couldn't have made it through this process without their love and support. I specially thank my amazing husband, James, for his continuous support and love, bearing with me through the stressful time of writing, and putting me first through his treatment. I dedicate this dissertation to my late mother-in-law, who left us so soon, and couldn't see the day I finish my PhD, as well as my beloved father, who passed away shortly after my defense.

Financial support statement: This work was supported by National Science Foundation (NSF) grant number 1543344, "Quantifying Surface Area in Muds from the Antarctic Dry Valleys: Implications for Weathering in Glacial Systems.", awarded to Drs. Lynn Soreghan and Megan Elwood Madden.

Dissertation Summary

Chemical weathering of silicate minerals is one of the most important Earth processes, moderating atmospheric carbon dioxide levels by consumption of carbon dioxide during hydrolysis of silicates (Nesbitt and Young, 1982; White and Peterson, 1990; Velbel, 1993; White and Blum, 1995; White et al., 1996; White and Brantley, 2003; White and Buss, 2014). Owing to its significance to the carbon cycle, and sensitivity to climatic conditions, chemical weathering and indices developed to determine the extent of weathering (i.e., Chemical Index of Alteration-CIA) have been the focus of significant studies aimed at investigating implications for paleoclimate in both terrestrial and extraterrestrial settings (i.e., Nesbitt and Young, 1982; Nesbitt and Young, 1989; Soreghan and Soreghan, 2007; Yang et al., 2016; Siebach et al., 2017; Deng et al., 2022). Chemical weathering leaves physical, chemical, and mineralogical signatures on rocks, sediments, and the aquatic environment, both via abiotic and biotic pathways. Therefore, weathering signatures studied on Earth are analogs for extraterrestrial signatures of surface alteration processes (i.e., Cannon et al., 2015; Olsson-Francis et al., 2017). However, abiotic and biotic weathering pathways in cold environments (i.e., within glacial settings) and subsequent weathering signatures remain poorly understood.

This dissertation investigates biotic and abiotic weathering signatures and pathways within various glaciated settings, with the focus on Antarctica and Iceland as climatic and mineralogical analogs of Mars. Non-glaciated settings are also investigated to compare weathering signatures generated within cold and hot climates. Chapters within this dissertation are formatted as peer-reviewed journal publications (in prep. or published).

The Chemical Index of Alteration (CIA) was developed to quantify the extent of weathering based on major oxides within silicates that are significantly associated with

weathering: Al_2O_3 , CaO , Na_2O and K_2O (Nesbitt and Young, 1982). CIA has been largely used to interpret paleoclimate, and correlated with climate parameters (mean annual temperature, MAT, and mean annual precipitation, MAP), especially with MAT within tropical soil profiles and watersheds on felsic bedrock (i.e., Nesbitt and Young, 1989, Rasmussen et al., 2011; Yang et al., 2016; Joo et al., 2018a). However, these correlations don't seem to apply to glaciated settings (Deng et al., 2022), and various studies discuss shortcomings of applying CIA when mafic rock types are involved, as mafic major oxide components (such as FeO and MgO) are not incorporated within CIA calculations, and CIA is highly dependent on CaO that can result in artificially underestimated CIA values when the source rock contains high CaO (Nesbitt et al., 1996; Siebach et al., 2017; Mangold et al., 2019; Berger et al., 2020). Despite these documented issues, CIA remains widely utilized for various depositional settings, including potentially glaciated environments on Earth and Mars (i.e., Nesbitt and Young, 1982; Balburg and Dobrzinski 2011; Marra et al., 2017; Hurrowitz et al., 2017; Wang et al., 2020).

In **Chapter 1**, I investigate and compare weathering signatures (mineralogy, chemistry, grain size and surface area) within mud-sized ($<63 \mu\text{m}$) sediments from both cold glaciated and hot non-glacial settings on felsic-intermediate bedrock to assess paleoclimatic implications of chemical weathering, attempting to decouple inherited provenance signatures from climatic signals. Use of ternary plots that are commonly used for chemical weathering and paleoclimate studies, such as A-CK-N, A-CKN-FM (Nesbitt and Young, 1982) and MFW (Ohta and Arai, 2007), illustrate that the effects of provenance and mafic mineral sorting (towards finer grain sizes) overshadow weathering trends (Nesbitt et al., 1996; von Eynatten et al., 2012; Mangold et al., 2019), except for tropical soils and fluvial muds from Puerto Rico. In addition, data from very different climatic settings have overlapping CIA values (indicative of weak to intermediate

weathering) that also clustered together on A-CK-N diagrams, suggesting that assessing climatic trends using this method may lead to erroneous interpretations. In an attempt to remove the provenance signature from the data, we normalized sediment CIA values to the CIA values determined for their bedrock sources and tested the correlation with MAT and MAP. Though R^2 values obtained from this multi-provenance and climate data set were enhanced, and showed better correlation of CIA with MAP, removing the tropical watershed from the data set eliminated any expected correlations. Overall, Chapter 1 shows that: 1) CIA and ternary plots for weathering are most useful when applied to tropical settings with uniform bedrock composition, where elemental weathering trends can be directly traced from the bedrock to first-cycle material (soil profiles/paleosols); 2) CIA values of muds from glacial settings overlap with values observed in hot and humid climates; and 3) no correlations were observed between climatic parameters (mean annual precipitation and temperature) and CIA in non-tropical fluvial sediments, suggesting that CIA is not a useful metric for modeling paleoclimate in glaciated settings.

Microbial organisms catalyze chemical weathering owing to their metabolic byproducts (organic acids, carbon dioxide, extracellular polymeric substances) which locally decrease the pH, and metabolic activity (i.e., photosynthesis) that significantly increases the pH of the overall weathering solution (Welch and Ullman, 1999; Montross et al., 2013; Olsson-Francis et al., 2012; Olson-Francis et al., 2017). Solute fluxes observed in the Antarctic McMurdo Dry Valleys (Gooseff et al., 2002; Marra et al., 2017; Stumpf et al., 2012) exceed expected abiotic weathering fluxes, which previous studies have attributed to microbial weathering (i.e., Lyons et al., 2015), as well as abiotic factors such as production of fresh high surface area silicates via glacial grinding priming them for chemical weathering (Anderson et al., 1997, Anderson, 2005; Stumpf

et al., 2012; Marra et al., 2017). However, the effects of psychrophilic microbes in chemical weathering processes in Antarctica (as well as other glaciated settings) are not well known. Permafrost soil surface temperatures can reach 12°C due to radiative austral summer heating (Balks et al., 2002; Dolgikh et al., 2015), providing optimum growth conditions for cold-tolerant cyanobacterial mats (e.g., Kleinteich et al., 2012) that are widespread in meltwater stream banks and cryptoendolithic habitats of the topsoil (Cary et al., 2010; Cowan et al., 2010).

In **Chapter 2**, I investigate the role of the Antarctic benthic mat-forming (non-axenic) cyanobacterium, *Leptolyngbya glacialis*, on chemical weathering of (felsic-intermediate, Antarctic and basaltic, Iceland) glacial sediments at 12°C, representing permafrost surface temperatures, testing the hypothesis that microbial life increases weathering rates and solute fluxes within glacial settings. Results show silicate weathering rates in felsic sediments are three times faster with microbes than without, whereas biotic and abiotic weathering rates observed in mafic sediments are comparable, likely due to faster chemical weathering rates in basaltic sediments which directly provide nutrients to the microbes, reducing the need for direct microbial-facilitated weathering (scavenging). Results also show that microbes increase the solution pH and lead to up to four times higher bicarbonate concentration, suggesting they may play a key role in carbonate deposition in both felsic and mafic settings. Production of Fe-(hydr)oxide nano minerals and neo-formed clays may be potential inorganic biosignatures as they are closely associated with microbial biofilms, and similar phases were not observed in abiotic reactors. Note that this chapter has been published in *Permafrost and Periglacial Processes* (Demirel-Floyd et al., 2022), partially fulfilling doctoral degree requirements for the OU School of Geosciences.

Cyanobacteria have also played important roles within Earth history such as atmospheric oxygenation and the evolution of multicellular life (Lyons et al., 2014), while also surviving across multiple climatic extremes such as the Neoproterozoic “Snowball Earth” episodes (Hoffman et al., 1998; Fairchild and Kennedy, 2007; Ye et al., 2015; Brocks et al., 2017; Shizuya et al., 2021). These resilient organisms also are known to endure multiple environmental extremes (UV radiation, desiccation, salt, cold, etc.) within Antarctic glacial habitats (Gilichinsky et al., 2007; Cary et al., 2010; Cowan et al., 2010, Anesio and Laybourn-Parry, 2012), where they lead the primary production and play a fundamental role in Antarctic biogeochemical cycles (McKnight et al., 2004; Smith et al., 2017). Antarctic cyanobacterial mats also increase weathering rates, and therefore impact nutrient fluxes at warmer surface soil temperatures (12°C), as described in Chapter 2 (Demirel-Floyd et al., 2022). Though they are widespread in cold meltwater streams (McKnight et al., 1999, 2004; Van Horn et al., 2016), the role of cyanobacterial mats in cold temperature weathering is not well known.

In **Chapter 3**, I investigate biotic and abiotic silicate weathering rates and nutrient release at different temperatures (4°C and 12°C) and nutrient conditions (10 and 1000 times diluted), using the same felsic-mixed sourced Antarctic glaciofluvial sediments and basaltic-sourced Icelandic glacio-volcanic outwash sediments used in Chapter 2, testing the hypothesis that polyextremophilic cyanobacterial weathering rates increase under colder and nutrient-stressed conditions via enhanced production of extracellular polymeric substance (EPS) resulting in release of organic acids. Results show limited evidence of biological weathering of silicate minerals at cold temperature, yet microbe-mineral interactions still affect nutrient concentrations, particularly for Ca, Mg, Mn, P and N. However, increased nutrient and salt concentrations also increased the rate of solute release from the silicate sediments, even under abiotic conditions.

These results indicate that concentration and chemistry of weathering solutes (salts) are important factors controlling weathering rates and nutrient fluxes in cold settings. This chapter will soon be submitted to *Geomicrobiology Journal* for initial peer review.

Chapter 1. Investigating weathering signatures in terrestrial muds: Can we separate climatic signatures from provenance?

Cansu Demirel-Floyd¹, Gerilyn S. Soreghan¹, Nina D.S. Webb², Autumn Roche¹, Kristen R. Marra³, Young Ji Joo⁴, Brenda Hall⁵, Joseph S. Levy⁶, Andrew S. Elwood Madden¹, and Megan E. Elwood Madden¹

¹School of Geosciences, University of Oklahoma, Norman, OK 73019, USA

²Impossible Sensing, St. Louis, MO 63118, USA

³USGS, Central Energy Resour. Sci. Center, Lakewood, CO 80226, USA

⁴ Pukyong National University, Busan 48513, Republic of Korea

⁵School of Earth and Climate Sciences and Climate Change Institute, University of Maine, Orono, ME 04469, USA

⁶Department of Geology, Colgate University, Hamilton, NY 13346, USA

Key Words: Chemical weathering; physical weathering; Chemical Index of Alteration; paleoclimate; glacial settings; sedimentary geochemistry

Data Availability Statement: All data tables associated with this manuscript are available at U.S. Antarctic Program Data Center (USAP-DC) at <https://www.usap-dc.org/view/dataset/601599>.

Abstract

Siliciclastic muds concentrate physical and chemical weathering products. However, both rock composition and climate can affect the mineralogy and geochemistry of these sediments. We quantitatively assessed the influence of provenance and climate on muds collected from end-member climates to identify potential weathering signatures indicative of climate. Granulometry, mineralogy, and geochemistry of these muds indicate that provenance and mineral sorting mask (paleo)climate signals. These effects permeate CIA (Chemical Index of Alteration) values, and MFW (mafic-felsic-weathering), A-CK-N, and A-CKN-FM ternary plots. CaO content is heavily weighted within the calculations, resulting in even felsic-sourced sediment commonly plotting as mafic, due to relative enrichment of CaO from preferential sorting of Ca-rich minerals into the mud-sized fraction during transport. These results cast doubt on the indiscriminate use of CIA values and ternary plots for interpreting chemical weathering and paleoclimate within muds, particularly from glacial systems.

Additionally, CIA values from fluvial sediments did not correlate with climatic parameters (mean annual temperature and mean annual precipitation) when sediments formed in non-glacial settings were removed from the datasets. This implies that CIA may only be a useful when applied to non-glacial systems in which the composition of the primary source material is well constrained—such as soil/paleosol profiles. Within this endmember climate dataset, CIA was only useful in discriminating hot-humid climates.

INTRODUCTION

Chemical weathering has been a fundamental component of Earth surface processes throughout geologic time, producing chemical, physical, and mineralogical signatures within siliciclastic sediments (White et al., 1996). Chemical weathering of silicates is controlled by lithology (composition and texture), climate (temperature and precipitation), biological activity (macro- and micro-), chemistry of weathering solutes (acidic, neutral, or basic; salty or fresh), and the reactive surface area of fine-grained sediments (White and Peterson, 1990; White and Blum, 1995; White et al., 1996; White and Brantley, 2003; White and Buss, 2014). Weathering products, such as clay minerals and Fe-oxides, are concentrated within the mud-sized (<63 μm) sediment fraction due to their small grain sizes (Nesbitt and Young, 1982). Climate regime and duration of weathering control the type and amount of secondary weathering products in general, where one would expect the highest intensity of chemical alteration and abundant secondary mineral products such as kaolinite and Fe-oxides in hot and humid (tropical) settings. On the other hand, negligible chemical weathering and less-aluminous clays (illite, smectite, and chlorite) are associated with dry, high-latitude regions including glacial systems (Biscaye, 1965; Barshad, 1966; Nesbitt and Young, 1982; Velbel, 1993; White et al., 1999; White and Brantley, 2003). However, high values of the Chemical Index of Alteration (CIA; Nesbitt and Young, 1982) have been reported within some glacial regions (e.g., Marra et al., 2017) comparable to those of tropical settings (i.e., Joo et al., 2018a; Webb et al., 2022).

Evidence of chemical weathering has long been utilized for paleoclimate interpretations based on weathering indices calculated from major oxides compositions of sediment developed on various basement rocks (i.e., CIA; Nesbitt and Young, 1982; Soreghan and Soreghan, 2007; Goldberg and Humayun, 2010; Xioa et al., 2010; Li and Yang, 2010; Bahlburg and Dobrzinski

2011; Yang et al., 2016; Ren et al., 2019; Wang et al., 2020; Deng et al., 2022). Relationships between climate parameters such as mean annual temperature (MAT) and mean annual precipitation (MAP), and CIA show moderate-strong correlations when applied to tropical and temperate regions where weathering trends can be easily observed within well-developed soil profiles (i.e., Nesbitt and Young, 1989, Rasmussen et al., 2011; Yang et al., 2016; Joo et al., 2018a). On the other hand, application of weathering indices, including CIA, in glacial regions produces values that do not follow the same trends observed in ice-free systems (Deng et al., 2022). In addition, physical sorting of grains during sediment transport can also affect chemical weathering signatures by concentrating mechanically weaker minerals (commonly mafic phases) in the finer size fractions (Nesbitt et al., 1996; von Eynatten et al., 2012). Sorting may lead to underestimated weathering index values within fine-grained sediments and regolith, due to relative enrichment of CaO in the fine-grained sediment fraction (i.e., Nesbitt et al., 1996; Siebach et al., 2017). Despite these complications, CIA and other weathering indices have been widely applied to fine-grained sediments from a large variety of depositional environments including glacial drifts and fluvial systems, where well-developed weathering profiles aren't available (i.e., Soreghan and Soreghan, 2007; Xioa et al., 2010; Bahlburg and Dobrzinski 2011; Yang et al., 2016; Marra et al., 2017; Siebach et al., 2017; Hurowitz et al., 2017; Ren et al., 2019; Wang et al., 2020).

While most previous studies of CIA and other weathering indices have focused primarily on temperate and tropical climate systems (i.e., Nesbitt and Young, 1989, Rasmussen et al., 2011; Yang et al., 2016; Joo et al., 2018a), the effects of extreme endmember climate conditions, including glacial environments, on terrestrial sediment composition, texture, and mineralogy have not been systematically compared and studied. Here we report the surface area, grain size,

mineralogy, and geochemistry of fine-grained glacial and pro-glacial siliciclastic sediments collected from cold-arid (Antarctica MDV), temperate-arid (Peru) and temperate-humid (Norway, Washington, Iceland) glacial systems, as well as to fluvial siliciclastic sediments and soils collected from hot-arid (Anza Borrego) and hot-humid (Puerto Rico) non-glacial environments to determine if statistically significant relationships are observed between weathering products and climate of these deposits. We focused on comparing sediments systematically collected from slackwater regions within fluvial settings on the similar bedrock types (granitic, granodioritic besides Iceland), treated and analyzed following same protocols between the samples, minimizing user error and sample treatment related variations in the results unlike studies based on collection of published data (e.g., Li and Yang, 2010; Deng et al., 2022).

GEOLOGICAL SETTING

We selected drainage basins sited on felsic-intermediate bedrock in Antarctica (Stumpf et al., 2012; Marra et al., 2014, 2015, 2017), Norway (Joo et al., 2018b), Peru, Washington, Puerto Rico (Joo et al., 2018a; Webb et al., 2022) and Southern California (Joo et al., 2016). For these sites, we attempted to keep bedrock composition as similar as possible, but variations occur. In addition, we also included samples collected from a basaltic watershed from Iceland to compare the effects of a mafic bedrock source in a glaciated system. Summary descriptions for each field area are described below and listed in Table 1, with further details available in supplementary material of this chapter as well as previous papers (Hall et al., 1993; Hall et al., 2000; Levy et al., 2011; Stumpf et al., 2012; Marra et al., 2014, 2015, 2017; Soreghan et al., 2016; Joo et al., 2016, 2018a, 2018b, 2022; Webb et al., 2022), including detailed maps showing specific sampling locations.

We collected sediment samples from cold-dry (n=106), temperate-dry (n=22), and temperate-wet (n=43) glacial environments, as well as hot-wet (n=31) and hot-dry (n=13) non-glacial settings. These samples represent primarily fluvial slackwater sediments, but they also include glacial drift, lake, and water-track sediment, as well as soils from both glacial and non-glacial systems. Soil profiles were sampled at 10-20 cm increments within the top ~10 cm to 1 m where possible. Table S1 provides complete sample descriptions and metadata. All sediment samples were frozen until analysis. We also collected bedrock from Antarctica, Peru, Puerto Rico and Anza Borrego, and rely on published work for bedrock compositions of Washington (Smith, 1903), Norway (Gordon et al., 2013) and Iceland (Kelly et al., 2014).

Antarctica

The McMurdo Dry Valleys (MDVs) are largely ice-free polar desert, with mean annual temperature (MAT) around -18°C (within -14°C to -30°C temperature range) and mean annual precipitation (MAP; mostly snowfall) of 100 mm/yr (Fountain et al., 1999; Doran et al., 2002, 2008). Nevertheless, chemical weathering occurs, as inferred from solute fluxes in meltwater streams (Nezat et al., 2001; Maurice et al., 2002; Gooseff et al., 2002; Stumpf et al., 2012; Lyons et al., 2015), and weathering products observed within rocks and soils (Guglielmin et al., 2005; Cuzzo et al., 2020). Fine grained sediments produced by limited glacial grinding, as well as eolian redistribution of fine-grained glacial deposits supply ample surface area for weathering reactions (Stumpf et al., 2012; Marra et al., 2017). Polyextremophilic microbial communities also likely contribute to nutrient and weathering fluxes (Demirel-Floyd et al., 2022). Poorly developed permafrost soils are mainly located on the valley slopes and flood plains, which are composed of drift deposits from previous cycles of glacial advance and retreat within the valleys (Campbell and Claridge, 2006; Bockheim et al., 2008; Levy et al., 2011).

Taylor Valley

Eastern Taylor Valley is largely covered by Last Glacial Maximum (LGM) aged Ross Sea Drift that contain clasts from the underlying granite and biotite orthogenesis, as well as basalt, sandstone, and dolerite clasts sourced out of the valley (Hall et al., 2000). The western portion of the valley is covered by undifferentiated pre-Bonney drifts that are also reworked by proglacial fluvial stream systems (Hall et al., 2000).

Water tracks

Water tracks are gully-like features that have darker toned surfaces and are observed on gentle to steep slopes of soils with high moisture. They have been attributed previously to briny groundwater activity (Levy et al., 2008, 2011; McEwen et al., 2011), causing seasonal bright salt efflorescence on Taylor Valley soils (Weidong et al., 2002). Water tracks are observed cutting through dry ephemeral stream channels and contribute to proglacial lake nutrient budgets by transporting weathering solutes. Therefore, water tracks are considered to be a component of hydrological cycles within Taylor Valley (Levy et al., 2011).

Wright Valley

The eastern end of the Wright Valley is underlain by granite, quartz monzonite, and granodiorite bedrock (Brownworth and Denton plutons) and filled with pre-LGM drifts (Brownworth, Trilogy, Loke, Loop, Peleus and various Alpine drifts) dating from mid-Quaternary to as old as Miocene that contain heterogeneous clasts from these bedrock types (Hall and Denton, 2005). Wright Valley soils are composed of these drifts, in addition to bedrock clasts of Ferrar dolerite, Olympus granite gneiss, Vida granite, and microdiorite (Hall and Denton, 2005; Campbell and Claridge, 2006; Bockheim and McLeod, 2008).

Peru

Llanganuco and Paron valleys are at high elevation within the Cordillera Blanca Mountain range that exhibits a cold and semi-arid climate regime with highly seasonal precipitation (MAT= 0-9°C; MAP= 800-1200 mm/yr) due to high elevation and El Niño– La Niña oscillations (Kaser et al., 1990, 2003; Vuille et al., 2008; Bury et al., 2011). Climate is heavily affected by the topography, where high peaks act as a barrier for moist air masses. The hydrological cycle during the dry season (June to September) consists of glacial streams and groundwater, but the water budget is reduced by sublimation (Vuille et al., 2008; Gordon et al. 2015). In contrast, rainfall is abundant from October to May. The wet season allows the western Cordillera Blanca glacial region to support vegetation in high-moisture soils that are underlain by lacustrine sediments and glacial till (Kaser et al., 2003; Baraer et al., 2015; Gordon et al., 2015). Llanganuco Valley is largely underlain by the granodioritic and tonalitic Cordillera Blanca batholith and locally by pyrite and sulfide mineral-rich marine black shales of the Upper Jurassic Chicama Formation, which is under ice cover (Wilson et al., 1995; Love et al., 2004), whereas the majority of the Paron valley is underlain by the Miocene batholith granodiorite complexes (Siame et al., 2006).

Norway

The Josteldalsbreen region has a cold and humid climate, with MAT of 4.5°C and MAP of 1769 mm/yr. The glaciomorphological sediment and landforms locally record glacial advance and retreat during the Little Ice Age (LIA) of the late Holocene (Bickerton and Matthews, 1993; Lewis and Birnie, 2001). Josteldalsbreen ice cap is located along the southwest coast of Norway, feeding S-NNW and N-S trending glacial valley streams that drain into lakes and fjords, including the Austerdalen and Langedalen valleys we sampled. Precambrian acidic gneiss (granite to granodiorite composition), which is a part of the broader Norwegian Caledonides,

underlies the western section of the Josteldalsbreen watershed (Rye et al., 1997). The bedrock composition and structure are affected by Precambrian and Caledonian orogenies, as well as ultrahigh- and high-pressure metamorphism (Rye et al., 1997) referred to generally as The Western Gneiss Region (Root et al., 2005; Butler et al., 2015).

Iceland

Iceland is a volcanic island in the South Atlantic Circle, underlain by volcanic rocks of 13 Ma to recent age. Silica-rich basaltic tephra eruptions have been frequent for the last 12,000 years (Andrews and Eberl, 2007). MAT ranges between 0-4°C, with MAP >600 mm/year contributing to a humid climate that supports vegetation (Olafsson et al., 2007). The Eyjafjallajökull volcanic eruption in 2010 (Sigmundsson et al. 2010) caused a catastrophic glacial outburst flood, which are common in the region. Both the outburst flood and aeolian processes (Arnalds et al. 2016) contribute to landform evolution and sediment budgets within the fluvial catchments, as they rework former deposits and transport large amounts of fresh volcanic sediments (Prospero et al. 2012).

Washington

Mt. Stuart is a glaciated peak within the Washington Cascades with a climate heavily affected by the topography, where high peaks act as a barrier for moist air masses (Reiners et al., 2003). MAP in the Northern Cascades region around Mt. Stuart is 1500-2000 mm/yr and MAT is ~8-10°C around Mt. Stuart (based on PRISM group 30-yr annual precipitation and temperature maps, Daly et al., 1994; Daly et al., 2008). Erosion rates across the Cascades show similar trends with precipitation profiles, reaching a maximum of 0.33 mm/yr, which is correlated with fluvial discharge (Reiners et al., 2003). Mt. Stuart is located on the Mt. Stuart Batholith, a Late Cretaceous calc-alkaline pluton that intruded the metamorphic basement (pre-Cretaceous

Chiwaukum Schist) of the Cascades (Erikson, 1977; Brown and Walker, 1993). The batholith varies spatially between tonalite, quartz diorite, granodiorite, granite, gabbro, and ultramafite, and may be intruded by mafic Tertiary dikes (Erikson, 1977). However, no mafic clasts or dikes were observed within the sampling area.

Puerto Rico

Southeastern Puerto Rico exhibits a hot and humid, tropical climate with MAT of 22°C and MAP of 4200 mm/yr (Joo et al., 2018a, 2018b). Puerto Rico is commonly in the path of tropical storms and hurricanes, which induce landslides (Lepore et al., 2012; Besette-Kirton et al., 2019). Rio Guayanés and Rio Guayabo watersheds in southeastern Puerto Rico are largely underlain by Late Cretaceous San Lorenzo granodiorite, as well as quartz diorite, and minor metavolcanics (Rogers et al., 1979). The granodioritic bedrock hosts thick layers of soil and saprolite (up to 1 m and 8 m, respectively; Fletcher et al., 2006; Murphy et al., 2012). At a larger scale, the field site is within the Cordillera Central Mountain range, largely underlain by Jurassic to Eocene igneous rocks (Monroe, 1980). The region is also tectonically active along the Puerto Rico Trench, characterized by 1 mm/yr uplift rates and moderate earthquakes (Mann et al., 2005).

Anza Borrego

The Anza Borrego Desert in the Sonoran Desert of Southern California has a hot and dry climate- MAT of 23°C and MAP of 150 mm/yr (Geiger & Pohl, 1953; Joo et al., 2016). Rare, intense precipitation events result in ephemeral fluvial transport (Joo et al., 2016; 2018b). This watershed is largely underlain by tonalitic bedrock, within a larger region that also contains Jurassic metamorphic and Cretaceous plutonic units affected by activity along the Elsinore fault,

and the uplift of the Peninsular Ranges batholith (Remeika & Lindsay, 1992; Axen & Fletcher, 1998; Dorsey et al., 2011).

METHODS

To obtain the mud (<63 μ m) silicate fractions of the sediment samples, we coned and quartered the thawed samples, then wet sieved for granulometry (total mud% <63 μ m, sand% <63 μ m-2mm, gravel% >2mm). We treated the mud fraction with acetic acid overnight and H₂O₂ until the reaction (fizzing) ceased (2-5 days) to remove carbonate and organic constituents, respectively (Marra et al., 2017; Demirel-Floyd et al., 2022). Then, we measured the grain size distribution of the muds using a Malvern Mastersizer 3000 Laser Particle Size Analyzer (LPSA), after treatment with sodium hexametaphosphate (Blott et al., 2004). Surface area of the muds were quantified using the Brunauer-Emmett-Teller (BET) nitrogen adsorption method (Brunauer et al., 1938). We performed X-Ray Diffraction (XRD) analyses using a Cu radiation source, employing the Bragg–Brentano method (2–70° 2 Θ angle interval with 0.02° step size and 2-second counting time, using fixed slits). We determined the quantitative mineral composition with MDI Jade software using Reitveld refinement method (Bish and Howard, 1988), in combination with ClaySIM software using the RockJock method (Eberl, 2003). Major oxide, rare earth element (REE), trace metal and heavy metal chemistry of the samples were determined by ALS labs, using ICP-MS by Li borate fusion and acid-digestion methods.

Weathering Indices and Ternary Plots

We removed loss of ignition (LOI) data from the major oxide results and closed our data to 100% prior to any calculations or data transformations. We also corrected CaO values for apatite (Equation 1.1) following Girty et al. (2013).

$$\text{CaO}^* = \text{CaO} - (3.3 * \text{P}_2\text{O}_5) \quad (1.1)$$

We calculated CIA (Equation 1.2)

$$\text{CIA} = \frac{\text{Al}_2\text{O}_3}{\text{Al}_2\text{O}_3 + \text{CaO}^* + \text{Na}_2\text{O} + \text{K}_2\text{O}} \times 100 \quad (1.2)$$

following Nesbitt and Young (1982) and MFW indices following Ohta and Arai (2007) using molar ratios obtained from major oxide analysis of the samples. as well as the Chemical Index of Weathering (CIW; Harnois, 1988), Plagioclase Index of Alteration (PIA; Fedo et al., 1995), and Weathering Index of Parker (WIP; Parker, 1970). In addition, we also generated A-CK-N, A-CKN-FM and MFW ternary plots after normalizing the components of the plots to 100%.

Statistical Analyses on Sediments

Our data set consists of both categorical (depositional setting, location, climate regime) and numerical data (BET surface area, geochemistry, granulometry, LPSA, mineralogy, MAP, MAT). The data set also includes below detection limit (BDL) values that are susceptible to rounded zero errors (Martin-Fernandez et al., 2003; Palarea-Albaladejo et al., 2014). The majority of the numerical data (geochemistry, mineralogy, granulometry) are also classified as compositional data, as they sum to 100% when considered as an independent dataset, which can impose the constant sum problem (Aitchinson, 1982; Aitchinson and Greenacre, 2002; Filzmoser et al., 2009; Grunsky et al. 2014). Multi-variate statistics is sensitive to issues such as rounded zeros and the constant sum problem within compositional data, biasing the results towards zero

values (Aitchinson, 1982; Aitchinson and Greenacre, 2002). Therefore, we imputed (replaced) missing and BDL values as described below and applied log-ratio transformation methods to mitigate these potential issues prior to statistical analyses when necessary (Aitchinson, 1982; Aitchinson and Greenacre, 2002).

Below Detection Limit and Missing Data Imputations

We imputed below detection limit data (rounded zeros) and missing values using either multiplicative simple replacement (employed when <10% of data points were imputed by replacing the BDL data with a value of 65% of the analytical detection limit) or robust Expectation-Maximization (EM) algorithms (employed when >10% of the data points were imputed through replacement of missing data based on other observations within the same sample group) using the R software packages (Templ et al., 2011; Martín-Fernández et al. 2012; Palarea-Albaladejo et al., 2014).

BDL imputation for major oxides, trace metals and REE

Our major oxide, REE and trace metal data had less than 10% BDL data. Therefore, we applied multiplicative simple replacement, where the BDL data are initially introduced as 0 within our data frame, and then substituted with 65% of the detection limit using the `multRepl` function of the `zCompositions` R package (Palarea-Albaladejo et al., 2014). Due to the differences in units, we applied this method to major oxide data (%), separate from the REE and trace metal data (ppm).

BDL and missing data imputation for heavy metals

We removed Ag, Cd, and Tl from our dataset, due to each element having >85% of sample values listed as BDL. After this filtering, we imputed the missing data in the remaining heavy metal dataset using the multReplus function of the zCompositions R package (Palarea-Albaladejo et al., 2014). Since our heavy metals dataset also contained >10% BDL we next applied a robust ilr-EM algorithm (Martín-Fernández et al., 2012), using the impRZilr function of the robCompositions R package that is used for data containing outliers (Templ et al., 2011; Palarea-Albaladejo et al., 2014). We applied this function separately to the data within each field site, as the BDL data are imputed drawing from other observations in the data set and individual components might have significant differences between field sites.

Data transformations

We applied data transformations to data groups that would result in the constant sum problem prior to statistical analysis of each group of variables (mineralogy, major oxides, REE, trace elements and heavy metals, individually). If these variables were combined as inputs (i.e., a data set composed of geochemistry and surface area combined), we did not complete the transformation step as there is no longer a constant sum issue.

We transformed our compositional data with the centered log ratio (clr) transformation, using the clr function of the compositions R package (Van den Boogaart and Tolosana-Delgado, 2008). The centered log ratio (clr) uses the geometric mean of the data set as a divisor, which is then converted to logarithm (Aitchinson, 1982), resulting in collinear data (Filzmoser et al., 2009). We chose the clr method due to its wide-spread application in multi-variate statistical analyses of geochemical data (i.e., Grunsky et al., 2014), superiority over alr (additive log ratio)

due to alr being subjective to a single reference divisor (Filzmoser et al., 2009), and simplicity as compared to ilr (isometric log ratio) (Grunsky et al., 2014).

Principal Component Analysis

We used GraphPad Prism 9 software to run Principal Component Analysis (PCA) using the Kaiser rule (eigen values >1) method, where principal components (PCs) are automatically selected based on maximum explained variance. PCA runs included multiple types of analyses (e.g., geochemistry, LPSA grain size, mineralogy and BET together in one dataset), so were not clr transformed, as the complete data set doesn't fall under the constant sum problem. However, we used the imputed and clr transformed data set when we ran PCA on individual compositional data sets (e.g., mineralogy, major oxides, REE, trace elements and heavy metals) separately.

Significance testing and correlations

We performed Two-way Analysis of Variance (ANOVA) using GraphPad Prism 9 to compare the significance of differences between the means calculated for categorical groups of individual numerical data subsets (i.e., means of CIA values belonging to different climatic regimes), coupled with Tukey's multiple comparisons. The family wise Alpha threshold was set to 0.05 and analyses were run within 95% confidence interval. We acknowledge that the statistical analyses are affected by the lack of replicate measurements from each sample. However, having multiple samples within individual watersheds from each field site lessens these effects. Multiple samples collected from each field site act as replicates, as we are selecting our categories based on general field site conditions and climatic regime.

RESULTS

Grain Size

The granulometry data obtained from wet sieving and Laser Particle Size Analysis (LPSA) analyses are provided in Table S1.2 and illustrated in Figures 1-3. Proglacial lakes have the highest amount of mud (~97%) amongst all depositional settings, with samples from Peru exhibiting higher mud content than those from Norway (Table S1.2, Figure 1.2). Peru soils and Puerto Rico saprolites are the other environments with high mud contents (Figure 1.2), up to ~71%, within the bulk fraction. Note that, overall, Antarctic samples exhibit the lowest mud contents amongst the field areas, with the exception of some Anza Borrego soils (Figure 1.2). However, anomalously high mud contents occur within some proglacial fluvial, water-track and glacial drift samples from Antarctica (Figure 1.2), where mud content reaches 54% (Table S1.2).

As depositional settings influence grain size distribution (via transport medium and energy, etc.), we focused on comparing the concentration of mud-sized grains within only fluvial settings (Figure 1.2), the setting for which we have the most data across all field sites. Fluvial sediments from Norway (26.2%) have higher mud content on average, followed by Peru (25.1%), Iceland (17.2%), Puerto Rico (10.3%), Antarctica (7.2%), Washington (3.5%) and Anza Borrego (3.5%).

When we integrate the LPSA results with the overall granulometry data to calculate the fraction of clay sized (<4 μm) sediment in the bulk samples, results varied significantly (Figure 1.3). Summary statistics of clay-sized (<4 μm) sediment *within the mud fraction* of different depositional settings show proglacial lakes had the highest percentage of clay (<4 μm) sized material (26%, n=4), followed by glacial drifts (19.7%, n=21), proglacial fluvial sediments

(16.2%, n=94), soils (0-10 cm topsoil, 16.4%, n=7), water-track sediments (16%, n=18), non-glacial fluvial sediments (13.5%, n=17), and saprolites (8.3%, n=9).

Comparing the concentration of clay within the mud fraction of fluvial sediments collected in different field sites (Figure 1.3), fluvial muds from Antarctica have the highest concentrations of clay-sized particles ($<4 \mu\text{m}$) on average (22.1%), followed by Anza Borrego (21.5%), Iceland (20.0%), Peru (13.4%), Puerto Rico (8.6%), Washington (4.9%) and Norway (2.7%).

Surface Area

Our BET surface area data from individual samples are provided in Table S1.2 and illustrated in Figure 1.4. Summary statistics of the BET results within different depositional settings showed that water track sediments exhibit the highest surface area on average ($32.9 \text{ m}^2/\text{g}$, n=18), followed by the non-glacial fluvial sediments ($19.7 \text{ m}^2/\text{g}$, n=24), top layers of soil profiles (0-10 cm; $19.6 \text{ m}^2/\text{g}$, n=6), glacial drifts ($18.0 \text{ m}^2/\text{g}$, n=22), saprolites ($17.4 \text{ m}^2/\text{g}$, n=9), proglacial fluvial sediments ($15.9 \text{ m}^2/\text{g}$, n=107), and proglacial lake sediments ($4.0 \text{ m}^2/\text{g}$, n=4). Viewed across all field sites and depositional settings combined (Figure 1.4), Antarctic Taylor Valley samples have significantly higher BET surface area values than the other sites, with an average of $63.6 \text{ m}^2/\text{g}$ within the CAMP soil profile samples (n=4), followed by the proglacial fluvial sediments ($39.3 \text{ m}^2/\text{g}$, n=27), water tracks ($32.9 \text{ m}^2/\text{g}$, n=18), and glacial drifts ($27.8 \text{ m}^2/\text{g}$, n=7 (Table S1.2). Delta Stream sediments within the Taylor Valley proglacial watershed display anomalously high BET values (Figure 1.4), reaching up to $70.6 \text{ m}^2/\text{g}$ (Table S1.2).

Mineralogy

Results of our quantitative XRD analyses are listed in Table S1.3 for each sample. Although we tried to keep the underlying lithology largely similar by targeting granitic to granodiorite composition bedrock sources (with the exception of Iceland), there are significant differences in the primary rock-forming minerals present in each field area (Figure 1.5), which are also reflected in PCA analyses as individual clusters belonging to field sites plotting away from each other (Figure 1.6). Summary statistics on individual field sites showed that Peru sediments contain the highest average fraction of primary rock-forming silicates within the mud fraction (95.1%, n=14), followed by Anza Borrego (85.2%, n=5), Washington (64%, n=11), Antarctica (64%, n=58), Iceland (63.1%, n=3), Norway (57%, n=15), and Puerto Rico (56%, n=23), in descending order. Clay mineral and miscellaneous secondary phyllosilicate mineral (serpentine, zeophyllite, pyrophyllite, clinozoisite) abundance (excluding primary mica minerals) follows an inverse order as expected (except for Iceland), with Puerto Rico having the highest average secondary mineral content (43.4%), followed by Norway (42%), Antarctica (34.4%), Washington (25%), Anza Borrego (14.4%), Iceland (5%), and Peru (4.7%). Zeolites were only observed within glacial settings, where the highest concentrations are observed within Washington muds (8.5% on average), followed by Norway (0.9%), Antarctica (0.7%), Iceland (0.7%), and Peru (0.2%). Note that Iceland sediments contain on average 30% amorphous material. Remaining mineral fractions are accessory minerals for all sediments. Further details regarding the primary rock-forming and accessory minerals, as well as zeolites and amorphous phases can be found in supplementary materials for this chapter.

Clay minerals

Secondary clay mineral assemblages (Table S1.3) within the Antarctic MDV muds collected from glaciofluvial and drift samples are dominated by illite, and also contain abundant chlorite group minerals (clinochlore >chamosite), smectites (montmorillonite and amorphous smectites), mixed layered clays (illite-smectite and chlorite-smectite) and, locally, small amounts of vermiculite. Montmorillonite is most abundant within water-track sediments. Vermiculite typically occurs in samples where biotite contents are relatively low. MDV permafrost soil samples contain varying illite-montmorillonite assemblages, where montmorillonite content is higher within the top 20 cm of the profiles in general, accompanied by relatively lower abundances of chlorite group minerals. Note that we did not detect kaolinite in our XRD analyses of MDV sediments, but kaolinite occurrences were previously reported within similar sediment samples from the Antarctic MDVs (Marra et al., 2017).

Secondary clays in Norway muds show a similar assemblage where illite dominates the fluvial sediments, montmorillonite occurs in drifts and soils, and chlorite is observed in proglacial lake, proglacial fluvial, and drift sediments. Note that Norway muds have significantly higher illite concentrations (~40% illite) compared to other field sites. Chlorite predominates in the relatively small concentration of clay minerals observed in Peru fluvial samples (clinochlore > chamosite), while palygorskite is also observed within proglacial lake sediments. Washington sediments are also enriched in chlorite minerals (mostly clinochlore) and have local occurrences of palygorskite, although montmorillonite and vermiculite are locally higher in abundance within meltwater stream sediments. Smectites predominate the clay minerals observed in Iceland muds (montmorillonite and some amorphous smectite).

The most distinctive difference in clay mineralogy observed between glacial and warmer climatic settings is the occurrence and abundance of kaolinite in Puerto Rico and Anza Borrego

(Table S1.3). Puerto Rico sediment muds contained up to 93% of kaolinite (40% kaolinite on average), where the highest kaolinite concentrations were observed in saprolites. The only secondary clay mineral observed in Puerto Rico fluvial muds is kaolinite, whereas the saprolite also contains chlorite and vermiculite in lower abundances. Clay minerals observed in Anza Borrego muds, on the other hand, are dominated by illite, followed by kaolinite and smectite.

Note that we are defining illite as the mineral specimen that has a d-spacing value of 10Å. Mechanical grinding of muscovite, which is especially pronounced in glacial sites via glacial grinding, also produces a 10Å d-spacing value. Therefore, amounts of illite within the samples reported in Table S1.3, and illustrated in Figure 1.5 might be artifacts of mechanical grinding, as well as being secondary products of biotite weathering.

Sediment Geochemistry

Major oxide results are reported in Table S1.4. We also analyzed heavy metals, trace metals and REE concentrations which can be found in Tables S5, S6 and S7, respectively. Overall, PCA analyses of major oxides, trace metals, heavy metals and rare earth element composition of the mud fraction samples (Figure 1.7) illustrate overlapping compositions as well as distinctive differences between samples collected from different field sites. Washington (square, dark blue) and Antarctic (asterisk, gray) mud compositions overlap, while fluvial Puerto Rico (circle, green) and Anza Borrego (triangle, red) samples cluster close to them. The Anza Borrego samples, however, display different heavy metal compositions than the Washington, Antarctica and Puerto Rico sediments. Examining the entire suite of geochemical data, (Tables S4-S7) the Puerto Rico saprolites, Norway muds, Icelandic basalts and the majority of the Peru sediments lie distinctively apart from the other samples on the PCA plots (Figure 1.7),

suggesting that they have significantly different chemical compositions compared to the other muds.

Figure S1.2 shows each individual major oxide component plotted against SiO₂ (%) content of individual observations. We calculated average major oxide concentrations for each field site normalized to average SiO₂ values (slopes within Figure S1.2 calculated for individual field sites, e.g., Al₂O₃/SiO₂). Aluminum is significantly higher in Puerto Rico sediments (Al₂O₃/SiO₂=0.52) as compared to other field sites, followed by Antarctica, Anza Borrego and Iceland that have similar Al₂O₃/SiO₂ ratios (~0.3), whereas Washington, Norway and Peru muds display lower Al₂O₃/SiO₂ values. Iron is significantly higher in Iceland basalts (Fe₂O₃/SiO₂=0.24) and significantly lower in Peru, Norway and Anza Borrego sediments (Fe₂O₃/SiO₂=0.04-0.07), whereas the rest of the field sites have similar Fe₂O₃/SiO₂ ratios (0.16-0.2). We note that TiO₂, Cr₂O₃, CaO, MnO and MgO abundances generally follow similar trends as Fe₂O₃, except for Puerto Rico sediments that have higher Fe₂O₃ concentrations, but lower TiO₂ and CaO. Puerto Rico, Washington and Antarctica display the lowest Na₂O/SiO₂ ratios (Na₂O/SiO₂=0.04-0.05), relative to other fields, which have Na₂O/SiO₂ ratios of ~0.06-0.07. Washington, Iceland, Puerto Rico and Anza Borrego have significantly lower K₂O/SiO₂ ratios (K₂O/SiO₂=0.02-0.03), reflecting lower K-feldspar contents, relative to other field sites (K₂O/SiO₂~0.05-0.06). Finally, Norway and Iceland muds have significantly higher P as compared to other field sites (P₂O₅/SiO₂=0.011 and 0.009, respectively), whereas Washington and Antarctica muds have moderate P₂O₅/SiO₂ values (0.007 and 0.006, respectively), and Puerto Rico, Anza Borrego and Peru muds display the lowest P₂O₅/SiO₂ ratios (0.002-0.004).

Weathering Indices and Trends

All weathering index values are reported in Table S1.8, and average values for fluvial muds are reported in Table 1.2. In general, the weathering index trends are similar, therefore we will focus primarily on CIA values in the remaining results and discussion. All CIA values observed fall between 46 and 99 (Table S1.8), considered indicative of incipient to extensive weathering, respectively, although CIA values are also influenced by source-rock lithology (Nesbitt and Young, 1982; Nesbitt et al., 1996; Nesbitt et al., 1997). Here we will focus primarily on the CIA values observed in the mud fraction of fluvial sediments, as these are the most abundant samples across all field sites and allow us to directly compare trends within the same depositional system. Comparisons between depositional systems observed within field sites are also discussed below.

Icelandic fluvial muds have the lowest average CIA value (46), indicative of fresh basalt, whereas Puerto Rico fluvial muds exhibit values of ~66, and saprolites and soil exhibit averaged values of ~81, indicating strong weathering (Table S1.8). Both trends can also be seen on the A-CN-K ternary plot in Figure 1.8. Note that in the A-CK-N diagram (Figure 1.8), Antarctica, Washington, Norway, Peru, and Anza Borrego data points overlap one another, with only Puerto Rico sediments distinctly illustrating an expected increasing weathering trend from bedrock to fluvial sediments to saprolite to soil, with values ranging from 55 to 96.

When we only compare the CIA values of fluvial muds (Table 1.2), we see that CIA values are the highest in Puerto Rico muds (62.2%), followed by Anza Borrego (60.6%), Peru (55.7%), Norway (53.2), Washington (52.1%), Antarctica (48.6%) and Iceland (46.4%). In an attempt to reduce the provenance effect on chemical trends, we normalized average fluvial mud CIA values to average values of bedrock from each field site (Table 1.2). The order of the

normalized CIA values (CIA_n) did not change, except for Iceland, demonstrating the effect of provenance on CIA values.

DISCUSSION

Controls on Grain Surface Area- Implications for Weathering and Climate

Sediment surface area reflects grain size and shape, as well as mineralogy and surface roughness. Therefore, both the concentration of clay-sized particles, as well as the mineralogy and amount of secondary minerals influence surface area. Granulometry, mineralogy, and surface roughness are affected by weathering processes, including mechanical, chemical, and biological processes that vary significantly across different climatic regimes and depositional settings. Therefore, based on the hypothesis that the mineralogy and chemical composition of fine-grained sediment, as well as physical properties (grain size, surface area and texture) derived by weathering are inherited from their depositional settings and climate, we investigated BET surface area and grain size as parameters that can inform interpretations of weathering and climate.

Theoretically, surface area is expected to correlate inversely with grain size (Horowitz and Elrick, 1987) and increase in warmer, wetter settings owing to production of abundant secondary clay minerals and iron (hydr)oxides attendant with chemical weathering (Velbel, 1993; White et al., 1999; White and Brantley, 2003). Surface-area values for muds from warm climates in our dataset, i.e., Anza Borrego (11-19.1 m^2/g ; hot, arid) and Puerto Rico (8.2-35.2 m^2/g ; hot, wet), follow this expectation, exhibiting higher surface areas than *most* of the glacially derived muds (0.3-70.6 m^2/g), with the exception of muds from the Antarctic MDVs (2.5-70.6 m^2/g ; see below). The Anza Borrego fluvial muds contain abundant clay-sized particles (21.5%) and

Puerto Rico muds on average contain a much higher concentration of clay minerals (~43%, Figure 1.5) than other field sites.

Within glacial settings, wet-based temperate glaciers produce abundant fine-grained material due to mechanical weathering associated with basal sliding (Anderson et al., 1997; Anderson, 2005). Therefore, temperate glacial deposits are expected to have high surface areas attributed to the abundance of silt and clay-sized glacial flour (Anderson et al., 1997). In contrast, cold-based glaciers, such as those in the MDVs, are not thought to produce abundant fine-grained sediments due to the lack of basal sliding. However, within the mud fraction, Antarctic sediments (especially from Taylor Valley) exhibit the highest surface area, even exceeding those from tropical regions (e.g., Puerto Rico). MDV sediments contain less mud-sized material as compared to the majority of the field sites; however, MDV muds, particularly those from Taylor Valley, contain more clay-sized particles within the mud fraction than the other glacial sites. Therefore, one reason Antarctic sediments have the highest surface area muds is that they contain abundant clay-sized particles. Marra et al. (2015) attributes the production and transport of high-surface area sediments, as well as the significant variability observed within Wright and Taylor Valley streams, to variations in eolian input and stream discharge rates, as well as the sediment properties within underlying drifts and potential enhanced weathering due to microbially-produced organic acids. Fine-grained sediments are also concentrated onto glacial surfaces (where they may undergo weathering) and released into the stream channels during melting during the austral summer (Marra et al., 2015).

The high BET surface areas observed in the Antarctic mud samples is surprising (Figure 1.4, Table S1.2), as one would expect a tropical region saprolite sample that is almost completely composed of clay minerals (e.g., Puerto Rico PM-RG-SAP-6A sample with $BET=21.9\text{m}^2/\text{g}$,

~93% kaolinite, Tables S2 and S3) to have the highest surface area within the whole data set. However, Antarctic sediments have higher smectite content, potentially due to inheritance from marine sediments (Robert and Kennett, 1992, 1994, 1997), weathering of volcanic clasts and ash inherited from Mt. Erebus (Ugolini, 1967), and older ages (potentially exposing grains to multiple cycles of weathering) compared to Anza Borrego and Puerto Rico muds, as well as other samples. Smectites have some of the highest BET surface areas amongst the wide range of Clay Mineral Society standards (Table S1.9, Dogan et al., 2006, 2007). Therefore, the relatively high smectite content of most of the Antarctic samples (Table S1.3) likely results in the anomalously high surface area values measured in these samples.

Sediment age also affects the chemical, mineralogical, and physical weathering signatures, including the surface area (White et al., 1996; Egli et al., 2001). Antarctic MDV sediments (ranging from LGM to Miocene age; Hall et al., 2000; Hall and Denton; 2005) are older than other sediments we investigated, which were otherwise all first-cycle. The Antarctic sediments may have experienced more than one cycle of weathering owing to multiple glacial advances and retreats as progressively older drifts were reworked and overprinted. (Anderson et al., 1997; Hall et al., 2000; Hall and Denton; 2005), providing multiple opportunities to further develop secondary weathering products and associated high surface area (White and Peterson, 1990; White et al., 1996). However, BET surface area values observed in the LGM-aged Taylor Valley samples significantly exceed values observed in older Wright Valley sediments, suggesting that sediment age is not the primary factor controlling the variability between surface area of these deposits.

To quantitatively investigate the effect of climatic parameters (MAP and MAT) on BET and % clay grain size fraction observed in fluvial sediments across all field areas, we

investigated correlations between these variables by constructing cross-plots (Figure 1.9). Results indicate that the correlations between BET and grain size with MAT and MAP are relatively weak and cannot be individually used as parameters to interpret climate, even though BET and grain size are byproducts of weathering of the source material (Figure 1.9). Therefore, our results indicate that climate is not a primary determinant of BET surface area and % clay in fluvial sediments (Figure 1.9).

Effects of Provenance

Despite selecting field areas underlain by broadly similar granitoid bedrock, we observed distinct differences in the chemistry of mud-sized sediments; however, these differences appear to have little to no link to climate. Indeed, the CIA values (Tables 2 and S8) and compositions plotted in A-CK-N space largely overlap (Figure 1.8), except for the saprolite and soil samples from PR that produce a strong chemical weathering signature (Figures 5-8; Tables S3-S7). We also observed differences in both primary and secondary minerals between all field sites (Figure 1.5). Mineralogical differences are often tied to climate and weathering but may also be due to subtle differences in provenance (Nesbitt et al., 1996; Ren et al., 2019; Mangold et al., 2019). For instance, low abundance of feldspar is often associated with the extent of weathering and linked to higher CIA values (Nesbitt and Young, 1982). However, variations in feldspar content and composition can also be due to provenance, leading to misinterpretations (Mangold et al., 2019). On the other hand, zeolite and clay minerals are associated with weathering conditions (weathering solute composition, weathered material, etc.) and climate (i.e., Barshad, 1966; Dickinson and Rosen, 2003; Wise, 2005; Jacobson et al., 2015), though it is not straightforward to link their presence and abundances to certain climatic regimes. Here we observed zeolites only

in the glacial muds within our dataset, and their occurrences has previously been associated with low-temperature weathering of volcanic and plagioclase-rich rocks (i.e., via brines in Antarctica; Dickinson and Rosen, 2003). However, they also can also form via other mechanisms (Wise, 2005), such as low-grade metamorphism of basalt in Iceland (i.e., Jacobson et al., 2015).

Speciation of clay minerals are also often tied to climate and weathering conditions. For instance, the presence of Fe/Mg bearing smectites on Mars is often linked to weathering of basalts by acidic hydrothermal solutions (Peretyazhko et al., 2016) and/or introduction of wet conditions to a previously dry environment (Bishop et al., 2018). However, Antarctic smectites may also be inherited from marine sediments during alternating wet-dry periods (Robert and Kennett, 1992, 1994, 1997) or sourced from weathering of volcanic clasts and ash from Mt. Erebus (Ugolini, 1967). Kaolinites are also linked to climate, where kaolinites are expected to form in areas with high precipitation, hot-humid climate regimes due to leaching of more soluble ions out of the system (Biscaye, 1965; Barshad, 1966), such as Puerto Rico (e.g., White et al., 1996; White et al., 1998; White and Buss, 2014; Joo et al., 2018a; Webb et al., 2022). However, though we didn't observe kaolinites in our XRD analysis (potentially due to falling below detection limit), other studies have reported kaolinite within Antarctic sediments (Robert and Kennett, 1992, 1994, 1997; Marra et al., 2017). This suggests that, though minerals can be linked to specific climatic regime and CIA is widely utilized in paleoclimate studies (i.e., Nesbitt and Young, 1982; Soreghan and Soreghan, 2007; Goldberg and Humayun, 2010; Xioa et al., 2010; Bahlburg and Dobrzinski 2011; Yang et al., 2016; Ren et al., 2019; Wang et al., 2020; Deng et al., 2022), paleoclimate implications are more complicated due to the ambiguity of the origin of most minerals, and complicated climatic history of the older sediments (Thiry, 2000).

The A-CKN-FM diagram in the right block of Figure 1.10 shows that, with the exception of the Puerto Rico samples, only a few Peru mud samples and a single Norway sample trend significantly towards the weathering apex (towards A). Similar trends observed on the A-CK-N diagram (Figure 1.8) indicate that only the Puerto Rico muds exhibit strong weathering trends. However, since the A-CKN-FM plot also incorporates Mg and Fe contents, it provides additional provenance information. The distribution of samples relative to the line that connects the FM apex and the point halfway between A and CKN is likely due to differences in provenance between samples (Nesbitt et al., 1996). We observed that Norway and Peru bedrock plot towards the felsic apex and Iceland bedrock plots towards mafic (as expected), whereas the underlying bedrock in Antarctica, Washington, Anza Borrego and Puerto Rico plot as mixed felsic-intermediate compositions. These differences indicate that while we attempted to normalize for bedrock by targeting areas underlain by granitic-granodioritic compositions, even relatively small differences in lithology can result in significantly different bulk compositions as visualized in these ternary spaces and also indicated by the significant differences in major oxide chemistry and primary mineralogy (Figure 1.6, Figure 1.7).

We also plotted the compositional data on a MFW diagram (Ohta and Arai, 2007; Figure 1.11) to further investigate the role of provenance in the mud chemistry and weathering trends. In contrast to the A-CKN-FM plot, fluvial samples from Iceland, Antarctica, Washington and Puerto Rico plot closest to the mafic apex, while Peru samples plot closest to felsic, and Norway and Anza Borrego samples lie mostly in the felsic-intermediate range. Note that the Antarctic Taylor Valley drifts (mainly Ross Sea Drift) contain up to ~17% mafic clasts from the Ferrar Dolerite and McMurdo volcanics; however, the rest of the clast composition (~83%) is largely granitic and granodioritic within the bulk fraction (Hall et al., 2000), suggesting significant

sorting effects lead to the Antarctic muds plotting within the mafic apex (Nesbitt et al., 1996; von Eynatten et al., 2012). Only the Puerto Rico soil and saprolite samples plot near the weathered apex (Figure 1.11), consistent with the A-CK-N plots (Figure 1.8) showing weathering trends only in the Puerto Rico samples. These results demonstrate that, amongst our endmember climate samples, MFW plots only indicate significant weathering signatures in tropical watersheds (i.e., Puerto Rico). However, CIA values and clay mineral assemblages indicative of moderate-intense weathering were also observed in Antarctic samples (Tables 2 and S8).

Further comparison of depositional settings within individual field sites (Figure 1.11) revealed that soil and saprolite samples tend to show more intense weathering signatures than bedrock or fluvial samples, except for soils collected in Washington and Anza Borrego which produced weathering indices indicating that they were *less* weathered than fluvial samples from the same watershed. Among Antarctic samples, we also observed that some bedrock and drift samples produced weathering indices that were higher than those observed in the soils and water track samples overlapped with soils (Levy et al., 2011). In addition, felsic bedrock from Antarctica and Puerto Rico (granite and granodiorite) plotted as mafic on the MFW plot, within the same region of the diagram with Iceland basalts, indicating that MFW plots may also produce misleading representations of lithology and provenance, in addition to being less sensitive to potential weathering trends.

Limitations of Ternary Diagrams for Fine-Grained Sediments

A-CK-N diagrams are generated using the Al_2O_3 , CaO, K_2O and N_2O contents of samples, and are often combined with CIA values to interpret weathering trends (Nesbitt and Young, 1982). A-CK-N plots were developed for, and are therefore more applicable to, chemical

weathering in felsic-intermediate lithologies, since mafic lithologies also contain abundant FeO, MgO, MnO, Cr₂O₃ and TiO₂. Ignoring these more mafic components can obfuscate interpretations of weathering trends in mafic planetary settings (i.e., Martian regolith; Siebach et al., 2017; Berger et al., 2020), as well as within our mixed-sourced (Antarctic) terrestrial muds. In contrast, A-CKN-FM diagrams account for FeO and MgO and MFW diagrams incorporate all of the major oxide components of the samples, removing the bias towards felsic components. However, these plots also produced surprising results that call into question the effectiveness of these tools as indicators of climate such as 1) sediments from significantly warmer and wetter climates have CIA values comparable to Antarctic sediments and plot in the same region on the A-CK-N diagram, 2) other than the Puerto Rico saprolites, samples with relatively high CIA values do not plot towards the weathered apex in MFW space, and finally, 3) Puerto Rico sediments derived from intermediate bedrock and felsic-intermediate Antarctic sediments both plot squarely in the mafic apex of MFW diagrams.

We posit that the discrepancies between the ternary diagram plots of the muds we investigated, and the bulk bedrock lithology and observed mud mineralogy sampled from field sites within various climatic regimes (Figures 9, 11, 12) are due to the calculations placing significant weight on CaO content. Minerals containing high abundances of CaO -particularly plagioclase, amphibole, and pyroxene) become concentrated within the fine fraction due to physical sorting mechanisms. This results in higher concentrations of more mafic minerals within the mud fraction (Nesbitt et al., 1996; von Eynatten et al., 2012; McLennan et al., 2014; Siebach et al., 2017; Hurowitz et al., 2017; Bedford et al., 2019), skewing the ternary diagram plots toward the mafic apex.

For example, CaO is a major component in all three diagrams, as well as being a primary variable in CIA calculations. The CaO values reported on the diagrams and included in the CIA calculations are representative of CaO within the siliciclastic components of the sediments since we removed carbonates prior to analyses and calculated CaO* values, which corrects CaO content to remove apatite (Equation 1.2; Girty et al., 2013). While other secondary minerals, including sulfates, can also contribute to elevated CaO content in fine-grained sediments (McLennan et al., 2014; Hurowitz et al., 2017; Bedford et al., 2019; Mangold et al., 2019), we do not see any evidence of gypsum or other sulfates in our samples and any secondary salts or carbonates were removed in our pre-analysis wet sieving, acid, and peroxide treatments. However, CaO content also can be elevated based on provenance, for example elevated anorthite compositions in a plagioclase-rich bedrock would also result in lower CIA values, even if the extent of weathering is comparable between field sites (Mangold et al., 2019). Thus, the effects of physical sorting, e.g., concentrating CaO and other mafic oxides within the mud fraction (i.e., Nesbitt et al., 1996), could explain why samples derived from predominantly felsic and felsic-intermediate lithology plot close to mafic apex in MFW diagrams.

Mafic minerals are also more susceptible to physical and chemical weathering than more felsic minerals (Goldich, 1938). These processes concentrate more mafic minerals in finer grained size fractions, whereas the felsic mineral content is more prevalent in coarser sediment fractions (Nesbitt et al., 1996; von Eynatten et al., 2012). This influences the composition of fine-grained sediments eroded from mafic rocks (Siebach et al., 2017), but the trend is more pronounced in intermediate- and mixed-sourced sediments where mafic minerals have relatively low concentrations in the bulk sediment but are heavily concentrated in the fine-grained fraction. In the case of intermediate- and mixed-source sediments, the regions that have higher

abundances of Ca-rich pyroxene (e.g., Antarctica) and amphibole (e.g., Washington) within the bedrock, as well as the regions with pronounced mechanical weathering (i.e., pulverization within glacial settings) are particularly susceptible to relative enrichment of mafic grains within the mud fraction, which could explain these regions plotting as mafic in the MFW plots.

The relative enrichment of metal oxides (Fe-, Mn- and Ti-oxides) within the mud fraction via preferential weathering and sorting of mafic minerals could also result in plotting at the mafic apex of the MFW diagram. Antarctic and Washington muds are notably rich in Fe_2O_3 , MnO, and TiO_2 , with concentrations comparable to Iceland muds, and their average Cr_2O_3 concentrations even exceed Iceland basalts (Table S1.4). However, fluvial Puerto Rico sediments derived from felsic-intermediate granodiorite also plot as mafic, potentially due to their relatively high Fe_2O_3 and MnO contents (~10% and 0.19%) which are concentrated within the mud fraction. These iron and manganese concentrations are similar to those observed in the mixed-source Antarctic (~10% and 0.16%) and basaltic Iceland muds (~12%). Note that Joo et al. (2018a) reported up to 1.4% Fe-oxides based on XRD analyses, (which is very close to the instrumental detection limit of 1%) within similar samples collected from Puerto Rico. We posit that the source of the Fe and Mn within Puerto Rico muds is likely secondary oxides resulting from chemical weathering within a tropical climate, that are concentrated in soils (Huang et al., 2016; Nguyen et al., 2019). These Fe and Mn rich soils are delivered to the fluvial system via slope failure or hurricane events that can transport soil to fluvial systems (Webb et al., 2022), including the B horizon which is often rich in metals leached from the horizon above.

Separating Weathering Signatures from Provenance to Interpret Climate

Ternary diagrams of weathering parameters are commonly used to interpret the climate within ancient sediments on Earth, as well as planetary samples derived from unknown bedrock sources (provenance), depositional environment, and climatic history. However, in this study comparing modern sediments produced in endmember climate systems these ternary plots failed to produce patterns that can be correlated with climate, as samples from different climate regimes largely overlap. Therefore, we took an alternative approach to investigate multiple weathering signatures all together, using BET surface area, major oxides, heavy metals, trace metals, rare earth elements, mineralogy, and grain size (percentage of clay-sized particles) within the mud fraction using PCA analyses (Figure 1.12). PCA analyses of our entire data set also produced partially overlapping clusters of temperate glacial (Washington) and tropical (Puerto Rico) data points, whereas other temperate glacial regions (Iceland, Peru, Norway) clustered away from them. These results, combined with provenance considerations inferred from A-CKN-FM and MFW diagrams on bedrock data (Figures 11A and 12A), the overlapping Antarctica, Washington and Puerto Rico data clusters within the PCA analyses of the mineralogy (Figure 1.6) and geochemistry (Figure 1.7), of our samples suggest that subtle differences in provenance significantly affects the “weathering” signatures observed in sediments collected across our climate endmember field sites, even though we tried to keep the bedrock compositions similar (granitic-granodioritic, with the exception of Iceland).

In a further attempt to separate the climate signature from provenance, we normalized the CIA values of the fluvial sediments to the average bedrock CIA values for each field site (Equation 1.3):

$$CIA_n = CIA_{mud} / CIA_{bedrock} \quad \text{(Equation 1.3)}$$

Then we compared these normalized CIA_n values with the mean annual temperature and mean annual precipitation observed in each field area to investigate if these climate parameters correlate with potential weathering signatures within fluvial settings. The correlation between the CIA values versus MAP ($R^2 = 0.6862$) and MAT ($R^2 = 0.5239$) were stronger than the correlation observed between bedrock normalized CIA_n values (R^2 for CIA_n vs. MAP= 0.5538 and R^2 for CIA_n vs. MAT = 0.4226) of the sediments (Figure 1.13), suggesting that provenance effects might lead to overestimated CIA-climate correlations.

We then removed the non-glacial (Anza Borrego and Puerto Rico muds) muds from the dataset to investigate the applicability of CIA-climate correlations within glaciofluvial settings, which diminished correlations between CIA and climate (for both raw and normalized data; Figure 1.14). Deng et al. (2022) also reported that CIA values of glaciofluvial muds do not fit traditional trends assumed for CIA- climatic correlations, though CIA and MAT correlated strongly for non-glacial fluvial muds from warmer settings ($R^2 = \sim 0.6$) in their study. This implies that CIA is not a useful metric for interpreting paleoclimate in glaciofluvial settings, and rather should be used for where the composition of the primary source material is well constrained—such as tropical soil/paleosol profiles (i.e., Joo et al., 2018a).

Synthesis and Implications for Paleoclimate Studies

In contrast to many paleoclimate/weathering studies that are limited to tropical settings or data mining from the literature, our study focused on systematically collected sediments from watersheds with similar bedrock composition (except for Iceland) from various glacial settings with different MAP and MAT, as well as hot-wet and hot-dry non-glacial systems, and various depositional settings to directly test the effects of climate on weathering signatures observed in

modern sediments. All samples were collected, treated, prepared, and analyzed the same way; therefore, analytical and operator-based variations are minimal. Despite these systematic and careful measures, our study revealed overlapping CIA values and composition trends on ternary plots (A-CK-N, A-CKN-FM, and MFW) suggesting that differences in provenance outweigh weathering processes, preventing accurate interpretations of climate from fine-grained sediments, especially in sediments derived from intermediate or mixed bedrock. Mafic minerals, as well as other Ca-rich minerals concentrate within the fine fraction during weathering and transport, resulting in relative enrichment of CaO and correspondingly underestimated CIA values, as also noted in previous literature (i.e., Nesbitt et al., 1996; Siebach et al., 2017; Mangold et al., 2019).

Most of the literature reporting strong correlations between CIA and climate are based on soil profiles or fluvial watersheds in tropical climates (Rasmussen et al., 2011; Yang et al., 2016; Joo et al., 2018a; Mao et al., 2022), which have well-defined chemical weathering trends (increasing Al_2O_3 and clay minerals with weathering, etc.). Our climate (MAP and MAT) and CIA correlation analyses based on sediments from a range of endmember climates on fluvial settings suggest that CIA is not a useful metric for glaciated settings in agreement with Deng et al. (2022), especially in systems that may contain older sediments that have experienced multiple rounds of weathering. Therefore, our results call for caution when applying CIA to interpret climate in fine grained sediments, especially those derived from glacial, intermediate, or mixed-source environments.

Our results combined with previous studies indicate that CIA and ternary plots may be useful tools for studying weathering in tropical settings with uniform bedrock composition, where elemental (weathering) trends can be directly linked between the bedrock to derived

sediment, such as soil profiles/paleosols. Since provenance often overwhelmed climate signals, even when comparing sites with similar underlying bedrock from very different endmember climate conditions, CIA is not suitable for comparisons between mixed-provenance data sets or where the provenance is unknown. Observations of overlapping CIA values of glacial muds with muds derived from hot climates suggest that relying on CIA can result in erroneous interpretations on weathering and paleoclimate. In addition, comparisons of CIA values observed in different glacial settings should not be directly compared to each other to determine the relative extent of weathering, but rather could be used within a single environment to determine changes in the extent of weathering, if the source rock is known (and is strictly uniform) and the depositional setting remains constant to avoid grain sorting effects.

CONCLUSIONS

Based on the sedimentologic and geochemical data from terrestrial sediments collected across endmember climatic regimes, we conclude that physical, chemical, and biological weathering processes all leave imprints on terrestrial sediments, as inferred from surface area, grain size, geochemistry, and mineralogy combined. However, the relatively minor differences in source rock lithology (mineralogy, geochemistry and texture) overwhelm any climatic signatures that may be present when comparing endmember climate conditions. In addition, grain size and BET surface area are not significant proxies for climate within a multi-provenance dataset of mud-sized sediments from various depositional settings, though they may be valuable for investigating weathering trends within individual field sites.

Weathering indices and ternary plots that are commonly used as proxies to interpret paleoclimate are most useful when applied to well-developed weathering profiles within tropical

settings (e.g., Puerto Rico), and are largely ineffective for identifying climate signals in fine-grained fluvial and glacial sediments formed in other climates. Though CIA values and ternary diagrams (A-CK-N, A-CKN-FM, MFW) have conventionally been used to interpret climate conditions based on the intensity of weathering, CIA values and position of data within ternary diagrams are heavily affected by the amount of silicate-bound CaO, as higher CaO concentrations result in lower CIA values and pull samples toward the mafic apex of MFW plots. Despite treating our samples to isolate the silicate fraction by removing soluble salts, carbonates and organic matter, our data set still contained significant variation in CaO content. Even if the weathering intensities of two regions are exactly the same, higher Ca content (plagioclase, Ca-pyroxene, Ca-rich amphiboles, etc.) leads to lower CIA values. In addition, CaO is relatively enriched in finer-grained sediments, as mechanically and chemically weaker mafic components rich in Ca are preferentially sorted into the mud fraction, while harder felsic minerals remain within the sand- and gravel-sized grains (i.e., Nesbitt et al., 1996; Mangold et al., 2019). This can result in muds derived from felsic rocks plotting as mafic within ternary plots, hindering interpretations of weathering extent. Therefore, use of CIA and ternary diagrams for fine-grained terrestrial and planetary sediments, especially sediments derived from intermediate or mixed composition sources require caution and additional proxies in order to make realistic climatic interpretations.

Plotting individual major oxide components from fine-grained sediments on ternary diagrams may intensify small differences in provenance, thus diluting the weathering signatures within the data set and hindering climatic interpretations. Normalizing sediment data based on bedrock composition to reduce the provenance effect reduced correlations with climate parameters (MAP and MAT), suggesting that provenance effect might lead to overestimated

CIA-climate correlations. However, these trends were absent when we excluded sediments formed in hot climates (Anza Borrego and Puerto Rico muds) from the dataset.

Synthesis of our overall findings suggest: 1) CIA and ternary plots for weathering are most useful when applied to tropical settings with uniform bedrock composition, where elemental (weathering) trends can be well-constrained from the bedrock to first-cycle material (soil profiles/paleosols); 2) CIA values of muds from glacial settings overlap with hot and humid climates; and 3) no correlations were observed between climatic parameters (mean annual precipitation and temperature) and CIA in glacial systems, suggesting that CIA is not a useful metric determining paleoclimate in glaciated settings.

ACKNOWLEDGEMENTS

This project is funded by National Science Foundation (NSF) grant #1543344. Project information can be found at USAP-DC website at <https://www.usap-dc.org/view/project/p0010181>. We thank Claire Curry, Zachary D. Tomlinson, J. Scott Greene, James G. Floyd, and Mark J. Laufersweiler for their valuable comments and suggestions on our data analysis methods.

REFERENCES

- Aitchison, J., 1982, *The Statistical Analysis of Compositional Data*: v. 44, p. 139–177, doi:<https://doi.org/10.1111/j.2517-6161.1982.tb01195.x>.
- Aitchison, J., and Greenacre, M., 2002, Biplots of compositional data: *Journal of the Royal Statistical Society: Series C (Applied Statistics)*, v. 51, p. 375–392, doi:[10.1111/1467-9876.00275](https://doi.org/10.1111/1467-9876.00275).
- Anderson, S.P., 2005, Glaciers show direct linkage between erosion rate and chemical weathering fluxes: *Geomorphology*, v. 67, p. 147–157, doi:[10.1016/j.geomorph.2004.07.010](https://doi.org/10.1016/j.geomorph.2004.07.010).
- Anderson, S.P., Drever, J.I., and Humphrey, N.F., 1997, Chemical weathering in glacial environments: *Geology*, v. 25 (5), p. 399-402.

- Andrews, J.T., and Eberl, D.D., 2007, Quantitative Mineralogy of Surface Sediments on the Iceland Shelf, and Application to Down-Core Studies of Holocene Ice-Rafted Sediments: *Journal of Sedimentary Research*, v. 77, p. 469–479, doi:[10.2110/jsr.2007.045](https://doi.org/10.2110/jsr.2007.045).
- Arnalds, O., Dagsson-Waldhauserova, P., and Olafsson, H., 2016, The Icelandic volcanic aeolian environment: Processes and impacts — A review: *Aeolian Research*, v. 20, p. 176–195, doi:[10.1016/j.aeolia.2016.01.004](https://doi.org/10.1016/j.aeolia.2016.01.004).
- Axen, G.J., and Fletcher, J.M., 1988, Late Miocene-Pleistocene Extensional Faulting, Northern Gulf of California, Mexico and Salton Trough, California: *International Geology Review*, v. 40, p. 217–244, doi:<https://doi.org/10.1080/00206819809465207>.
- Bahlburg, H., and Dobrzinski, N., 2011, Chapter 6 A review of the Chemical Index of Alteration (CIA) and its application to the study of Neoproterozoic glacial deposits and climate transitions: *Geological Society, London, Memoirs*, v. 36, p. 81–92, doi:10.1144/M36.6.
- Baraer, M., McKenzie, J., Mark, B.G., Gordon, R., Bury, J., Condom, T., Gomez, J., Knox, S., and Fortner, S.K., 2015, Contribution of groundwater to the outflow from ungauged glacierized catchments: a multi-site study in the tropical Cordillera Blanca, Peru: *Hydrological Processes*, v. 29, p. 2561–2581, doi:[10.1002/hyp.10386](https://doi.org/10.1002/hyp.10386).
- Barshad, J., 1966, The effect of a variation of precipitation on the nature of clay mineral formation in soils from acid and basic igneous rocks, *in Proc. Int. Clay Conf. (Jerusalem)*, v. 1, p. 167–173.
- Beck, H.E., Zimmermann, N.E., McVicar, T.R., Vergopolan, N., Berg, A., and Wood, E.F., 2018, Present and future Köppen-Geiger climate classification maps at 1-km resolution: *Scientific Data*, v. 5, p. 180214, doi:10.1038/sdata.2018.214.
- Bedford, C.C., Bridges, J.C., Schwenzer, S.P., Wiens, R.C., Rampe, E.B., Frydenvang, J., and Gasda, P.J., 2019, Alteration trends and geochemical source region characteristics preserved in the fluviolacustrine sedimentary record of Gale crater, Mars: *Geochimica et Cosmochimica Acta*, v. 246, p. 234–266, doi:[10.1016/j.gca.2018.11.031](https://doi.org/10.1016/j.gca.2018.11.031).
- Berger, J. et al., 2020, Elemental Composition and Chemical Evolution of Geologic Materials in Gale Crater, Mars: APXS Results From Bradbury Landing to the Vera Rubin Ridge: *Journal of Geophysical Research: Planets*, v. 125, doi:[10.1029/2020JE006536](https://doi.org/10.1029/2020JE006536).
- Besette-Kirton, E.K., Cerovski-Darriau, C., Schulz, W.H., Coe, J.A., Kean, J.W., Godt, J.W., Thomas, M.A., and Hughes, S.K., 2019, Landslides Triggered by Hurricane Maria: Assessment of an Extreme Event in Puerto Rico: *GSA Today*, v. 29, p. 4–10, doi:[10.1130/GSATG383A.1](https://doi.org/10.1130/GSATG383A.1).
- Bickerton, R.W., and Matthews, J.A., 1993, ‘Little ice age’ variations of outlet glaciers from the jostedalbreen ice-cap, Southern Norway: A regional lichenometric-dating study of ice-marginal moraine sequences and their climatic significance: *Journal of Quaternary Science*, v. 8, p. 45–66, doi:[10.1002/jqs.3390080105](https://doi.org/10.1002/jqs.3390080105).
- Biscaye, P.E., 1965, Mineralogy and Sedimentation of Recent Deep-Sea Clay in the Atlantic Ocean and Adjacent Seas and Oceans: *GSA Bulletin*, v. 76, p. 803–832, doi:[10.1130/0016-7606\(1965\)76\[803:MASORD\]2.0.CO;2](https://doi.org/10.1130/0016-7606(1965)76[803:MASORD]2.0.CO;2).

- Bish, D.L., and Howard, S.A., 1988, Quantitative phase analysis using the Rietveld method: *Journal of Applied Crystallography*, v. 21, p. 86–91, doi:[10.1107/S0021889887009415](https://doi.org/10.1107/S0021889887009415).
- Bishop, J.L., Fairén, A.G., Michalski, J.R., Gago-Duport, L., Baker, L.L., Velbel, M.A., Gross, C., and Rampe, E.B., 2018, Surface clay formation during short-term warmer and wetter conditions on a largely cold ancient Mars: *Nature Astronomy*, v. 2, p. 206–213, doi:[10.1038/s41550-017-0377-9](https://doi.org/10.1038/s41550-017-0377-9).
- Blott, S.J., Croft, D.J., Pye, K., Saye, S.E., and Wilson, H.E., 2004, Particle size analysis by laser diffraction: Geological Society, London, Special Publications, v. 232, p. 63–73, doi:[10.1144/GSL.SP.2004.232.01.08](https://doi.org/10.1144/GSL.SP.2004.232.01.08).
- Bockheim, J.G., and McLeod, M., 2008, Soil distribution in the McMurdo Dry Valleys, Antarctica: *Geoderma*, v. 144, p. 43–49, doi:[10.1016/j.geoderma.2007.10.015](https://doi.org/10.1016/j.geoderma.2007.10.015).
- van den Boogaart, K.G., and Tolosana-Delgado, R., 2008, “compositions”: A unified R package to analyze compositional data: *Computers & Geosciences*, v. 34, p. 320–338, doi:[10.1016/j.cageo.2006.11.017](https://doi.org/10.1016/j.cageo.2006.11.017).
- Brown, E.H., and Walker, N.W., 1993, A magma-loading model for Barrovian metamorphism in the southeast Coast Plutonic Complex, British Columbia and Washington: *GSA Bulletin*, v. 105, p. 479–500, doi:[10.1130/0016-7606\(1993\)105<0479:AMLMFB>2.3.CO;2](https://doi.org/10.1130/0016-7606(1993)105<0479:AMLMFB>2.3.CO;2).
- Brunauer, S., Emmett, P.H., and Teller, E., 1938, Adsorption of Gases in Multimolecular Layers: *Journal of the American Chemical Society*, v. 60, p. 309–319, doi:[10.1021/ja01269a023](https://doi.org/10.1021/ja01269a023).
- Bury, J.T., Mark, B.G., McKenzie, J.M., French, A., Baraer, M., Huh, K.I., Zapata Luyo, M.A., and Gómez López, R.J., 2011, Glacier recession and human vulnerability in the Yanamarey watershed of the Cordillera Blanca, Peru: *Climatic Change*, v. 105, p. 179–206, doi:[10.1007/s10584-010-9870-1](https://doi.org/10.1007/s10584-010-9870-1).
- Butler, J., Beaumont, C., and Jamieson, R., 2015, Paradigm lost: Buoyancy thwarted by the strength of the Western Gneiss Region (ultra)high-pressure terrane, Norway: *Lithosphere*, v. 7, doi:[10.1130/L426.1](https://doi.org/10.1130/L426.1).
- Campbell, I.B., and Claridge, G.G.C., 2006, Permafrost Properties, Patterns and Processes in the Transantarctic Mountains Region: *Permafrost and Periglacial Processes*, v. 17, p. 215–232, doi:[10.1002/ppp](https://doi.org/10.1002/ppp).
- Cowan, D.A., Khan, N., Pointing, S.B., and Cary, S.C., 2010, Diverse hypolithic refuge communities in the McMurdo Dry Valleys: *Antarctic Science*, v. 22, p. 714–720, doi:[10.1017/S0954102010000507](https://doi.org/10.1017/S0954102010000507).
- Cuozzo, N., Sletten, R.S., Hu, Y., Liu, L., Teng, F.-Z., and Hagedorn, B., 2020, Silicate weathering in antarctic ice-rich permafrost: Insights using magnesium isotopes: *Geochimica et Cosmochimica Acta*, v. 278, p. 244–260, doi:[10.1016/j.gca.2019.07.031](https://doi.org/10.1016/j.gca.2019.07.031).
- Dickinson, W.W., and Rosen, M.R., 2003, Antarctic permafrost: An analogue for water and diagenetic minerals on Mars: *Geology*, v. 31, p. 199–202, doi:[10.1130/0091-7613\(2003\)031<0199:APAAFW>2.0.CO;2](https://doi.org/10.1130/0091-7613(2003)031<0199:APAAFW>2.0.CO;2).

- Daly, C., Halbleib, M., Smith, J.I., Gibson, W.P., Doggett, M.K., Taylor, G.H., Curtis, J., and Pasteris, P.P., 2008, Physiographically sensitive mapping of climatological temperature and precipitation across the conterminous United States: *International Journal of Climatology*, v. 28, p. 2031–2064, doi:[10.1002/joc.1688](https://doi.org/10.1002/joc.1688).
- Daly, C., Neilson, R.P., and Phillips, D.L., 1994, A Statistical-Topographic Model for Mapping Climatological Precipitation over Mountainous Terrain: *Journal of Applied Meteorology and Climatology*, v. 33, p. 140–158, doi:[10.1175/1520-0450\(1994\)033<0140:ASTMFM>2.0.CO;2](https://doi.org/10.1175/1520-0450(1994)033<0140:ASTMFM>2.0.CO;2).
- Demirel-Floyd, C. (2022) "Data and metadata for "Quantifying surface area in muds from the Antarctic Dry Valleys: Implications for weathering in glacial systems"" U.S. Antarctic Program (USAP) Data Center. doi: <https://doi.org/10.15784/601599>.
- Demirel-Floyd, C., Soreghan, G.S., and Madden, M.E.E., 2022, Cyanobacterial weathering in warming periglacial sediments: Implications for nutrient cycling and potential biosignatures: *Permafrost and Periglacial Processes*, v. 33, p. 63–77, doi:[10.1002/ppp.2133](https://doi.org/10.1002/ppp.2133).
- Deng, K., Yang, S., and Guo, Y., 2022, A global temperature control of silicate weathering intensity: *Nature Communications*, v. 13, p. 1781, doi:[10.1038/s41467-022-29415-0](https://doi.org/10.1038/s41467-022-29415-0).
- Dogan, A.U., Dogan, M., Onal, M., Sarikaya, Y., Aburub, A., and Wurster, D.E., 2006, Baseline studies of the Clay Minerals Society source clays: specific surface area by the Brunauer Emmett Teller (BET) method: *Clays and Clay Minerals*, v. 54, p. 62–66, doi:[10.1346/CCMN.2006.0540108](https://doi.org/10.1346/CCMN.2006.0540108).
- Dogan, M., Dogan, A.U., Yesilyurt, F.I., Alaygut, D., Buckner, I., and Wurster, D.E., 2007, Baseline studies of The Clay Minerals Society special clays: specific surface area by the Brunauer Emmett Teller (BET) method: *Clays and Clay Minerals*, v. 55, p. 534–541, doi:[10.1346/CCMN.2007.0550508](https://doi.org/10.1346/CCMN.2007.0550508).
- Doran, P.T., McKay, C.P., Clow, G.D., Dana, G.L., Fountain, A.G., Nylén, T., and Lyons, W.B., 2002, Valley floor climate observations from the McMurdo dry valleys, Antarctica, 1986–2000: *Journal of Geophysical Research: Atmospheres*, v. 107, p. ACL 13-1-ACL 13-12, doi:[10.1029/2001JD002045](https://doi.org/10.1029/2001JD002045).
- Doran, P.T., McKay, C.P., Fountain, A.G., Nylén, T., McKnight, D.M., Jaros, C., and Barrett, J.E., 2008, Hydrologic response to extreme warm and cold summers in the McMurdo Dry Valleys, East Antarctica: *Antarctic Science*, v. 20, p. 499–509, doi:[10.1017/S0954102008001272](https://doi.org/10.1017/S0954102008001272).
- Dorsey, R.J., Housen, B.A., Janecke, S.U., Fanning, C.M., and Spears, A.L.F., 2011, Stratigraphic record of basin development within the San Andreas fault system: Late Cenozoic Fish Creek–Vallecito basin, southern California: *GSA Bulletin*, v. 123, p. 771–793, doi:[10.1130/B30168.1](https://doi.org/10.1130/B30168.1).
- Eberl, D.D., 2003, User Guide to RockJock - A Program for Determining Quantitative Mineralogy from X-Ray Diffraction Data:, doi:[10.3133/ofr200378](https://doi.org/10.3133/ofr200378).

- Egli, M., Fitze, P., and Mirabella, A., 2001, Weathering and evolution of soils formed on granitic, glacial deposits: results from chronosequences of Swiss alpine environments: *CATENA*, v. 45, p. 19–47, doi:[10.1016/S0341-8162\(01\)00138-2](https://doi.org/10.1016/S0341-8162(01)00138-2).
- Erikson, E.H., 1977, Petrology and petrogenesis of the Mount Stuart batholith — Plutonic equivalent of the high-alumina basalt association? *Contributions to Mineralogy and Petrology*, v. 60, p. 183–207, doi:[10.1007/BF00372281](https://doi.org/10.1007/BF00372281).
- von Eynatten, H., Tolosana-Delgado, R., and Karius, V., 2012, Sediment generation in modern glacial settings: Grain-size and source-rock control on sediment composition: *Sedimentary Geology*, v. 280, p. 80–92, doi:[10.1016/j.sedgeo.2012.03.008](https://doi.org/10.1016/j.sedgeo.2012.03.008).
- Fedo, C.M., Wayne Nesbitt, H., and Young, G.M., 1995, Unraveling the effects of potassium metasomatism in sedimentary rocks and paleosols, with implications for paleoweathering conditions and provenance: *Geology*, v. 23, p. 921–924, doi:[10.1130/0091-7613\(1995\)023<0921:UTEOPM>2.3.CO;2](https://doi.org/10.1130/0091-7613(1995)023<0921:UTEOPM>2.3.CO;2).
- Filzmoser, P., Hron, K., and Reimann, C., 2009, Principal component analysis for compositional data with outliers: *Environmetrics*, v. 20, p. 621–632, doi:[10.1002/env.966](https://doi.org/10.1002/env.966).
- Fischer, E.R., Hansen, B.T., Nair, V., Hoyt, F.H., and Dorward, D.W., 2012, Scanning Electron Microscopy: *Current Protocols in Microbiology*, v. 25, doi:[10.1002/9780471729259.mc02b02s25](https://doi.org/10.1002/9780471729259.mc02b02s25).
- Fletcher, R.C., Buss, H.L., and Brantley, S.L., 2006, A spheroidal weathering model coupling porewater chemistry to soil thicknesses during steady-state denudation: *Earth and Planetary Science Letters*, v. 244, p. 444–457, doi:[10.1016/j.epsl.2006.01.055](https://doi.org/10.1016/j.epsl.2006.01.055).
- Fountain, A.G. et al., 1999, Physical Controls on the Taylor Valley Ecosystem, Antarctica: *BioScience*, v. 49, p. 961–971, doi:[10.1525/bisi.1999.49.12.961](https://doi.org/10.1525/bisi.1999.49.12.961).
- Geiger, R., and Pohl, W., 1953, Revision of the Köppen-Geiger Klimakarte der Erde:
- Girty, G.H., Colby, T.A., Rayburn, J.Z., Parizek, J.R., and Voyles, E.M., 2013, Biotite-controlled linear compositional weathering trends in tonalitic to quartz dioritic saprock, Santa Margarita Ecological Reserve, southern California, USA: *CATENA*, v. 105, p. 40–51, doi:[10.1016/j.catena.2013.01.001](https://doi.org/10.1016/j.catena.2013.01.001).
- Goldberg, K., and Humayun, M., 2010, The applicability of the Chemical Index of Alteration as a paleoclimatic indicator: An example from the Permian of the Paraná Basin, Brazil: *Palaeogeography, Palaeoclimatology, Palaeoecology*, v. 293, p. 175–183, doi:[10.1016/j.palaeo.2010.05.015](https://doi.org/10.1016/j.palaeo.2010.05.015).
- Goldich, S.S., 1938, A Study in Rock-Weathering: *The Journal of Geology*, v. 46, p. 17–58.
- Gooseff, M.N., McKnight, D.M., Lyons, W.B., and Blum, A.E., 2002, Weathering reactions and hyporheic exchange controls on stream water chemistry in a glacial meltwater stream in the McMurdo Dry Valleys: *Water Resources Research*, v. 38, p. 15-1-15–17, doi:[10.1029/2001WR000834](https://doi.org/10.1029/2001WR000834).

- Gordon, R.P., Lautz, L.K., McKenzie, J.M., Mark, B.G., Chavez, D., and Baraer, M., 2015, Sources and pathways of stream generation in tropical proglacial valleys of the Cordillera Blanca, Peru: *Journal of Hydrology*, v. 522, p. 628–644, doi:[10.1016/j.jhydrol.2015.01.013](https://doi.org/10.1016/j.jhydrol.2015.01.013).
- Gordon, S.M., Whitney, D.L., Teyssier, C., and Fossen, H., 2013, U–Pb dates and trace-element geochemistry of zircon from migmatite, Western Gneiss Region, Norway: Significance for history of partial melting in continental subduction: *Lithos*, v. 170–171, p. 35–53, doi:[10.1016/j.lithos.2013.02.003](https://doi.org/10.1016/j.lithos.2013.02.003).
- Grunsky, E.C., Mueller, U.A., and Corrigan, D., 2014, A study of the lake sediment geochemistry of the Melville Peninsula using multivariate methods: Applications for predictive geological mapping: *Journal of Geochemical Exploration*, v. 141, p. 15–41, doi:[10.1016/j.gexplo.2013.07.013](https://doi.org/10.1016/j.gexplo.2013.07.013).
- Guglielmin, M., Cannone, N., Strini, A., and Lewkowicz, A.G., 2005, Biotic and abiotic processes on granite weathering landforms in a cryotic environment, Northern Victoria Land, Antarctica: *Permafrost and Periglacial Processes*, v. 16, p. 69–85, doi:[10.1002/ppp.514](https://doi.org/10.1002/ppp.514).
- Hall, B.L., and Denton, G.H., 2005, Surficial geology and geomorphology of eastern and central Wright Valley, Antarctica: *Geomorphology*, v. 64, p. 25–65, doi:[10.1016/j.geomorph.2004.05.002](https://doi.org/10.1016/j.geomorph.2004.05.002).
- Hall, B.L., Denton, G.H., and Hendy, C.H., 2000, Evidence from Taylor Valley for a Grounded Ice Sheet in the Ross Sea, Antarctica: *Geografiska Annaler. Series A, Physical Geography*, v. 82, p. 275–303.
- Hall, B.L., Denton, G.H., Lux, D.R., and Bockheim, J.G., 1993, Late Tertiary Antarctic Paleoclimate and Ice-Sheet Dynamics Inferred from Surficial Deposits in Wright Valley: *Physical Geog.: Geografiska Annaler., Series A*, v. 75, p. 239–267.
- Harnois, L., 1988, The CIW index: A new chemical index of weathering: *Sedimentary Geology*, v. 55, p. 319–322, doi:[10.1016/0037-0738\(88\)90137-6](https://doi.org/10.1016/0037-0738(88)90137-6).
- Huang, X., Jiang, H., Li, Y., Ma, Y., Tang, H., Ran, W., and Shen, Q., 2016, The role of poorly crystalline iron oxides in the stability of soil aggregate-associated organic carbon in a rice–wheat cropping system: *Geoderma*, v. 279, p. 1–10, doi:[10.1016/j.geoderma.2016.05.011](https://doi.org/10.1016/j.geoderma.2016.05.011).
- Hurowitz, J.A. et al., 2017, Redox stratification of an ancient lake in Gale crater, Mars: *Science*, v. 356, p. eaah6849, doi:[10.1126/science.aah6849](https://doi.org/10.1126/science.aah6849).
- Jacobson, A.D., Grace Andrews, M., Lehn, G.O., and Holmden, C., 2015, Silicate versus carbonate weathering in Iceland: New insights from Ca isotopes: *Earth and Planetary Science Letters*, v. 416, p. 132–142, doi:[10.1016/j.epsl.2015.01.030](https://doi.org/10.1016/j.epsl.2015.01.030).
- Joo, Y.J., Elwood Madden, M.E., and Soreghan, G.S., 2018a, Anomalously low chemical weathering in fluvial sediment of a tropical watershed (Puerto Rico): *Geology*, v. 46, p. 691–694, doi:[10.1130/G40315.1](https://doi.org/10.1130/G40315.1).
- Joo, Y.J., Elwood Madden, M.E., and Soreghan, G.S., 2016, Chemical and physical weathering in a hot-arid, tectonically active alluvial system of Anza Borrego Desert, California: *Sedimentology*, v. 63, p. 1065–1083, doi:[10.1111/sed.12249](https://doi.org/10.1111/sed.12249).

- Joo, Y.J., Sim, M.S., Elwood Madden, M.E., and Soreghan, G.S., 2022, Significance of the Terrestrial Sink in the Biogeochemical Sulfur Cycle: *Geophysical Research Letters*, v. 49, p. e2021GL097009, doi:[10.1029/2021GL097009](https://doi.org/10.1029/2021GL097009).
- Joo, Y.J., Soreghan, A.M., Madden, M.E.E., and Soreghan, G.S., 2018b, Quantification of particle shape by an automated image analysis system: a case study in natural sediment samples from extreme climates: *Geosciences Journal*, v. 22, p. 525–532, doi:[10.1007/s12303-018-0025-0](https://doi.org/10.1007/s12303-018-0025-0).
- Kaser, G., Ames, A., and Zamora, M., 1990, Glacier Fluctuations and Climate in the Cordillera Blanca, Peru: *Annals of Glaciology*, v. 14, p. 136–140, doi:[10.3189/S0260305500008430](https://doi.org/10.3189/S0260305500008430).
- Kaser, G., Juen, I., Georges, C., Gómez, J., and Tamayo, W., 2003, The impact of glaciers on the runoff and the reconstruction of mass balance history from hydrological data in the tropical Cordillera Blanca, Perú: *Journal of Hydrology*, v. 282, p. 130–144, doi:[10.1016/S0022-1694\(03\)00259-2](https://doi.org/10.1016/S0022-1694(03)00259-2).
- Kelly, L.C., Cockell, C.S., Thorsteinsson, T., Marteinson, V., and Stevenson, J., 2014, Pioneer Microbial Communities of the Fimmvörðuháls Lava Flow, Eyjafjallajökull, Iceland: *Microbial Ecology*, v. 68, p. 504–518, doi:[10.1007/s00248-014-0432-3](https://doi.org/10.1007/s00248-014-0432-3).
- Lepore, C., Kamal, S.A., Shanahan, P., and Bras, R.L., 2012, Rainfall-induced landslide susceptibility zonation of Puerto Rico: *Environmental Earth Sciences*, v. 66, p. 1667–1681, doi:[10.1007/s12665-011-0976-1](https://doi.org/10.1007/s12665-011-0976-1).
- Levy, J.S., Fountain, A.G., Gooseff, M.N., Welch, K.A., and Lyons, W.B., 2011, Water tracks and permafrost in Taylor Valley, Antarctica: Extensive and shallow groundwater connectivity in a cold desert ecosystem: *Bulletin of the Geological Society of America*, v. 123, p. 2295–2311, doi:[10.1130/B30436.1](https://doi.org/10.1130/B30436.1).
- Levy, J.S., Head, J.W., and Marchant, D.R., 2008, The role of thermal contraction crack polygons in cold-desert fluvial systems: *Antarctic Science*, v. 20, p. 565–579, doi:[10.1017/S0954102008001375](https://doi.org/10.1017/S0954102008001375).
- Lewis, S., and Birnie, J., 2001, Little ice age alluvial fan development in Langedalen, western Norway: *Geografiska Annaler Series A Physical Geography*, v. 83A, p. 179–190, doi:[10.1111/1468-0459.00153](https://doi.org/10.1111/1468-0459.00153).
- Li, C., and Yang, S., 2010, Is chemical index of alteration (CIA) a reliable proxy for chemical weathering in global drainage basins? *American Journal of Science*, v. 310, p. 111–127, doi:[10.2475/02.2010.03](https://doi.org/10.2475/02.2010.03).
- Love, D.A., Clark, A.H., and Glover, J.K., 2004, The Lithologic, Stratigraphic, and Structural Setting of the Giant Antamina Copper-Zinc Skarn Deposit, Ancash, Peru: *Economic Geology*, v. 99, p. 887–916, doi:[10.2113/econgeo.99.5.887](https://doi.org/10.2113/econgeo.99.5.887).
- Lyons, W.B., Dailey, K.R., Welch, K.A., Deuerling, K.M., Welch, S.A., and McKnight, D.M., 2015, Antarctic streams as a potential source of iron for the Southern Ocean: *Geology*, v. 43, p. 1003–1006, doi:[10.1130/G36989.1](https://doi.org/10.1130/G36989.1).
- Mangold, N. et al., 2019, Chemical alteration of fine-grained sedimentary rocks at Gale crater: *Icarus*, v. 321, p. 619–631, doi:[10.1016/j.icarus.2018.11.004](https://doi.org/10.1016/j.icarus.2018.11.004).

- Mann, P., Hippolyte, J.-C., Grindlay, N.R., and Abrams, L.J., 2005, Neotectonics of southern Puerto Rico and its offshore margin, doi:[10.1130/0-8137-2385-X.173](https://doi.org/10.1130/0-8137-2385-X.173).
- Mao, H.-R., Cui, L.-F., Zhang, Z.-J., Xu, S., Liu, C.-Q., and Zhao, Z.-Q., 2022, Influence of Monsoon Climate on Chemical Weathering of Granitic Regoliths: Global Biogeochemical Cycles, v. 36, p. e2022GB007362, doi:[10.1029/2022GB007362](https://doi.org/10.1029/2022GB007362).
- Marra, K.R., Madden, M.E.E., Soreghan, G.S., and Hall, B.L., 2015, BET surface area distributions in polar stream sediments: Implications for silicate weathering in a cold-arid environment: *Applied Geochemistry*, v. 52, p. 31–42, doi:<https://doi.org/10.1016/j.apgeochem.2014.11.005>.
- Marra, K.R., Madden, M.E.E., Soreghan, G.S., and Hall, B.L., 2017, Chemical weathering trends in fine-grained ephemeral stream sediments of the McMurdo Dry Valleys, Antarctica: *Geomorphology*, v. 281, p. 13–30, doi:[10.1016/j.geomorph.2016.12.016](https://doi.org/10.1016/j.geomorph.2016.12.016).
- Marra, K.R., Soreghan, G.S., Elwood Madden, M.E., Keiser, L.J., and Hall, B.L., 2014, Trends in grain size and BET surface area in cold–arid versus warm–semiarid fluvial systems: *Geomorphology*, v. 206, p. 483–491, doi:[10.1016/j.geomorph.2013.10.018](https://doi.org/10.1016/j.geomorph.2013.10.018).
- Martín-Fernández, J.A., Barceló-Vidal, C., and Pawlowsky-Glahn, V., 2003, Dealing With Zeros and Missing Values in Compositional Data Sets Using Nonparametric Imputation: *Mathematical Geology*, v. 35, p. 253–278, doi:[10.1023/A:1023866030544](https://doi.org/10.1023/A:1023866030544).
- Martín-Fernández, J.A., Hron, K., Templ, M., Filzmoser, P., and Palarea-Albaladejo, J., 2012, Model-based replacement of rounded zeros in compositional data: Classical and robust approaches: *Computational Statistics & Data Analysis*, v. 56, p. 2688–2704, doi:[10.1016/j.csda.2012.02.012](https://doi.org/10.1016/j.csda.2012.02.012).
- Maurice, P.A., McKnight, D.M., Leff, L., Fulghum, J.E., and Gooseff, M., 2002, Direct observations of aluminosilicate weathering in the hyporheic zone of an Antarctic Dry Valley stream: *Geochimica et Cosmochimica Acta*, v. 66, p. 1335–1347, doi:[10.1016/S0016-7037\(01\)00890-0](https://doi.org/10.1016/S0016-7037(01)00890-0).
- McEwen, A.S., Ojha, L., Dundas, C.M., Mattson, S.S., Byrne, S., Wray, J.J., Cull, S.C., Murchie, S.L., Thomas, N., and Gulick, V.C., 2011, Seasonal Flows on Warm Martian Slopes: *Science*, v. 333, p. 740–743, doi:[10.1126/science.1204816](https://doi.org/10.1126/science.1204816).
- McLennan, S.M. et al., 2014, Elemental Geochemistry of Sedimentary Rocks at Yellowknife Bay, Gale Crater, Mars: *Science*, v. 343, p. 1244734, doi:[10.1126/science.1244734](https://doi.org/10.1126/science.1244734).
- Monroe, W.H., 1980, *Geology of the middle Tertiary formations of Puerto Rico*: U.S. Government Printing Office Professional Paper USGS Numbered Series 953, doi:[10.3133/pp953](https://doi.org/10.3133/pp953).
- Murphy, S.F., Stallard, R.F., Larsen, M.C., and Gould, W.A., 2012, Physiography, geology, and land cover of four watersheds in Eastern Puerto Rico: Professional Paper 1789-A. Reston, VA (?): U.S. Department of the Interior, U.S. Geological Survey., <http://www.fs.usda.gov/treearch/pubs/41669> (accessed July 2022).

- Nesbitt, H.W., Fedo, C.M., and Young, G.M., 1997, Quartz and Feldspar Stability, Steady and Non-Steady-State Weathering, and Petrogenesis of Siliciclastic Sands and Muds: *The Journal of Geology*, v. 105, p. 173–192, doi:[10.1086/515908](https://doi.org/10.1086/515908).
- Nesbitt, H.W., and Young, G.M., 1982, Early Proterozoic climates and plate motions inferred from major element chemistry of lutites: *Nature*, v. 299, p. 715–717, doi:[10.1038/299715a0](https://doi.org/10.1038/299715a0).
- Nesbitt, H.W., and Young, G.M., 1989, Formation and Diagenesis of Weathering Profiles: *The Journal of Geology*, v. 97, p. 129–147.
- Nesbitt, H.W., Young, G.M., McLennan, S.M., and Keays, R.R., 1996, Effects of Chemical Weathering and Sorting on the Petrogenesis of Siliciclastic Sediments, with Implications for Provenance Studies: *The Journal of Geology*, v. 104, p. 525–542.
- Nezat, C.A., Lyons, W.B., and Welch, K.A., 2001, Chemical weathering in streams of a polar desert (Taylor Valley, Antarctica): *Geological Society of America Bulletin*, p. 8.
- Nguyen, M.L., Goldfarb, J.L., Plante, A.F., Lau, B.L.T., and Hockaday, W.C., 2019, Sorption temperature and the stability of iron-bound soil organic matter: *Geoderma*, v. 341, p. 93–99, doi:[10.1016/j.geoderma.2019.01.040](https://doi.org/10.1016/j.geoderma.2019.01.040).
- Ohta, T., and Arai, H., 2007, Statistical empirical index of chemical weathering in igneous rocks: A new tool for evaluating the degree of weathering: *Chemical Geology*, v. 240, p. 280–297, doi:[10.1016/j.chemgeo.2007.02.017](https://doi.org/10.1016/j.chemgeo.2007.02.017).
- Ólafsson, H., Furger, M., and Brümmer, B., 2007, The weather and climate of Iceland: *Meteorologische Zeitschrift*, v. 16, p. 5–8, doi:[10.1127/0941-2948/2007/0185](https://doi.org/10.1127/0941-2948/2007/0185).
- Palarea-Albaladejo, J., Martín-Fernández, J.A., and Buccianti, A., 2014, Compositional methods for estimating elemental concentrations below the limit of detection in practice using R: *Journal of Geochemical Exploration*, v. 141, p. 71–77, doi:[10.1016/j.gexplo.2013.09.003](https://doi.org/10.1016/j.gexplo.2013.09.003).
- Parker, A., 1970, An Index of Weathering for Silicate Rocks: *Geological Magazine*, v. 107, p. 501–504, doi:[10.1017/S0016756800058581](https://doi.org/10.1017/S0016756800058581).
- Peretyazhko, T.S., Sutter, B., Morris, R.V., Agresti, D.G., Le, L., and Ming, D.W., 2016, Fe/Mg smectite formation under acidic conditions on early Mars: *Geochimica et Cosmochimica Acta*, v. 173, p. 37–49, doi:[10.1016/j.gca.2015.10.012](https://doi.org/10.1016/j.gca.2015.10.012).
- Prospero, J.M., Bullard, J.E., and Hodgkins, R., 2012, High-Latitude Dust Over the North Atlantic: Inputs from Icelandic Proglacial Dust Storms: *Science*, v. 335, p. 1078–1082, doi:[10.1126/science.1217447](https://doi.org/10.1126/science.1217447).
- Rasmussen, C., Brantley, S., Richter, D. deB., Blum, A., Dixon, J., and White, A.F., 2011, Strong climate and tectonic control on plagioclase weathering in granitic terrain: *Earth and Planetary Science Letters*, v. 301, p. 521–530, doi:[10.1016/j.epsl.2010.11.037](https://doi.org/10.1016/j.epsl.2010.11.037).
- Reiners, P.W., Ehlers, T.A., Mitchell, S.G., and Montgomery, D.R., 2003, Coupled spatial variations in precipitation and long-term erosion rates across the Washington Cascades: *Nature*, v. 426, p. 645–647, doi:[10.1038/nature02111](https://doi.org/10.1038/nature02111).

- Remeika, P., and Lindsey, L., 1992, *Geology of Anza-Borrego: Edge of Creation*: Sunbelt Publications, San Diego, CA, 218 p., <https://sunbeltpublications.com/shop/geology-of-anza-borrego/>
- Ren, X., Nie, J., Saylor, J.E., Li, H., Bush, M.A., and Horton, B.K., 2019, Provenance Control on Chemical Weathering Index of Fluvio-Lacustrine Sediments: Evidence From the Qaidam Basin, NE Tibetan Plateau: *Geochemistry, Geophysics, Geosystems*, v. 20, p. 3216–3224, doi:10.1029/2019GC008330.
- Robert, C., and Kennett, J.P., 1997, Antarctic continental weathering changes during Eocene-Oligocene cryosphere expansion: Clay mineral and oxygen isotope evidence: *Geology*, v. 25, p. 587, doi:[10.1130/0091-7613\(1997\)025<0587:ACWCDE>2.3.CO;2](https://doi.org/10.1130/0091-7613(1997)025<0587:ACWCDE>2.3.CO;2).
- Robert, C., and Kennett, J.P., 1994, Antarctic subtropical humid episode at the Paleocene-Eocene boundary: Clay-mineral evidence: *Geology*, v. 22, p. 211, doi:[10.1130/0091-7613\(1994\)022<0211:ASHEAT>2.3.CO;2](https://doi.org/10.1130/0091-7613(1994)022<0211:ASHEAT>2.3.CO;2).
- Robert, C., and Kennett, J.P., 1992, Paleocene and Eocene kaolinite distribution in the South Atlantic and Southern Ocean: Antarctic climatic and paleoceanographic implications: *Marine Geology*, v. 103, p. 99–110, doi:[10.1016/0025-3227\(92\)90010-F](https://doi.org/10.1016/0025-3227(92)90010-F).
- Rogers, C.S., Cram, C.M., Jr, M.H.P., and Tischler, M.S., 1979, Geologic map of the Yabucoa and Punta Tuna quadrangles, Puerto Rico: IMAP, doi:[10.3133/i1086](https://doi.org/10.3133/i1086).
- Root, D.B., Hacker, B.R., Gans, P.B., Ducea, M.N., Eide, E.A., and Mosenfelder, J.L., 2005, Discrete ultrahigh-pressure domains in the Western Gneiss Region, Norway: implications for formation and exhumation: *Journal of Metamorphic Geology*, v. 23, p. 45–61, doi:[10.1111/j.1525-1314.2005.00561.x](https://doi.org/10.1111/j.1525-1314.2005.00561.x).
- Rye, N., Nesje, A., Lien, R., Blikra, L.H., Eiken, O., Hole, P.A., and Torsnes, I., 1997, Glacial geology and deglaciation chronology of the area between inner Nordfjord and Jostedalsbreen Strynefjellet, western Norway: *NORSK GEOLOGISK TIDSSKRIFT*, p. 13.
- Siame, L.L., Sébrier, M., Bellier, O., and Bourles, D., 2006, Can cosmic ray exposure dating reveal the normal faulting activity of the Cordillera Blanca Fault, Peru? *Revista de la Asociación Geológica Argentina*, v. 61, p. 536–544.
- Siebach, K.L., Baker, M.B., Grotzinger, J.P., McLennan, S.M., Gellert, R., Thompson, L.M., and Hurowitz, J.A., 2017, Sorting out compositional trends in sedimentary rocks of the Bradbury group (Aeolis Palus), Gale crater, Mars: *Journal of Geophysical Research: Planets*, v. 122, p. 295–328, doi:[10.1002/2016JE005195](https://doi.org/10.1002/2016JE005195).
- Sigmundsson, F. et al., 2010, Intrusion triggering of the 2010 Eyjafjallajökull explosive eruption: *Nature*, v. 468, p. 426–430, doi:[10.1038/nature09558](https://doi.org/10.1038/nature09558).
- Smith, G.O., 1903, *DESCRIPTION OF THE MOUNT STUART QUADRANGLE.*: USGS, <https://pubs.usgs.gov/gf/106/text.pdf>.
- Soreghan, G.S., Joo, Y.J., Elwood Madden, M.E., and Van Deventer, S.C., 2016, Silt production as a function of climate and lithology under simulated comminution: *Quaternary International*, v. 399, p. 218–227, doi:[10.1016/j.quaint.2015.05.010](https://doi.org/10.1016/j.quaint.2015.05.010).

- Soreghan, M.J., and Soreghan, G.S. (Lynn), 2007, Whole-rock geochemistry of upper Paleozoic loessite, western Pangaea: Implications for paleo-atmospheric circulation: *Earth and Planetary Science Letters*, v. 255, p. 117–132, doi:[10.1016/j.epsl.2006.12.010](https://doi.org/10.1016/j.epsl.2006.12.010).
- Stumpf, A.R., Elwood Madden, M.E., Soreghan, G.S., Hall, B.L., Keiser, L.J., and Marra, K.R., 2012, Glacier meltwater stream chemistry in Wright and Taylor Valleys, Antarctica: Significant roles of drift, dust and biological processes in chemical weathering in a polar climate: *Chemical Geology*, v. 322–323, p. 79–90, doi:[10.1016/j.chemgeo.2012.06.009](https://doi.org/10.1016/j.chemgeo.2012.06.009).
- Templ, M., Filzmoser, P., and Hron, K., 2011, Analysis of Compositional Data using Robust Methods. The R-package robCompositons: *Computational Statistics & Data Analysis*, v. 54, p. 3095–3107, doi:[10.1016/j.csda.2009.11.023](https://doi.org/10.1016/j.csda.2009.11.023).
- Thiry, M., 2000, Palaeoclimatic interpretation of clay minerals in marine deposits: an outlook from the continental origin: *Earth-Science Reviews*, v. 49, p. 201–221, doi:[10.1016/S0012-8252\(99\)00054-9](https://doi.org/10.1016/S0012-8252(99)00054-9).
- Ugolini, F.C., 1967, Soils of Mount Erebus, Antarctica: *New Zealand Journal of Geology and Geophysics*, v. 10, p. 431–442, doi:[10.1080/00288306.1967.10426747](https://doi.org/10.1080/00288306.1967.10426747).
- Velbel, M.A., 1993, Temperature dependence of silicate weathering in nature: How strong a negative feedback on long-term accumulation of atmospheric CO₂ and global greenhouse warming? *Geology*, v. 21, p. 1059–1062, doi:[10.1130/0091-7613\(1993\)021<1059:TDOSWI>2.3.CO;2](https://doi.org/10.1130/0091-7613(1993)021<1059:TDOSWI>2.3.CO;2).
- Vuille, M., Francou, B., Wagnon, P., Juen, I., Kaser, G., Mark, B.G., and Bradley, R.S., 2008, Climate change and tropical Andean glaciers: Past, present and future: *Earth-Science Reviews*, v. 89, p. 79–96, doi:[10.1016/j.earscirev.2008.04.002](https://doi.org/10.1016/j.earscirev.2008.04.002).
- Webb, N., Regmi, N., Soreghan, G., Madden, A., Sylvester, J., Colon, F., Demirel-Floyd, C., and Elwood Madden, M., 2022, Effects of Mass Wasting on the Physiochemical Properties of Fluvial Sediments in Puerto Rico Following Hurricane Maria: *Journal of Geophysical Research: Earth Surface*, v. 127, doi:[10.1029/2021JF006509](https://doi.org/10.1029/2021JF006509).
- Weidong, L., Baret, F., Xingfa, G., Qingxi, T., Lanfen, Z., and Bing, Z., 2002, Relating soil surface moisture to reflectance: *Remote Sensing of Environment*, v. 81, p. 238–246, doi:[10.1016/S0034-4257\(01\)00347-9](https://doi.org/10.1016/S0034-4257(01)00347-9).
- White, A.F., and Blum, A.E., 1995, Effects of climate on chemical weathering in watersheds: *Geochimica et Cosmochimica Acta*, v. 59, p. 1729–1747, doi:[10.1016/0016-7037\(95\)00078-E](https://doi.org/10.1016/0016-7037(95)00078-E).
- White, A.F., Blum, A.E., Schulz, M.S., Vivit, D.V., Stonestrom, D.A., Larsen, M., Murphy, S.F., and Eberl, D., 1998, Chemical Weathering in a Tropical Watershed, Luquillo Mountains, Puerto Rico: I. Long-Term Versus Short-Term Weathering Fluxes: *Geochimica et Cosmochimica Acta*, v. 62, p. 209–226, doi:[10.1016/S0016-7037\(97\)00335-9](https://doi.org/10.1016/S0016-7037(97)00335-9).
- White, A.F., Blum, A.E., Bullen, T.D., Vivit, D.V., Schulz, M., and Fitzpatrick, J., 1999, The effect of temperature on experimental and natural chemical weathering rates of granitoid rocks: *Geochimica et Cosmochimica Acta*, v. 63, p. 3277–3291, doi:[10.1016/S0016-7037\(99\)00250-1](https://doi.org/10.1016/S0016-7037(99)00250-1).

- White, A.F., Blum, A.E., Schulz, M.S., Bullen, T.D., Harden, J.W., and Peterson, M.L., 1996, Chemical weathering rates of a soil chronosequence on granitic alluvium: I. Quantification of mineralogical and surface area changes and calculation of primary silicate reaction rates: *Geochimica et Cosmochimica Acta*, v. 60, p. 2533–2550, doi:[10.1016/0016-7037\(96\)00106-8](https://doi.org/10.1016/0016-7037(96)00106-8).
- White, A.F., and Brantley, S.L., 2003, The effect of time on the weathering of silicate minerals: why do weathering rates differ in the laboratory and field? *Chemical Geology*, p. 28.
- White, A.F., and Buss, H.L., 2014, 7.4 - Natural Weathering Rates of Silicate Minerals, *in* Holland, H.D. and Turekian, K.K. eds., *Treatise on Geochemistry (Second Edition)*, Oxford, Elsevier, p. 115–155, doi:[10.1016/B978-0-08-095975-7.00504-0](https://doi.org/10.1016/B978-0-08-095975-7.00504-0).
- White, A.F., and Peterson, M.L., 1990, Role of Reactive-Surface-Area Characterization in Geochemical Kinetic Models, *in* *Chemical Modeling of Aqueous Systems II*, American Chemical Society, ACS Symposium Series 416, v. 416, p. 461–475, doi:[10.1021/bk-1990-0416.ch035](https://doi.org/10.1021/bk-1990-0416.ch035).
- Wilson, J.J., Reyes Rivera, L., and Garayar S., J., 1995, - Geología de los cuadrángulos de Pallasca, Tayabamba, Corongo, Pomabamba, Carhuaz y Huari. Hojas: 17-h, 17-i, 18-h, 18-i, 19-h, y 19-i – [Boletín A 60]: Instituto Geológico, Minero y Metalúrgico - INGEMMET, <https://repositorio.ingemmet.gob.pe/handle/20.500.12544/182> (accessed July 2022).
- Wise, W.S., 2005, MINERALS | Zeolites, *in* Selley, R.C., Cocks, L.R.M., and Plimer, I.R. eds., *Encyclopedia of Geology*, Oxford, Elsevier, p. 591–600, doi:10.1016/B0-12-369396-9/00270-7.
- Xiao, S., Liu, W., Li, A., Yang, S., and Lai, Z., 2010, Pervasive autocorrelation of the chemical index of alteration in sedimentary profiles and its palaeoenvironmental implications: *Sedimentology*, v. 57, p. 670–676, doi:10.1111/j.1365-3091.2009.01113.x.
- Yang, J., Cawood, P.A., Du, Y., Li, W., and Yan, J., 2016, Reconstructing Early Permian tropical climates from chemical weathering indices: *GSA Bulletin*, v. 128, p. 739–751, doi:[10.1130/B31371.1](https://doi.org/10.1130/B31371.1).

TABLES

Table 1.1. Summary of the field site characteristics. Climate classes are according to Köppen-Geiger climate classification (Geiger and Pohl, 1953; Beck et al., 2018).

Field Area	Latitude	Longitude	Bedrock	Climate	MAT (°C)	MAP (mm/yr)
<u>Glacial</u>						
MDV, Antarctica	-77.24	162.48	Granite, granodiorite, hornblende-biotite orthogenesis	Polar-Ice cap	-18	100
Cordillera Blanca, Peru	-9.01	-77.69	Granodiorite, tonalite	Cold-Semiarid	8	588
Jostedalbreen, Norway	61.59	6.99	Quartz monzonite, granitic gneiss, granodiorite	Subpolar oceanic	4.5	1769
Eyjafjallajökull, Iceland	63.67	-19.63	Basalt	Polar-Tundra	3	1000
Mt. Stuart, Washington	47.49	-120.9	Granite, granodiorite	Subpolar oceanic	8	1270
<u>Non-glacial</u>						
SE Puerto Rico	18.07	-65.93	Granodiorite, metavolcanics, diorite	Tropical rainforest	22	4200
Anza Borrego, California	32.88	-116.21	Tonalite	Hot desert	23	150

Table 1.2. CIA (Nesbitt and Young, 1982), Chemical Index of Weathering (CIW; Harnois, 1988), Plagioclase Index of Alteration (PIA; Fedo et al., 1995), and Weathering Index of Parker (WIP; Parker, 1970) calculations for fluvial muds and bedrock and bedrock normalized values, on average, for each field site. Note that CaO values are corrected for apatite (Equation 1.1) following Girty et al. (2013). Standard deviations for muds are given in parathesis.

Field Area	Sample	CIA	CIW	PIA	WIP
Antarctica	Fluvial mud	48.6 (4.0)	52.9 (5.1)	48.5 (4.6)	72.4 (2.1)
	Bedrock	47.9	54.7	47.8	76.6
	Mud/Bedrock	1.01	0.97	1.01	0.95
Peru	Fluvial mud	55.7 (2.5)	64.1 (3.2)	57.7 (3.4)	71.9 (5.7)
	Bedrock	51.0	59.7	51.4	79.4
	Mud/Bedrock	1.09	1.07	1.12	0.91
Washington	Fluvial mud	52.1 (1.8)	55.1 (2.3)	52.4 (2.1)	65.7 (0.3)
	Bedrock	50.4	54.3	50.4	74.4
	Mud/Bedrock	1.03	1.01	1.04	0.88
Norway	Fluvial mud	53.2 (0.5)	61.6 (1.4)	54.5 (0.8)	74.9 (3.0)
	Bedrock	51.2	53.5	51.4	77.2
	Mud/Bedrock	1.04	1.15	1.06	0.97
Iceland	Fluvial mud	46.4 (0.2)	48.3 (0.0)	46.1 (0.2)	71.4 (1.1)
	Bedrock	42.2	43.2	41.9	76.3
	Mud/Bedrock	1.1	1.12	1.1	0.94
Puerto Rico	Fluvial mud	66.2 (14.3)	68.6 (14.7)	67.6 (14.6)	45.7 (10.7)
	Bedrock	43.9	45.3	43.6	70.3
	Mud/Bedrock	1.51	1.51	1.55	0.65
Anza Borrego	Fluvial mud	60.6 (1.7)	65.9 (2.5)	62.7 (2.3)	63.3 (1.8)
	Bedrock	51.9	55.4	52.2	61.6
	Mud/Bedrock	1.17	1.19	1.2	1.03

FIGURES

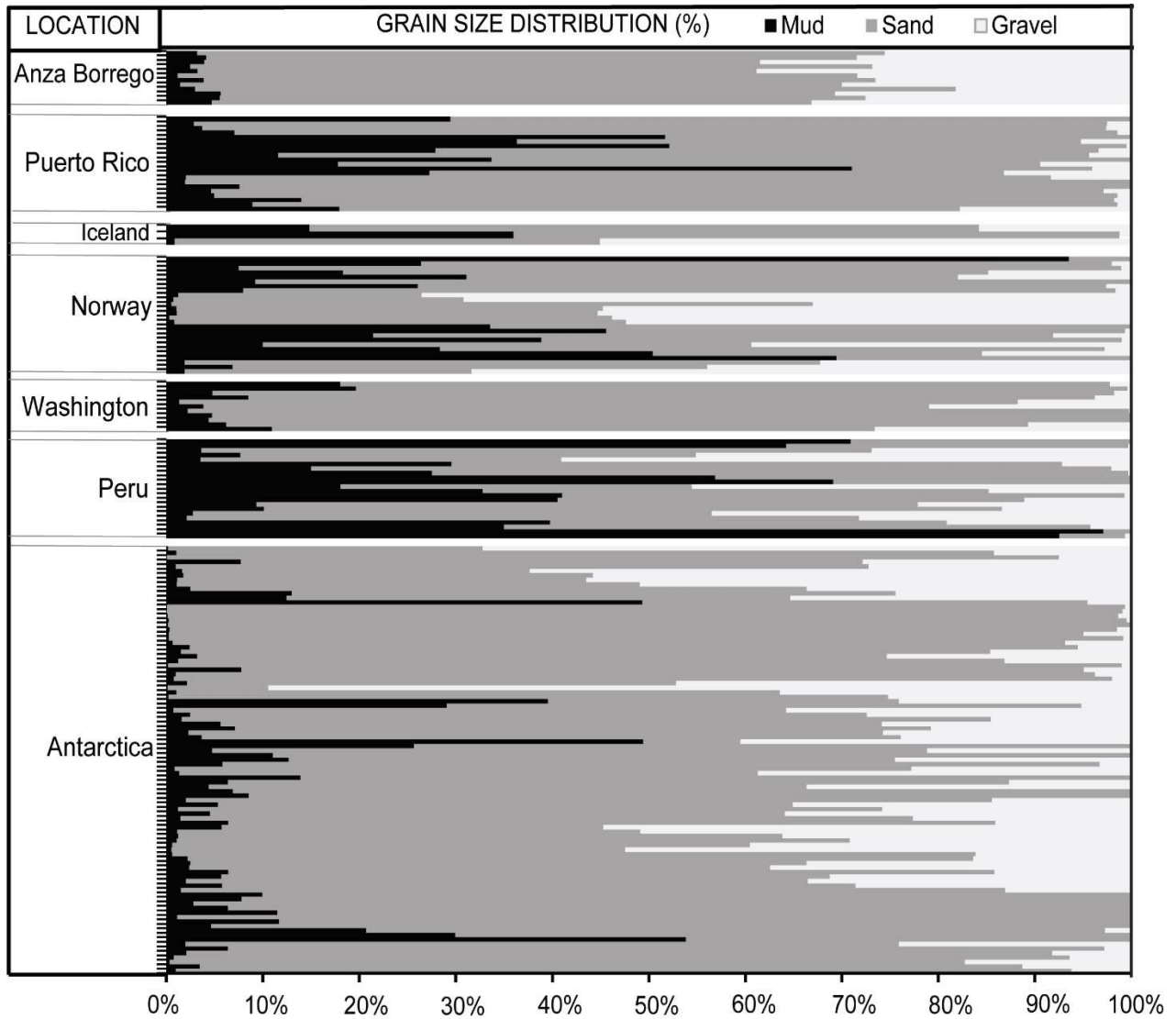


Figure 1.1. All granulometric data represented in stacked area chart, showing % mud (<63 μm , black), % sand (>63 μm - < 2mm, dark grey) and % gravel (>2 mm, light grey) grain size distribution within the bulk fraction of the samples. Antarctica sediments, except for a few glacial drifts, have the coarsest grain size within the bulk fractions. Y-axis shows individual samples from indicated locations.

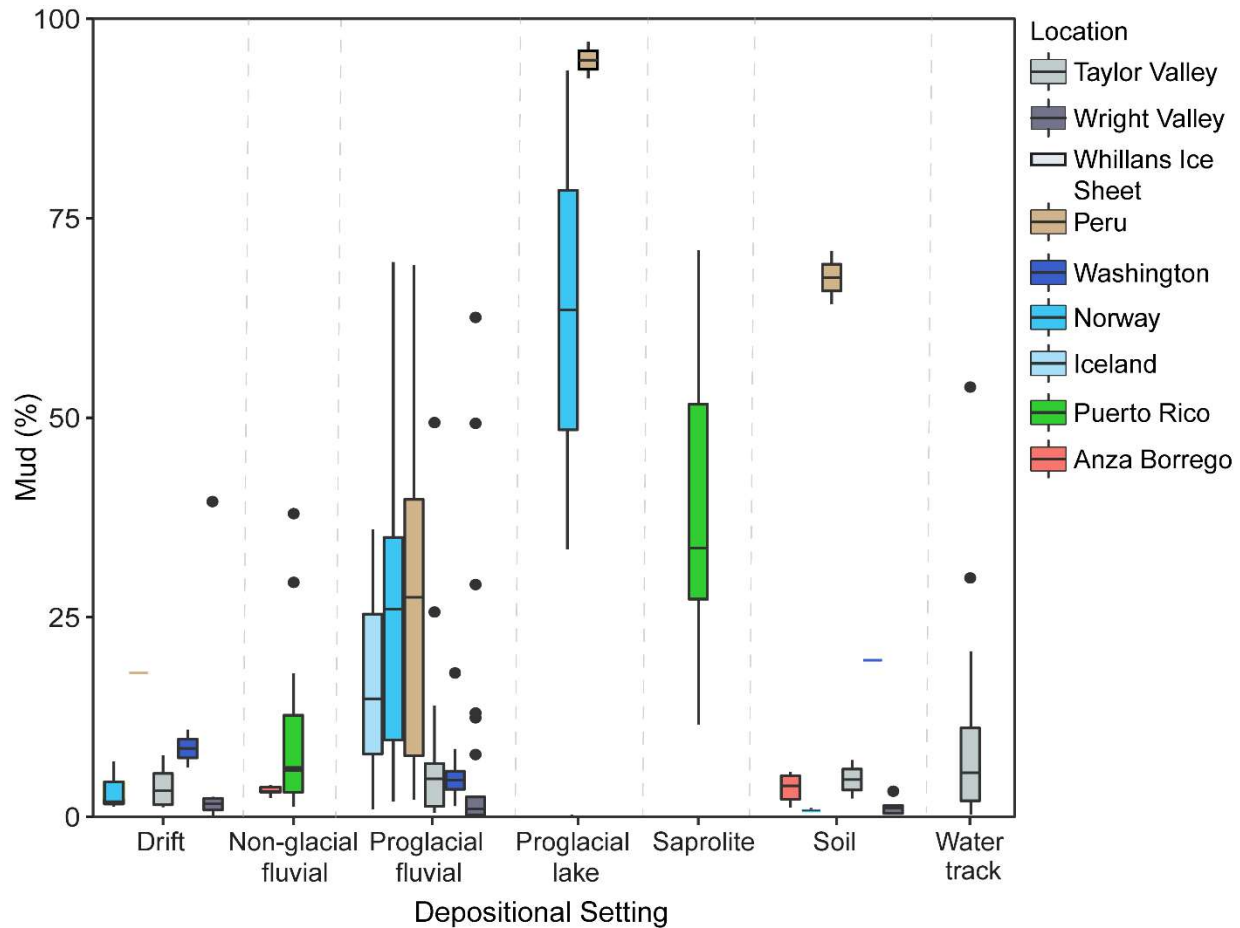


Figure 1.2. Boxplots showing the % distribution of mud sized (<63 μm) sediments within depositional settings at each field site, based on granulometry analysis of bulk fractions. There are no discernable trends of mud amount with climate (based on Table 1.1). Overall, proglacial lakes, saprolites, and Peruvian soils are the depositional environments with high amounts of mud-sized grains, followed by proglacial fluvial sediments, showing depositional setting is the overriding factor, masking any climatic trends.

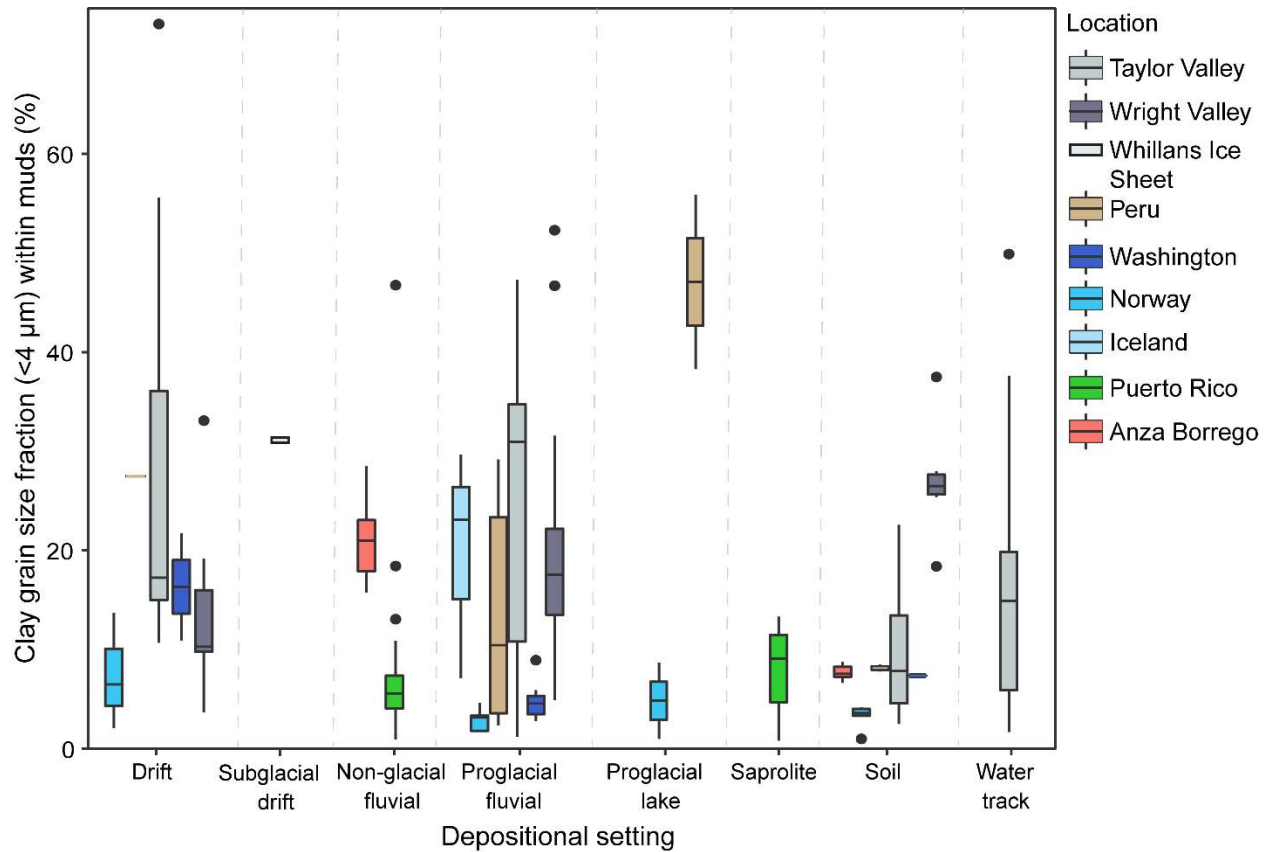


Figure 1.3. Boxplots showing the % distribution of clay-sized (<4 μm) grains within depositional settings at each field site, based on LPSA analysis of mud fractions. Overall, Peruvian proglacial lakes, Wright Valley soils and all Taylor Valley depositional environments are the settings with high amounts of clay-sized grains. Within fluvial setting, muds from Antarctica have higher concentrations of clay-sized particles (<4 μm) on average (22.1%), followed by Anza Borrego (21.5%), Iceland (20.0%), Peru (13.4%), Puerto Rico (8.6%), Washington (4.9%) and Norway (2.7%).

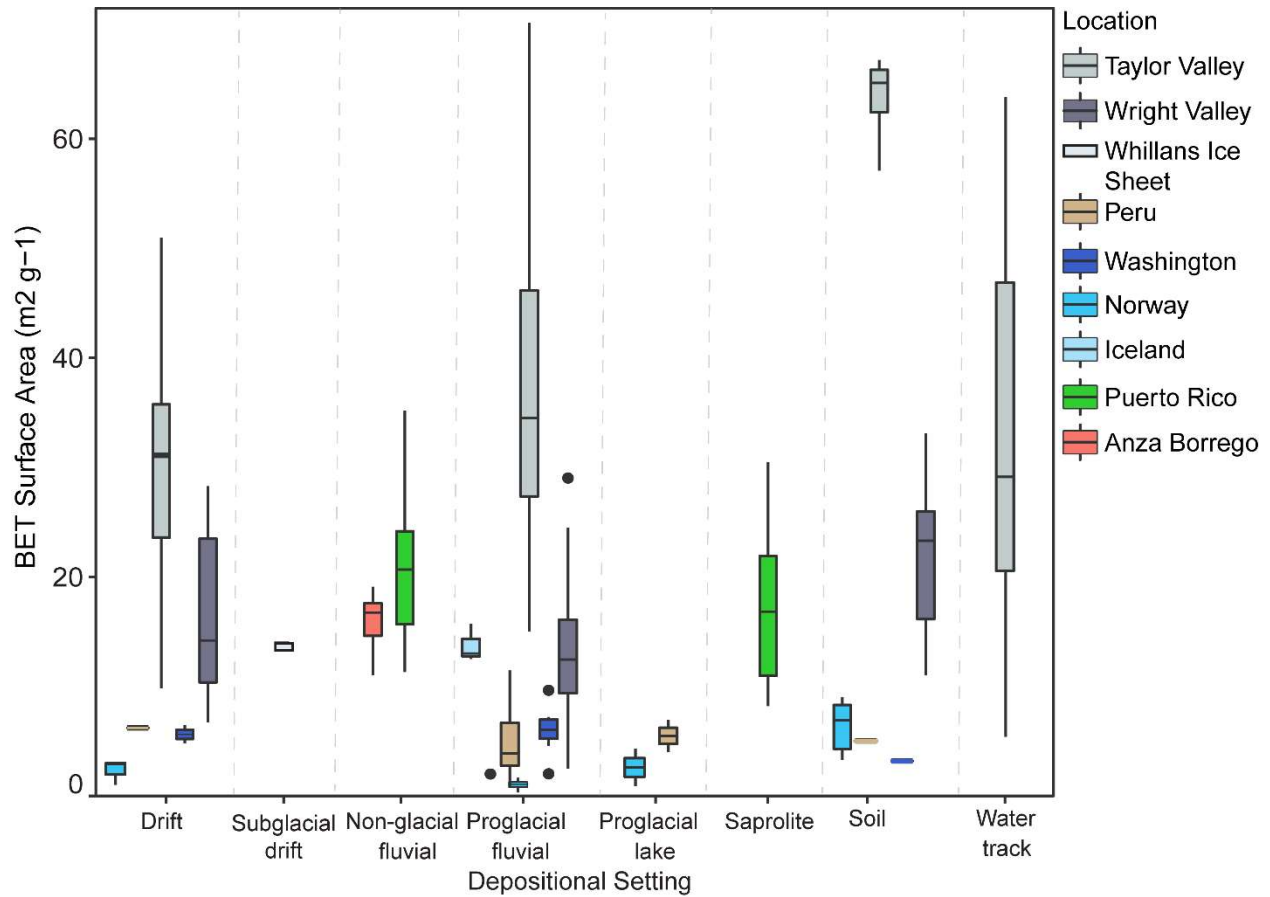


Figure 1.4. Boxplots showing the distribution of grain surface area ($\text{m}^2 \text{g}^{-1}$, measured by BET) of muds within depositional settings at each field site. The surface area of Antarctic Taylor Valley muds significantly exceeds other field sites within all depositional settings, where data is available. There are no discernable trends of mud surface area with climate.

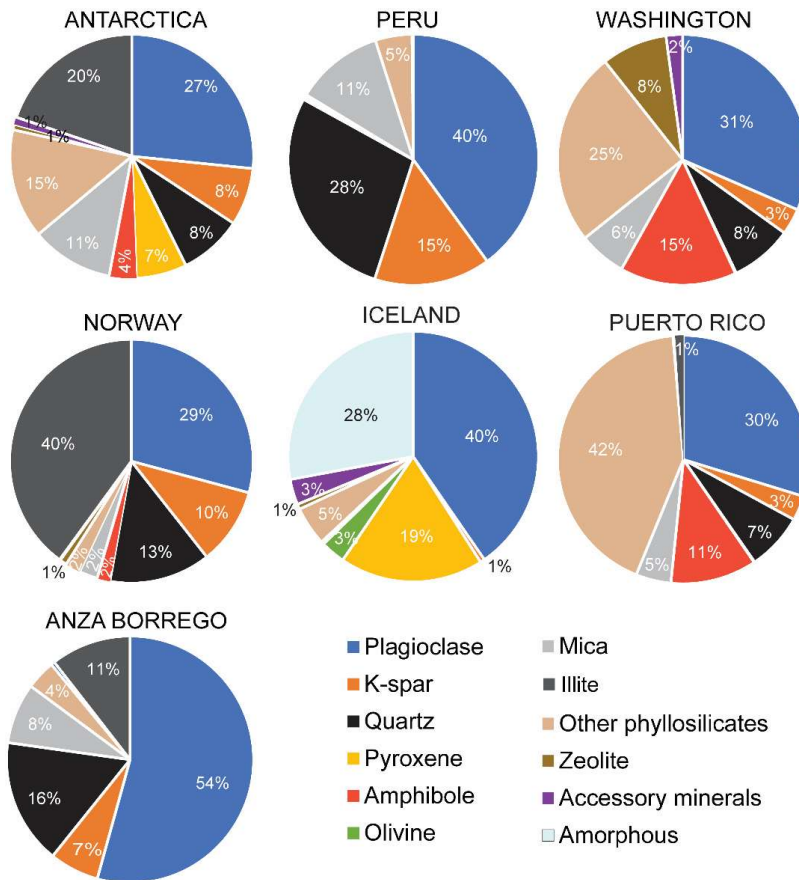


Figure 1.5. Pie charts illustrating the representative quantitative mineralogical compositions of muds from each field site, based on averaged values. Despite choosing field sites with similar underlying bedrock (except for Iceland), mineralogical composition of the muds varied significantly between field sites. Note that we are defining illite as the mineral specimen that has a d-spacing value of 10Å. Mechanical grinding of muscovite, which is especially pronounced in glacial sites via glacial grinding, also produces a 10Å d-spacing value. Therefore, amounts of illite illustrated in Figure 1.5 might be artifacts of mechanical grinding, which especially pronounced in Norway mineralogy, as well as being secondary products of biotite weathering.

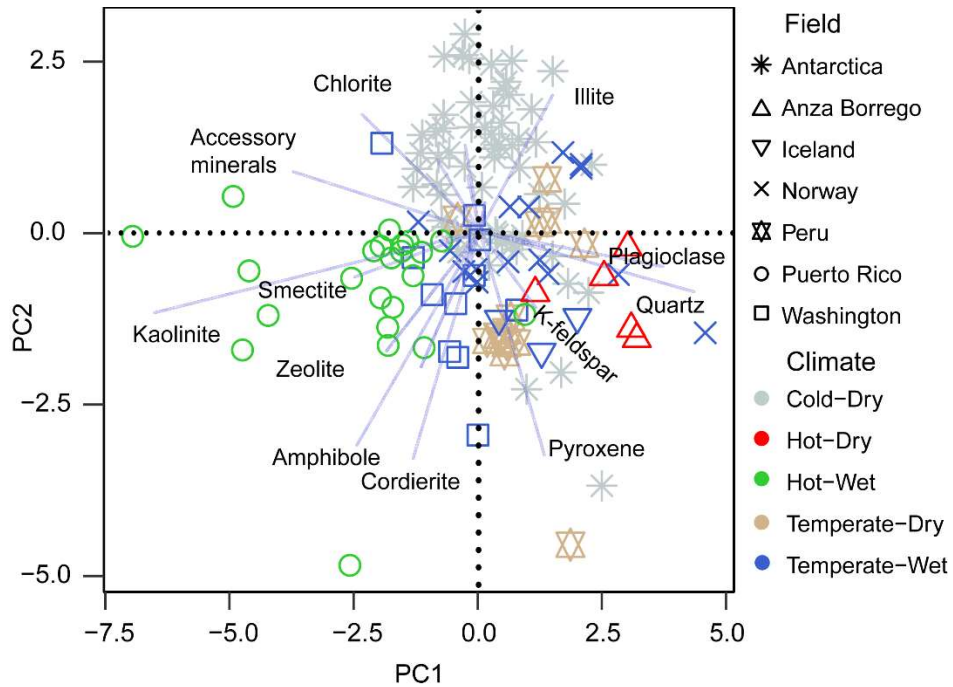


Figure 1.6. Principal Component Analysis (PCA) of the quantitative mineralogy of the muds from all field sites, colored with regards to climate regime. Vectors represent loadings (variables) in PCA, and their magnitudes represent their relative significance in terms of the differences observed in mineralogy (i.e., higher magnitudes are more significant). Vectors pointing towards particular data points or within the same quadrant, indicate that those data points significantly control the differences in concentration represented by the loading vectors. Note that we only labeled the significant vectors for clarity of illustration. The signs of the principal components (PC) are not representative of physical differences in the sample but are simply an artifact of the PCA analysis process.

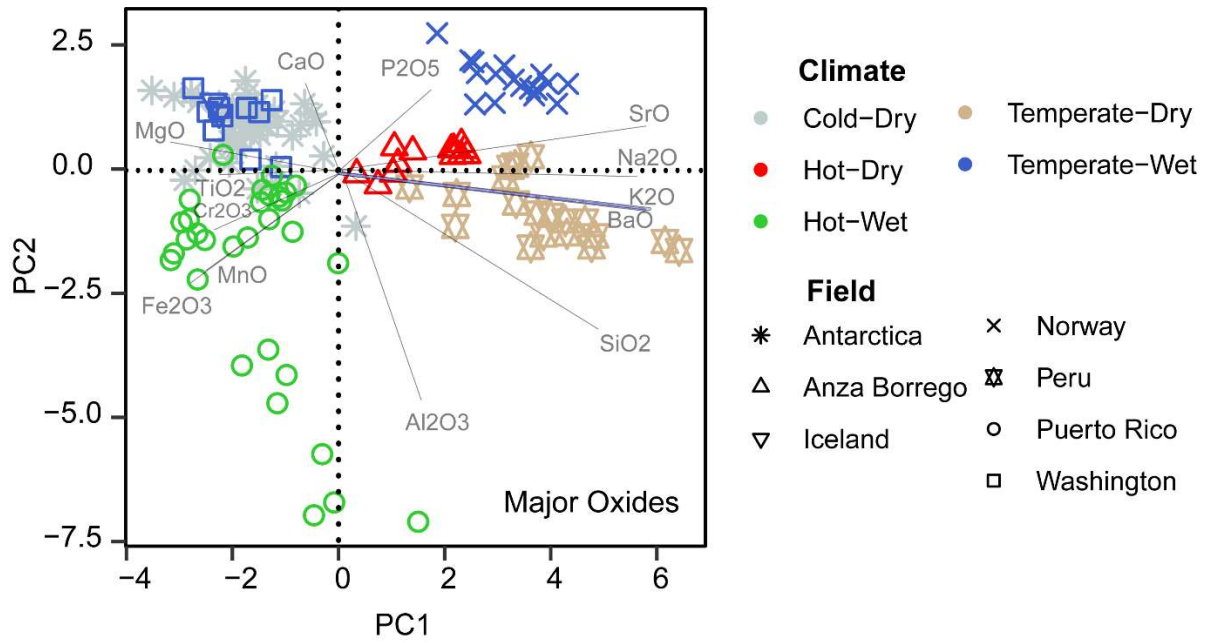


Figure 1.7. PCA of the major oxide chemistry of the muds from all field sites, colored based on climate regime. Note that we only included loading vectors to major oxides, as major oxide chemistry is the focus of the discussions.

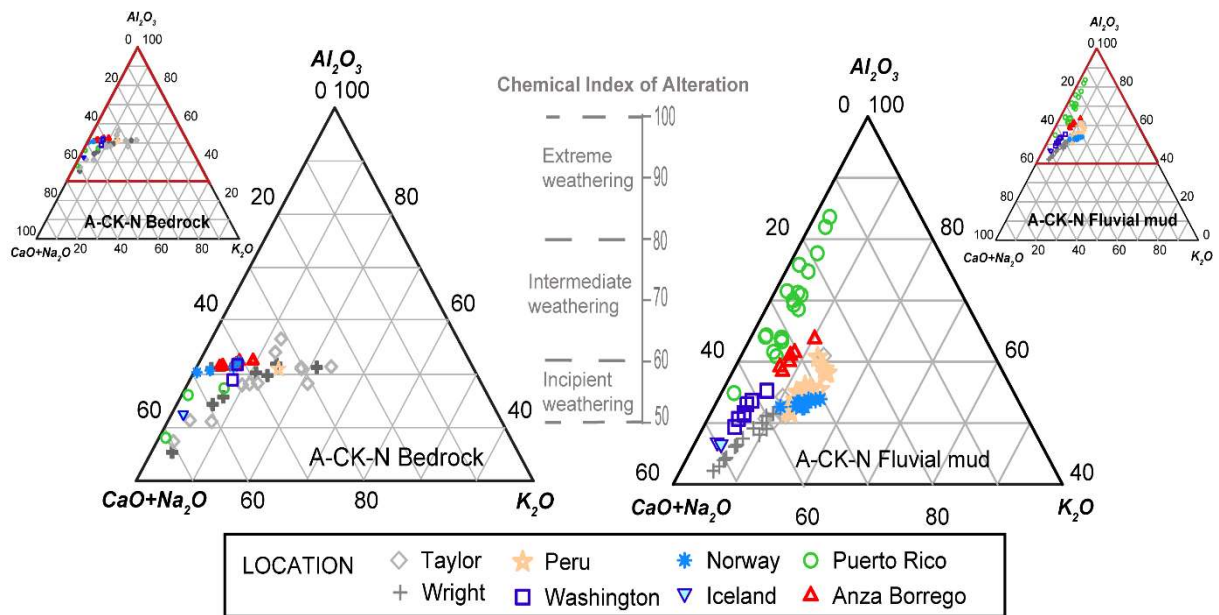


Figure 1.8. A-CK-N ternary plots of the bedrock (left) and fluvial muds (right) from all field sites. We are focusing on the red triangles on the smaller ternary plots for scaling. Location of the bedrock data points are indicative of fresh bedrock, except for a few Antarctic Taylor Valley samples. Geochemical data collected from almost all locations show incipient to intermediate chemical weathering, while Puerto Rico muds show a trend ranging from incipient to extreme weathering. Except for Puerto Rico muds, there are no discernable weathering trends between climatic regimes, as the muds ranging from cold to hot climates cluster together in the same region of the diagram.

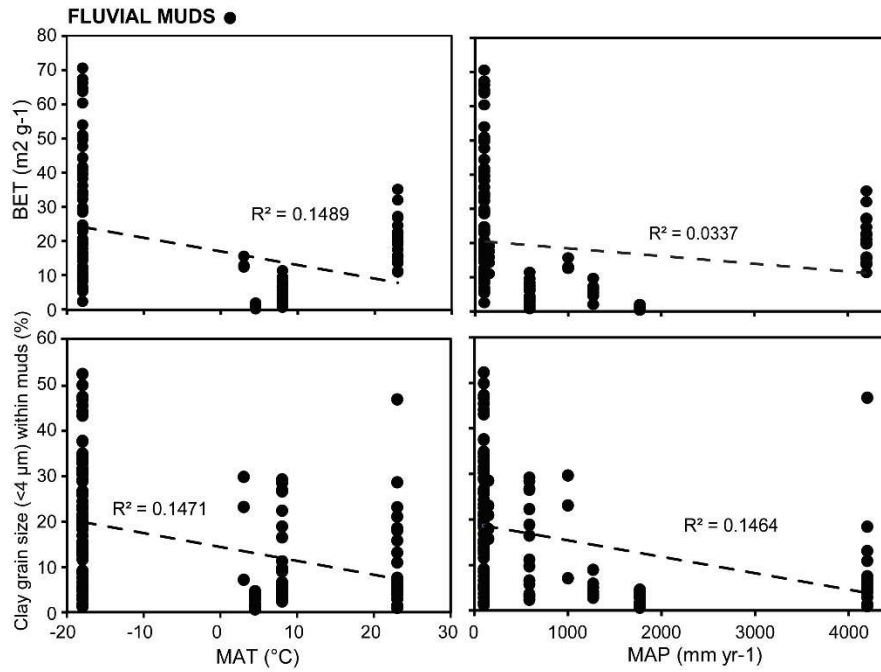


Figure 1.9. Correlation of BET surface area and clay grain size fraction within muds with mean annual temperature (MAT) and mean annual precipitation (MAP), based on fluvial samples. R^2 values suggest that there are no strong correlations between these variables.

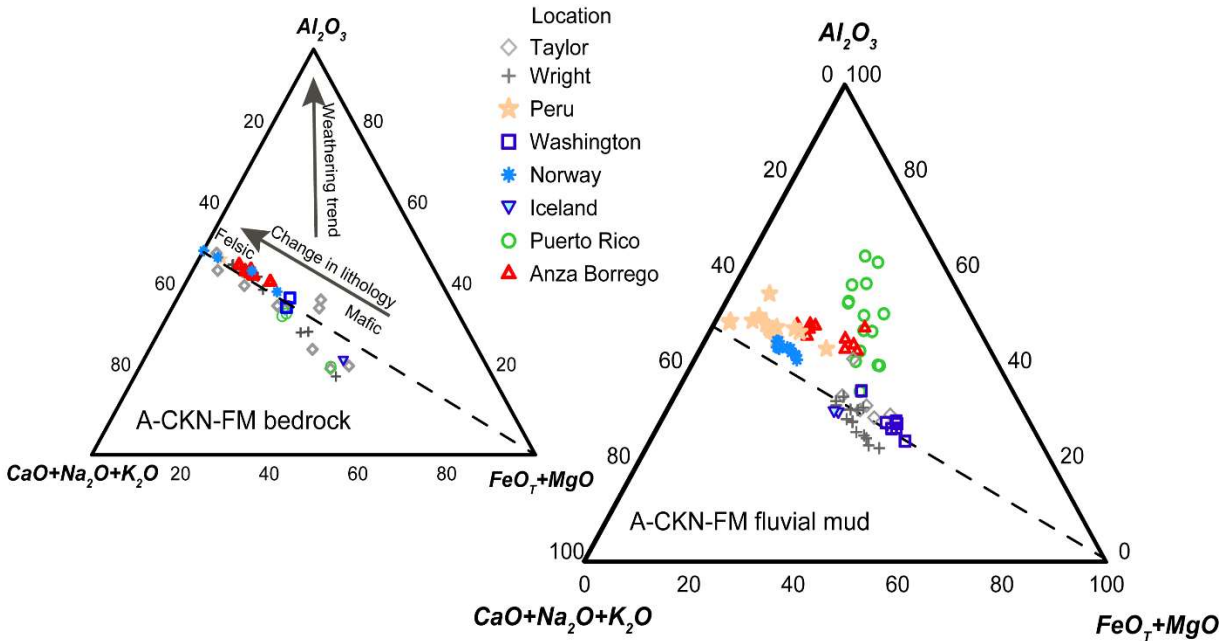


Figure 1.10. A-CKN-FM ternary plots of the bedrock (left) and fluvial muds (right) from all field sites. Variations along the dashed line indicate differences in lithology, changing from mafic to felsic in the arrow direction on the bedrock plot. Lithology is also variable within the fluvial muds, showing that Peru, Norway and majority of the Anza Borrego muds are felsic, while a few Anza Borrego and Peru muds show intermediate composition. Antarctica and Washington and some Puerto Rico data points show intermediate-mafic composition, plotting close with Iceland muds. Puerto Rico muds, as well as a few Antarctica, Peru and Norway muds show weathering trends, approaching the A apex.

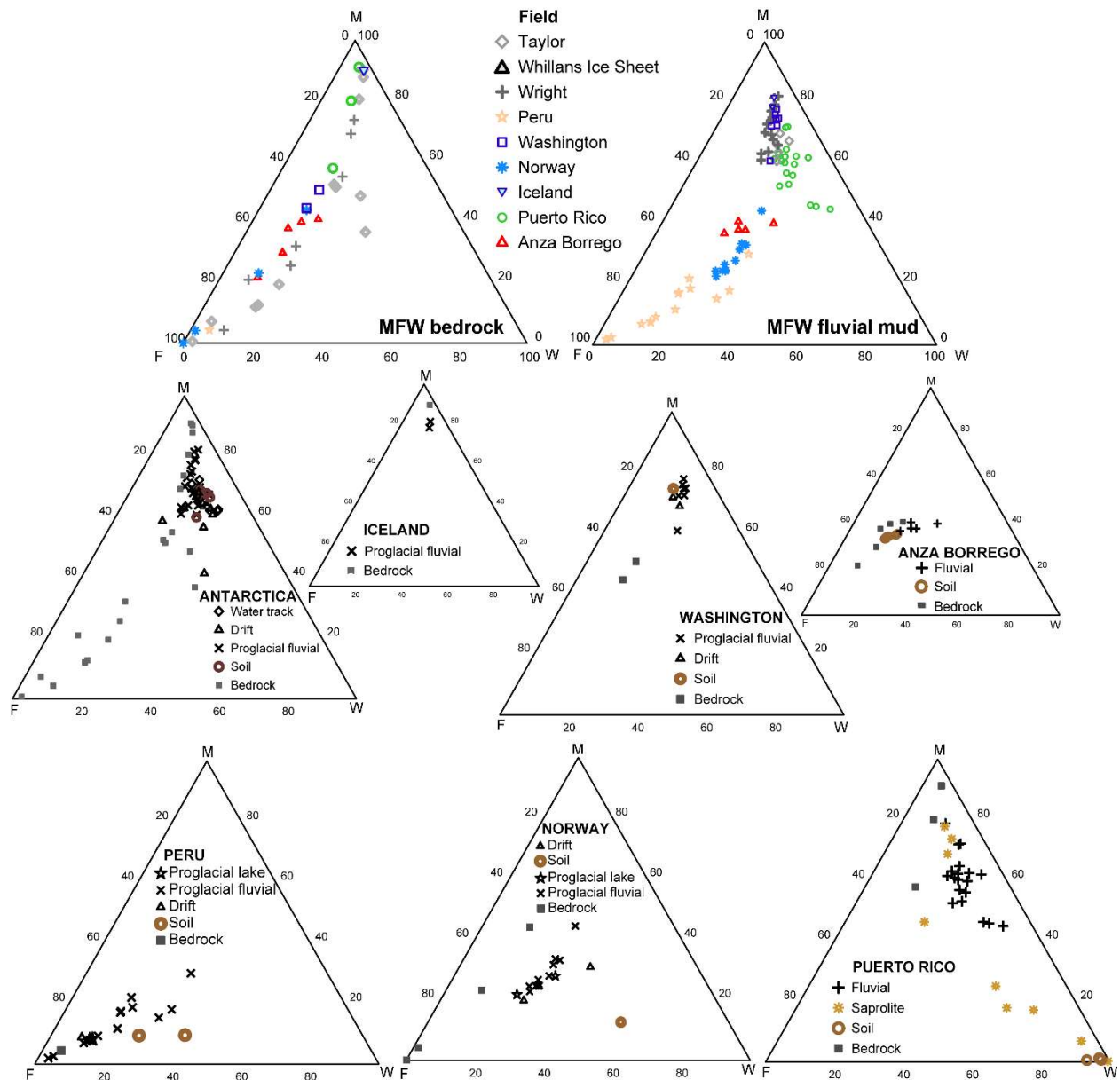


Figure 1.11. MFW ternary plots of the bedrock and fluvial muds from all field sites (top two plots). We additionally plotted MFW for individual field sites, illustrating various depositional settings of muds with different shapes (bottom). Individual investigations of depositional settings within each field site showed soil and saprolite samples tend to show weathering trends except in Washington and Anza Borrego where soil samples plot as less weathered than fluvial samples. The most obvious weathering trend is observed in Puerto Rico, in agreement with A-CK-N and

A-CKN-FM plots. We additionally noted felsic bedrock plotted as mafic in Antarctica and Puerto Rico, suggesting limitations for both provenance and weathering interpretations.

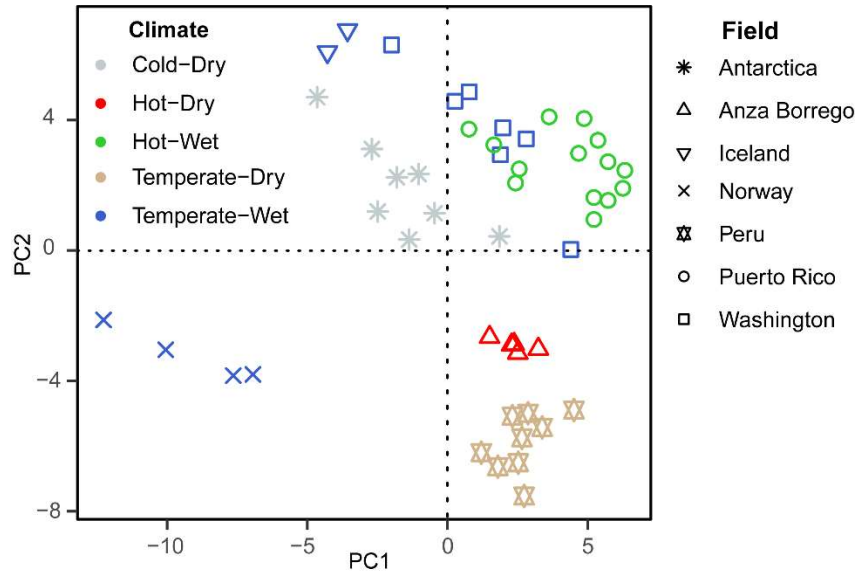


Figure 1.12. PCA of all variables (mineralogy, grain size- % clay <4 μm , surface area, geochemistry). The signs of the principal components (PC) are not representative of physical differences in the sample but are simply an artifact of the PCA analysis process. Data points are colored with respect to climate regime. Overall, no significant trends were observed with climate. Instead, the data clustered with respect to provenance.

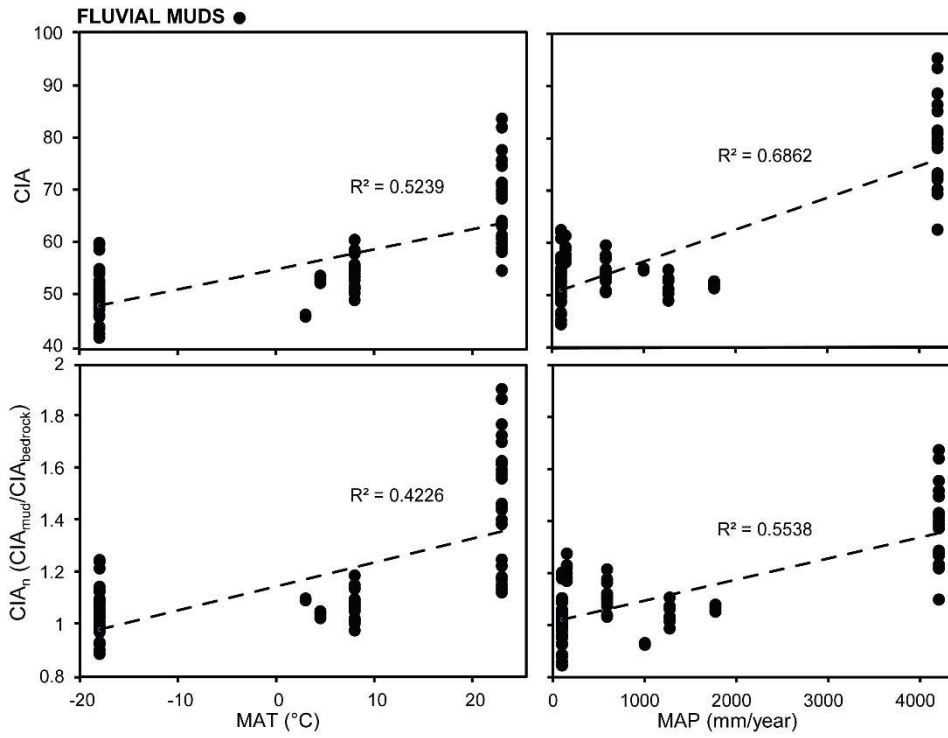


Figure 1.13. Correlations between Chemical Index of Alteration (CIA) and bedrock normalized CIA values (CIA_n), and climatic parameters (MAP and MAT) based on fluvial samples of all field sites. CIA_n corrections reduced the correlation between CIA and climatic parameters, suggesting provenance was leading to overestimated correlations between climate and weathering.

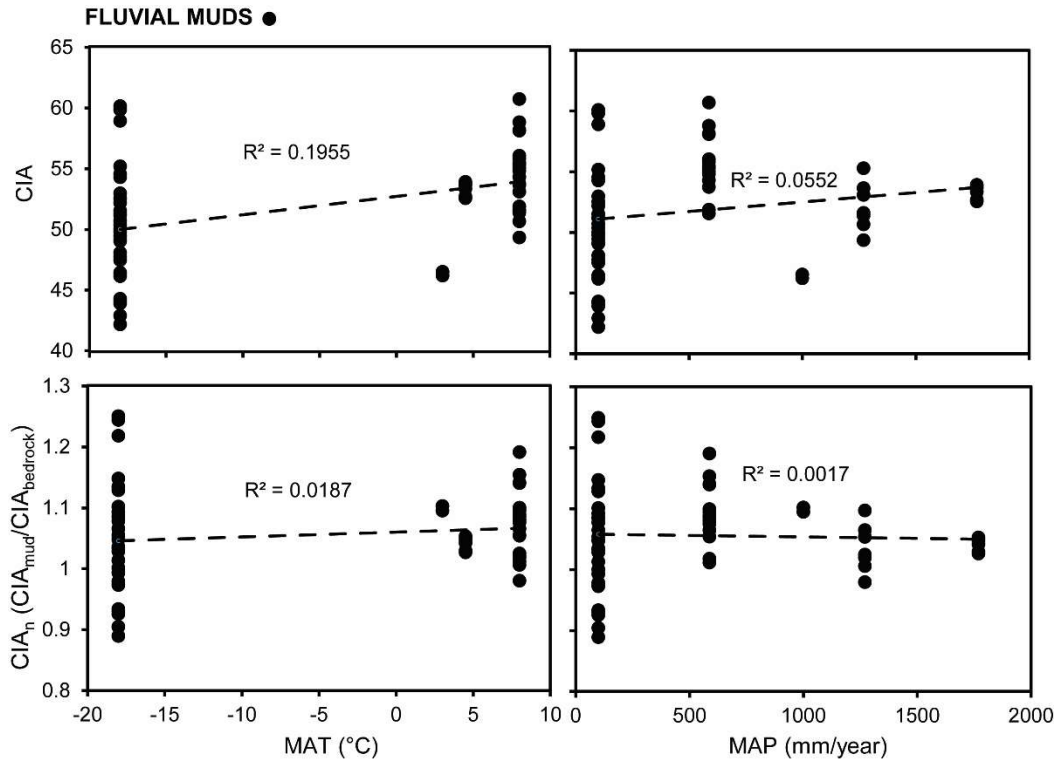


Figure 1.14. Correlations between Chemical Index of Alteration (CIA) and bedrock normalized CIA values (CIA_n), and climatic parameters (MAP and MAT) based on proglacial fluvial muds. These plots illustrate that there are no significant correlations between CIA and climate parameters within the glacial environments (Puerto Rico and Anza Borrego are removed).

Chapter 2. Cyanobacterial weathering in warming periglacial sediments: Implications for nutrient cycling and potential biosignatures

Cansu Demirel-Floyd¹, Gerilyn S. Soreghan¹, Megan E. Elwood Madden¹

¹School of Geosciences, University of Oklahoma, Norman, OK 73019, USA

Key Words: Antarctic Dry Valleys, Biosignature, Cyanobacteria, Glacial, Mars, Silicate
Weathering

Copyright Statement:

*This chapter is derived from an article published in *Permafrost and Periglacial Processes*, 2022, copyright John Wiley & Sons, Inc., available online: doi.org/10.1002/ppp.2133*

Citation:

*Demirel-Floyd, C., Soreghan, G.S., and Madden, M.E.E., 2022, Cyanobacterial weathering in warming periglacial sediments: Implications for nutrient cycling and potential biosignatures: *Permafrost and Periglacial Processes*, v. 33, p. 63–77, doi:[10.1002/ppp.2133](https://doi.org/10.1002/ppp.2133).*

Abstract

The cryosphere hosts a widespread microbial community, yet microbial influences on silicate weathering have been historically neglected in cold-arid deserts. Here we investigate bio weathering by a cold-tolerant cyanobacteria (*Leptolyngbya glacialis*) via laboratory experiments using glaciofluvial drift sediments at 12°C, analogous to predicted future permafrost surface temperatures. Our results show threefold enhanced Si weathering rates in pre-weathered, mixed-lithology Antarctic biotic reactors compared to abiotic controls, indicating the significant influence of microbial life on weathering. Although biotic and abiotic weathering rates are similar in Icelandic sediments, neo-formed clay and Fe-(oxy)hydroxide minerals observed in association with biofilms in biotic reactors are common on Icelandic mafic minerals, similar to features observed in unprocessed Antarctic drifts. This suggests that microbes enhance weathering in systems where they must scavenge for nutrients that are not easily liberated via abiotic pathways; potential biosignatures may form in nutrient-rich systems as well. In both sediment types we also observed up to fourfold higher bicarbonate concentrations in biotic reactors relative to abiotic reactors, indicating that, as warming occurs, psychrotolerant biota will enhance bicarbonate flux to the oceans, thus stimulating carbonate deposition and providing a negative feed-back to increasing atmospheric CO₂.

INTRODUCTION

Occupying 10% of the Earth's land surface and comprising 90% of the cryosphere, the Antarctic continent is a climatically sensitive environment that has major influences on global biogeochemical cycles (Anesio and Laybourn-Parry, 2012; Bockheim, 2015). This environment is also experiencing some of the most extreme effects of anthropogenic climate change (Bockheim, 2015; Ugolini and Bockheim, 2008). Increased mean annual temperatures of 3.4°C

over the past 50 years resulted in melting icesheets, unusual flooding events in the McMurdo Dry Valley (MDV) streams and lakes (Nielsen et al., 2012), retreat of alpine glaciers (Fountain et al., 1999), expanding hyporheic zones (Levy et al., 2011), thickening active layer (Guglielmin and Cannone, 2012; Guglielmin et al., 2014), permafrost loss (Bockheim et al., 2013), and similar changes (Bockheim, 2015). Whereas current mean annual soil temperatures range between 15°C and 40°C, surface temperatures up to +12°C are recorded in the Molodezhynaya station (Dolgikh et al., 2015) and can reach up to 20°C in the Ross Sea region during the austral summer (Balks et al., 2002). Because microbial diversity is related to soil chemistry (Aislabie et al., 2008), that is, in turn, influenced by microclimatic conditions (Campbell and Claridge, 2006), dynamically changing permafrost conditions accompanying climate change will likely cause shifts in the cryosphere's microbial population (Yergeau, 2012).

Antarctic soils record signatures of climate change as well as information on the glacial history of the MDVs (Bockheim, 2008, 2015; Cannone et al., 2008; Hall and Denton 2005). These hyper arid soils form through an interplay between cryogenic (fragmentation by glacial retreat and mechanical and chemical weathering) and microclimatic processes (precipitation, katabatic winds, and ice sublimation). However, despite the impressive microbial diversity within a range of cryospheric habitats (Anesio and Laybourn-Parry, 2012; Cary et al., 2010; Cowan et al., 2010), the role of psychrotolerant (cold-tolerant) bacteria in silicate weathering has not been deeply investigated, except in organic-rich and relatively humid soils of eastern Antarctica (Dolgikh et al., 2015).

All polar glacial settings exert extreme environmental conditions such as high ultraviolet (UV) light fluxes, extreme cold, nutrient deficiency, high salinity, and aridity (Seckback and Rampelotto, 2015). As one moves from the coastal regions to inland, the microclimatic zones

gradually become hyperarid and colder from mixed xerous in the MDVs (50–200 mm/year precipitation) to ultraxerous (0–50 mm/year precipitation) zones in high-altitude mountain ranges (Bockheim, 2015; Bockheim and McLeod, 2015), thus potentially decreasing biological diversity and curtailing microbial activity. However, polyextremophilic microbes have evolved multiple survival strategies such as pigment, exopolymeric substance (EPS), cold-adaptive enzymes, and osmo-protectant production that allow them to cope with their extreme environments (Seckback and Rampelotto, 2015; Edwards et al., 2004; Margesin and Miteva, 2011). Moreover, microbial cells can persist within ice (Karl et al., 1999; Raymond et al., 2008) and permafrost up to a few million years and may still be capable of sustaining basic metabolic activities (Bidle et al., 2007; Gilichinsky et al., 2007; Rivkina et al., 2018). Therefore, we hypothesize that as permafrost warms, microbial communities may enhance silicate weathering in polar environments, even in xerous and ultraxerous settings.

Previous studies of Antarctic ephemeral meltwater streams revealed that solute fluxes indicate active chemical weathering of drift sediments, even under kinetically limited extremely cold conditions and short periods of liquid water availability (Gooseff et al., 2002; Marra et al., 2017; Stumpf et al., 2012). Higher-than-expected nutrient concentrations of these streams also show evidence of additional microbial silicate weathering contributing to chemical weathering pathways along these streams (Lyons et al., 2015). In addition, biotically promoted weathering in arid settings of the MDV such as rock crevices and pores occur as a result of micro-acidic conditions produced within the EPS layer and mechanical weathering via EPS expansion along with lichen and filament placement (De Los Rios et al., 2014; Friedmann et al., 1988; Friedmann et al., 1987; Friedmann, 1982; Guglielmin et al., 2005; Johnston and Vestal, 1993). MDV soils also have C and N isotopic signatures, indicative of partial soil formation by microbial life within

endolithic environments (Mergelov et al., 2018). Furthermore, cyanobacteria may have formed primordial soils of early Earth, and prospective extraterrestrial soil formation processes on Mars and other bodies may also be tied to bioweathering by polyextremophiles (Rivkina et al., 2018; Mergelov et al., 2018). Traces of such biological surface alteration can be used as inorganic biosignatures, which are defined as the chemical, morphological, and mineralogical (biomineral) biproducts of microbe–mineral interactions (Demirel-Floyd et al., 2020; Hays et al., 2017).

Considering the compelling evidence of chemical and potentially biological weathering from previous studies in Antarctica (e.g., (De Los et al., 2014; Friedmann et al., 1988; Friedmann et al., 1987; Friedman, 1982; Guglielmin et al., 2005; Johnston and Vestal, 1993; Mergelov et al., 2018)) and the role of microbes in accelerating silicate weathering (e.g., Montross et al., 2013; Olsson-Francis et al., 2012; Olson-Francis et al., 2017; Welch and Ullman, 1999), we hypothesize that cyanobacterial mats in polar environments have the potential to enhance chemical weathering rates via both elevated pH in the solution and locally generated micro-acidic regions within their EPS on the grains via cell-surface attachment. Therefore, we predict that the cyanobacterial mats could cause significant changes in the aquatic chemistry and detectable mineralogical changes in sediments and/or protosoils within glaciated planetary settings. Here we report the results from comparative biotic and abiotic silicate weathering experiments at 12°C on mixed felsic-mafic, fine-grained (<63µm), pre-weathered proglacial sediments of the Onyx River (Wright Valley [WV]) that derive from MDV drifts. Although the focus is on Antarctic bioweathering and the relationship to biogeochemical processes in the permafrost, we include a separate set of experiments on basaltic glacio-volcanic outwash deposits from Iceland to compare bioweathering effects on fresh mafic sources in Arctic regions and predict potential bioweathering processes on other icy planets such as Mars.

MATERIALS AND METHODS

Starting Material: Source, Preparation, and Characterization

To quantify the weathering rates of silicate minerals derived from different bedrock compositions in glacial regions, we used glacial melt-water sediments collected from Antarctica (mixed felsic-mafic source materials) and Iceland (uniform mafic source), representing glacial drift deposits. Sediments were collected by G.S. Soreghan, M.E. Elwood Madden, and previous researchers from slackwater regions of marginal channel bars (Stumpf et al., 2012; Marra et al., 2014, 2015, 2017) and stored at 21°C until further analysis. We obtained the Antarctic sediments from the Onyx River (n=3; 77° 27.003' S, 162° 29.858' E; 77° 27.318' S, 162° 28.581' E; 77° 27.787' S, 162° 26.567' E, collected in January 2010), a MDV meltwater stream emanating from cold-based Wright Lower Glacier and Clark Glacier in WV. The Onyx River drains from Lake Brownworth and passes through pre-Last Glacial Maximum glacial sediments derived from the Ferrar Dolerite, and plutons composed of diorite, granite, granodiorite, and quartz monazite flowing into Lake Vanda (Hall and Denton, 2005; Stumpf et al., 2012). We additionally collected various drift deposits, meltwater stream sediments, and soil samples from both Wright and Taylor Valleys to compare their microtexture and weathering features with the ones to be produced in experimental samples. We obtained the basaltic Iceland sediments from the modern glacial outwash stream of the Eyjafjallajökull volcano (n=3; 63° 40.858' N, 19° 38.032' W; 63° 40.976' N, 19° 38.168' W; 63° 40.178' N, 19° 37.504' W; collected in May 2017) to investigate abiotic and biotic weathering of fresh mafic glacio-volcanic deposits, similar to those expected on Mars (Ehlmann et al., 2012).

Before any sample was processed, we sputter-coated a subsample of the Antarctic sediments with Au/Pb and imaged them using scanning electron microscopy (SEM) with energy

dispersive X-ray spectroscopy (EDS). This imaging enabled the observation of the natural state of the samples and examination of any preexisting weathering features and biofilms (Figure 2.1).

We merged the three Onyx River sediments together into one batch and three Eyjafjallajökull outwash sediments into another and then wet sieved the two samples through a <math><63\text{-}\mu\text{m}</math> mesh to obtain the “glacial-fine” (Anderson, 2005) mud-sized fraction. We focus on the fine-grained components of the sediments because these have the most abundant surface area for alteration, allowing us to observe solute fluxes in short-term weathering reactors. Although weathering also occurs on larger grains, it proceeds more slowly and does not generate significant weathering fluxes (Anderson, 2005, 2007). We treated the samples with glacial acetic acid (24 hours) and hydrogen peroxide (3 days) to remove secondary carbonate and organic remnants (cell, biofilm, and other organic matter) and/or sulfide fractions, respectively (Marra et al., 2017; Demirel-Floyd et al. 2020). These treatments isolated the silicate fraction, thus simplifying the design and allowing us to focus on the aqueous and mineralogical changes resulting solely from silicate weathering and microbial activity.

Following the chemical treatments, we determined the clay and silt fractions within these glacial fines (Table 2.1) using a Malvern Mastersizer 3000 laser particle size analyzer, after treatment with sodium hexametaphosphate as a dispersant (Blott et al., 2004). We quantified the specific surface area of the glacial fines (Table 2.1) using the Brunauer–Emmett–Teller (BET) nitrogen adsorption method, with a Quantachrome Nova 2000e gas adsorption analyzer (Brunauer et al., 1938; Bish and Howard, 1988), and determined the mineralogy of the glacial fines with X-ray powder diffraction (XRD) using a Rigaku Ultima IV with a Cu radiation source and graphite monochromator (Figures S2.2 and S2.3). We mounted the sediments in standard glass sample holders and employed the Bragg–Brentano method (2–70 2θ angle interval).

Analyses were performed with 0.02° step size and 2-second counting time, using fixed slits. We determined the mineral composition quantitatively (Table 2.2) with MDI Jade software using the Reitveld refinement method (Bish and Howard, 1988; Demirel et al., 2018) in combination with ClaySIM software using the RockJock method (Eberl, 2003). Finally, we sent our samples to ALS Labs (ALS USA Inc., Reno, NV, USA) for whole rock geochemistry (Inductively Coupled Plasma Mass Spectrometry (ICP-MS), Li borate fusion method) and trace element and base metal geochemistry (Inductively Coupled Plasma Atomic Emission Spectroscopy (ICP-AES), acid-digestion methods).

Culture Growth and Experimental Design

We purchased the polyextremophilic culture, *Leptolyngbya glacialis* (ULC073), from Belgian Coordinated Collections of Microorganisms. This culture is non-axenic (also contains some heterotrophic cells) due to the difficulties in isolating filamentous cyanobacteria (Cornet et al., 2018; Fernandez-Carazo et al., 2011). We grew the culture at 12°C in 1x BG11 freshwater medium (Sigma-Aldrich, St. Louis, MO, USA, catalog #C3061, adjusted pH 7 with 1 M KOH) in a rotary shaking incubator (Inova 42R with cyanobacterial growth lamp) at 60 rpm for 3 weeks, providing an 8-hour dark/16-hour light cycle (Figure S2.1b), representing optimal conditions for the strain. Then, we inoculated 25 mg of wet cells into 50-ml sterile glass Erlenmeyer flasks containing 25-ml sterile 0.1x BG11 and 0.25 g of UV-sterilized muds, in triplicates to set up biological weathering experiments. We set up abiotic controls containing UV-sterilized mud and 25-ml 0.1x BG11. Each separate batch reactor experiment lasted 0, 1–2, 3, or 4 weeks, representing varying durations of the Antarctic melt season. In addition, we set up parallel culture growth controls (without adding sediments) to monitor the pH and microbial growth in the absence of nutrient flux from weathering. We monitored the cyanobacterial growth

in 0.1x BG11 medium for 6 weeks to obtain data points at all phases on its growth curve (lag, exponential, stationary, and death).

Sampling and Analyses During the Experiments

We sampled individual batch reactors (in triplicate) of Icelandic biotic weathering experiments at week 0, 2, 3, and 4. Chlorophyll-a (Chl-a) measurements demonstrate that the culture showed considerable growth in the first week (Demirel-Floyd et al., 2020). Therefore, we added a week-1 sampling time point to the later Antarctic weathering experiments. During each sampling, we filtered supernatants through 0.2- μm syringe-tip filters to remove particulates and cells from the solution, and we periodically measured the pH of the filtrates. We sent separate aliquots of the filtrates (untreated) for ion chromatography and acidified (1 M HNO_3) aliquots of the filtrates for ICP-AES analyses (The Advanced Water Technology Center and J. Ranville Lab at the Colorado School of Mines, Golden, CO, USA) to monitor all released anions and cations. We also monitored the changing alkalinity via bicarbonate and carbonate ion measurements (flow injection method, OSU Soil Labs, Still-water, OK, USA).

Weathering Rate Calculations

Weathering rates were measured based on aqueous silica concentrations observed during both the abiotic and biotic weathering experiments. We calculated Si weathering rates by plotting aqueous Si concentrations (obtained by ICP-AES) normalized to BET surface area of sediments versus time elapsed (Figure 2.2) and then fitting the curve with a polynomial equation. We used the first derivative of the polynomial to determine the rate of biological and abiotic weathering (Rimstidt, 2013).

Microbial Growth Monitoring

We monitored cyanobacterial growth within both the biotic weathering experiments and culture growth controls via Chl-a measurements on microbial mats. We harvested and weighed cell pellets weekly (centrifuged at 12,000g for 10 minutes in pre-weighed tubes). We extracted Chl-a in 90% methanol at 25°C in the dark and measured the absorbance values of the extract at 663 nm using UV/Vis spectrophotometry (Genesys 6, Thermo Scientific, Waltham, MA, USA). We also measured the absorbance values at 750 nm to correct for interference and calculated Chl-a concentrations using Equation 2.1 (Fiore et al., 2000; Li et al., 2012; Meeks and Castenholz, 1971).

$$\text{Chl-a } (\mu\text{g}/\mu\text{l}) = \text{Absorbance (663nm-750nm)} * 12.7 \quad (2.1)$$

We also performed the same extractions and spectrophotometric measurements on the sediments of the abiotic experiments to account for remnant Chl-a (if any) or other green pigments coming from the field. Then we corrected the absorbance values of biotic experiments by subtracting the absorbance values of abiotic experiments. This correction allowed us to ensure that our results represent only cyanobacterial growth.

Imaging Microbial Mats, Weathering Features, and Secondary Mineral Formation

To preserve the biofilm structure for SEM imaging, we fixed sediment–microbe aggregates on pre-sputter-coated glass slides immediately on harvesting using a mixture of 2.5% glutaraldehyde, 50mM lysine, and 0.1 M HEPES buffer (pH 7). Then we successively applied a secondary fixation (1% OsO₄ in 0.1 M HEPES), EtOH dehydration (25%, 50%, 75%, 95%, and 100%), and finally chemical drying (HMDS:EtOH ratio 1:2, 1:1, and 2:1) protocols suggested for microbial biofilms (Fischer et al., 2012; Kyle et al., 2007). We sputter-coated with Au/Pd (10-nm coating) to create conductive specimens and then imaged biofilms, cells, and potential

microbial weathering features (e.g., cell-shaped pits) using SEM. We also coupled EDS measurement with our imaging to determine elemental composition changes on the grains and characterized secondary precipitates, thus identifying and characterizing inorganic biosignatures of surface alteration (Demirel-Floyd et al., 2020). We performed our SEM-EDS studies at the OU Samuel Roberts Noble Microscopy Laboratory, using Zeiss NEON 40 EsB field emission SEM with an Oxford Electron Backscattered Diffraction camera and INCA Energy 250 energy dispersive X-ray microanalysis system. We used a combination of secondary electron, backscattered diffraction, and InLens detectors alternating between 5 and 15 kV, depending on surface charging, organic matter content, and scale of the mineral or bacteria to image.

Statistical Analyses

To determine the significance of our results, we performed four multi-variate statistical analyses (Ramette, 2007; Till, 1974; Wackernagel, 2003) on abiotic and biotic weathering experiments, separately for Antarctica and Iceland reactors, using GraphPad Prism 9.0.2 software. We performed PCA (principal component analysis (Ramette, 2007) with principal components (PCs) with eigen values greater than 1.0 (Kaiser rule). Plots of PCs are grouped based on the presence of microbes (biotic or abiotic) and overlapped with loading vectors showing which water chemistry variables (solutes and pH) are driving the most significant differences. We also performed multiple unpaired t-tests using two-stage step-up Benjamini, Krieger, and Yekutieli procedure controlling the false discovery rate (Benjamini et al., 2006), comparing the water chemistry at each time point between abiotic and biotic experiments to identify the significant differences. Finally, we plotted r-scores from Pearson's correlation matrix to prepare separate heatmaps for Antarctica and Iceland experiments to determine which water chemistry changes are significantly correlated with each other in both biotic and abiotic reactors.

High positive correlation is indicated by *r* scores between 0.5 and 1, increasing in degree with higher *r*-scores, whereas high negative correlation between the two variables is indicated by *r*-scores between 0.5 and 1. Finally, we supplemented these tests with two-way ANOVA (analyses of variance) coupled with Tukey's multiple comparisons (Till, 1974) on our solute chemistry, using $p < 0.05$ threshold as an indication of significant microbial influence on silicate weathering. Here we also investigated the significance of pH and Chl-*a* increase between comparable biological weathering and culture growth experiment time points using two-way ANOVA coupled with Šídák's multiple comparisons.

RESULTS

Weathering Features Observed in the Field

SEM imaging of the untreated field samples shows mechanical, biological, and abiotic weathering textures in Antarctic drift sediments and soils (Figure 2.1). Side-by-side comparisons of colonized and uncolonized samples (Figure 2.1a) illustrate that biofilm cover results in the disintegration of the grain surfaces, whereas uncolonized grains do not disintegrate. Chemical incongruent dissolution features were discernable as smooth-pitting and blade-like Ca-rich secondary precipitates, Fe-bearing carbonates, and potential Fe coatings on pit walls (Figure 2.1b; Table S2.6). Biofilms and filaments also contribute to mechanical and chemical weathering by separating the grains (Figure 2.1c,d), dissolving them (Figure 2.1e), and leaving nano-phase secondary precipitates (Figure 2.1f). Exfoliation structures observed (Figure 2.1c,d) may be artifacts of both mechanical disintegration by the microbial mats and weathering by acidic chemical solutions. SEM coupled with EDS measurements revealed that nano-phase potentially neo-formed precipitates are Fe-(oxy) hydroxide minerals on mafic grains impacted by biofilms (Figure 2.1f).

Characteristics of the Treated Starting Material

Specific BET surface area values of the Antarctic and Icelandic sediments are 8.2 and 11.5 m²/g, respectively. The bulk SiO₂ and Al₂O₃ contents, as well as the grain size (silt/clay), are comparable (Tables 2.1 and 2.2). The primary difference between the Antarctic and Icelandic samples is their contrasting mineralogy. The Antarctic sample contains more felsic primary minerals and clay minerals (largely smectite and illite), whereas the Iceland sample contains more mafic phases and amorphous materials (Table 2.2; Figures S2.2 and S2.3).

Silica Release Rates

Silica release rates in all of the Antarctic mixed-source experiments were significantly slower than the silica release rates observed in the mafic Icelandic experiments, in both the biotic reactors and abiotic controls (Table 2.3; Figure 2.2). Within the mafic Icelandic sediments, we observed little difference between the bioweathering and abiotic weathering rates. However, in the more felsic, mixed-source Antarctic sediments, the bioweathering rates were up to three times faster than the abiotic controls (Table 2.3; Figure 2.2).

Aqueous Chemistry and Chlorophyll Production

We observed increasing Si, Al, and HCO₃⁻ concentrations in both biotic and abiotic reactors for the Antarctic and Icelandic silicate weathering experiments; however, the final concentrations of Si, Al, and HCO₃⁻ were significantly higher in the presence of microbial life (Figure 2.3; Table S2.1). Nutrients important for biota (Ca, Fe, Mg, Mn, P, NO₃⁻, SO₄²⁻) decreased significantly in all biotic reactors (Figures 2.3 and 2.4; Table S2.1). These solutes changed only slightly or remained constant in all abiotic reactors (Figures 2.3 and 2.4; Table S2.1). This trend is also observed in the Fe plots, where Fe was nearly depleted in the solution by

the end of week 2 in the biological experiments and then increased, whereas Fe decreased throughout the abiotic experiments.

Solution pH increased from 6.5 through 7 in abiotic weathering experiments and up to 8 in biological weathering experiments and culture growth controls (Figure 2.5; Table S2.2). pH increases in the biotic reactors were accompanied by increasing Chl-a (Chl-a) pigmentation (Figure 2.5; Table 2.2). Differences in Chl-a between each of the three biotic replicates likely result from sampling both microbial cells and biofilm within the microbial mat. Chl-a concentrations depend on the amount of the active cyanobacterial cells; however, the weight of the biofilm (e.g., EPS components) and the actual cells cannot be differentiated. For example, the highest Chl-a concentrations within the three replicates should correspond to the highest weight of cyanobacterial cell density within the sampled microbial mat, even though the total microbial mat (cell + biofilm) weights are almost the same.

Statistical Analyses

PCA analyses (Figure S2.4) revealed that pH, Si, HCO_3^- , Al, and Fe solute concentrations resulted in the most significant differences in both Iceland and Antarctic experiments, where pH, Si, HCO_3^- , and Al correlate strongly with biotic pathways, whereas Fe solute concentrations show the most difference in abiotic experiments. Significant differences in water chemistry between biotic and abiotic weathering experiments occur starting with the first and second weeks of the experiments but accentuated in the third and fourth weeks. As expected, no significant differences occurred between week 0 samples. The results of the t-tests (Table S2.3) are in agreement with all PCA results. t-Test analyses also show that Ca, Mn, Al, Mg, P, SO_4^{2-} , and NO_3^- are significantly different between biotic and abiotic experiments due to significant decreases in aqueous concentrations in biotic experiments (Figures 2.3 and 2.4; Table S2.1). Pairwise comparisons

indicate that all investigated water chemistry variables, except Fe, are significantly different between biotic and abiotic experiments at the end of 4 weeks. Two-way ANOVA pairwise comparisons of biotic and abiotic solute chemistry (Table S2.4) are in agreement with PCA and t-test results. In addition, pairwise comparisons of biotic and culture growth comparisons of pH and Chl-a results indicate no significant differences between comparable time points, besides higher mean Chl-a in biotic at weeks 3 and 4 of Antarctic and Icelandic experiments, respectively (Table S2.5). Finally, Pearson's correlation tests (Figure 2.6) of both biotic and abiotic experiments showed high positive correlation between Fe-P and Ca-Mg. These results are in strong agreement with the PCA analyses; Si is highly correlated with pH, HCO_3^- , and Chl-a in all biotic reactors, with the addition of high correlation to Al in Iceland biotic experiments, indicating a high positive correlation of silicate weathering to photosynthesis. In addition, microbially important nutrients (Ca, Mg, Mn, P, SO_4^{2-} , and NO_3^-) are highly positively correlated with one another in both Antarctic and Icelandic biotic experiments, whereas similar trends and/or strong correlations are not observed in abiotic experiments. Overall, the combined statistical results are in agreement pointing to significant differences in water chemistry driven by *L. glacialis*.

SEM observations

Although we did not observe any discernable textural changes in the abiotic experiments (Figure 2.7a), we did observe a few chemically weathered surfaces (Figure 2.7b), where weathering starts from a corner and regularly moves across the grain surface, leaving a very shallow pitted surface (Figure 2.7c) that is different from its biogenic counterparts (e.g., Figure 2.7f). We observed several features indicating biological weathering in the SEM images collected from Icelandic biotic experiments (Figure 2.7d–f). For example, the cyanobacteria physically trapped grains within a mesh of filaments and were bound to the sediments with their

biofilms (Figure 2.7d). Biofilm and cell attachment also dissolved the grains, leaving filament or coccus-shaped etch pits (Figures 2.7e, f and 2.8a) on grain surfaces, and potentially aided the formation of secondary Fe-oxy (hydroxide) and flakey clay precipitates on mineral and cell surfaces (Figures 2.7e and 2.8b,c). Botryoidal etch pits resembling coccus colonies (Figure 2.7f) were also observed and may potentially reflect heterotrophic communities (potentially *Deinococcus* sp. in MDV soils (Hirsch et al., 2004) that came with the microbial mat.

DISCUSSION

Enhanced Weathering by Microbes in Sediments

These results show that *L. glacialis* enhance Si release rates up to threefold relative to abiotic weathering (Table 2.3; Figure 2.2) in the mixed-source Onyx River sediments, comparable to Si release rates at 25°C from *Leptolyngbya* strains collected in temperate glacial environments (Olsson-Francis et al., 2012). Increased weathering rates in biotic reactors relative to abiotic controls likely relate to acidic microenvironments developed beneath microbial biofilms (e.g., De Los Rios et al., 2003), forming the cell-shaped etch pits observed by SEM imaging (Figure 2.7). Organic acids produced within the EPS also likely facilitated the extremely high Al release observed (Figure 2.3; Table S2.1) (Johnston et al., 1993). However, the overall pH increases in biotic experiments (up to ~8) track closely with the pH observed in the culture growth controls, accompanied by increasing Chl-a, suggesting that the overall pH is largely controlled by photosynthesis (Figures 2.5 and 2.6; Table S2.5). This overall increase in pH in the bioweathering experiments likely contributed to enhanced Si release (Olsson-Francis et al., 2012). Chl-a pigmentation in the microbial mats peaked at weeks 2–3 and was replaced with carotenoid pigments likely as a result of prolonged exposure to UV radiation (Figure S2.1d and S2.1e) and NO₃⁻ depletion (Miller and Castenholz, 2001) (Figure 2.4). Decreasing Chl-a

concentrations after weeks 2–3 also suggest that *L. glacialis* reached the stationary phase of their life cycle; solute concentrations also either stay constant or change more slowly (observed by relatively gentle slopes, Figures 2.3 and 2.4) around the same time, further relating solute release rates to microbial activity.

We observed faster weathering rates in both the biotic and abiotic mafic Icelandic weathering experiments compared to the mixed- lithology Antarctic experiments (Table 2.3), likely attributable to differences in chemistry and mineralogy (Table 2.2; Figures S2.2 and S2.3). Icelandic muds contain higher concentrations of fresh reactive mafic minerals (olivine and pyroxene) and volcanic glass, whereas nearly 38% of the Antarctic muds contain clay minerals (Table 2.2), which are less reactive. Because chemical weathering of the mafic minerals proceeds faster than rates observed for felsic minerals or clays, (Goldich, 1938; Rimstidt, 2013) sufficient nutrients may be abiotically delivered to the bacteria in the mafic Iceland experiments, eliminating the need to scavenge nutrients through enhanced chemical weathering, leading to similar weathering rates observed in both the biotic and abiotic weathering experiments. In contrast, we posit that microbes stimulated chemical weathering in the Antarctic sediment experiments due to the lower nutrient release rates from less-reactive clays and felsic phases, resulting in nutrient- poor conditions that caused microbes to actively scavenge nutrients through biologically enhanced mineral dissolution reactions.

The Antarctic sediments have a complex weathering history dating from the Early-Mid Quaternary (Hall et al., 1993), whereas Iceland sediments were freshly supplied by recent volcano-glaciogenic events (Oddsson et al., 2016). Thus, the Antarctic sediments experienced prolonged “pre-weathering” before our experiments and thus were less reactive due to aging, in addition to differences in the source lithology. Wild et al. (2018) found a nearly 10-fold increase in abiotic

weathering rates from fresh labradorite and olivine minerals compared to artificially acid-aged samples in laboratory experiments.

Our water chemistry results show that nutrients essential for photosystems (i.e., Ca, Fe, Mn, Mg, and P) (Shcolnich and Keren, 2006) decreased with increasing Chl-a production (Figures 2.3–2.5), consistent with potential secondary mineral precipitation and/or cellular intake by *L. glacialis*. SEM observations coupled with EDS measurements revealed potential neo-formed flakey secondary clay minerals (Figure 2.8c) and spherical nano-phase iron oxy/hydroxides (Figures 2.7e and 2.8b) associated with EPS and cell surfaces that are similar to the nano-phase minerals observed on biofilm-impacted grains in the field (Figure 2.1f). Previous studies suggest that such minerals in association with biofilms are potential biosignatures of microbial surface alteration (Mergelov et al., 2018; Olsson-Francis et al., 2017; McKinley and Stevens, 2000; Phillips-Lander et al., 2020). These secondary phases also consume cations from solution, resulting in lower aqueous concentrations, thus lowering the apparent weathering rates. In addition, survival mechanisms observed in polyextremophilic cultures (e.g., EPS and carotenoid production; Figure S2.1d and S2.1e) might consume added nutrients.

Increasing Si dissolution (Figure 2.3) with increasing Chl-a production (Figure 2.5) indicates that weathering was enhanced by microbial activity in the biotic reactors. Overall, our results and statistical analyses indicate strong impacts of cold-tolerant cyanobacterial mats on silicate weathering, even in cold-arid conditions such as the Antarctic Dry Valleys. Our results also suggest that cyanobacteria likely play an important role in facilitating pedogenesis via silicate weathering in the MDV (Mergelov et al., 2018).

Implications

Carbonate Production, Chemical Weathering, and Nutrient Cycling on Earth

Psychrotolerant polar cyanobacterial mats both enhance silicate weathering, releasing nutrients that promote primary production, and provide refugia for other organisms within their EPS. Cyanobacterial mats also trap and bind mud-sized grains (Frantz et al., 2015), creating an inorganic nutrition bank during prolonged nutrient-limited conditions (Vincent et al., 2000). EPS excreted by psychrophilic cyanobacteria (Figure 2.7d,2.7e) likely helped some eukaryotes like microalgae (e.g., Ye et al., 2015) survive through cold climates and adapt to warmer environments by acting as a physical barrier (Schulze-Makuch et al., 2005). Thus, psychrotolerant polyextremophilic cyanobacteria may have been crucial to sustain terrestrial life during paleoclimatic extremes, including Proterozoic glaciations such as Snowball Earth. Most of the Antarctic cyanobacteria, including those belonging to *Leptolyngbya* genus, are known for their cold tolerance and functionality across a wide range of temperatures (i.e., 4°C–23°C), making them good candidates for monitoring the effects of global warming (Kleinteich et al., 2012) on soil processes such as weathering fluxes from silicate minerals.

Fresh, fine-grained sediment supplied by glacial milling and/or volcanoclastic processes fertilizes phototrophs (Shoenfelt et al., 2019), stimulating further (bio)weathering and associated nutrient release and thus further enhancing phototroph activity in a positive-feedback cycle that greatly accelerates CO₂ drawdown. In our experiments, increased photosynthetic activity carried out by the cyanobacteria increased the pH due to CO₂ consumption, shifting the carbon speciation toward HCO₃⁻ (Andersen, 2002), thus resulting in four times higher HCO₃⁻ concentrations compared to the abiotic weathering controls (Figure 2.3). Enhanced bicarbonate concentrations and cations released due to biological weathering of silicates could thus supersaturate oceans and promote the precipitation of carbonates, similar to those observed associated with Snowball Earth glaciations (Hoffman and Schrag, 2002).

The results of our experiments provide insights into the effects of future warming of permafrost soils on the global C cycle. Although warming temperatures might cause the death of some strictly psychrophilic communities, growth rates of the psychrotolerant cyanobacteria will increase (Kleinteich et al., 2012) in parallel with increasing nutrient fluxes that accompany higher chemical weathering rates. Nutrients resulting from combined abiotic and biotic chemical weathering pathways carried by meltwaters will fertilize the oceans (Lyons et al., 2015) and periglacial soils. In addition, as microbial diversity is closely related with the chemistry of permafrosts (Aislabie et al., 2008), we posit that soil chemistry and mineralogy will change with intensifying weathering reactions and cause ecological shifts in soil microbial populations within glaciated settings. Based on our observations from untreated MDV sediments and our laboratory experiments, we posit that the Antarctic cyanobacterial mats have the potential to influence soil-forming processes and chemistry via enhanced silicate weathering and nutrient release, resulting in secondary mineral precipitation.

Weathering and Biosignatures on Mars

Microbe–mineral interactions leave biosignatures in the rock record and permafrost soils on Earth, providing clues to interpret similar chemical and mineralogical transformations within planetary soils. In our experiments we observed neo-formed clay and nano-phase Fe-(oxy)hydroxide precipitates (Figures 2.7e and 2.8b,c) similar to features also observed in unprocessed field samples (see Figure 2.1f and Mergelov et al., 2018; Olsson-Francis., 2012; McKinley et al., 2000; Phillips-Lander et al., 2020). While secondary Fe and clay precipitates can also be precipitated solely by abiotic pathways, we did not observe them in our abiotic experiments. However, minerals observed on EPS and cell surfaces indicate the role of microbes in precipitating secondary phases through their biofilms. We observed these potential bio-

minerals primarily on mafic minerals in unprocessed Antarctic drifts (Figure 2.1f) and throughout the bioweathered Icelandic sediments (Figures 2.7e and 2.8b,c).

Our findings suggest that cyanobacterial mats have the potential to produce putative biosignatures in mafic extraterrestrial terrains, thus providing biosignatures within the soils on other icy planets, especially Mars (Demirel-Floyd et al., 2020; Demirel et al., 2019). Even though our experiments are not set up in Mars conditions, our felsic and mafic starting materials are sampled from sites (Antarctica and Iceland) considered to share climatic and mineralogic similarities to the Mars surface (Demirel-Floyd et al., 2020; Ehlmann et al., 2012; Demirel et al., 2019; Demirel et al., 2018; Cannon et al., 2015). Finding similar inorganic biosignatures, including spherical nano-phase Fe-(oxy)hydroxide minerals and clays associated with biofilm sheet-like etch surfaces and cell-shaped etch pits from mixed mafic-felsic terrains under SEM imaging (Figures 2.7e and 2.8b,c) in returned samples from the Perseverance Rover, might indicate the potential presence of past life on Mars.

CONCLUSIONS

Our study demonstrates that psychrotolerant cyanobacterial mats significantly accelerate silicate weathering in mixed-source, pre-aged sediments by increasing the pH due to photosynthesis and EPS production, under warming polar temperature conditions. Even though the weathering rates are higher, in general, in mafic and volcanic glass-rich polythermal terrains in more temperate settings, chemical and biological weathering are almost of equal importance in terms of nutrient release as fresh mafic minerals can be easily weathered by abiotic pathways. In terms of the global C cycle, the biotic pathways accelerate atmospheric CO₂ withdrawal and bicarbonate production through weathering and shifting the saturation state toward carbonate via pH increase. As anthropogenic climate change (warming) continues, we posit cyanobacterial mats

will contribute increasingly to significant changes in the permafrost in the MDV, altering the soil chemistry through enhancing fluxes of Si, Al, and HCO_3^- , thus promoting the formation of clay and carbonate deposits. Such psychrotolerant polyextremophilic mats would also leave their biosignatures of surface alteration in the form of spherical nano-phase Fe-(oxy)hydroxide minerals on micron-scale biofilm sheet-like etch marks and cell-shaped pits on mafic minerals within mixed mafic-felsic planetary terrains. Therefore, the occurrence of such putative bio- minerals in future sample return missions would indicate microbial influences on geochemical cycling within planetary regoliths and thus the presence of past extraterrestrial life.

ACKNOWLEDGEMENTS

We thank Kristin Marra, Brenda Hall, and Alison Stumpf for sample collection; Nina D.S. Webb for her assistance in sample processing; Preston Larson for his help in SEM imaging; Andy E. Elwood Madden for his help in XRD data analysis; and Claire Curry for her help in statistical data analysis. We also thank Amy Callaghan, Boris Wavrick, Bradley S. Stevenson, Paul Lawson, and Anne Dunn for providing access to microbiology lab equipment and facilities. Finally, we thank the anonymous reviewers' comments that helped us improve the quality of our publication.

This project is funded by NSF grant number 1543344, “Quantifying Surface Area in Muds from the Antarctic Dry Valleys: Implications for Weathering in Glacial Systems.”

REFERENCES

- Aislabie, J.M., Jordan, S., and Barker, G.M., 2008, Relation between soil classification and bacterial diversity in soils of the Ross Sea region, Antarctica: *Geoderma*, v. 144, p. 9–20, doi:[10.1016/j.geoderma.2007.10.006](https://doi.org/10.1016/j.geoderma.2007.10.006).
- Andersen, C.B., 2002, Understanding Carbonate Equilibria by Measuring Alkalinity in Experimental and Natural Systems: *Journal of Geoscience Education*, v. 50, p. 389–403, doi:[10.5408/1089-9995-50.4.389](https://doi.org/10.5408/1089-9995-50.4.389).

- Anderson, S.P., 2007, Biogeochemistry of Glacial Landscape Systems: Annual Review of Earth and Planetary Sciences, v. 35, p. 375–399, doi:[10.1146/annurev.earth.35.031306.140033](https://doi.org/10.1146/annurev.earth.35.031306.140033).
- Anderson, S.P., 2005, Glaciers show direct linkage between erosion rate and chemical weathering fluxes: *Geomorphology*, v. 67, p. 147–157, doi:<https://doi.org/10.1016/j.geomorph.2004.07.010>.
- Anesio, A.M., and Laybourn-Parry, J., 2012, Glaciers and ice sheets as a biome: Trends in Ecology and Evolution, v. 27, p. 219–225, doi:[10.1016/j.tree.2011.09.012](https://doi.org/10.1016/j.tree.2011.09.012).
- Balks, M.R., López-Martínez, J., Goryachkin, S.V., Mergelov, N.S., Schaefer, C.E.G.R., Simas, F.N.B., Almond, P.C., Claridge, G.G.C., McLeod, M., and Scarrow, J., 2013, Windows on Antarctic soil-landscape relationships: comparison across selected regions of Antarctica: Geological Society, London, Special Publications, v. 381, p. 397–410, doi:[10.1144/SP381.9](https://doi.org/10.1144/SP381.9).
- Balks, M.R., Paetzold, R.O.N.F., Kimble, J.M., Aislabie, J.M., and Campbell, I.B., 2002, Effects of hydrocarbon spills on the temperature and moisture regimes of Cryosols in the Ross Sea region: *Antarctic Science*, v. 14, p. 319–326, doi:[10.1017/S0954102002000135](https://doi.org/10.1017/S0954102002000135).
- Benjamini, Y., Krieger, A.M., and Yekutieli, D., 2006, Adaptive linear step-up procedures that control the false discovery rate: *Biometrika*, v. 93, p. 491–507, doi:[10.1093/biomet/93.3.491](https://doi.org/10.1093/biomet/93.3.491).
- Bidle, K.D., Lee, S.H., Marchant, D.R., and Falkowski, P.G., 2007, Fossil genes and microbes in the oldest ice on Earth: *Proceedings of the National Academy of Sciences of the United States of America*, v. 104, p. 13455–13460, doi:[10.1073/pnas.0702196104](https://doi.org/10.1073/pnas.0702196104).
- Bish, D.L., and Howard, S.A., 1988, Quantitative phase analysis using the Rietveld method: *Journal of Applied Crystallography*, v. 21, p. 86–91, doi:[10.1107/S0021889887009415](https://doi.org/10.1107/S0021889887009415).
- Blott, S.J., Croft, D.J., Pye, K., Saye, S.E., and Wilson, H.E., 2004, Particle size analysis by laser diffraction: Geological Society, London, Special Publications, v. 232, p. 63–73, doi:[10.1144/GSL.SP.2004.232.01.08](https://doi.org/10.1144/GSL.SP.2004.232.01.08).
- Bockheim, J.G., 2008, Functional diversity of soils along environmental gradients in the Ross Sea region, Antarctica: *Geoderma*, v. 144, p. 32–42, doi:[10.1016/j.geoderma.2007.10.014](https://doi.org/10.1016/j.geoderma.2007.10.014).
- Bockheim, J.G., 1990, Soil development rates in the Transantarctic Mountains: *Geoderma*, v. 47, p. 59–77, doi:[10.1016/0016-7061\(90\)90047-D](https://doi.org/10.1016/0016-7061(90)90047-D).
- Bockheim, J.G. (Ed.), 2015, *The Soils of Antarctica*: Springer International Publishing, doi:[10.1007/978-3-319-05497-1](https://doi.org/10.1007/978-3-319-05497-1).
- Bockheim, J.G., and McLeod, M., 2015, Soils of Central Victoria Land, the McMurdo Dry Valleys: 117–148 p., doi:[10.1007/978-3-319-05497-1_8](https://doi.org/10.1007/978-3-319-05497-1_8).
- Bockheim, J., Vieira, G., Ramos, M., López-Martínez, J., Serrano, E., Guglielmin, M., Wilhelm, K., and Nieuwendam, A., 2013, Climate warming and permafrost dynamics in the Antarctic Peninsula region: *Global and Planetary Change*, v. 100, p. 215–223, doi:[10.1016/j.gloplacha.2012.10.018](https://doi.org/10.1016/j.gloplacha.2012.10.018).

- Brunauer, S., Emmett, P.H., and Teller, E., 1938, Adsorption of Gases in Multimolecular Layers: *Journal of the American Chemical Society*, v. 60, p. 309–319, doi:[10.1021/ja01269a023](https://doi.org/10.1021/ja01269a023).
- Campbell, I.B., and Claridge, G.G.C., 2006, Permafrost Properties, Patterns and Processes in the Transantarctic Mountains Region: *Permafrost and Periglacial Processes*, v. 17, p. 215–232, doi:[10.1002/ppp](https://doi.org/10.1002/ppp).
- Cannon, K.M., Mustard, J.F., and Salvatore, M.R., 2015, Alteration of immature sedimentary rocks on Earth and Mars: Recording aqueous and surface–atmosphere processes: *Earth and Planetary Science Letters*, v. 417, p. 78–86, doi:[10.1016/j.epsl.2015.02.017](https://doi.org/10.1016/j.epsl.2015.02.017).
- Cannone, N., Guglielmin, M., Malfasi, F., Hubberten, H.W., and Wagner, D., 2021, Rapid soil and vegetation changes at regional scale in continental Antarctica: *Geoderma*, v. 394, p. 115017, doi:<https://doi.org/10.1016/j.geoderma.2021.115017>.
- Cary, S.C., McDonald, I.R., Barrett, J.E., and Cowan, D.A., 2010, On the rocks: The microbiology of Antarctic Dry Valley soils: *Nature Reviews Microbiology*, v. 8, p. 129–138, doi:[10.1038/nrmicro2281](https://doi.org/10.1038/nrmicro2281).
- Cornet, L., Bertrand, A.R., Hanikenne, M., Javaux, E.J., Wilmotte, A., and Baurain, D., 2018, Metagenomic assembly of new (Sub)polar cyanobacteria and their associated microbiome from non-axenic cultures: *Microbial Genomics*, v. 4, doi:[10.1099/mgen.0.000212](https://doi.org/10.1099/mgen.0.000212).
- Cowan, D.A., Khan, N., Pointing, S.B., and Cary, S.C., 2010, Diverse hypolithic refuge communities in the McMurdo Dry Valleys: *Antarctic Science*, v. 22, p. 714–720, doi:[10.1017/S0954102010000507](https://doi.org/10.1017/S0954102010000507).
- Demirel, C., McCollom, N., Marra, K., Madden, A.S.E., Hall, B., Levy, J., Soreghan, G.S., and Madden, M.E.E., 2019, Potential Biosignatures of Surface Alteration on Mars Inferred from Terrestrial Analog Regoliths, *in* Goldschmidt Abstracts, p. 769.
- Demirel, C., Soreghan, G.S., McCollom, N., Madden, A.S.E., Marra, K., and Madden, M.E.E., 2018, XRD Characterization of Antarctic Glacial Drift Deposits: Implications for Quantifying Weathering Products on Earth and Mars, *in* 49th Lunar and Planetary Science Conference, Lunar and Planetary Institute, p. Abstract #1542, <http://www.lpi.usra.edu/meetings/lpsc2018/pdf/1542.pdf>.
- Demirel-Floyd, C., Madden, A.S.E., Soreghan, G.S., and Madden, M.E.E., 2020, Determination of Inorganic Biosignatures Based on Terrestrial Analogs: Preliminary Results from Glacio-Fluvial Sediments from Iceland, *in* 51st Lunar and Planetary Science Conference, Lunar and Planetary Institute, p. Abstract #2238, <http://www.lpi.usra.edu/meetings/lpsc2020/pdf/2238.pdf>.
- Dolgikh, A.V., Mergelov, N.S., Abramov, A.A., Lupachev, A.V., and Goryachkin, S.V., 2015, Soils of Enderby Land, *in* Bockheim, J.G. ed., *The Soils of Antarctica*, Cham, Springer International Publishing, World Soils Book Series, p. 45–63, doi:[10.1007/978-3-319-05497-1_4](https://doi.org/10.1007/978-3-319-05497-1_4).
- Eberl, D.D., 2003, User Guide to RockJock - A Program for Determining Quantitative Mineralogy from X-Ray Diffraction Data:, doi:[10.3133/ofr200378](https://doi.org/10.3133/ofr200378).

- Edwards, H.G.M., Oliveira, L.F.C. de, Cockell, C.S., Ellis-Evans, J.C., and Wynn-Williams, D.D., 2004, Raman spectroscopy of senescing snow algae: Pigmentation changes in an Antarctic cold desert extremophile: *International Journal of Astrobiology*, v. 3, p. 125–129, doi:[10.1017/S1473550404002034](https://doi.org/10.1017/S1473550404002034).
- Ehlmann, B.L., Bish, D.L., Ruff, S.W., and Mustard, J.F., 2012, Mineralogy and chemistry of altered Icelandic basalts : Application to clay mineral detection and understanding aqueous environments on Mars: *JOURNAL OF GEOPHYSICAL RESEARCH*, v. 117, p. E00J16, doi:[10.1029/2012JE004156](https://doi.org/10.1029/2012JE004156).
- Fernandez-Carazo, R., Hodgson, D.A., Convey, P., and Wilmotte, A., 2011, Low cyanobacterial diversity in biotopes of the Transantarctic Mountains and Shackleton Range (80–82°S), Antarctica: *FEMS Microbiology Ecology*, v. 77, p. 503–517, doi:[10.1111/j.1574-6941.2011.01132.x](https://doi.org/10.1111/j.1574-6941.2011.01132.x).
- Fiore, M.F., Moon, D.H., Tsai, S.M., Lee, H., and Trevors, J.T., 2000, Miniprep DNA isolation from unicellular and filamentous cyanobacteria: *Journal of Microbiological Methods*, v. 39, p. 159–169, doi:[10.1016/S0167-7012\(99\)00110-4](https://doi.org/10.1016/S0167-7012(99)00110-4).
- Fischer, E.R., Hansen, B.T., Nair, V., Hoyt, F.H., and Dorward, D.W., 2012, Scanning Electron Microscopy: *Current Protocols in Microbiology*, v. 25, doi:[10.1002/9780471729259.mc02b02s25](https://doi.org/10.1002/9780471729259.mc02b02s25).
- Fountain, A.G. et al., 2015, Physical Controls on Ecosystem ,: v. 49, p. 961–971.
- Frantz, C.M., Petryshyn, V.A., and Corsetti, F.A., 2015, Grain trapping by filamentous cyanobacterial and algal mats: Implications for stromatolite microfabrics through time: *Geobiology*, v. 13, p. 409–423, doi:[10.1111/gbi.12145](https://doi.org/10.1111/gbi.12145).
- Friedmann, I., 1982, Endolithic Microorganisms in the Antarctic Cold Desert: *Science*, v. 215, p. 1045–1053.
- Friedmann, E.I., Hua, M., and Ocampo-Freidmann, R., 1988, 3 . 6 Cryptoendolithic Lichen and Cyanobacterial Communities of the Ross Desert , Antarctica: *Polarforschung*, v. 58, p. 251–259.
- Friedmann, E.J., and Weed, R., 1987, Abiotic Weathering in the Antarctic Cold Desert: *Science*, v. 236, p. 703–705.
- Gilichinsky, D.A. et al., 2007, Microbial populations in Antarctic permafrost: Biodiversity, stage, age, and implication for astrobiology: *Astrobiology*, v. 7, p. 275–311, doi:[10.1089/ast.2006.0012](https://doi.org/10.1089/ast.2006.0012).
- Goldich, S.S., 1938, A Study in Rock-Weathering: *The Journal of Geology*, v. 46, p. 17–58.
- Gooseff, M.N., Mcknight, D.M., Lyons, W.B., and Blum, A.E., 2002, Weathering reactions and hyporheic exchange controls on stream water chemistry in a glacial meltwater stream in the McMurdo Dry Valleys: v. 38, doi:[10.1029/2001WR000834](https://doi.org/10.1029/2001WR000834).
- Guglielmin, M., and Cannone, N., 2012, A permafrost warming in a cooling Antarctica ? *Climatic Change*, v. 111, p. 177–195, doi:[10.1007/s10584-011-0137-2](https://doi.org/10.1007/s10584-011-0137-2).

- Guglielmin, M., Cannone, N., Strini, A., and Lewkowicz, A.G., 2005, Biotic and abiotic processes on granite weathering landforms in a cryotic environment, Northern Victoria Land, Antarctica: *Permafrost and Periglacial Processes*, v. 16, p. 69–85, doi:[10.1002/ppp.514](https://doi.org/10.1002/ppp.514).
- Guglielmin, M., Fratte, M.D., and Cannone, N., 2014, Permafrost warming and vegetation changes in continental Antarctica: *Environ. Res. Lett.*, v. 9, p. 045001, doi:[10.1088/1748-9326/9/4/045001](https://doi.org/10.1088/1748-9326/9/4/045001).
- Hall, B.L., and Denton, G.H., 2005, Surficial geology and geomorphology of eastern and central Wright Valley, Antarctica: *Geomorphology*, v. 64, p. 25–65, doi:<https://doi.org/10.1016/j.geomorph.2004.05.002>.
- Hall, B.L., Denton, G.H., Lux, D.R., and Bockheim, J.G., 1993, Late Tertiary Antarctic Paleoclimate and Ice-Sheet Dynamics Inferred from Surficial Deposits in Wright Valley: *Physical Geog.: Geografiska Annaler., Series A*, v. 75, p. 239–267.
- Hays, L.E., Graham, H.V., Marais, D.J.D., Hausrath, E.M., Horgan, B., McCollom, T.M., Parenteau, M.N., Potter-McIntyre, S.L., Williams, A.J., and Lynch, K.L., 2017, Biosignature Preservation and Detection in Mars Analog Environments: *Astrobiology*, v. 17, p. 363–400, doi:[10.1089/ast.2016.1627](https://doi.org/10.1089/ast.2016.1627).
- Hirsch, P., Gallikowski, C.A., Siebert, J., Peissl, K., Kroppenstedt, R., Schumann, P., Stackebrandt, E., and Anderson, R., 2004, *Deinococcus frigans* sp. nov., *Deinococcus saxicola* sp. nov., and *Deinococcus marmoris* sp. nov., Low Temperature and Draught-tolerating, UV-resistant Bacteria from Continental Antarctica: *Systematic and Applied Microbiology*, v. 27, p. 636–645, doi:[10.1078/0723202042370008](https://doi.org/10.1078/0723202042370008).
- Hoffman, P.F., and Schrag, D.P., 2002, The snowball Earth hypothesis: testing the limits of global change: *Terra Nova*, v. 14, p. 129–155, doi:<https://doi.org/10.1046/j.1365-3121.2002.00408.x>.
- Johnston, C.G., and Vestal, J.R., 1993, Biogeochemistry of oxalate in the antarctic cryptoendolithic lichen-dominated community: *Microbial Ecology*, v. 25, p. 305–319, doi:[10.1007/BF00171895](https://doi.org/10.1007/BF00171895).
- Karl, D.M., Bird, D.F., Björkman, K., Houlihan, T., Shackelford, R., and Tupas, L., 1999, Microorganisms in the accreted ice of Lake Vostok, Antarctica: *Science*, v. 286, p. 2144–2147, doi:[10.1126/science.286.5447.2144](https://doi.org/10.1126/science.286.5447.2144).
- Kleinteich, J., Wood, S.A., Küpper, F.C., Camacho, A., Quesada, A., Frickey, T., and Dietrich, D.R., 2012, Temperature-related changes in polar cyanobacterial mat diversity and toxin production: *Nature Climate Change*, v. 2, p. 356–360, doi:[10.1038/nclimate1418](https://doi.org/10.1038/nclimate1418).
- Kyle, J.E., Schroeder, P.A., and Wiegel, J., 2007, Microbial silicification in sinters from two terrestrial hot springs in the Uzon Caldera, Kamchatka, Russia: *Geomicrobiology Journal*, v. 24, p. 627–641, doi:[10.1080/01490450701672158](https://doi.org/10.1080/01490450701672158).
- Levy, J.S., Fountain, A.G., Gooseff, M.N., Welch, K.A., and Lyons, W.B., 2011, Water tracks and permafrost in Taylor Valley, Antarctica: Extensive and shallow groundwater

- connectivity in a cold desert ecosystem: *Bulletin of the Geological Society of America*, v. 123, p. 2295–2311, doi:[10.1130/B30436.1](https://doi.org/10.1130/B30436.1).
- Li, Y., Scales, N., Blankenship, R.E., Willows, R.D., and Chen, M., 2012, Extinction coefficient for red-shifted chlorophylls: Chlorophyll d and chlorophyll f: *Biochimica et Biophysica Acta - Bioenergetics*, v. 1817, p. 1292–1298, doi:[10.1016/j.bbabi.2012.02.026](https://doi.org/10.1016/j.bbabi.2012.02.026).
- Lyons, W.B., Dailey, K.R., Welch, K.A., Deuerling, K.M., Welch, S.A., and McKnight, D.M., 2015, Antarctic streams as a potential source of iron for the Southern Ocean: *Geology*, v. 43, p. 1003–1006, doi:[10.1130/G36989.1](https://doi.org/10.1130/G36989.1).
- Marchant, D.R., and Head, J.W., 2007, Antarctic dry valleys: Microclimate zonation, variable geomorphic processes, and implications for assessing climate change on Mars: *Icarus*, v. 192, p. 187–222, doi:[10.1016/j.icarus.2007.06.018](https://doi.org/10.1016/j.icarus.2007.06.018).
- Margesin, R., and Miteva, V., 2011, Diversity and ecology of psychrophilic microorganisms.: *Research in microbiology*, v. 162, p. 346–361, doi:[10.1016/j.resmic.2010.12.004](https://doi.org/10.1016/j.resmic.2010.12.004).
- Marra, K.R., Madden, M.E.E., Soreghan, G.S., and Hall, B.L., 2015, BET surface area distributions in polar stream sediments: Implications for silicate weathering in a cold-arid environment: *Applied Geochemistry*, v. 52, p. 31–42, doi:<https://doi.org/10.1016/j.apgeochem.2014.11.005>.
- Marra, K.R., Madden, M.E.E., Soreghan, G.S., and Hall, B.L., 2017, Chemical weathering trends in fine-grained ephemeral stream sediments of the McMurdo Dry Valleys, Antarctica: *Geomorphology*, v. 281, p. 13–30, doi:[10.1016/j.geomorph.2016.12.016](https://doi.org/10.1016/j.geomorph.2016.12.016).
- Marra, K.R., Soreghan, G.S., Madden, M.E.E., Keiser, L.J., and Hall, B.L., 2014, Trends in grain size and BET surface area in cold–arid versus warm–semiarid fluvial systems: *Geomorphology*, v. 206, p. 483–491, doi:<https://doi.org/10.1016/j.geomorph.2013.10.018>.
- McKinley, J.P., Stevens, T.O., and Westall, F., 2000, Microfossils and paleoenvironments in deep subsurface basalt samples: *Geomicrobiology Journal*, v. 17, p. 43–54, doi:[10.1080/014904500270486](https://doi.org/10.1080/014904500270486).
- Meeks, J.C., and Castenholz, R.W., 1971, Growth and photosynthesis in an extreme thermophile, *Synechococcus lividus* (Cyanophyta): *Archiv für Mikrobiologie*, v. 78, p. 25–41, doi:[10.1007/BF00409086](https://doi.org/10.1007/BF00409086).
- Mergelov, N. et al., 2018, Alteration of rocks by endolithic organisms is one of the pathways for the beginning of soils on Earth: *Scientific Reports*, v. 8, p. 1–15, doi:[10.1038/s41598-018-21682-6](https://doi.org/10.1038/s41598-018-21682-6).
- Miller, S.R., and Castenholz, R.W., 2001, Ecological Physiology of *Synechococcus* sp. Strain SH-94-5, a Naturally Occurring Cyanobacterium Deficient in Nitrate Assimilation: *Applied and Environmental Microbiology*, v. 67, p. 3002–3009, doi:[10.1128/AEM.67.7.3002-3009.2001](https://doi.org/10.1128/AEM.67.7.3002-3009.2001).
- Montross, S.N., Skidmore, M., Tranter, M., Kivimäki, A.L., and Parkes, R.J., 2013, A microbial driver of chemical weathering in glaciated systems: *Geology*, v. 41, p. 215–218, doi:[10.1130/G33572.1](https://doi.org/10.1130/G33572.1).

- Nielsen, U.N., Wall, D.H., Adams, B.J., Virginia, R.A., Ball, B.A., Gooseff, M.N., and McKnight, D.M., 2012, The ecology of pulse events: insights from an extreme climatic event in a polar desert ecosystem: *Ecosphere*, v. 3, p. art17, doi:<https://doi.org/10.1890/ES11-00325.1>.
- Oddsson, B., Gudmundsson, M.T., Edwards, B.R., Thordarson, T., Magnússon, E., and Sigurðsson, G., 2016, Subglacial lava propagation, ice melting and heat transfer during emplacement of an intermediate lava flow in the 2010 Eyjafjallajökull eruption: *Bulletin of Volcanology*, v. 78, p. 48, doi:[10.1007/s00445-016-1041-4](https://doi.org/10.1007/s00445-016-1041-4).
- Olsson-Francis, K., Pearson, V.K., Steer, E.D., and Schwenzer, S.P., 2017, Determination of Geochemical Bio-Signatures in Mars-Like Basaltic Environments: *Frontiers in microbiology*, v. 8, p. 1668, doi:[10.3389/fmicb.2017.01668](https://doi.org/10.3389/fmicb.2017.01668).
- Olsson-Francis, K., Simpson, A.E., Wolff-Boenisch, D., and Cockell, C.S., 2012, The effect of rock composition on cyanobacterial weathering of crystalline basalt and rhyolite: *Geobiology*, v. 10, p. 434–444, doi:<https://doi.org/10.1111/j.1472-4669.2012.00333.x>.
- Phillips-Lander, C.M., Harrold, Z., Hausrath, E.M., Lanzirrotti, A., Newville, M., Adcock, C.T., Raymond, J.A., Huang, S., Tschauner, O., and Sanchez, A., 2020, Snow Algae Preferentially Grow on Fe-containing Minerals and Contribute to the Formation of Fe Phases: *Geomicrobiology Journal*, v. 37, p. 572–581, doi:[10.1080/01490451.2020.1739176](https://doi.org/10.1080/01490451.2020.1739176).
- Ramette, A., 2007, Multivariate analyses in microbial ecology: *FEMS Microbiol Ecol*, v. 62, p. 142–160, doi:[10.1111/j.1574-6941.2007.00375.x](https://doi.org/10.1111/j.1574-6941.2007.00375.x).
- Raymond, J.A., Christner, B.C., and Schuster, S.C., 2008, A bacterial ice-binding protein from the Vostok ice core: *Extremophiles*, v. 12, p. 713–717, doi:[10.1007/s00792-008-0178-2](https://doi.org/10.1007/s00792-008-0178-2).
- Rimstidt, J.D., 2013, *Geochemical Rate Models: An Introduction to Geochemical Kinetics*: Cambridge University Press, doi:[10.1017/CBO9781139342773](https://doi.org/10.1017/CBO9781139342773).
- Ríos, A.D.L., Wierzchos, J., and Ascaso, C., 2014, The lithic microbial ecosystems of Antarctica's McMurdo Dry Valleys: *Antarctic Science*, v. 25, p. 459–477, doi:[10.1017/S0954102014000194](https://doi.org/10.1017/S0954102014000194).
- Ríos, A.D.L., Wierzchos, J., Sancho, L.G., and Ascaso, C., 2003, Acid microenvironments in microbial biofilms of antarctic endolithic microecosystems: *Environmental Microbiology*, v. 5, p. 231–237, doi:[10.1046/j.1462-2920.2003.00417.x](https://doi.org/10.1046/j.1462-2920.2003.00417.x).
- Rivkina, E., Abramov, A., Spirina, E., Petrovskaya, L., Shatilovich, A., Shmakova, L., Scherbakova, V., and Vishnivetskaya, T., 2018, Earth's perennially frozen environments as a model of cryogenic planet ecosystems: *Permafrost and Periglacial Processes*, v. 29, p. 246–256, doi:[10.1002/ppp.1987](https://doi.org/10.1002/ppp.1987).
- Schulze-Makuch, D., Irwin, L.N., Lipps, J.H., LeMone, D., Dohm, J.M., and Fairén, A.G., 2005, Scenarios for the evolution of life on Mars: *Journal of Geophysical Research E: Planets*, v. 110, p. 1–12, doi:[10.1029/2005JE002430](https://doi.org/10.1029/2005JE002430).
- Seckbach, J., Oren, A., and Stan-Lotter, H. (Eds.), 2013, *Polyextremophiles: Life Under Multiple Forms of Stress*: Dordrecht, Springer Netherlands, Cellular Origin, Life in Extreme Habitats and Astrobiology, v. 27, doi:[10.1007/978-94-007-6488-0](https://doi.org/10.1007/978-94-007-6488-0).

- Shcolnick, S., and Keren, N., 2006, Metal homeostasis in cyanobacteria and chloroplasts. Balancing benefits and risks to the photosynthetic apparatus: *Plant Physiology*, v. 141, p. 805–810, doi:[10.1104/pp.106.079251](https://doi.org/10.1104/pp.106.079251).
- Shoenfelt, E.M., Winckler, G., Annett, A.L., Hendry, K.R., and Bostick, B.C., 2019, Physical Weathering Intensity Controls Bioavailable Primary Iron(II) Silicate Content in Major Global Dust Sources: *Geophysical Research Letters*, v. 46, p. 10854–10864, doi:[10.1029/2019GL084180](https://doi.org/10.1029/2019GL084180).
- Stumpf, A.R., Madden, M.E.E., Soreghan, G.S., Hall, B.L., Keiser, L.J., and Marra, K.R., 2012, Glacier meltwater stream chemistry in Wright and Taylor Valleys, Antarctica: Significant roles of drift, dust and biological processes in chemical weathering in a polar climate: *Chemical Geology*, v. 322–323, p. 79–90, doi:[10.1016/j.chemgeo.2012.06.009](https://doi.org/10.1016/j.chemgeo.2012.06.009).
- Till, R., 1974, *Statistical Methods for the Earth Scientist*: Macmillan Education UK, doi:[10.1007/978-1-349-15536-1](https://doi.org/10.1007/978-1-349-15536-1).
- Ugolini, F.C., and Bockheim, J.G., 2008, Antarctic soils and soil formation in a changing environment: A review: *Geoderma*, v. 144, p. 1–8, doi:[10.1016/j.geoderma.2007.10.005](https://doi.org/10.1016/j.geoderma.2007.10.005).
- Vincent, W.F., Gibson, J.A.E., Pienitz, R., Villeneuve, V., Broady, P.A., Hamilton, P.B., and Howard-Williams, C., 2000, Ice shelf microbial ecosystems in the high arctic and implications for life on snowball earth: *Naturwissenschaften*, v. 87, p. 137–141, doi:[10.1007/s001140050692](https://doi.org/10.1007/s001140050692).
- Wackernagel, H., 2003, *Multivariate Geostatistics*: Springer Berlin Heidelberg, doi:[10.1007/978-3-662-05294-5](https://doi.org/10.1007/978-3-662-05294-5).
- Welch, S.A., and Ullman, W.J., 1999, The effect of microbial glucose metabolism on bytownite feldspar dissolution rates between 5° and 35°C: *Geochimica et Cosmochimica Acta*, v. 63, p. 3247–3259, doi:[https://doi.org/10.1016/S0016-7037\(99\)00248-3](https://doi.org/10.1016/S0016-7037(99)00248-3).
- Wild, B., Imfeld, G., Guyot, F., and Daval, D., 2018, Early stages of bacterial community adaptation to silicate aging: *Geology*, v. 46, p. 555–558, doi:[10.1130/G40283.1](https://doi.org/10.1130/G40283.1).
- Ye, Q., Tong, J., Xiao, S., Zhu, S., An, Z., Tian, L., and Hu, J., 2015, The survival of benthic macroscopic phototrophs on a Neoproterozoic snowball Earth: *Geology*, v. 43, p. 507–510, doi:[10.1130/G36640.1](https://doi.org/10.1130/G36640.1).
- Yergeau, E., Bokhorst, S., Kang, S., Zhou, J., Greer, C.W., Aerts, R., and Kowalchuk, G.A., 2012, Shifts in soil microorganisms in response to warming are consistent across a range of Antarctic environments: *The ISME Journal*, v. 6, p. 692–702, doi:[10.1038/ismej.2011.124](https://doi.org/10.1038/ismej.2011.124).

TABLES

Table 2.1. Physical characteristics of Antarctic and Icelandic sediments

Location	BET (m ² /g)	Clay (<4μm) grain size (%)	Silt (4-63 μm) grain size (%)
Antarctica	8.2	3.8	96.2
Iceland	11.5	2	98

Table 2.2. Chemical and mineralogical characteristics of Antarctic and Icelandic sediments

Location	SiO ₂ (%)	Al ₂ O ₃ (%)	P ₂ O ₅ (%)	Fe ₂ O ₃ (%)	MnO (%)	Mafic minerals (%)	Quartz + K-spar (%)	Plagioclase (%)	Clay minerals (%)	Amorphous phases (%)
Antarctica	56.4	15	0.3	8.6	0.1	12.2	16.2	28.8	37.6	3.2
Iceland	52.9	15.6	0.5	11.8	0.2	25.9	0	38.7	0	31.6

Table 2.3. BET normalized comparative Si release rates (mol/m²s)

Replicate	<i>Antarctica</i>			<i>Iceland</i>		
	Biotic	Abiotic	Biotic/Abiotic	Biotic	Abiotic	Biotic/Abiotic
1	7.0 x 10 ⁻¹⁵	4.0 x 10 ⁻¹⁵	1.8	1.0 x 10 ⁻¹⁴	9.0 x 10 ⁻¹⁵	1.1
2	1.0 x 10 ⁻¹⁴	3.0 x 10 ⁻¹⁵	3.3	9.0 x 10 ⁻¹⁵	1.0 x 10 ⁻¹⁴	0.9
3	9.0 x 10 ⁻¹⁵	2.0 x 10 ⁻¹⁵	4.5	1.0 x 10 ⁻¹⁴	9.0 x 10 ⁻¹⁵	1.1
Average	8.7 x 10 ⁻¹⁵	3.0 x 10 ⁻¹⁵	3.2	9.7 x 10 ⁻¹⁵	9.0 x 10 ⁻¹⁵	1.0
Standard deviation	1.3 x 10 ⁻¹⁵	8.2 x 10 ⁻¹⁶	1.1	4.7 x 10 ⁻¹⁶	8.2 x 10 ⁻¹⁶	0.1

FIGURES

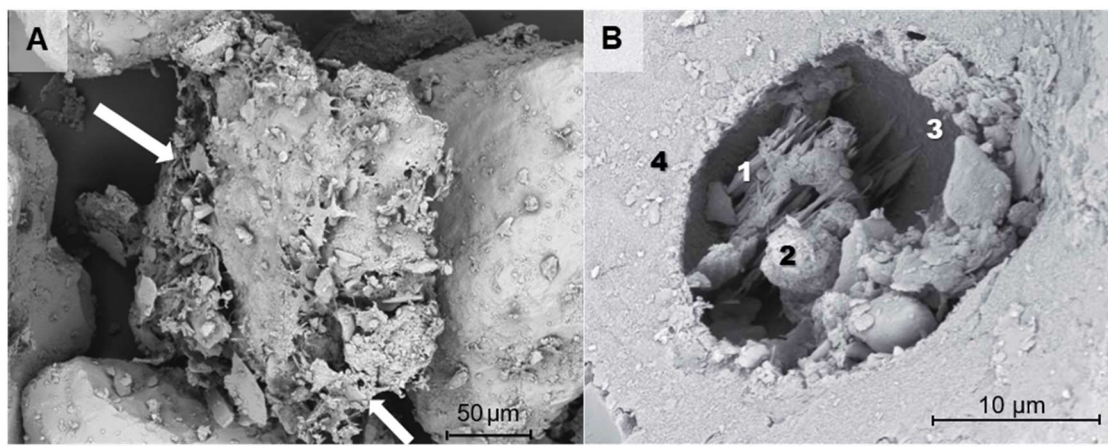


Figure 2.1. SEM images of untreated Antarctic drift (B: Ross Sea Drift, TV), sediment (A, E, F: Delta Stream, TV; D: Clark Glacier Stream, WV) and soil (C: Upper Onyx River, WV) samples. Numbers indicate EDS measurement locations (Table S2.6). A: Side-by-side comparison of a biofilm covered (arrow) and uncolonized smooth grain shows that biofilms effectively disintegrate the sediments. B: Incongruent dissolution pits formed via abiotic weathering and secondary blade-like potential Ca-carbonates (EDS #1) and spherical Fe-bearing carbonates (EDS #2) are observed. C: Exfoliation (flaking) of the mineral surface (arrows). D: Exfoliation features are generally associated with biofilms (arrows). E: EPS covering mineral surfaces leave large grooves on mineral surfaces via etching (arrows). F: Close-up of the etched grooves in Fig.

1E (white box) shows nanophase spherical Fe precipitates (putative inorganic biosignatures) nucleating on and within the biofilm layer.

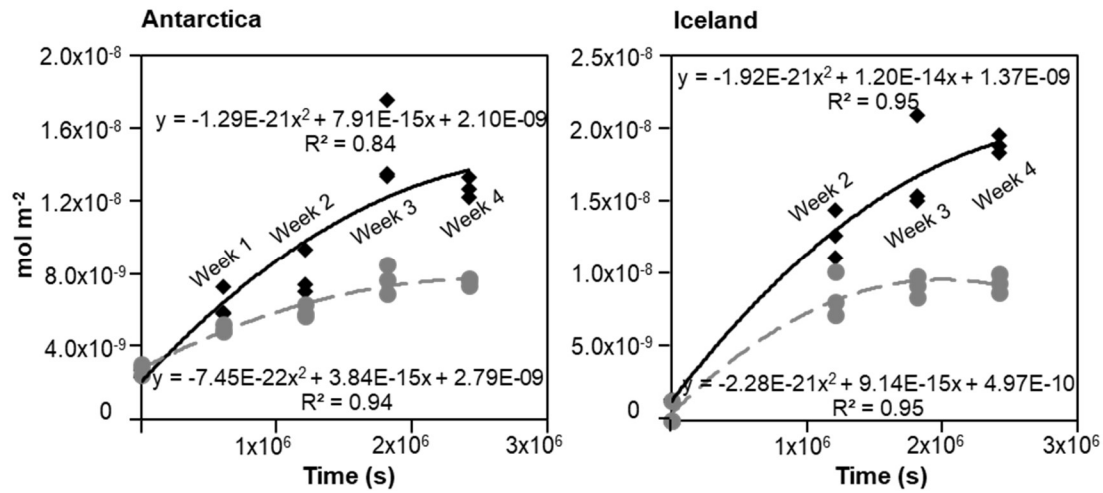


Figure 2.2. Antarctic and Icelandic silica release normalized to BET surface area (mol/m^2). Solid black and dashed gray lines are biotic and abiotic weathering trend lines, respectively. Note the higher biotic weathering rates (diamonds) as compared to abiotic weathering rates (circles).

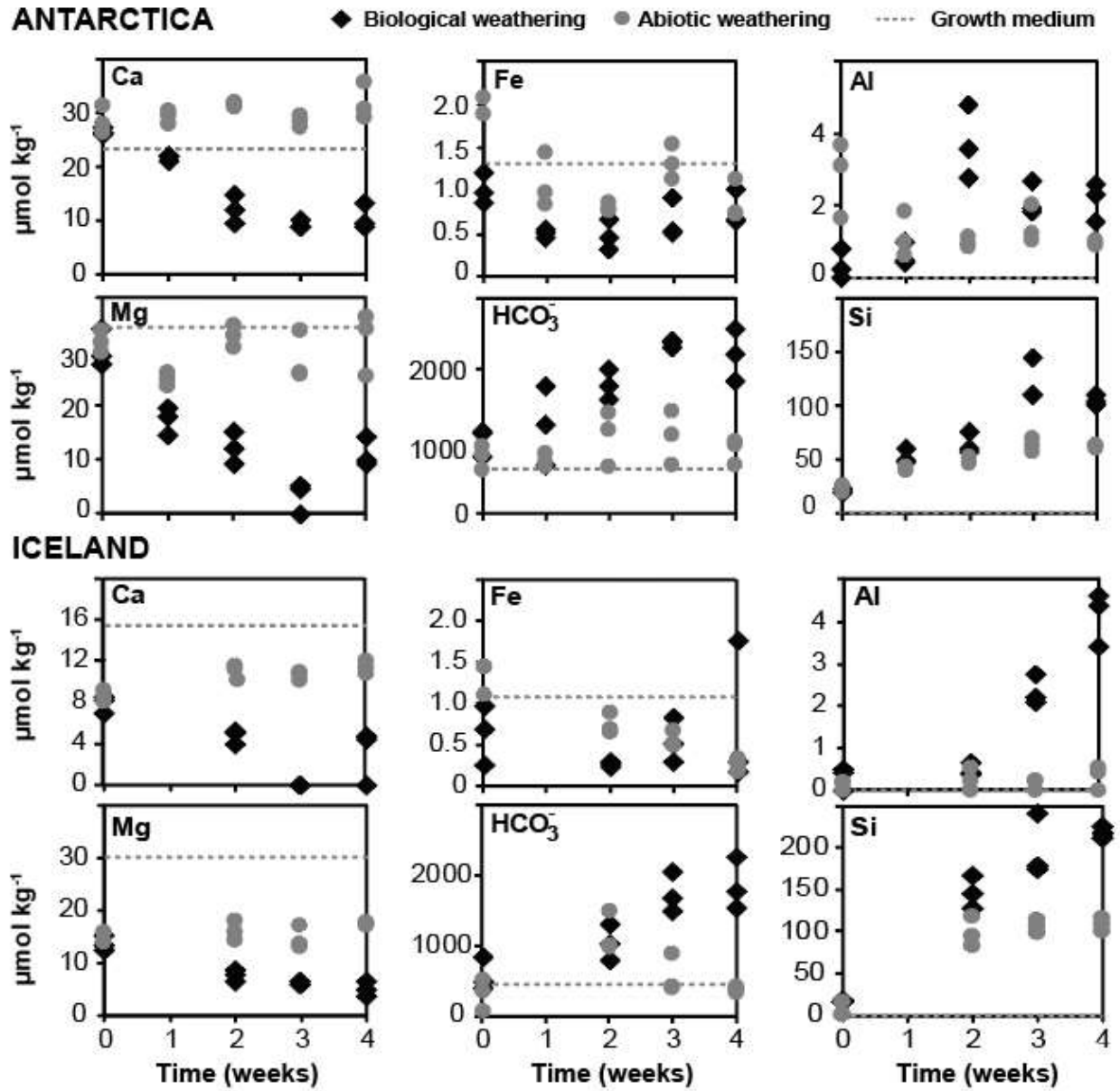


Figure 2.3. Changes in solute chemistry during Antarctic and Icelandic biotic (diamonds) and abiotic (circles) experiments. Dotted lines mark initial concentrations in the growth medium. Note the significant biotic intake of bio-essential nutrients (Ca, Mg, Fe), while HCO_3^- , Al and Si increase due to silicate weathering.

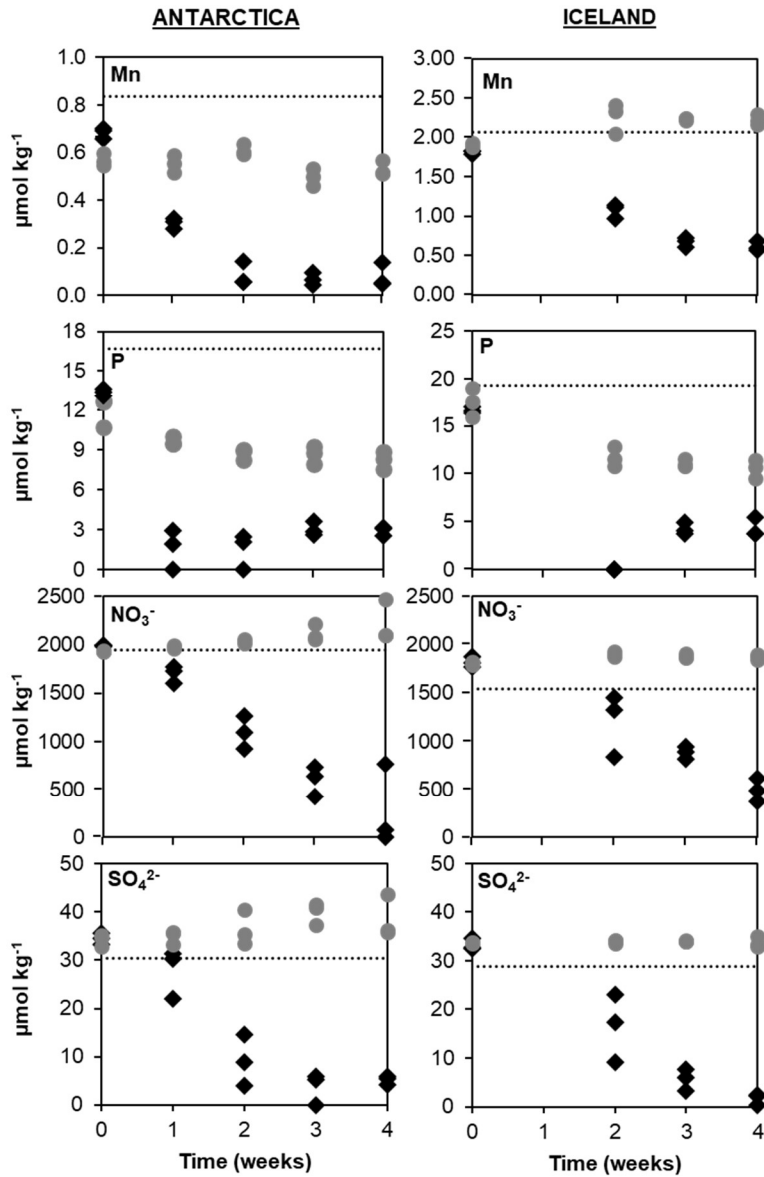


Figure 2.4. Changes in Mn, P, NO₃⁻, and SO₄²⁻ concentrations during Antarctica and Iceland biotic (diamonds) and abiotic (circles) weathering experiments. Mn, P and NO₃⁻ are consumed by *L. glacialis* as they are essential for the photosystems. SO₄²⁻ depletion in the biological experiments is likely due to microbial use.

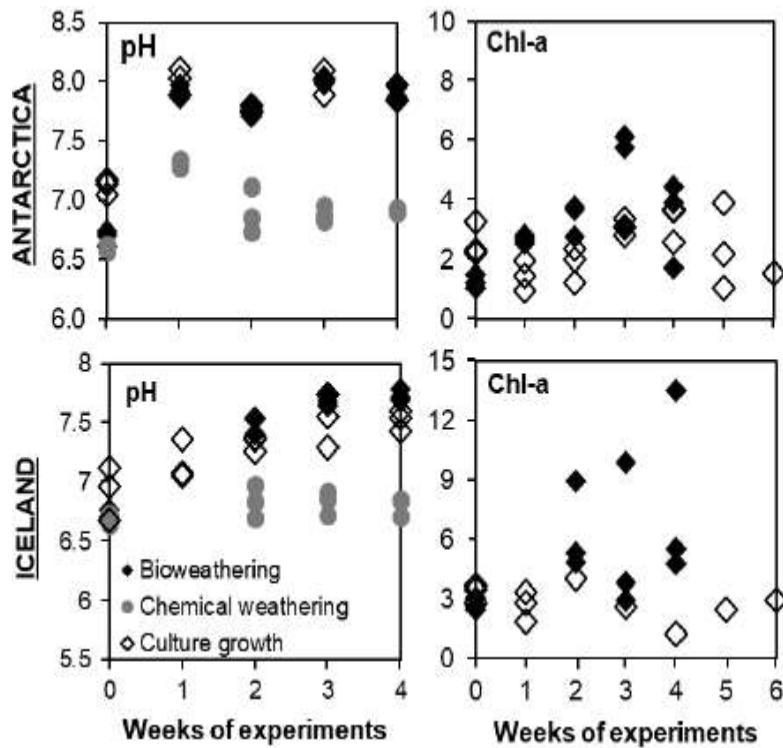


Figure 2.5. Changes in pH and chlorophyll-a (Chl-a; $\mu\text{g/ml}$) during Antarctic and Icelandic biotic (solid diamonds) and abiotic (circles) experiments. Hollow diamonds indicate culture growth experiments. Note the increase in pH with Chl-a in bioweathering and culture growth experiments due to photosynthesis, as opposed to nearly constant abiotic pH.

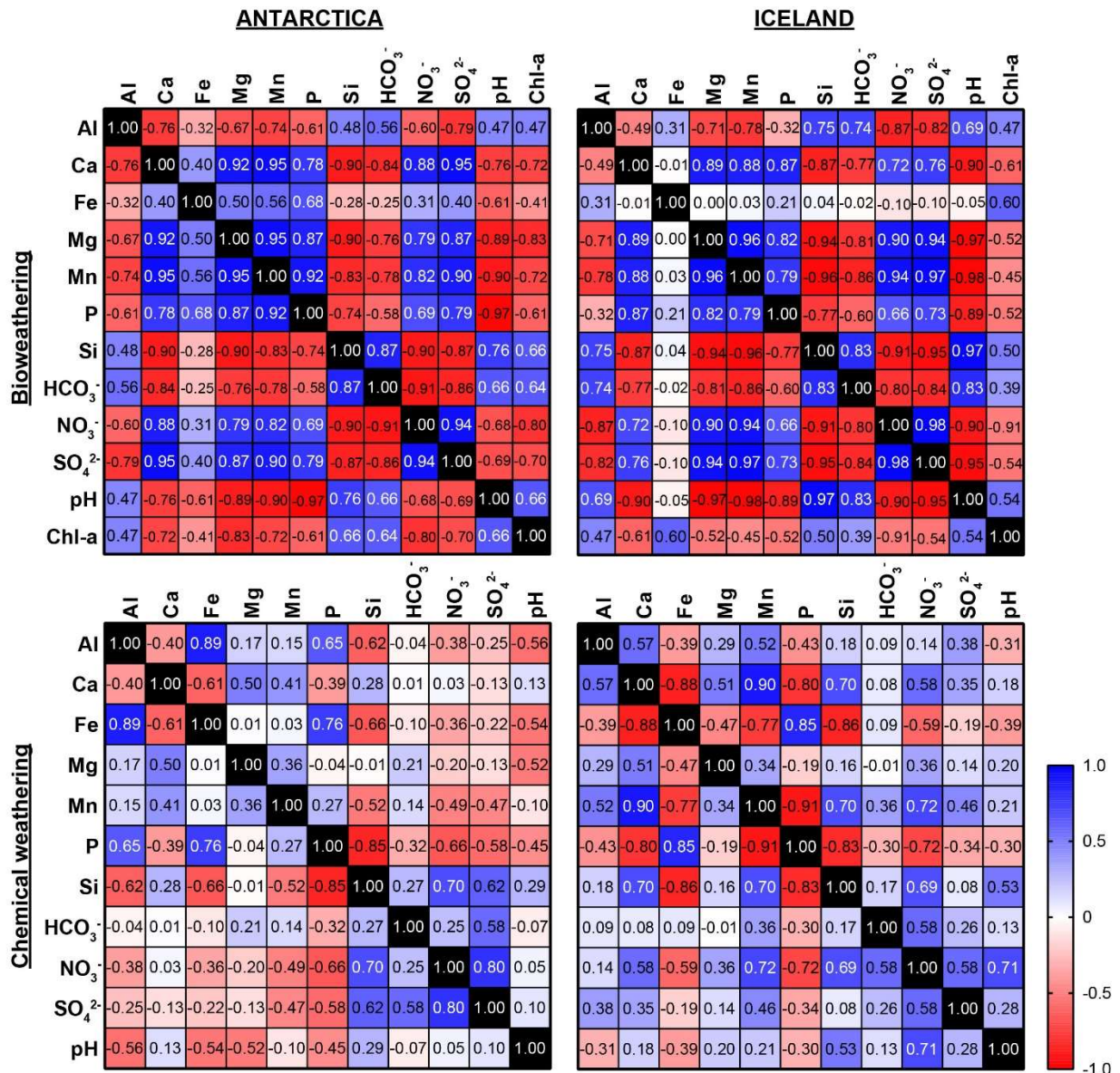


Figure 2.6. Pearson's Correlation matrices of Antarctic (A), and Icelandic (B) bioweathering and abiotic weathering experiments. Numbers in the cells are calculated r scores, while color transitions from dark to light correspond to their graduation from higher to lower correlation. Red colors (negative values) indicate negative, and blue colors (positive values) indicate positive correlation between the variables.

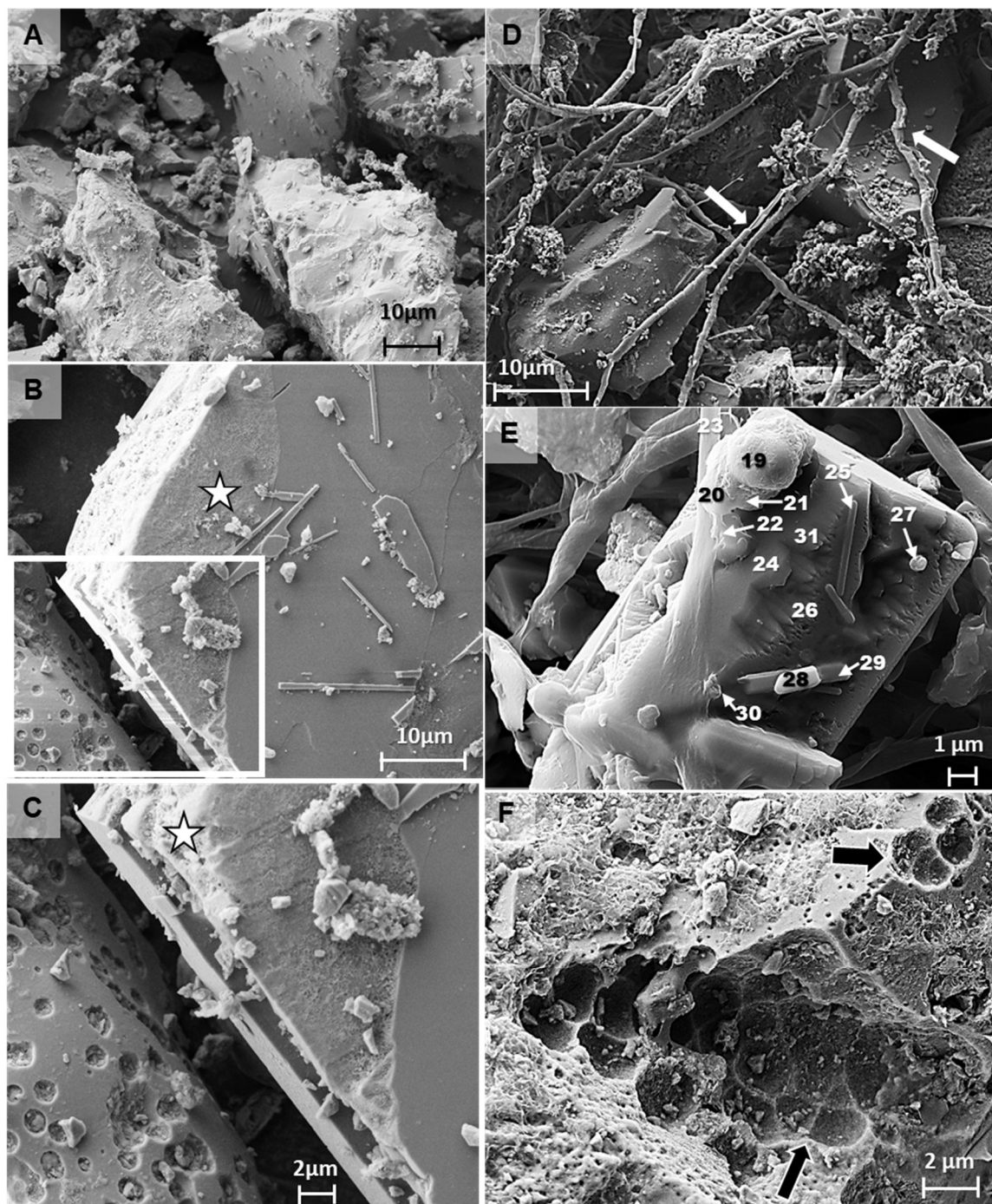


Figure 2.7. SEM images from the fourth week of Icelandic abiotic and biological weathering experiments. Numbers indicate EDS measurement locations (Table S6). A: Illustration of the overall case for abiotic experiments at a magnification of 1.17 kX. Sediments in abiotic experiments illustrate mostly smooth surfaces. B: An etched surface (star) detected on a potential

plagioclase grain. C: Close-up look at the boxed area in Figure 2.7B. As expected, abiotic chemical weathering starts from the corner of the mineral (star) and creates a somewhat smoother surface as opposed to deep-pitted bioweathered minerals (e.g., Figure 2.7F). Note that the lower left grain with pits is a vesicular basalt, not a weathered grain. D: *L. glacialis* filaments forms a mesh trapping sediments and binding them with their EPS (arrows). E: A highly weathered Mg- and Fe-rich mineral (potentially olivine; EDS #24, 31) covered with biofilm (EDS #23) and colonized by bacteria (e.g. EDS #25), showing spherical secondary Fe-(hydr)oxide precipitation (EDS #20-21, 27, 30). Note that there are apatite minerals (EDS #28, 29) detected on the surface, which might make the mineral favorable for colonization. F: Etch pits (arrows) left by coccus (tetrad) shaped colonies resembling to Figure 2.7B, indicating that other microbes in the mat assist weathering. Note that mineral surface around the pits are flakey.

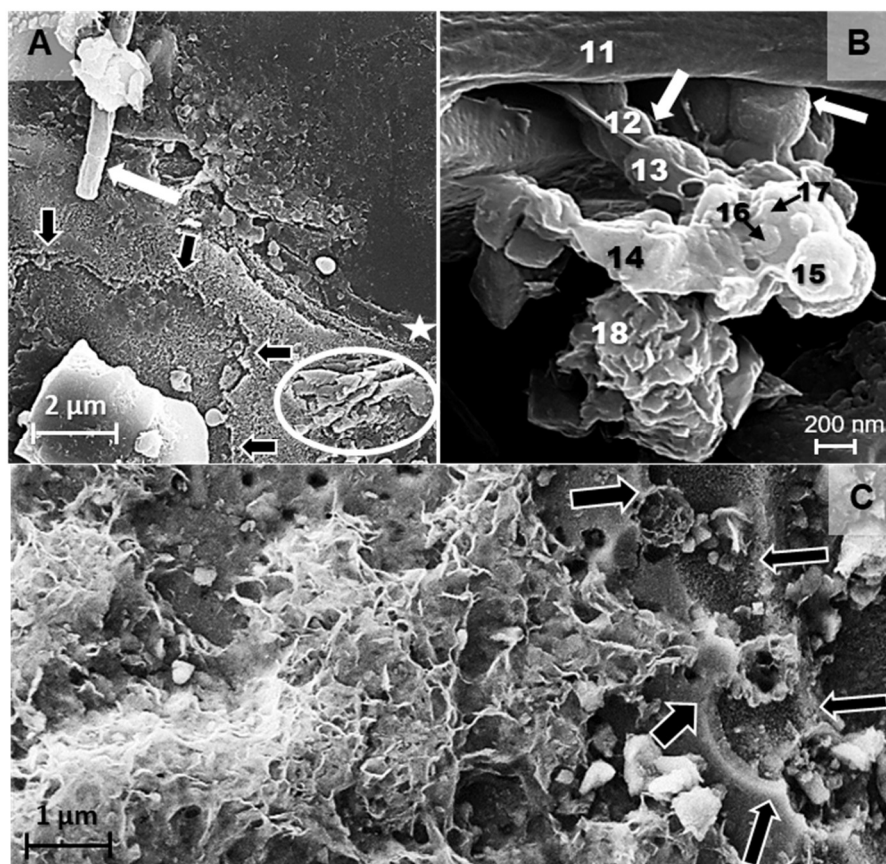


Figure 2.8. SEM images showing cyanobacteria filament shaped etch pits, biominerals nucleating on cells and flakey surface deposits in Icelandic bioweathering experiments. Numbers indicate EDS measurement locations (Table S2.6). A: *L. glacialis* (white arrow), filament shaped etch-pit (star) on a mineral surface. Notice that the mineral surface displays other etching features associated with biofilm attachment (black arrows) and chemical dissolution (circle). B: Secondary nano-phase Fe-(hydr)oxides (EDS #15-17) nucleating on coccus-shaped cell surfaces (white arrows) and a potential clay precipitate associated with biofilms (EDS #18). C: Close-up on a region of flakey surfaces shown in Figure 2.7F. These honeycomb-like features are potentially neo-formed clays produced by bioweathering. Notice the stepwise etching associated with cells and biofilm traced by black arrows.

Chapter 3. Limited bioweathering by cyanobacteria in cold, nutrient-limited conditions: Implications for microbe-mineral interactions and aquatic chemistry in cold environments

Cansu Demirel-Floyd¹, G. S. Soreghan¹, J. G. Floyd² and M. E. Elwood Madden¹

¹School of Geosciences, University of Oklahoma, Norman, OK 73019, USA

²Cemvita Factory, Westminster, CO

Key Words: Antarctica; cyanobacteria; bioweathering; chemical weathering, nutrient fluxes; salt weathering

Abstract

Solute fluxes in Antarctic meltwaters indicate microbial processes influence chemical weathering. Antarctic cyanobacterial mats dominated by *Leptolyngbya glacialis* enhance weathering rates at 12°C, yet their effects on nutrient fluxes in colder, nutrient-limited conditions similar to environments in the McMurdo Dry Valleys is unknown. Here we investigate biotic and abiotic weathering rates of glaciofluvial sediments at 4°C and compare results to previous experiments at 12°C. We also examine the effects of nutrient and salt concentrations on weathering fluxes by comparing the effects of different media concentrations (0.1X and 0.001X: 10 and 1000 times diluted) at both temperature conditions. Our results show limited evidence of biologically mediated silica release at 4°C, yet microbe-mineral interactions still affect nutrient fluxes, particularly for Ca, Mg, Mn, P and N. However, increased initial salt concentrations (0.001X to 0.1X media) also increased the amount of solutes release under abiotic conditions. These results indicate that both aqueous solutes and temperature are important factors controlling weathering rates and nutrient fluxes in cold settings.

INTRODUCTION

Throughout the last ~3 Ga, cyanobacteria have survived across climatic extremes (i.e., Costa et al., 2018), as well as being tolerant of multiple other environmental stressors, including extremes in UV radiation, salinity, nutrient availability, etc. (Wynn-Williams and Edwards, 2002). Polyextremophilic cyanobacterial mats are therefore model organisms for extraterrestrial life (Wynn-Williams and Edwards, 2002), as well as for investigating potential extraterrestrial biosignatures (i.e., Demirel-Floyd et al., 2022) and early Earth biogeochemical cycling (e.g., Mergelov et al., 2018). Cyanobacterial mats also provide oxygenated oases and refugia for

benthic mat communities, as inferred by fossil algae occurrences, as well as steroid and lipid data within Marinoan-aged glaciogenic units (Ye et al., 2015; Brocks et al., 2017; Shizuya et al., 2021) which document cyanobacteria survival during rapidly shifting conditions in the Neoproterozoic Snowball Earth intervals (Hoffman et al., 1998; Hoffman and Schrag, 2002; Fairchild and Kennedy, 2007). Therefore, cold-tolerant benthic phototrophic mats may significantly affect nutrient fluxes within cold and nutrient-limited settings, such as glacial meltwaters.

Cyanobacterial EPS (Extracellular Polymeric Substances) production (micro-environmental pH decrease due to organic acids) and photosynthesis-related pH increase are associated with weathering for a range of environments and lithologies (Omelon, 2008), as demonstrated by observations of chemical weathering products in South African sandstones (Büdel, 2004), as well as Antarctic MDV and East Antarctica granites, gneiss and sandstone (de los Ríos et al., 2003, 2007; Büdel et al., 2008; Archer et al., 2017), where neo-formed Fe-(hydr)oxides and clays were found associated with biofilms within weathered zones (Mergelov et al., 2018). However, few studies have investigated silicate weathering and measurements of weathering rates by cyanobacteria experimentally in the laboratory (i.e., Olsson-Francis et al., 2012; Demirel-Floyd et al., 2022). The few previous experimental studies reported in the literature were conducted at the upper limits of psychrophilic (12°C, Demirel-Floyd et al., 2022) or mesophilic (25°C, Olsson-Francis et al., 2012) temperatures where cyanobacteria can easily grow, leaving weathering at cold-temperatures analogous to Antarctic meltwater streams unstudied.

Though formerly considered a barren desert due to frigid conditions, Antarctic soils, ice, lakes, cryoconite holes and fluvial systems host a diverse microbial community that contributes

to biogeochemical cycles at rates comparable to temperate environments (McKnight et al., 1999, 2004; Price, 2000; Karr et al., 2003; de la Torre et al., 2003; Gilichinsky et al., 2007; Cary et al., 2010; Cowan et al., 2010, Anesio and Laybourn-Parry, 2012; Van Horn et al., 2016; Smith et al., 2017). Based on Smith et al. (2017)'s study of an Antarctic McMurdo Dry Valley (MDV) supraglacial stream emanating from Cotton Glacier, photosynthetic primary production exceeds heterotrophic respiration and heterotrophic communities rely on annual supplies of microbially produced organic C within meltwaters. Algal mats within the MDVs additionally affect inorganic N and P cycles via significant nitrate and phosphate uptake, as inferred from in-situ nutrient injection experiments (McKnight et al., 2004). These C, N, and P nutrient pools and their relationships with microbial metabolic processes are well studied individually. However, microbe-mediated silicate weathering may additionally impact Antarctic nutrient fluxes, contributing to global biogeochemical cycles through both atmospheric CO₂ drawdown via photosynthesis and bicarbonate production and release of nutrients that feed the Southern Ocean communities (Lyons et al., 2015, Demirel-Floyd et al., 2022). Yet our understanding of the factors controlling bioweathering and subsequent nutrient fluxes at cold temperatures observed in glacial settings is limited (i.e., Montross et al., 2013).

Numerous studies suggest that EPS produced by Antarctic cyanobacterial mats can weather sandstone, granite and gneiss based on SEM-EDS (Scanning Electron Microscopy – Energy-Dispersive X-Ray Spectroscopy, TEM (Transmission Electron Microscopy), CSLM (Confocal Scanning Laser Microscopy), and NanoSIMS (Nanoscale Secondary Ion Mass Spectrometry) studies (i.e., de los Ríos et al., 2003, 2007; Büdel et al., 2008; Archer et al., 2017; Mergelov et al., 2018). De los Ríos et al. (2003) used a pH indicator dye to show that the EPS around cyanobacterial cells had a pH of 3.5, suggesting that organic acids produced by

cyanobacteria can chemically weather silicates. EPS layer and filamentous cyanobacteria were also observed in association with exfoliation structures (de los Ríos et al., 2003, 2007, Mergelov et al., 2018), suggesting that they also contribute to physical weathering, which increases reactive surface area for chemical weathering.

Microbial mats that are largely dominated by filamentous cyanobacteria commonly occur in Antarctic MDV meltwater streams (McKnight et al., 1999, 2004; Van Horn et al., 2016). These mats are mostly composed of *Oscillatoria* sp., *Phormidium* sp., *Nostoc* sp., and *Leptolyngbya* sp. (Howard-Williams and Vincent, 1989; Vincent and James, 1996). We previously studied bioweathering with a cold-tolerant non-axenic cyanobacterial mat dominated by *Leptolyngbya glacialis* (*L. glacialis*) at 12°C, the average optimal growth temperature of Antarctic cyanobacterial mats (Kleinteich et al., 2012; Cornet et al., 2018). However, 12°C is at the highest range of surface soil temperatures observed on the continent (Balks et al., 2002; Dolgikh et al., 2015). Results revealed that this benthic mat community enhances Si weathering rates by three-fold compared to abiotic weathering under identical conditions at 12°C (Demirel-Floyd et al., 2022). We hypothesized that polyextremophilic cyanobacteria weathering rates would increase further under colder and nutrient-stressed conditions due to enhanced production of extracellular polymeric substance (EPS), resulting in release of organic acids. In this study we test this hypothesis by investigating biotic and abiotic silicate weathering and nutrient release at different temperature (4°C and 12°C) and nutrient conditions (0.1X and 0.001X) using the same felsic-mixed sourced Antarctic glaciofluvial sediments and basaltic Iceland glacio-volcanic outwash sediments used in the Demirel-Floyd et al. (2022) experiments.

METHODS

Sampling and Geological Setting

In order to investigate the effects of cyanobacteria on silicate weathering rates, we chose to use fine-grained, heterogeneous siliciclastic sediments collected in natural systems. We used the mud (<63 μm) fraction of felsic-mixed source Antarctic and basaltic Icelandic glaciofluvial sediments collected from slackwater regions of marginal channel bars in previous field campaigns (Stumpf et al., 2012; Marra et al., 2014, 2015, 2017; Demirel-Floyd et al., 2022).

Antarctic sediments were collected from Wright Valley, one of the E-W trending, virtually ice-free valleys within the Antarctic McMurdo Dry Valleys (MDV), where mean annual temperature (MAT) ranges from -14°C to -30°C and mean annual precipitation (MAP; mostly snowfall) is 100 mm/yr, creating cold desert conditions (Fountain et al., 1999; Doran et al., 2002, 2008). We collected the Antarctic sediments used in this study from the Onyx River ($n = 3$; 77 27.0030 S, 162 29.8580 E; 77 27.3180 S, 162 28.5810 E; 77 27.7870 S, 162 26.5670 E) which is fed by meltwater from cold-based Wright Lower Glacier and Clark Glacier within Wright Valley. The Onyx River drains over and potentially contains sediments derived from several glacial drifts that were deposited before the Last Glacial Maximum (LGM, e.g., Brownworth, Valkyrie, Loop, Peleus and various Alpine drifts), as well as glacial sediments derived from the Ferrar Dolerite and underlying plutons composed of diorite, granite, granodiorite, and quartz monazite (Hall et al., 1993; Hall and Denton, 2005). Samples were collected during the January 2010 field season (Stumpf et al., 2012; Marra et al., 2014, 2015, 2017) and remained frozen until sample processing for use in experiments.

Additional glaciofluvial samples were also collected from Iceland in May 2017. Iceland is underlain by mafic volcanic rocks erupted from 13 Mya-present (Andrews and Eberl, 2007). The MAT ranges between $0-4^{\circ}\text{C}$, with a MAP >600 mm/year that supports vegetation (Olafsson et al., 2007). Glacio-volcanic processes (magma-ice interactions) occasionally cause explosive

basaltic magma eruptions, followed by meltwater flooding known as glacial outburst floods (Sigmundsson et al., 2010). We sampled basaltic Iceland sediments from one of the modern glacial outwash streams of the Eyjafjallajökull volcano that feeds into the Katla glaciovolcanic outwash flood plains (n = 3; 63 40.8580 N, 19 38.0320 W; 6340.9760 N, 19 38.1680 W; 6340.1780 N, 19 37.5040 W) to investigate Si weathering rates of fresh, mafic, glacial deposits, compared to felsic-mixed sourced sediments (Demirel-Floyd et al., 2022).

Sample Processing and Characterization

We used subsamples of the same sediment previously processed for our 12°C bioweathering studies (Demirel-Floyd et al. 2022) to keep our results directly comparable. We merged Onyx River sediments to represent felsic-mixed sourced Antarctic fluvial watersheds, and also separately merged the Eyjafjallajökull outwash sediments. We wet-sieved the two merged samples through a <63- μ m mesh to obtain fine-grained sediments with relatively high surface area (glacial muds). Any water-soluble salts are also washed away in the sieving process. We treated these glacial muds with acetic acid (overnight) and hydrogen peroxide (3 days) to remove any carbonates, as well as sulfide mineral and organic fractions, allowing us to focus on solute fluxes released from the silicate mineral fraction. We added dispersant and analysed the grain size (clay% and silt%) of the treated glacial muds using a Malvern Mastersizer 3000 laser particle size analyzer and quantified their specific surface area using the Brunauer-Emmett-Teller (BET) nitrogen adsorption method, with a Quantachrome Nova 2000e gas adsorption analyzer (refer to Table 2.1. in Chapter 2). We determined the mineralogy of the treated sediments with X-ray powder diffraction (XRD) using a Rigaku Ultima IV with a Cu radiation source and graphite monochromator, employing the Bragg–Brentano method (2–70° 2 θ angle

interval), using 0.02° step size and 2-second counting time and fixed slits settings. We determined the mineral composition quantitatively with MDI Jade software using the Reitveld refinement method (Table 3.1). Bulk chemical compositions of our samples were analysed by ALS Labs (ALS USA Inc., Reno, NV, USA) using the Li borate fusion method by Inductively Coupled Plasma Mass Spectrometry (ICP-MS) for whole rock geochemistry, and by acid-digestion method using Inductively Coupled Plasma Atomic Emission Spectroscopy (ICP-AES) for trace elements and base metals. Major oxide compositions of these sediments are reported in Table 3.3. Refer to supplementary materials for the whole suite of chemical analysis results (Table S3.1).

Culture Growth

We used subcultures of a non-axenic benthic mat-forming *L. glacialis* (ULC073) culture that was purchased from the Belgian Coordinated Collections of Microorganisms (Fernandez-to Carazo et al., 2011; Cornet et al., 2018) and used by Demirel-Floyd et al. (2022) in the previous 12°C experiments. The starting culture was initially grown at 12°C in BG11 freshwater medium (Sigma-Aldrich, St. Louis, MO, USA, catalog #C3061, adjusted pH 7 with 1 M KOH) in a rotary shaking incubator (Inova 42R with cyanobacterial growth lamp) at 60 rpm for 3 weeks, providing an 8-hour dark/16-hour light cycle, representing optimal conditions for the strain (Demirel-Floyd et al., 2022). We subcultured this initial growth in 1X BG11 at 4°C and 12°C separately for comparative temperature experiments, following the procedure above, but extended the growth period to 4 weeks to allow the cultures more time to grow under cold conditions (4°C).

Experimental Design

We set up separate biotic and abiotic weathering experiments to test the effects of temperature and aqueous solute concentrations independently, with each experiment replicated in triplicate (Figure 3.1). The first batch reactor experiments, referred to subsequently as *cold weathering experiments* were set up to measure weathering rates at 4°C and 0.1X BG11 (10 times diluted freshwater medium), replicating the experimental conditions in Demirel-Floyd et al. (2022) for direct comparison with previous results at 12 °C. A second set of batch reactor endpoint experiments were also conducted to compare solute fluxes as a function of both weathering solute concentration (0.1X BG11 and 0.001X BG11; Table 3.2) and temperature (4°C and 12°C). These are referred to subsequently as variable *weathering solute experiments*. Additionally, we conducted culture growth controls for each experimental condition to monitor aquatic chemistry changes without sediments. We set up each experiment in autoclave-sterilized 50 ml Erlenmeyer flasks with 25 ml of autoclave-sterilized BG11 medium that was adjusted to pH 7 with 0.5M KOH. Biotic experiments (biotic weathering and culture growth) were inoculated with ~25 mg of wet filamentous mat harvested by centrifuging at 12,000 rpm, followed by washing with autoclave-sterilized double-distilled water. All weathering experiments (biotic and abiotic) also contained 0.25g of UV-sterilized glacial mud. Each biotic and abiotic reactor in the *cold weathering experiments* lasted 0, 1, 2, 3, or 4 weeks, to determine weathering rates over a time period analogous to Antarctica's short and relatively dry austral summer. The *variable weathering solute experiments* were sampled only at the 0- and 4-week time points to quantify the concentrations of solutes accumulated during short-term weathering. Experiments were placed within an Inova 42R temperature-controlled incubator at 4°C or 12°C without shaking (so as not to disturb the microbial mats), with an 8-hour dark/16-hour light cycle via cyanobacterial growth lights of the incubator.

Sampling and Analyses

We sampled leachates from individual reactors of *cold weathering experiments* each week for four weeks, and *variable nutrient experiments* at week 0 and week 4, for pH, aquatic chemistry (major anions and cations), and alkalinity monitoring. Supernatants were withdrawn from each reactor and filtered with 0.2- μm syringe-tip filters to remove particulates and cells from the solution. We measured pH using an Orion pH meter on small aliquots of the unprocessed filtrates. Additional aliquots of unprocessed filtrates were sent to OSU Soil Labs (Stillwater, OK, USA) for bicarbonate and carbonate ion measurements via flow injection. Unprocessed filtrates were analysed by IC (Ion Chromatography) for major anions and acidified filtrates (with 1M HNO_3) were analysed by ICP-AES (Inductively Couple Plasma Atomic Emission Spectroscopy) for total elemental analysis at the Advanced Water Technology Center and J. Ranville Lab (Colorado School of Mines, Golden, CO, USA).

We used aqueous Si concentrations measured by ICP-AES to calculate BET surface area-normalized silicate weathering rates for Antarctica and Iceland. First, we plotted the surface area-normalized Si concentrations versus time elapsed, then fitted the curve with a polynomial equation, and finally, used the first derivative of the polynomial to determine the rate of biological and abiotic weathering (Rimstidt, 2013; Demirel-Floyd et al., 2022).

We sampled microbial mat samples from the biotic (biotic weathering and culture growth) reactors of the *cold weathering experiments* for microbial growth monitoring via Chlorophyll-a (Chl-a) measurements for 4 weeks. We extracted Chl-a from the microbial mats in 90% methanol at 25°C in the dark and measured the absorbance (A) values of the extract at 663 nm (for Chl-a) and 750 nm (to correct for interference) using UV/VIS spectrophotometry

(Genesys 6, Thermo Scientific, Waltham, MA, USA). Chl-a concentrations were calculated using Equation 3.1 (Fiore et al., 2000; Demirel-Floyd et al., 2022):

$$\text{Chl-a } (\mu\text{g}/\mu\text{l}) = (A_{663\text{nm}} - A_{750\text{nm}}) \times 12.7 \quad (3.1)$$

We also collected additional sediment and microbial mat samples from all experiments to monitor secondary weathering products (etch-pits, secondary minerals, etc.) via SEM.

Immediately after sampling, we fixed our samples with 2.5% glutaraldehyde, 50 mM lysine, and 0.1 M HEPES buffer (pH 7), followed by secondary fixation (1% OsO₄ in 0.1 M HEPES), stepwise EtOH dehydration (25%, 50%, 75%, 95%, and 100%), and finally stepwise chemical drying (HMDS:EtOH ratio 1:2, 1:1, and 2:1) to preserve the biofilms until imaging (Kyle et al., 2007; Fischer et al., 2012). Prior to imaging, we mounted our samples on Al studs using C tape, then we sputter-coated the samples with Au/Pd (10-nm coating) to create conductive specimens. We performed SEM coupled with EDS (Electron Dispersive Spectroscopy) analysis at the OU Samuel Roberts Noble Microscopy Laboratory, using a ThermoFisher Quattro ESEM (Environmental SEM) coupled with EDS at 15 kV and low vacuum conditions to reduce the surface charging effect.

Statistical Analyses

We performed multivariate statistical analyses to determine the most significant components driving the differences between biotically- and abiotically-derived aquatic chemistry after short-term weathering of glacial muds at different weathering conditions. Prior to statistical analysis, we performed multiplicative simple replacement to replace values below detection limits (BDL) (Palarea-Albaladejo and Martín-Fernández, 2013) by manually replacing each BDL with a value equal to 65% of the analytical detection limit. We included variables from multiple

data sets, thereby avoiding the constant sum problem (Aitchinson, 1982; Aitchinson and Greenacre, 2002; Filzmoser et al., 2009; Palarea-Albaladejo and Martín-Fernández, 2013).

We performed multivariate statistical analyses on the Antarctic and Icelandic data separately to identify variables contributing to significant differences between leachates produced by the different experimental groups using GraphPad Prism 9.0.2 software. We performed two-way ANOVA analyses of variance coupled with Tukey's multiple comparisons (Till, 1974) on our solute chemistry, using $p < 0.05$ threshold as an indication of significant microbial influence on silicate weathering, following methods discussed in detail throughout the existing reffliterature on compositional data analysis (Aitchinson, 1982; Aitchinson and Greenacre, 2002; Filzmoser et al., 2009; Palarea-Albaladejo and Martín-Fernández, 2013; Palarea-Albaladejo et al., 2014). Then we performed Principal Component Analysis (PCA), using GraphPad to apply the Kaiser rule and select for principal components (PCs) with eigenvalues >1 (Ramette, 2007).

RESULTS

Cold Temperature Weathering

In both the Antarctic and Icelandic experiments, the pH of the solution increased from pH 6.5-7 to ~7.3-7.6 within both the culture growth and biotic weathering reactors, while pH of the Antarctic abiotic weathering reactors stayed nearly constant, and pH only slightly increased from 6.4 to 6.8 in abiotic Icelandic experiments (Figure 3.2). Chlorophyll-a (Chl-a) concentrations within microbial mats increased throughout all experiments, recording microbial growth and photosynthetic activity. Note that Chl-a concentrations measured in the bioweathering experiments might not be representative of the relative mass of microbial mats within the

reactors due to mixing of sediment and microbial mats. Sediments might be attached to the mats, affecting the mass of mat sampled and resulting in lower apparent Chl-a concentrations. Refer to Table S3.2 and Table S3.3 for pH and Chl-a measurements, in addition to Figure 3.2.

Bicarbonate concentrations significantly increased in both Antarctic and Icelandic cold temperature biotic weathering reactors, while bicarbonate stayed relatively constant during abiotic experiments (Figure 3.3). Nitrate and sulfate concentrations showed similar trends between biotic and abiotic reactors. While nitrate increased in Antarctic reactors, we observed a decrease in nitrate after 4 weeks in both the biotic and abiotic Iceland weathering experiments (Figure 3.3). Complete datasets of the major anion chemistry are reported in Table S3.4.

Cation chemistry observed in both the biotic and abiotic weathering reactors largely show similar trends between Antarctic (Figure 3.4) and Icelandic (Figure 3.5) experiments. Concentrations of Al, Fe, P, and K decreased over time, while Si and Na increased within both biotic and abiotic reactors at 4°C. However, Ca and Mg concentrations decreased within biotic Antarctic weathering experiments but increased in the abiotic weathering experiments. Mn and P also steeply decreased in the biotic reactors, while Mn stayed constant, and P slightly decreased within the abiotic experiments (Figure 3.4). Within the Icelandic weathering experiments, Mn concentrations increased within abiotic reactors and Mg decreased in both the biotic and abiotic reactors (Figure 3.5). Note that we added KOH to the weathering solutes to adjust the pH, therefore, changes in K concentrations are not entirely representative of weathering processes. Complete datasets of total anion and cation analyses are reported in Table S3.5.

At the end of 4 weeks, $\sim 35 \mu\text{mol kg}^{-1}$ (biotic) and $45 \mu\text{mol kg}^{-1}$ (abiotic) of Si was released to the aquatic environment in Antarctic experiments (Figure 3.4, Table S3.5). Although

the abiotic reactors seemingly released more Si, weathering rates calculated by taking the derivative of the rate equation obtained by polynomial fitting of the surface-area-normalized Si release through time (Figure 3.6) showed comparable weathering rates in the biotic ($3.44 \times 10^{-15} \text{ mol m}^{-2} \text{ s}^{-1}$) and abiotic experiments ($3.40 \times 10^{-15} \text{ mol m}^{-2} \text{ s}^{-1}$, Table 3.3). Biotic reactors containing Iceland sediments released slightly more Si ($\sim 60 \mu\text{mol kg}^{-1}$) than the abiotic reactors ($\sim 56 \mu\text{mol kg}^{-1}$; Figure 3.5, Table S3.5). Biotic weathering rates calculated for Iceland experiments ($4.29 \times 10^{-15} \text{ mol m}^{-2} \text{ s}^{-1}$) exceed the abiotic weathering rates ($3.44 \times 10^{-15} \text{ mol m}^{-2} \text{ s}^{-1}$), as well as the weathering rates calculated for all Antarctic reactors (Figure 3.6, Table 3.3).

Variable Solute Concentration Experiments

Within the variable weathering solute experiments, the pH was always the highest in the presence of cyanobacteria, which is most abundant at 12°C and $0.1x$ weathering solute conditions (Figure 3.7 and Table S3.6). At cold conditions (4°C), the pH increase is slightly higher in Iceland experiments (6.4-7.5, on average) as compared to Antarctic ones (7.0-7.4, on average). However, at 12°C the Antarctic bioweathering reactors displayed higher pH values than the Icelandic experiments. Note that pH values observed in the biotic weathering reactors exceeded culture growth pH values at all nutrient-limited (dilute weathering solute, $0.001x$) conditions, while they are comparable in the higher nutrient reactors ($0.1x$).

To compare the differences in nutrient release between experiments that contained different concentrations of the starter medium, we normalized each nutrient concentration at the end of 4 weeks to their starting concentrations at week 0, thus determining the ratio of final: initial concentrations for each individual component. Then we took the logarithm of these ratios

(which we will refer to as log ratio changes) to avoid scaling issues within our illustrations and statistical analyses. We illustrate the results of our log ratio change total elemental analysis in Figures 3.8 (Antarctica) and 3.9 (Iceland). The complete dataset can be found at Table S3.7. Results of selected major anions are illustrated in Figure 3.10 (see Table S3.8 for the complete dataset).

Overall trends in solute concentrations show that differences between the biotic and abiotic reactors for many of the components (Al, Si, Fe, Mg, Mn, and P) were most pronounced in the biotic experiments conducted at 12°C with higher concentrations of weathering solutes (0.1x) (Figure 3.8 and Figure 3.9), with the exception of a significant Al increase within bioweathering experiments at 4°C in 0.1x, which is more pronounced within the Iceland reactors. At cold conditions, most of the reactors behave similarly, while higher log change ratios were observed within reactors with 0.001x starter weathering solutes, except for Si in all cases and Al in biotic weathering reactors. We additionally note decreasing concentrations of solutes within both the Antarctic (Si, Ca, Fe, Mg, Mn, P, and K) and Iceland (Si, Ca, Mg, Mn, P, and K) low concentration weathering solute (0.001x) experiments conducted at 12°C. Note that we added KOH to the weathering solutes to adjust the pH, therefore the magnitude of log changes in K might not be representative of weathering, although the direction of change in K concentration under various conditions is likely valid.

Our investigation of log ratio changes in selected major anions (Figure 3.10) shows that overall, bicarbonate increases were always more pronounced in the presence of cyanobacteria, with the largest change observed at 12°C in the higher concentration weathering solute experiments. We noted decreasing bicarbonate concentrations for all of the low-concentration weathering solute reactors, while decreases were more pronounced within the biological reactors.

Within abiotic reactors, we observed increasing sulfate concentrations at the 4°C experiments, except the 0.001x reactors. On the other hand, within biotic reactors, sulfate decreased in all 4°C reactors, except for the 0.001x culture growth reactors. Nitrite was always observed in the presence of cyanobacteria, with increasing concentrations observed within the low concentration (0.001x) weathering solute experiments, but decreasing concentrations observed within the higher weathering solute (0.1x) experiments. We observed decreasing nitrate concentrations within both the biological weathering and culture growth experiments at 12°C, while nitrate significantly decreased in the 12°C 0.001x abiotic reactors. However, we observed increasing nitrate concentrations within all of the 4°C, 0.001x reactors.

DISCUSSION

Effects of Cyanobacteria on Weathering Rates at Cold Temperatures

At cold conditions (4°C), biotic weathering rates ($3.44 \times 10^{-15} \text{ mol m}^{-2} \text{ s}^{-1}$) are slightly, but not significantly, higher than abiotic weathering rates ($3.40 \times 10^{-15} \text{ mol m}^{-2} \text{ s}^{-1}$) in Antarctic reactors, whereas the biotic weathering rates ($4.29 \times 10^{-15} \text{ mol m}^{-2} \text{ s}^{-1}$) are notably higher than abiotic weathering rates ($3.49 \times 10^{-15} \text{ mol m}^{-2} \text{ s}^{-1}$) in Iceland reactors. These results indicate that microbial weathering is more pronounced in mafic lithologies compared to felsic-intermediate lithologies in cold-weathering conditions, which is expected given the greater susceptibility of mafic minerals to chemical weathering (Goldich, 1983).

PCA analysis of the aquatic chemistry resulting from cold (4°C) biotic and abiotic weathering of Antarctica and Iceland glacial muds (Figure 3.11) show biotic and abiotic data points clustering away from each other at the end of 4 weeks, suggesting that cyanobacterial weathering significantly affects the aquatic chemistry in both mafic and felsic systems.

Simultaneous pH increases with increasing Chl-a concentrations in all biotic weathering and culture growth experiments (Figure 3.2), as well as increasing Si and bicarbonate concentrations within biotic weathering reactors (Figures 3.3-3.5) suggest that silicate weathering occurs as a result of photosynthetic activity, in agreement with other reports of biotic weathering at warmer temperatures (Büdel et al., 2005; Olsson-Francis et al., 2012; Demirel-Floyd et al., 2022).

Carbon fixation via photosynthesis likely occurs at higher rates than atmospheric CO₂ diffusion, leading to higher HCO₃⁻ concentrations and producing OH⁻ ions that increase the pH observed in the macroenvironment (see Dupraz et al., 2009 for further details).

PCA analysis also indicates that Si, as well as Al and P concentrations are controlled by both biotic and abiotic factors in both felsic and mafic lithologies. We noted steep decreases in Mg, Ca, Mn and P concentrations in biotic reactors as compared to the abiotic experiments (Figure 3.4 and Figure 3.5), suggesting biotic uptake of these macro- and micro- nutrients which are needed for microbial metabolism and photosystems (Shcolnich and Keren, 2006). However, concentrations of these nutrients are also likely influenced by abiotic factors, based on the loading vectors of these components from our PCA at cold temperatures pointing towards abiotic weathering data points (Figure 3.11).

Effects of Temperature on Aquatic Chemistry and Weathering Rates

Increasing temperature from 4°C to 12°C resulted in a more than 2-fold increase in weathering rates in the Antarctic biotic weathering experiments (from $3.44 \times 10^{-15} \text{ mol m}^{-2} \text{ s}^{-1}$ to $7.91 \times 10^{-15} \text{ mol m}^{-2} \text{ s}^{-1}$), while abiotic weathering rates only increased slightly, resulting in no significant change with temperature (from $3.40 \times 10^{-15} \text{ mol m}^{-2} \text{ s}^{-1}$ to $3.84 \times 10^{-15} \text{ mol m}^{-2} \text{ s}^{-1}$; Table 3.3). In the Icelandic experiments, both biotic and abiotic weathering rates increased by 3-

fold (from $4.29 \times 10^{-15} \text{ mol m}^{-2} \text{ s}^{-1}$ to $1.20 \times 10^{-14} \text{ mol m}^{-2} \text{ s}^{-1}$ and $3.49 \times 10^{-15} \text{ mol m}^{-2} \text{ s}^{-1}$ to $9.14 \times 10^{-15} \text{ mol m}^{-2} \text{ s}^{-1}$, respectively) over the same temperature range (Table 3.3). These results suggest that temperature has a more pronounced effect on weathering rates in mafic lithologies as compared to felsic-intermediate lithologies. This conflicts with lower activation energies reported for volcanic glass, basalt, and basaltic river sediments (42 - 50 kJ/mol, Dessert et al., 2001; Wolff-Boenisch et al., 2004; Navarre Sitchler and Brantley, 2007) compared to granites, granitic regolith, and felsic rocks (61-74 kJ/mol; White and Blum, 1995; West et al., 2005; Rasmussen et al., 2011). Arrhenius equation calculations (Rimstidt, 2003) using the published activation energies demonstrate that the higher activation energies reported for granite (61 kJ/mol) are expected to result in a larger increase in dissolution rate with increasing temperature ($2.1 \text{ M}^{-1} \text{ s}^{-1}$) as compared to basalt (50 kJ/mol, yielding $1.8 \text{ M}^{-1} \text{ s}^{-1}$ increase in rate) between 4°C vs. 12°C . However, the Antarctic muds contain higher concentrations of clay minerals (Table 3.1), while Iceland sediments are relatively fresh and largely composed of volcanic glass, which may also explain the higher apparent weathering rates within Iceland sediments as compared to Antarctic sediments, where a smaller fraction of the sediment is likely to be reactive.

Within the felsic to intermediate Antarctic sediments, biotic weathering rates are more significantly affected by temperature than abiotic weathering, suggesting increased cyanobacterial growth at higher temperatures accelerates silicate weathering. Although the rates are slow compared to warmer temperatures, weathering still occurred, likely due to the general pH increase with photosynthesis (given increasing aqueous Si concentrations; Figures 3.4 and 3.5) and via acidic microenvironments that develop under EPS (e.g., de los Ríos et al., 2003). We observed etch-pits associated with microbial biofilms, as well as nano-phase secondary Fe-(hydr)oxide formation (Figure 3.13) as a byproduct of weathering, similar to those observed by

Demirel-Floyd et al. (2022) at 12°C. Note that we treated all the sediments with hydrogen peroxide to remove microbial mats prior to weathering experiments, so these microbes and the related textural/mineral context likely formed within the 4-week weathering experiments.

PCA also identified differences between cold- and warm-weathering processes and products based on aquatic chemistry (Figure 3.12). The PCA plots show that biotic and abiotic weathering results in different aquatic chemistry in all conditions, as indicated by biotic and abiotic data points clustering away from each other. In addition, comparative PCA showed that Si and bicarbonate concentrations, as well as pH are largely correlated with bioweathering at warmer conditions in both felsic and mafic lithologies. PCA results also indicate that Al was largely modulated by microbial processing in cold conditions, whereas every other component is controlled by both biotic and abiotic factors.

Based on previous microscopy-focused studies documenting cyanobacterial mediated chemical weathering in the MDV (i.e., de los Ríos et al., 2003, 2007; Büdel et al., 2008; Archer et al., 2017; Mergelov et al., 2018) and other literature reporting enhanced EPS production under environmental stress conditions (Dupraz et al., 2009; Marx et al., 2009; Margesin and Miteva, 2011), including observations of Antarctic microbes secreting more EPS at colder temperatures (Mancuso Nichols et al., 2004; Nevot et al., 2008), we initially hypothesized that cold-tolerant mat-forming cyanobacteria would increase biotic weathering rates at low temperatures and/or nutrient-deficient conditions due to enhanced EPS production under environmental stressors ((Dupraz et al., 2009; Marx et al., 2009; Margesin and Miteva, 2011; Mancuso Nichols et al., 2004; Nevot et al., 2008). However, our cold-weathering experiments at 4°C resulted in slower biologic weathering rates at cold conditions that are comparable to or only slightly faster than abiotic weathering rates (Table 3.3). Our results suggest that biologic weathering occurs at cold

temperatures with both felsic and mafic sediments, based on Si release and SEM images showing etch-pits in the vicinity of biofilms (Figure 3.13), but at 2-3-fold slower rates than those observed at warmer conditions (12°C) (Table 3.3; Demirel-Floyd et al., 2022). Previous studies showed that basalt weathering by various cyanobacterial strains (including a strain of *Leptolyngbya* sp.) also resulted in significantly faster Icelandic basalt weathering rates ($6.3 \times 10^{-13} \text{ mol m}^{-2} \text{ s}^{-1}$), at 25°C in distilled water spiked with 10 mM NaNO₂, (Table 3.3, Olsson-Francis et al., 2012), further indicating that weathering accelerates at optimum growth conditions when peak photosynthesis is reached.

Effects of Solute Concentration on Nutrient Release

Nutrient fluxes produced via both biotic and abiotic chemical weathering at 4°C differ significantly between experiments with different weathering solute concentrations (Figures 3.10 and 3.13). While solute concentrations did not considerably affect the culture growth experiments, potentially due to very limited growth of *L. glacialis* at 4°C (Kleinteich et al., 2012), ANOVA analyses showed significant differences in initial/final solute ratios 4°C with between experiments with different initial solute concentration in both the abiotic Antarctica and Iceland experiments ($p = <0.0001$ and 0.0049 , respectively). However, significant differences were not observed in the Antarctica and Iceland biotic weathering experiments with different initial weathering solute concentrations ($p = 0.9642$ and 0.9927 , respectively). These results suggest that in cold abiotic systems, solute concentrations can have a significant effect on weathering processes and products, but the presence of a biological mediator outweighs any differences in solute chemistry. While cyanobacterial weathering occurs at cold temperatures, evidenced by slightly higher biotic weathering rates as compared to abiotic rates within cold weathering experiments, and by the etch pits observed on colonized grains (Figure 3.13),

apparent nutrient release rates due to biotic weathering are similar to those observed in the abiotic experiments. However, at 12°C biotic and abiotic weathering, as well as the culture growth produce significantly different nutrient fluxes under different initial weathering solute concentrations.

We observed significant decreases in solute concentrations within the low-concentration weathering solute experiments at 12°C for both the Antarctic (Si, Ca, Fe, Mg, Mn, P, and K) and Iceland experiments (Si, Ca, Mg, Mn, P, and K) (Figure 3.8 and Figure 3.9). Our PCA results (Figure 3.14) suggest that these components are largely controlled by abiotic factors at warm temperatures in more dilute weathering solutes. We postulate that precipitation rates of these solutes exceed apparent weathering rates in dilute weathering solutes at 12°C, leading to the observed decrease in solute concentrations with time.

Effect of Environmental Conditions on Nitrogen Cycling Within Glacial Catchments

These results also indicate that N cycling in aquatic environments may be controlled by both the concentration of weathering solutes and temperature, in addition to the presence of microbial life. Previous work using nutrient injection experiments at Green Creek showed that microbial N cycles within the Antarctic MDV streams are controlled by nutrient availability, based on excessive algal nitrate uptake and nitrite and ammonium production following dissimilatory nitrate reduction (McKnight et al. 2004). Nitrogen fixation and denitrification has also been observed for Antarctic MDV and marine cyanobacteria (Howard-Williams et al., 1989; Perez et al., 2022). The temperature-controlled laboratory experiments reported here directly compare the effects of varying amounts of nutrients on microbially mediated nutrient fluxes, as

well as in abiotic controls, providing useful insights into N cycling in various glacial environmental conditions.

When nitrate is more available (within all 0.1X reactors) and temperature is not a growth-limiting factor (at 12°C), nitrate concentrations decreased along with nitrite within both biotic weathering and culture growth reactors likely due to microbial uptake; nitrate also decreased in abiotic reactors and nitrite was below detection (Figure 3.10). Alternatively, nitrate increased with nitrite in the cold- and nutrient-limited experiments (Figure 3.10), which might be indicative of nitrogen fixation under multiple growth-limiting conditions, supporting observations reported in Moisander et al. (2018) which indicated that dissolved inorganic nitrogen could decrease nitrogen-fixing gene (*nifH*) expression. Though studies suggest that micronutrient limitation (i.e., Fe and Mo) decreases nitrogen fixation activity (Rueter and Petersen, 1987; Bergman-Frank, 2007), and nitrogen fixation is largely an anaerobic process (Bergman et al., 1997), aerobic diazotrophic activity is observed in non-heterocystous Antarctic cyanobacteria (Benerjee and Verma, 2009; Pandey et al., 2004). Note that we provided alternating light (16 hr) and dark (8 hr) cycle to our culture and literature reviews note the nitrogen fixing ability of cyanobacteria in dark conditions (i.e., Bergman et al., 1997; Dupraz et al., 2009). At optimum growth temperature (12°C), but nutrient-limited conditions (0.001X), nitrate decreased in *L. glacialis* containing reactors, while nitrite increased (Figure 3.10), which is suggestive of intracellular nitrate reduction to nitrite upon assimilation when exposed to nitrogen limitation. Synthesis of the results and literature summarized here suggest environmental factors have significant effects on microbially mediated N cycles, while abiotic reactions (as inferred by results from the abiotic weathering reactors) also control inorganic nitrogen fluxes.

Abiotic Weathering by Dilute Solutions at Cold Temperatures: Salt Weathering

Our overall interpretations suggest that, at low-temperature conditions where abiotic dissolution rates are significantly slower (e.g., 4°C, cold weathering conditions), aqueous solute chemistry exerts a significant influence on chemical weathering rates and the resulting aquatic chemistry changes. We observed more abiotic silicate weathering in the experiments with higher initial salt concentrations (0.1x), compared to the 0.001x reactors, as inferred by increased Si release (Table S3.7; Figures 3.8 and 3.9). The initial weathering solution is dominated by Na (Table 3.2); previous studies have shown that increasing NaCl concentrations (up to 0.5 mol kg⁻¹) within dilute weathering solutions enhanced quartz weathering over a range of temperature (25°C-200°C) and pH conditions (Dove, 1999; Dove and Elston, 1992; Dove and Nix, 1997; and Icenhower and Dove, 2000). These studies suggest that SiO₃-Na complexes at the water-mineral interface (at pH 8) enhanced weathering by 12-fold due to the increased probability of Si-O bond hydrolysis. However, at higher concentrations, Phillips-Lander et al. (2019) observed that pyroxene weathering slowed with increasing NaCl concentrations (from 0.35 mol kg⁻¹ to 5.7 mol kg⁻¹) at 25°C. These observations suggest that silicate dissolution rates are less sensitive to differences in Na⁺ concentration in more concentrated solutions. However, Phillips-Lander et al. (2019) also reported faster weathering rates with increasing Na₂SO₄ concentrations (from 0.35 mol kg⁻¹ to 5.7 mol kg⁻¹), suggesting anion chemistry may also play an important role. Our abiotic weathering experiment results are similar to those observed in Dove and Elston (1992), suggesting increasing Na concentrations (from 4.5x10⁻⁵ mol kg⁻¹ to 2.2x10⁻³) in very dilute weathering solutes (Table 1) result in faster silicate weathering, as indicated by ~7-fold (4°C)

and 2-fold (12°C) increase in Si concentrations after 4 weeks of weathering in the experiments with higher initial solute concentrations (Figure 3.8, Figure 3.9, Table S3.7).

CONCLUSIONS

We initially hypothesized that cold-tolerant mat-forming cyanobacteria would increase biotic weathering rates at low temperatures and/or nutrient-deficient conditions due to higher production of EPS under environmental stressors. However, weathering rates observed at 4°C were 2-3-fold slower than the weathering rates calculated at 12°C, affirming that both biotic and abiotic factors affect weathering rates in cold aqueous systems. However, when environmental factors limit biological activity (e.g., cold weathering conditions, or nutrient limitation), abiotic weathering has a more pronounced effect on nutrient fluxes in aqueous settings. At 4°C, Si release rates were largely dependent on initial weathering solute chemistry, where increased weathering solute concentrations (higher concentrations of mixed cations and anions, including Na⁺, in the initial growth medium, from 0.001x to 0.1x) resulted in significantly more Si release over 4 weeks, suggesting that solute chemistry strongly influences chemical weathering in cold, nutrient-limited environments. Though biological growth and weathering is limited at cold- and nutrient-limited conditions, photosynthetic activity can still significantly affect aquatic chemistry, particularly concentrations of micro- and macro-nutrients including Ca, Mg, Mn, P and N.

ACKNOWLEDGEMENTS

We thank Kristin Marra, Brenda Hall, and Alison Stumpf for sample collection; Nina D.S. Webb for her assistance in sample processing; Preston Larson for his help in SEM imaging; Andy E. Elwood Madden for his help in XRD data analysis; and Claire Curry for her help in

statistical data analysis. We also thank Amy Callaghan, Boris Wavrick, Bradley S. Stevenson, Paul Lawson, and Anne Dunn for providing access to microbiology lab equipment and facilities. This project is funded by NSF grant number 1543344, “Quantifying Surface Area in Muds from the Antarctic Dry Valleys: Implications for Weathering in Glacial Systems.”

REFERENCES

- Aitchison, J., 1982, *The Statistical Analysis of Compositional Data*: v. 44, p. 139–177, doi:<https://doi.org/10.1111/j.2517-6161.1982.tb01195.x>.
- Aitchison, J., and Greenacre, M., 2002, Biplots of compositional data: *Journal of the Royal Statistical Society: Series C (Applied Statistics)*, v. 51, p. 375–392, doi:[10.1111/1467-9876.00275](https://doi.org/10.1111/1467-9876.00275).
- Andrews, J.T., and Eberl, D.D., 2007, Quantitative Mineralogy of Surface Sediments on the Iceland Shelf, and Application to Down-Core Studies of Holocene Ice-Rafted Sediments: *Journal of Sedimentary Research*, v. 77, p. 469–479, doi:[10.2110/jsr.2007.045](https://doi.org/10.2110/jsr.2007.045).
- Anesio, A.M., and Laybourn-Parry, J., 2012, Glaciers and ice sheets as a biome: *Trends in Ecology and Evolution*, v. 27, p. 219–225, doi:[10.1016/j.tree.2011.09.012](https://doi.org/10.1016/j.tree.2011.09.012).
- Archer, S.D.J., de los Ríos, A., Lee, K.C., Niederberger, T.S., Cary, S.C., Coyne, K.J., Douglas, S., Lacap-Bugler, D.C., and Pointing, S.B., 2017, Endolithic microbial diversity in sandstone and granite from the McMurdo Dry Valleys, Antarctica: *Polar Biology*, v. 40, p. 997–1006, doi:[10.1007/s00300-016-2024-9](https://doi.org/10.1007/s00300-016-2024-9).
- Balks, M.R., Paetzold, R.O.N.F., Kimble, J.M., Aislabie, J.M., and Campbell, I.B., 2002, Effects of hydrocarbon spills on the temperature and moisture regimes of Cryosols in the Ross Sea region: *Antarctic Science*, v. 14, p. 319–326, doi:[10.1017/S0954102002000135](https://doi.org/10.1017/S0954102002000135).
- Banerjee, M., and Verma, V., 2009, Nitrogen fixation in endolithic cyanobacterial communities of the McMurdo Dry Valley, Antarctica: *ScienceAsia*, v. 35, p. 215, doi:[10.2306/scienceasia1513-1874.2009.35.215](https://doi.org/10.2306/scienceasia1513-1874.2009.35.215).
- Bergman, B., Gallon, J.R., Rai, A.N., and Stal, L.J., 1997, N₂ Fixation by non-heterocystous cyanobacteria: *FEMS Microbiology Reviews*, v. 19, p. 139–185, doi:[10.1111/j.1574-6976.1997.tb00296.x](https://doi.org/10.1111/j.1574-6976.1997.tb00296.x).
- Berman-Frank, I., Quigg, A., Finkel, Z.V., Irwin, A.J., and Haramaty, L., 2007, Nitrogen-fixation strategies and Fe requirements in cyanobacteria: *Limnology and Oceanography*, v. 52, p. 2260–2269, doi:[10.4319/lo.2007.52.5.2260](https://doi.org/10.4319/lo.2007.52.5.2260).
- Brocks, J.J., Jarrett, A.J.M., Sirantoine, E., Hallmann, C., Hoshino, Y., and Liyanage, T., 2017, The rise of algae in Cryogenian oceans and the emergence of animals: *Nature*, v. 548, p. 578–581, doi:[10.1038/nature23457](https://doi.org/10.1038/nature23457).

- Büdel, B., Bendix, J., Bicker, F.R., and Allan Green, T.G., 2008, Dewfall as a Water Source Frequently Activates the Endolithic Cyanobacterial Communities in the Granites of Taylor Valley, Antarctica: *Journal of Phycology*, v. 44, p. 1415–1424, doi:[10.1111/j.1529-8817.2008.00608.x](https://doi.org/10.1111/j.1529-8817.2008.00608.x).
- Büdel, B., Weber, B., Kühl, M., Pfan, H., Sültemeyer, D., and Wessels, D., 2004, Reshaping of sandstone surfaces by cryptoendolithic cyanobacteria: bioalkalization causes chemical weathering in arid landscapes: *Geobiology*, v. 2, p. 261–268, doi:[10.1111/j.1472-4677.2004.00040.x](https://doi.org/10.1111/j.1472-4677.2004.00040.x).
- Cary, S.C., McDonald, I.R., Barrett, J.E., and Cowan, D.A., 2010, On the rocks: The microbiology of Antarctic Dry Valley soils: *Nature Reviews Microbiology*, v. 8, p. 129–138, doi:[10.1038/nrmicro2281](https://doi.org/10.1038/nrmicro2281).
- Cornet, L., Bertrand, A.R., Hanikenne, M., Javaux, E.J., Wilmotte, A., and Baurain, D., 2018, Metagenomic assembly of new (Sub)polar cyanobacteria and their associated microbiome from non-axenic cultures: *Microbial Genomics*, v. 4, doi:[10.1099/mgen.0.000212](https://doi.org/10.1099/mgen.0.000212).
- Costa, O.Y.A., Raaijmakers, J.M., and Kuramae, E.E., 2018, Microbial Extracellular Polymeric Substances: Ecological Function and Impact on Soil Aggregation: *Frontiers in Microbiology*, v. 9, <https://www.frontiersin.org/article/10.3389/fmicb.2018.01636> (accessed June 2022).
- Cowan, D.A., Khan, N., Pointing, S.B., and Cary, S.C., 2010, Diverse hypolithic refuge communities in the McMurdo Dry Valleys: *Antarctic Science*, v. 22, p. 714–720, doi:[10.1017/S0954102010000507](https://doi.org/10.1017/S0954102010000507).
- De Los Ríos, A., Grube, M., Sancho, L.G., and Ascaso, C., 2007, Ultrastructural and genetic characteristics of endolithic cyanobacterial biofilms colonizing Antarctic granite rocks: *FEMS Microbiology Ecology*, v. 59, p. 386–395, doi:[10.1111/j.1574-6941.2006.00256.x](https://doi.org/10.1111/j.1574-6941.2006.00256.x).
- De Los Ríos, A., Wierchos, J., Sancho, L.G., and Ascaso, C., 2003, Acid microenvironments in microbial biofilms of antarctic endolithic microecosystems: *Environmental Microbiology*, v. 5, p. 231–237, doi:[10.1046/j.1462-2920.2003.00417.x](https://doi.org/10.1046/j.1462-2920.2003.00417.x).
- Demirel-Floyd, C., Soreghan, G.S., and Madden, M.E.E., 2022, Cyanobacterial weathering in warming periglacial sediments: Implications for nutrient cycling and potential biosignatures: *Permafrost and Periglacial Processes*, v. 33, p. 63–77, doi:[10.1002/ppp.2133](https://doi.org/10.1002/ppp.2133).
- Dessert, C., Dupré, B., François, L.M., Schott, J., Gaillardet, J., Chakrapani, G., and Bajpai, S., 2001, Erosion of Deccan Traps determined by river geochemistry: impact on the global climate and the $^{87}\text{Sr}/^{86}\text{Sr}$ ratio of seawater: *Earth and Planetary Science Letters*, v. 188, p. 459–474, doi:[10.1016/S0012-821X\(01\)00317-X](https://doi.org/10.1016/S0012-821X(01)00317-X).
- Dolgikh, A.V., Mergelov, N.S., Abramov, A.A., Lupachev, A.V., and Goryachkin, S.V., 2015, Soils of Enderby Land, *in* Bockheim, J.G. ed., *The Soils of Antarctica*, Cham, Springer International Publishing, World Soils Book Series, p. 45–63, doi:[10.1007/978-3-319-05497-1_4](https://doi.org/10.1007/978-3-319-05497-1_4).
- Doran, P.T., McKay, C.P., Clow, G.D., Dana, G.L., Fountain, A.G., Nylen, T., and Lyons, W.B., 2002, Valley floor climate observations from the McMurdo dry valleys, Antarctica, 1986–

- 2000: *Journal of Geophysical Research: Atmospheres*, v. 107, p. ACL 13-1-ACL 13-12, doi:[10.1029/2001JD002045](https://doi.org/10.1029/2001JD002045).
- Doran, P.T., McKay, C.P., Fountain, A.G., Nylén, T., McKnight, D.M., Jaros, C., and Barrett, J.E., 2008, Hydrologic response to extreme warm and cold summers in the McMurdo Dry Valleys, East Antarctica: *Antarctic Science*, v. 20, p. 499–509, doi:[10.1017/S0954102008001272](https://doi.org/10.1017/S0954102008001272).
- Dove, P.M., 1999, The dissolution kinetics of quartz in aqueous mixed cation solutions: *Geochimica et Cosmochimica Acta*, v. 63, p. 3715–3727, doi:[10.1016/S0016-7037\(99\)00218-5](https://doi.org/10.1016/S0016-7037(99)00218-5).
- Dove, P.M., and Elston, S.F., 1992, Dissolution kinetics of quartz in sodium chloride solutions: Analysis of existing data and a rate model for 25°C: *Geochimica et Cosmochimica Acta*, v. 56, p. 4147–4156, doi:[10.1016/0016-7037\(92\)90257-J](https://doi.org/10.1016/0016-7037(92)90257-J).
- Dove, P.M., and Nix, C.J., 1997, The influence of the alkaline earth cations, magnesium, calcium, and barium on the dissolution kinetics of quartz: *Geochimica et Cosmochimica Acta*, v. 61, p. 3329–3340, doi:[10.1016/S0016-7037\(97\)00217-2](https://doi.org/10.1016/S0016-7037(97)00217-2).
- Dupraz, C., Reid, R.P., Braissant, O., Decho, A.W., Norman, R.S., and Visscher, P.T., 2009, Processes of carbonate precipitation in modern microbial mats: *Earth-Science Reviews*, v. 96, p. 141–162, doi:[10.1016/j.earscirev.2008.10.005](https://doi.org/10.1016/j.earscirev.2008.10.005).
- Fairchild, I.J., and Kennedy, M.J., 2007, Neoproterozoic glaciation in the Earth System: *Journal of the Geological Society*, v. 164, p. 895–921, doi:[10.1144/0016-76492006-191](https://doi.org/10.1144/0016-76492006-191).
- Fernandez-Carazo, R., Hodgson, D.A., Convey, P., and Willemotte, A., 2011, Low cyanobacterial diversity in biotopes of the Transantarctic Mountains and Shackleton Range (80–82°S), Antarctica: *FEMS Microbiology Ecology*, v. 77, p. 503–517, doi:[10.1111/j.1574-6941.2011.01132.x](https://doi.org/10.1111/j.1574-6941.2011.01132.x).
- Filzmoser, P., Hron, K., and Reimann, C., 2009, Principal component analysis for compositional data with outliers: *Environmetrics*, v. 20, p. 621–632, doi:[10.1002/env.966](https://doi.org/10.1002/env.966).
- Fiore, M.F., Moon, D.H., Tsai, S.M., Lee, H., and Trevors, J.T., 2000, Miniprep DNA isolation from unicellular and filamentous cyanobacteria: *Journal of Microbiological Methods*, v. 39, p. 159–169, doi:[10.1016/S0167-7012\(99\)00110-4](https://doi.org/10.1016/S0167-7012(99)00110-4).
- Fischer, E.R., Hansen, B.T., Nair, V., Hoyt, F.H., and Dorward, D.W., 2012, Scanning Electron Microscopy: *Current Protocols in Microbiology*, v. 25, doi:[10.1002/9780471729259.mc02b02s25](https://doi.org/10.1002/9780471729259.mc02b02s25).
- Fountain, A.G. et al., 1999, Physical Controls on the Taylor Valley Ecosystem, Antarctica: *BioScience*, v. 49, p. 961–971, doi:[10.1525/bisi.1999.49.12.961](https://doi.org/10.1525/bisi.1999.49.12.961).
- Gilichinsky, D.A. et al., 2007, Microbial populations in Antarctic permafrost: Biodiversity, stage, age, and implication for astrobiology: *Astrobiology*, v. 7, p. 275–311, doi:[10.1089/ast.2006.0012](https://doi.org/10.1089/ast.2006.0012).
- Goldich, S.S., 1938, A Study in Rock-Weathering: *The Journal of Geology*, v. 46, p. 17–58.

- Hall, B.L., and Denton, G.H., 2005, Surficial geology and geomorphology of eastern and central Wright Valley, Antarctica: *Geomorphology*, v. 64, p. 25–65, doi:[10.1016/j.geomorph.2004.05.002](https://doi.org/10.1016/j.geomorph.2004.05.002).
- Hall, B.L., Denton, G.H., Lux, D.R., and Bockheim, J.G., 1993, Late Tertiary Antarctic Paleoclimate and Ice-Sheet Dynamics Inferred from Surficial Deposits in Wright Valley: *Physical Geog.: Geografiska Annaler., Series A*, v. 75, p. 239–267.
- Hoffman, P.F., Kaufman, A.J., Halverson, G.P., and Schrag, D.P., 1998, A Neoproterozoic Snowball Earth: *Science*, v. 281, p. 1342–1346, doi:[10.1126/science.281.5381.1342](https://doi.org/10.1126/science.281.5381.1342).
- Hoffman, P.F., and Schrag, D.P., 2002, The snowball Earth hypothesis: testing the limits of global change: *Terra Nova*, v. 14, p. 129–155, doi:<https://doi.org/10.1046/j.1365-3121.2002.00408.x>.
- Howard-Williams, C., Priscu, J.C., and Vincent, W.F., 1989, Nitrogen dynamics in two antarctic streams: *Hydrobiologia*, v. 172, p. 51–61, doi:[10.1007/BF00031612](https://doi.org/10.1007/BF00031612).
- Howard-Williams, C., and Vincent, W.F., 1989, Microbial communities in southern Victoria Land streams (Antarctica) I. Photosynthesis: *Hydrobiologia*, v. 172, p. 27–38, doi:[10.1007/BF00031610](https://doi.org/10.1007/BF00031610).
- Icenhower, J.P., and Dove, P.M., 2000, The dissolution kinetics of amorphous silica into sodium chloride solutions: effects of temperature and ionic strength: *Geochimica et Cosmochimica Acta*, v. 64, p. 4193–4203, doi:[10.1016/S0016-7037\(00\)00487-7](https://doi.org/10.1016/S0016-7037(00)00487-7).
- Karr, E.A., Sattley, W.M., Jung, D.O., Madigan, M.T., and Achenbach, L.A., 2003, Remarkable Diversity of Phototrophic Purple Bacteria in a Permanently Frozen Antarctic Lake: *Applied and Environmental Microbiology*, v. 69, p. 4910–4914, doi:[10.1128/AEM.69.8.4910-4914.2003](https://doi.org/10.1128/AEM.69.8.4910-4914.2003).
- Kleinteich, J., Wood, S.A., Küpper, F.C., Camacho, A., Quesada, A., Frickey, T., and Dietrich, D.R., 2012, Temperature-related changes in polar cyanobacterial mat diversity and toxin production: *Nature Climate Change*, v. 2, p. 356–360, doi:[10.1038/nclimate1418](https://doi.org/10.1038/nclimate1418).
- Kyle, J.E., Schroeder, P.A., and Wiegel, J., 2007, Microbial silicification in sinters from two terrestrial hot springs in the Uzon Caldera, Kamchatka, Russia: *Geomicrobiology Journal*, v. 24, p. 627–641, doi:[10.1080/01490450701672158](https://doi.org/10.1080/01490450701672158).
- Lyons, W.B., Dailey, K.R., Welch, K.A., Deuerling, K.M., Welch, S.A., and McKnight, D.M., 2015, Antarctic streams as a potential source of iron for the Southern Ocean: *Geology*, v. 43, p. 1003–1006, doi:[10.1130/G36989.1](https://doi.org/10.1130/G36989.1).
- Mancuso Nichols, C.A., Garon, S., Bowman, J.P., Raguenes, G., and Guezennec, J., 2004, Production of exopolysaccharides by Antarctic marine bacterial isolates: *Journal of Applied Microbiology*, v. 96, p. 1057–1066, doi:[10.1111/j.1365-2672.2004.02216.x](https://doi.org/10.1111/j.1365-2672.2004.02216.x).
- Marra, K.R., Madden, M.E.E., Soreghan, G.S., and Hall, B.L., 2015, BET surface area distributions in polar stream sediments: Implications for silicate weathering in a cold-arid environment: *Applied Geochemistry*, v. 52, p. 31–42, doi:<https://doi.org/10.1016/j.apgeochem.2014.11.005>.

- Marra, K.R., Madden, M.E.E., Soreghan, G.S., and Hall, B.L., 2017, Chemical weathering trends in fine-grained ephemeral stream sediments of the McMurdo Dry Valleys, Antarctica: *Geomorphology*, v. 281, p. 13–30, doi:[10.1016/j.geomorph.2016.12.016](https://doi.org/10.1016/j.geomorph.2016.12.016).
- Marra, K.R., Soreghan, G.S., Elwood Madden, M.E., Keiser, L.J., and Hall, B.L., 2014, Trends in grain size and BET surface area in cold–arid versus warm–semiarid fluvial systems: *Geomorphology*, v. 206, p. 483–491, doi:[10.1016/j.geomorph.2013.10.018](https://doi.org/10.1016/j.geomorph.2013.10.018).
- Marx, J.G., Carpenter, S.D., and Deming, J.W., 2009, Production of cryoprotectant extracellular polysaccharide substances (EPS) by the marine psychrophilic bacterium *Colwellia psychrerythraea* strain 34H under extreme conditions This article is one of a selection of papers in the Special Issue on Polar and Alpine Microbiology.: *Canadian Journal of Microbiology*, v. 55, p. 63–72, doi:[10.1139/W08-130](https://doi.org/10.1139/W08-130).
- McKnight, D.M., Niyogia, E., Algera, L., Conovitz, E., and Tate, A., 1999, Dry Valley Streams in Antarctica: Ecosystems Waiting for Water: , p. 11.
- McKnight, D.M., Runkel, R.L., Tate, C.M., Duff, J.H., and Moorhead, D.L., 2004, Inorganic N and P dynamics of Antarctic glacial meltwater streams as controlled by hyporheic exchange and benthic autotrophic communities: *Journal of the North American Benthological Society*, v. 23, p. 171–188, doi:[10.1899/0887-3593\(2004\)023<0171:INAPDO>2.0.CO;2](https://doi.org/10.1899/0887-3593(2004)023<0171:INAPDO>2.0.CO;2).
- Mergelov, N. et al., 2018, Alteration of rocks by endolithic organisms is one of the pathways for the beginning of soils on Earth: *Scientific Reports*, v. 8, p. 1–15, doi:[10.1038/s41598-018-21682-6](https://doi.org/10.1038/s41598-018-21682-6).
- Moisander, P.H., Paerl, H.W., and Zehr, J.P., 2008, Effects of inorganic nitrogen on taxa-specific cyanobacterial growth and nifH expression in a subtropical estuary: *Limnology and Oceanography*, v. 53, p. 2519–2532, doi:[10.4319/lo.2008.53.6.2519](https://doi.org/10.4319/lo.2008.53.6.2519).
- Montross, S.N., Skidmore, M., Tranter, M., Kivimäki, A.L., and Parkes, R.J., 2013, A microbial driver of chemical weathering in glaciated systems: *Geology*, v. 41, p. 215–218, doi:[10.1130/G33572.1](https://doi.org/10.1130/G33572.1).
- Navarre-Sitchler, A., and Brantley, S., 2007, Basalt weathering across scales: *Earth and Planetary Science Letters*, v. 261, p. 321–334, doi:[10.1016/j.epsl.2007.07.010](https://doi.org/10.1016/j.epsl.2007.07.010).
- Nevot, M., Deroncelé, V., Montes, M.J., and Mercade, E., 2008, Effect of incubation temperature on growth parameters of *Pseudoalteromonas antarctica* NF 3 and its production of extracellular polymeric substances: *Journal of Applied Microbiology*, v. 105, p. 255–263, doi:[10.1111/j.1365-2672.2008.03769.x](https://doi.org/10.1111/j.1365-2672.2008.03769.x).
- Ólafsson, H., Furger, M., and Brümmer, B., 2007, The weather and climate of Iceland: *Meteorologische Zeitschrift*, v. 16, p. 5–8, doi:[10.1127/0941-2948/2007/0185](https://doi.org/10.1127/0941-2948/2007/0185).
- Olsson-Francis, K., Simpson, A.E., Wolff-Boenisch, D., and Cockell, C.S., 2012, The effect of rock composition on cyanobacterial weathering of crystalline basalt and rhyolite: *Geobiology*, v. 10, p. 434–444, doi:<https://doi.org/10.1111/j.1472-4669.2012.00333.x>.
- Omelon, C.R., 2008, Endolithic Microbial Communities in Polar Desert Habitats: *Geomicrobiology Journal*, v. 25, p. 404–414, doi:[10.1080/01490450802403057](https://doi.org/10.1080/01490450802403057).

- Palarea-Albaladejo, J., and Martín-Fernández, J.A., 2013, Values below detection limit in compositional chemical data: *Analytica Chimica Acta*, v. 764, p. 32–43, doi:[10.1016/j.aca.2012.12.029](https://doi.org/10.1016/j.aca.2012.12.029).
- Palarea-Albaladejo, J., Martín-Fernández, J.A., and Buccianti, A., 2014, Compositional methods for estimating elemental concentrations below the limit of detection in practice using R: *Journal of Geochemical Exploration*, v. 141, p. 71–77, doi:[10.1016/j.gexplo.2013.09.003](https://doi.org/10.1016/j.gexplo.2013.09.003).
- Pandey, K.D., Shukla, S.P., Shukla, P.N., Giri, D.D., Singh, J.S., Singh, P., and Kashyap, A.K., 2004, Cyanobacteria in antarctica: ecology, physiology and cold adaptation: *Cellular and Molecular Biology*, v. 50, p. 575–584.
- Pérez, C.A., Kim, M., Aravena, J.C., and Silva, W., 2022, Diazotrophic activity and denitrification in two long-term chronosequences of maritime Antarctica: *Science of The Total Environment*, v. 809, p. 152234, doi:[10.1016/j.scitotenv.2021.152234](https://doi.org/10.1016/j.scitotenv.2021.152234).
- Phillips-Lander, C.M., Elwood Madden, A.S., Hausrath, E.M., and Elwood Madden, M.E., 2019, Aqueous alteration of pyroxene in sulfate, chloride, and perchlorate brines: Implications for post-Noachian aqueous alteration on Mars: *Geochimica et Cosmochimica Acta*, v. 257, p. 336–353, doi:[10.1016/j.gca.2019.05.006](https://doi.org/10.1016/j.gca.2019.05.006).
- Price, P.B., 2000, A habitat for psychrophiles in deep Antarctic ice: *Proceedings of the National Academy of Sciences*, v. 97, p. 1247–1251, doi:[10.1073/pnas.97.3.1247](https://doi.org/10.1073/pnas.97.3.1247).
- Ramette, A., 2007, Multivariate analyses in microbial ecology: *FEMS Microbiol Ecol*, v. 62, p. 142–160, doi:[10.1111/j.1574-6941.2007.00375.x](https://doi.org/10.1111/j.1574-6941.2007.00375.x).
- Rasmussen, C., Brantley, S., Richter, D. deB., Blum, A., Dixon, J., and White, A.F., 2011, Strong climate and tectonic control on plagioclase weathering in granitic terrain: *Earth and Planetary Science Letters*, v. 301, p. 521–530, doi:[10.1016/j.epsl.2010.11.037](https://doi.org/10.1016/j.epsl.2010.11.037).
- Rimstidt, J.D., 2013, *Geochemical Rate Models: An Introduction to Geochemical Kinetics*: Cambridge University Press, doi:[10.1017/CBO9781139342773](https://doi.org/10.1017/CBO9781139342773).
- Rueter, J.G., and Petersen, R.R., 1987, Micronutrient effects on cyanobacterial growth and physiology: *New Zealand Journal of Marine and Freshwater Research*, v. 21, p. 435–445, doi:[10.1080/00288330.1987.9516239](https://doi.org/10.1080/00288330.1987.9516239).
- Shcolnick, S., and Keren, N., 2006, Metal homeostasis in cyanobacteria and chloroplasts. Balancing benefits and risks to the photosynthetic apparatus: *Plant Physiology*, v. 141, p. 805–810, doi:[10.1104/pp.106.079251](https://doi.org/10.1104/pp.106.079251).
- Shizuya, A., Kaiho, K., and Tong, J., 2021, Marine biomass changes during and after the Neoproterozoic Marinoan global glaciation: *Global and Planetary Change*, v. 205, p. 103610, doi:[10.1016/j.gloplacha.2021.103610](https://doi.org/10.1016/j.gloplacha.2021.103610).
- Sigmundsson, F. et al., 2010, Intrusion triggering of the 2010 Eyjafjallajökull explosive eruption: *Nature*, v. 468, p. 426–430, doi:[10.1038/nature09558](https://doi.org/10.1038/nature09558).
- Smith, H.J., Foster, R.A., McKnight, D.M., Lisle, J.T., Littmann, S., Kuypers, M.M.M., and Foreman, C.M., 2017, Microbial formation of labile organic carbon in Antarctic glacial environments: *Nature Geoscience*, v. 10, p. 356–359, doi:[10.1038/ngeo2925](https://doi.org/10.1038/ngeo2925).

- Stumpf, A.R., Elwood Madden, M.E., Soreghan, G.S., Hall, B.L., Keiser, L.J., and Marra, K.R., 2012, Glacier meltwater stream chemistry in Wright and Taylor Valleys, Antarctica: Significant roles of drift, dust and biological processes in chemical weathering in a polar climate: *Chemical Geology*, v. 322–323, p. 79–90, doi:[10.1016/j.chemgeo.2012.06.009](https://doi.org/10.1016/j.chemgeo.2012.06.009).
- de la Torre, J.R., Goebel, B.M., Friedmann, E.I., and Pace, N.R., 2003, Microbial Diversity of Cryptoendolithic Communities from the McMurdo Dry Valleys, Antarctica: *Applied and Environmental Microbiology*, v. 69, p. 3858–3867, doi:[10.1128/AEM.69.7.3858-3867.2003](https://doi.org/10.1128/AEM.69.7.3858-3867.2003).
- Van Horn, D.J., Wolf, C.R., Colman, D.R., Jiang, X., Kohler, T.J., McKnight, D.M., Stanish, L.F., Yazzie, T., and Takacs-Vesbach, C.D., 2016, Patterns of bacterial biodiversity in the glacial meltwater streams of the McMurdo Dry Valleys, Antarctica (M. Häggblom, Ed.): *FEMS Microbiology Ecology*, v. 92, p. fiw148, doi:[10.1093/femsec/fiw148](https://doi.org/10.1093/femsec/fiw148).
- Vincent, W.F., and James, M.R., 1996, Biodiversity in extreme aquatic environments: Lakes, ponds and streams of the Ross Sea sector, Antarctica: *Biodiversity and Conservation*, v. 5, p. 1451–1471, doi:[10.1007/BF00051987](https://doi.org/10.1007/BF00051987).
- White, A.F., and Blum, A.E., 1995, Effects of climate on chemical weathering in watersheds: *Geochimica et Cosmochimica Acta*, v. 59, p. 1729–1747, doi:[10.1016/0016-7037\(95\)00078-E](https://doi.org/10.1016/0016-7037(95)00078-E).
- Wolff-Boenisch, D., Gislason, S.R., Oelkers, E.H., and Putnis, C.V., 2004, The dissolution rates of natural glasses as a function of their composition at pH 4 and 10.6, and temperatures from 25 to 74°C: *Geochimica et Cosmochimica Acta*, v. 68, p. 4843–4858, doi:[10.1016/j.gca.2004.05.027](https://doi.org/10.1016/j.gca.2004.05.027).
- Wynn-Williams, D.D., and Edwards, H.G.M., 2002, Environmental UV Radiation: Biological Strategies for Protection and Avoidance, *in* Horneck, G. and Baumstark-Khan, C. eds., *Astrobiology: The Quest for the Conditions of Life*, Berlin, Heidelberg, Springer, p. 245–260, doi:[10.1007/978-3-642-59381-9_17](https://doi.org/10.1007/978-3-642-59381-9_17).
- Ye, Q., Tong, J., Xiao, S., Zhu, S., An, Z., Tian, L., and Hu, J., 2015, The survival of benthic macroscopic phototrophs on a Neoproterozoic snowball Earth: *Geology*, v. 43, p. 507–510, doi:[10.1130/G36640.1](https://doi.org/10.1130/G36640.1).

TABLES

Table 3.1. Quantitative mineralogy of the starter sediments

Mineralogy	Antarctica	Iceland
Plagioclase	28.80	38.74
K-spar	3.60	0.00
Quartz	12.60	0.00
Pyroxene	8.50	19.32
Amphibole	3.70	0.00

Cordierite	2.00	0.00
Biotite+Muscovite	3.10	0.00
Illite	23.00	0.00
Chlorite	6.90	0.00
Smectite	4.60	0.00
Olivine	0.00	6.61
Fe (oxy)hydroxide	0.00	2.40
Ilmenite	0.00	1.30
Amorphous	3.20	31.63

Table 3.2. Total elemental and major anion concentrations measured within the initial medium

Medium	B	Ca	Fe	K	Mg	Mn	Na	P
0.1X	8.5×10^{-6}	2.3×10^{-5}	1.6×10^{-6}	6.6×10^{-5}	3.3×10^{-5}	9.3×10^{-7}	2.2×10^{-3}	1.9×10^{-5}
0.001X	3.1×10^{-6}	BDL	BDL	2.0×10^{-5}	2.7×10^{-7}	BDL	4.6×10^{-5}	BDL
Medium	S	Si	Cl ⁻	NO ₂ ⁻	NO ₃ ⁻	PO ₄ ³⁻	SO ₄ ²⁻	HO ₃ ⁻
0.1X	4.1×10^{-5}	8.0×10^{-6}	1.8×10^{-4}	7.0×10^{-6}	2.1×10^{-3}	4.2×10^{-6}	3.5×10^{-5}	2.7×10^{-3}
0.001X	BDL	3.5×10^{-6}	1.7×10^{-5}	7.8×10^{-6}	1.6×10^{-6}	BDL	2.9×10^{-6}	2.9×10^{-4}

Table 3.3. Biotic and abiotic Si-based weathering rates ($\text{mol m}^{-2} \text{s}^{-1}$) calculated from the derivative of rate equations obtained by polynomial fitted trends in Figure 5. Data for 12°C experiments is obtained from Demirel-Floyd et al. (2022).

	Antarctica		Iceland	
	Biotic	Abiotic	Biotic	Abiotic
4°C	3.44×10^{-15}	3.40×10^{-15}	4.29×10^{-15}	3.49×10^{-15}
12°C	7.91×10^{-15}	3.84×10^{-15}	1.20×10^{-14}	9.14×10^{-15}

FIGURES

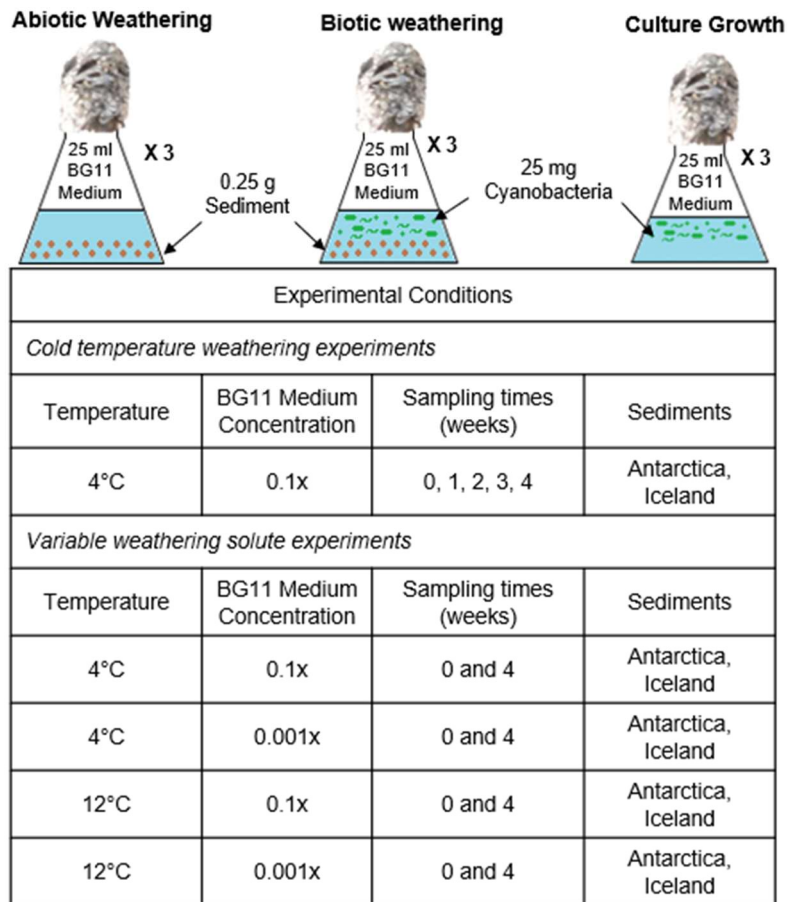


Figure 3.1. Schematic illustration of the experimental design for all experimental sets and summary of the experimental variables. *Cold temperature weathering* experiments were conducted at 4°C and in 0.1x BG11 medium. *Variable weathering solute* experiments were conducted at 4°C in 0.1x BG11 and 0.001x medium, and at 12°C in 0.1x BG11 and 0.001x medium, representing weathering at cold and warm conditions via dilute solutions differing 100-fold in total concentration.

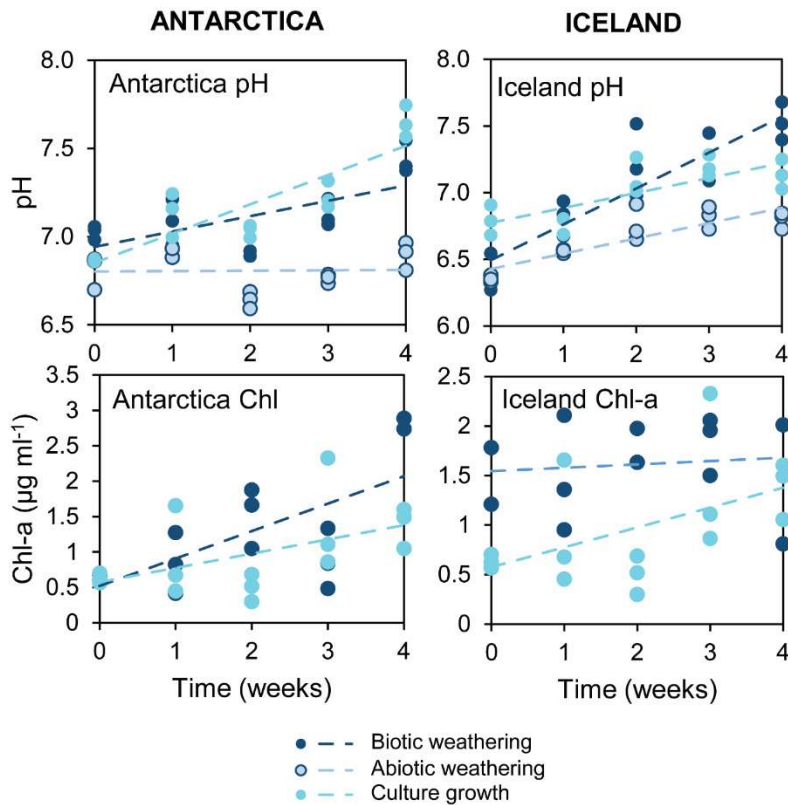
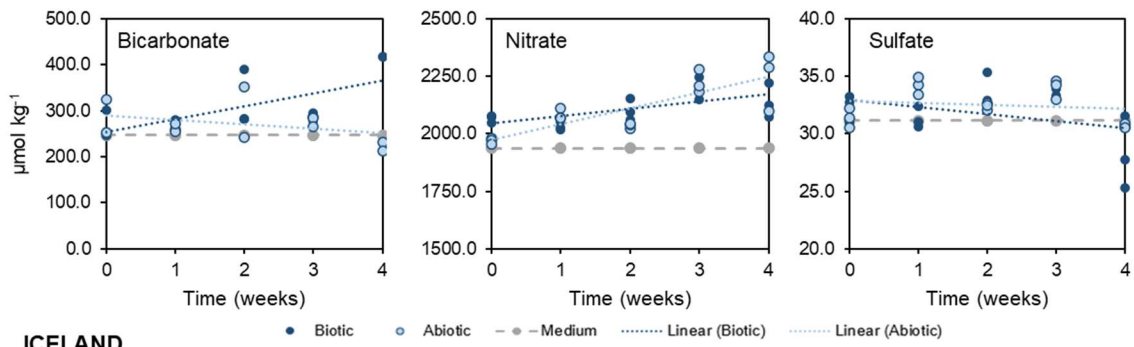


Figure 3.2. Changes in pH and Chlorophyll-a (Chl-a) concentrations during 4 weeks of Antarctic and Icelandic cold temperature biotic weathering, abiotic weathering, and culture growth experiments. Dotted lines show linear fit trends at each experiment. Trends show simultaneous increase of pH in all biotic and culture growth reactors with increasing Chl-a concentrations in the culture growth experiments.

ANTARCTICA



ICELAND

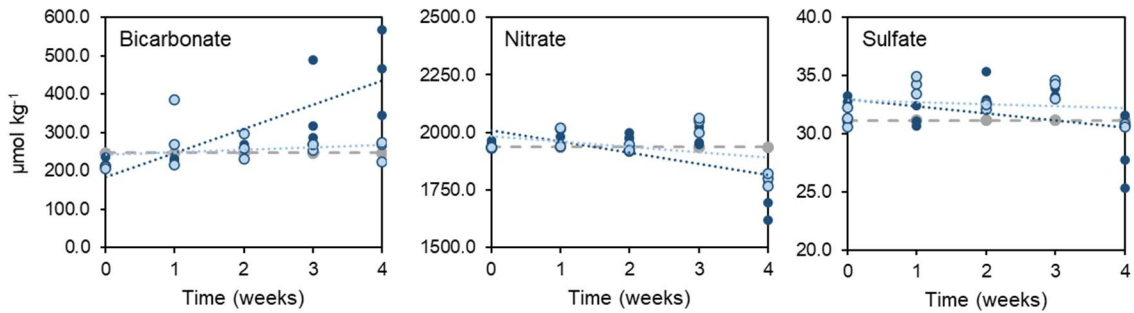


Figure 3.3. Changes in bicarbonate, nitrate and sulfate concentrations during 4 weeks of Antarctic and Icelandic cold temperature biotic and abiotic weathering experiments. Dotted lines show linear fit trends for each experiment; the grey dashed lines indicate initial media concentrations.

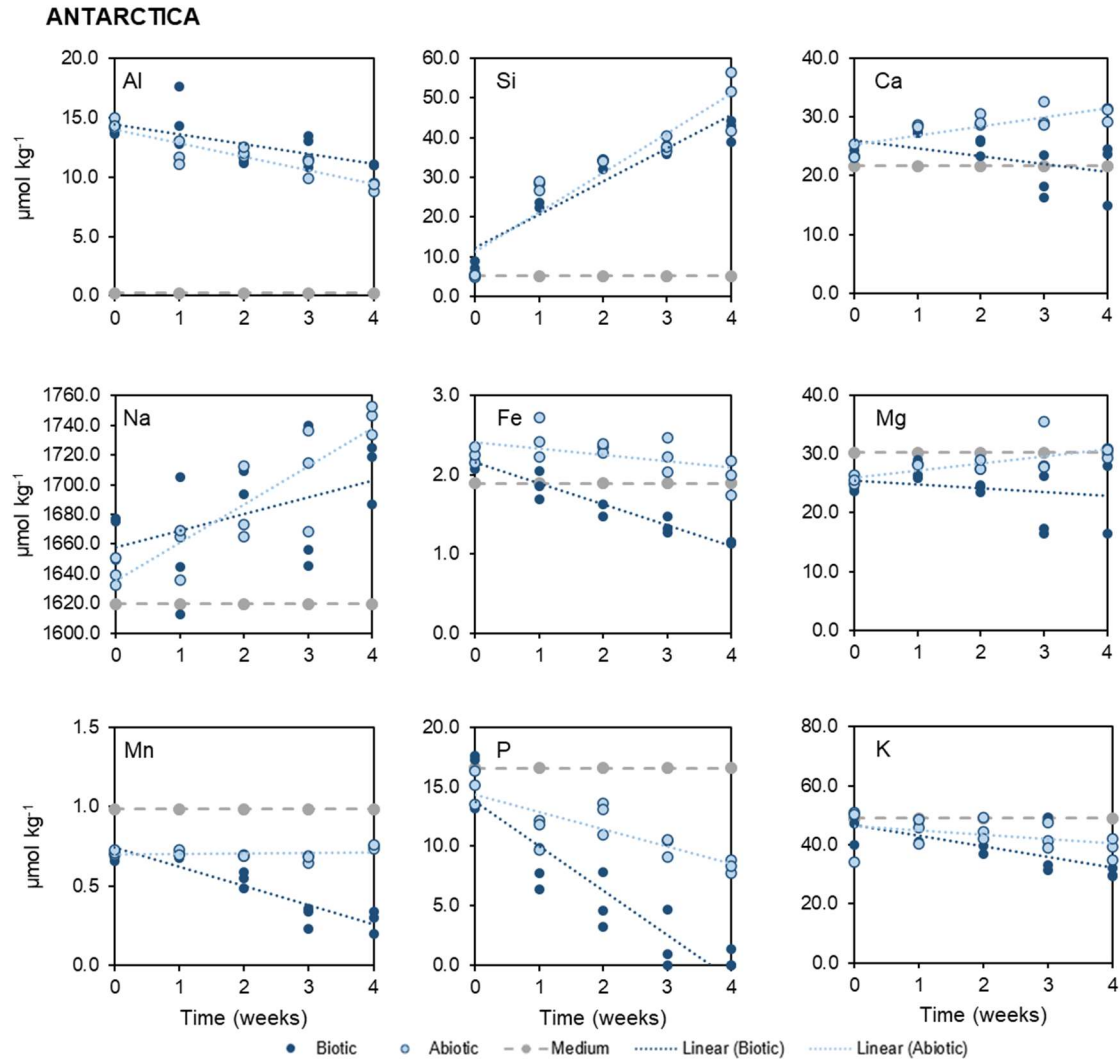


Figure 3.4. Changes in selected total solute concentrations during 4 weeks of Antarctic biotic and abiotic cold temperature weathering experiments. Dotted lines show linear fit trends at each experiment, whereas the grey dashed lines indicate initial media concentrations.

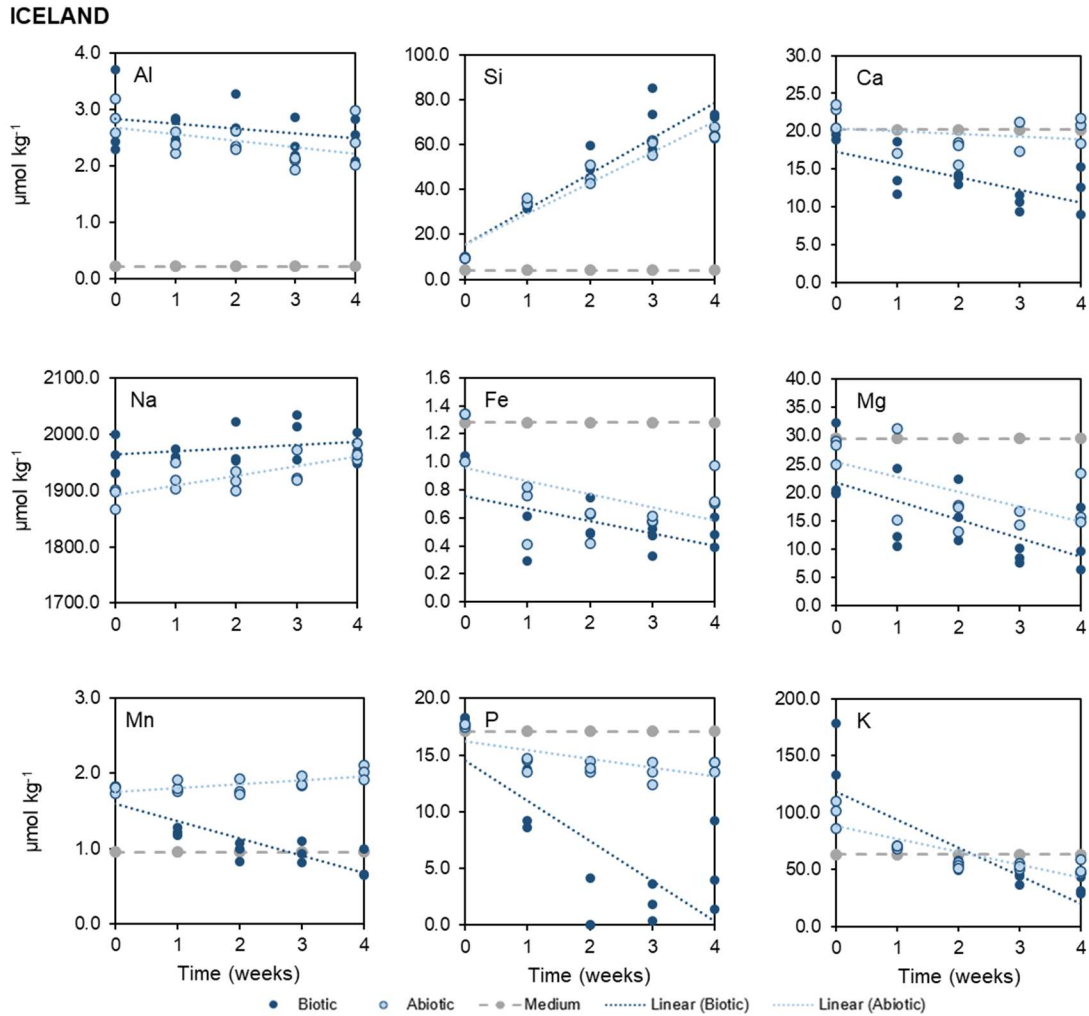


Figure 3.5. Changes in selected total nutrient concentrations during 4 weeks of Icelandic biotic and abiotic cold temperature weathering experiments. Dotted lines show linear fit trends at each experiment, whereas the grey dashed lines indicate starter medium concentrations.

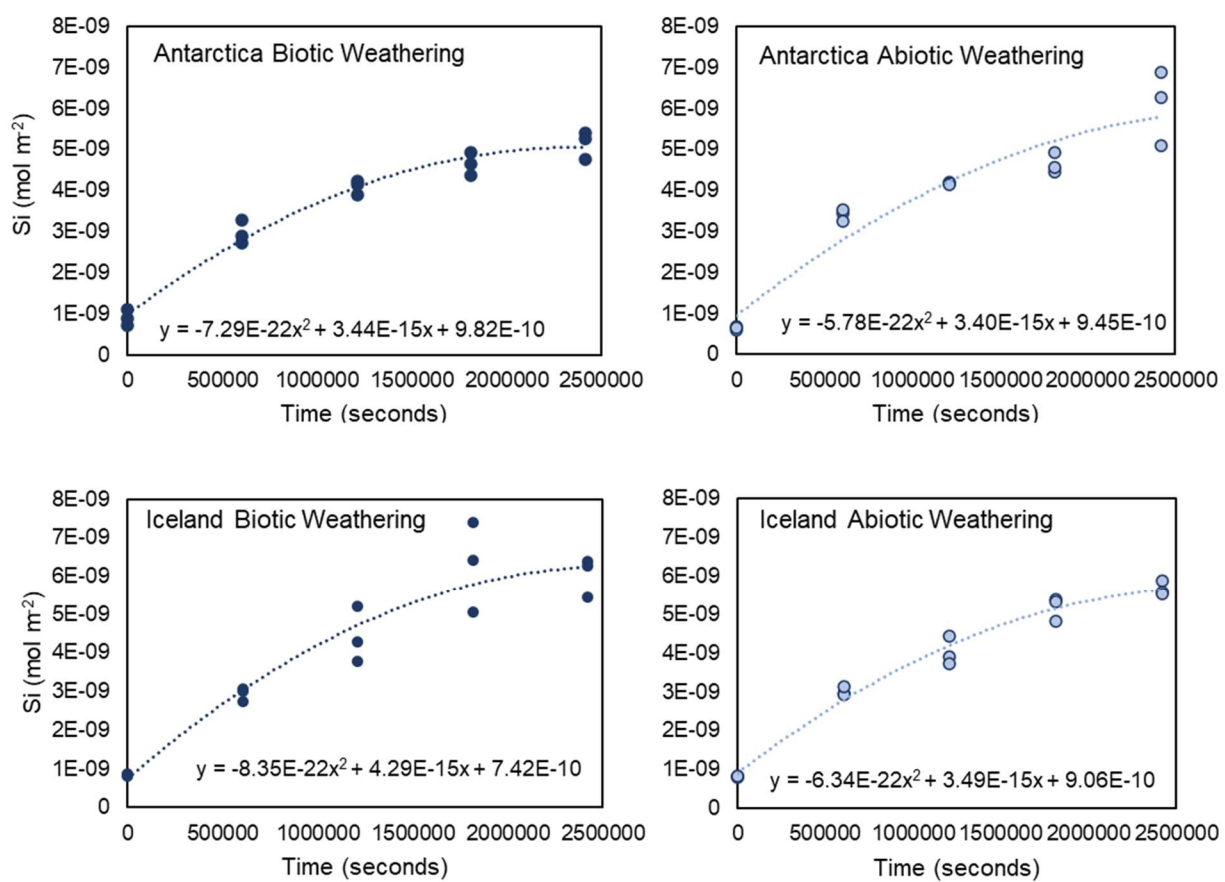


Figure 3.6. Biotic and abiotic Si release (normalized to BET surface area, mol m⁻²) during 4 weeks of Antarctic and Icelandic cold temperature weathering experiments and weathering rate equations obtained by polynomial fitted trends.

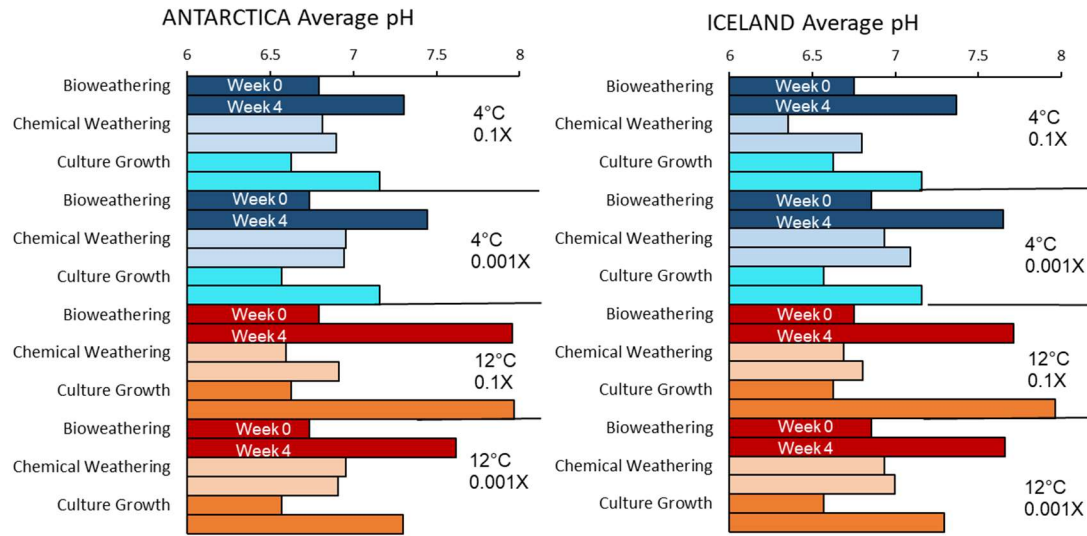


Figure 3.7. Changes in pH during 4 weeks of Antarctic and Icelandic biotic weathering, abiotic weathering, and culture growth experiments weathered by 0.1x and 0.001x concentrated freshwater medium in variable weathering solute experiments. Shades of blue and red refer to cold (4°C- blue) and warmer temperature (12°C-red) experiments. In this figure, pH values within each reactor are presented as averages of the triplicate values measured at the beginning (Week 0) and the end (Week 4) of the experiments.

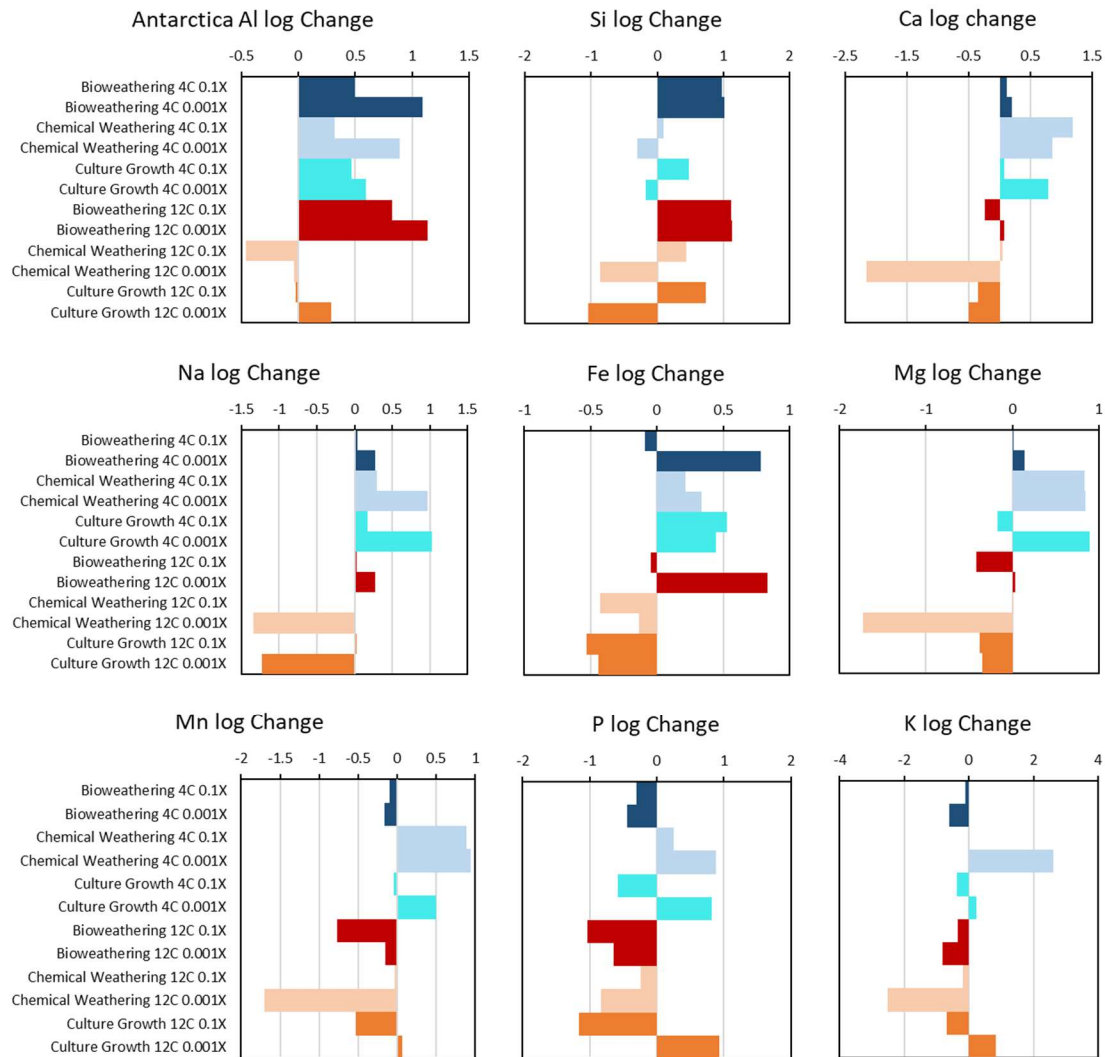


Figure 3.8. Average logarithmic change ratios in solute concentrations after 4 weeks (average of $\log [\text{concentration}_{\text{week 4}} / \text{concentration}_{\text{week 0}}]$) in Antarctic biotic weathering, abiotic weathering and culture growth experiments weathered by 0.1x and 0.001x concentrated freshwater medium in variable weathering solute experiments. Shades of blue refer to cold (4°C) conditions, while red shades refer warmer temperature (12°C) experiments. In this figure, 0 represents no change in concentrations of solutes, as compared to starting conditions. Positive bars represent net increased concentration, while negative bars represent decreased solute concentrations. The length of the bar represents the magnitude of the change.

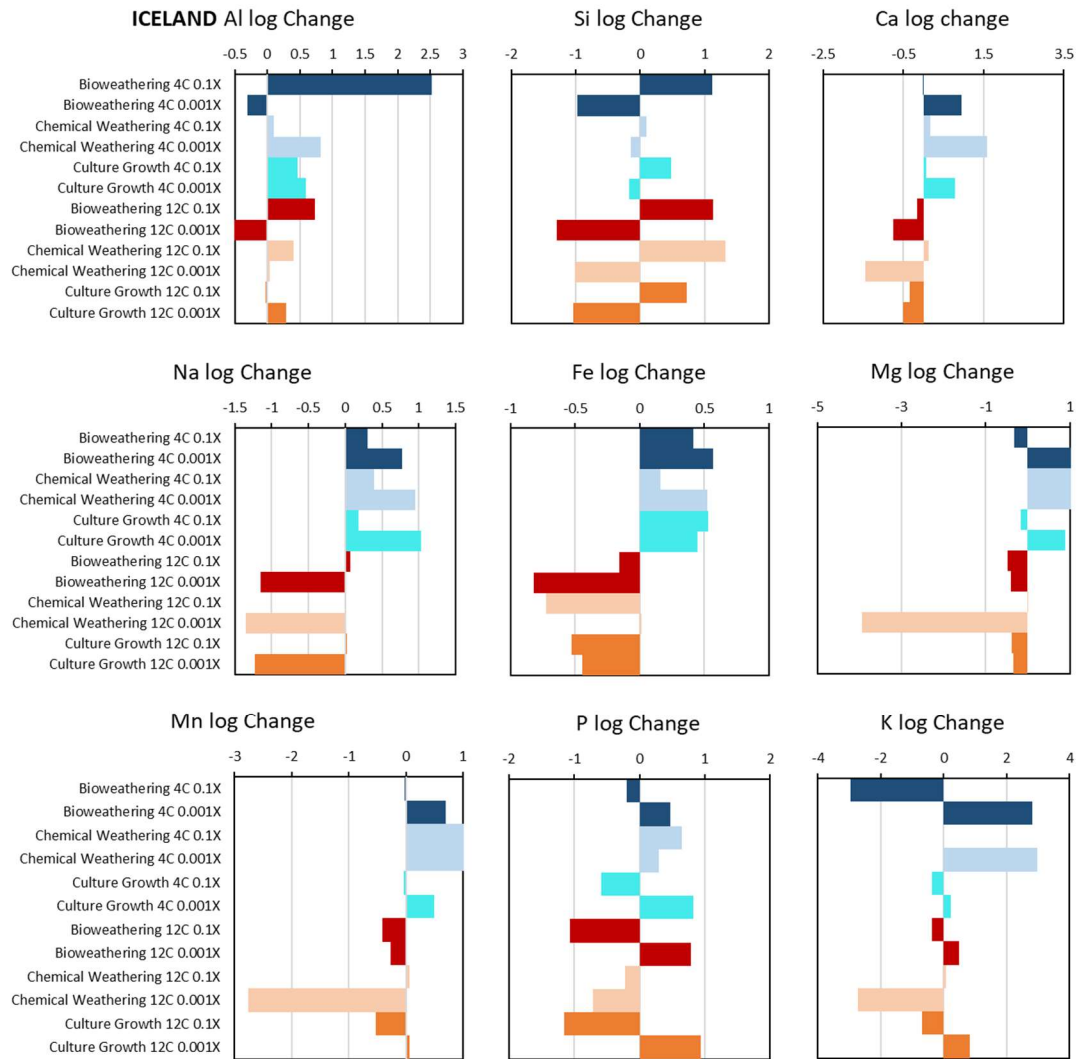


Figure 3.9. Average logarithmic change ratios in solute concentrations after 4 weeks (average of $\log[\text{week 4} / \text{week 0}]$) in Icelandic biotic weathering, abiotic weathering and culture growth experiments weathered by 0.1x and 0.001x concentrated freshwater medium in variable weathering solute experiments. Shades of blue refer to cold (4°C) conditions, while and red shades refer warmer temperature (12°C) experiments. In this figure, 0 represents no change in concentrations of solutes, as compared to starting conditions. Positive bars represent net increased concentration, while negative bars represent decreased solute concentrations. The length of the bar represents the magnitude of the change.

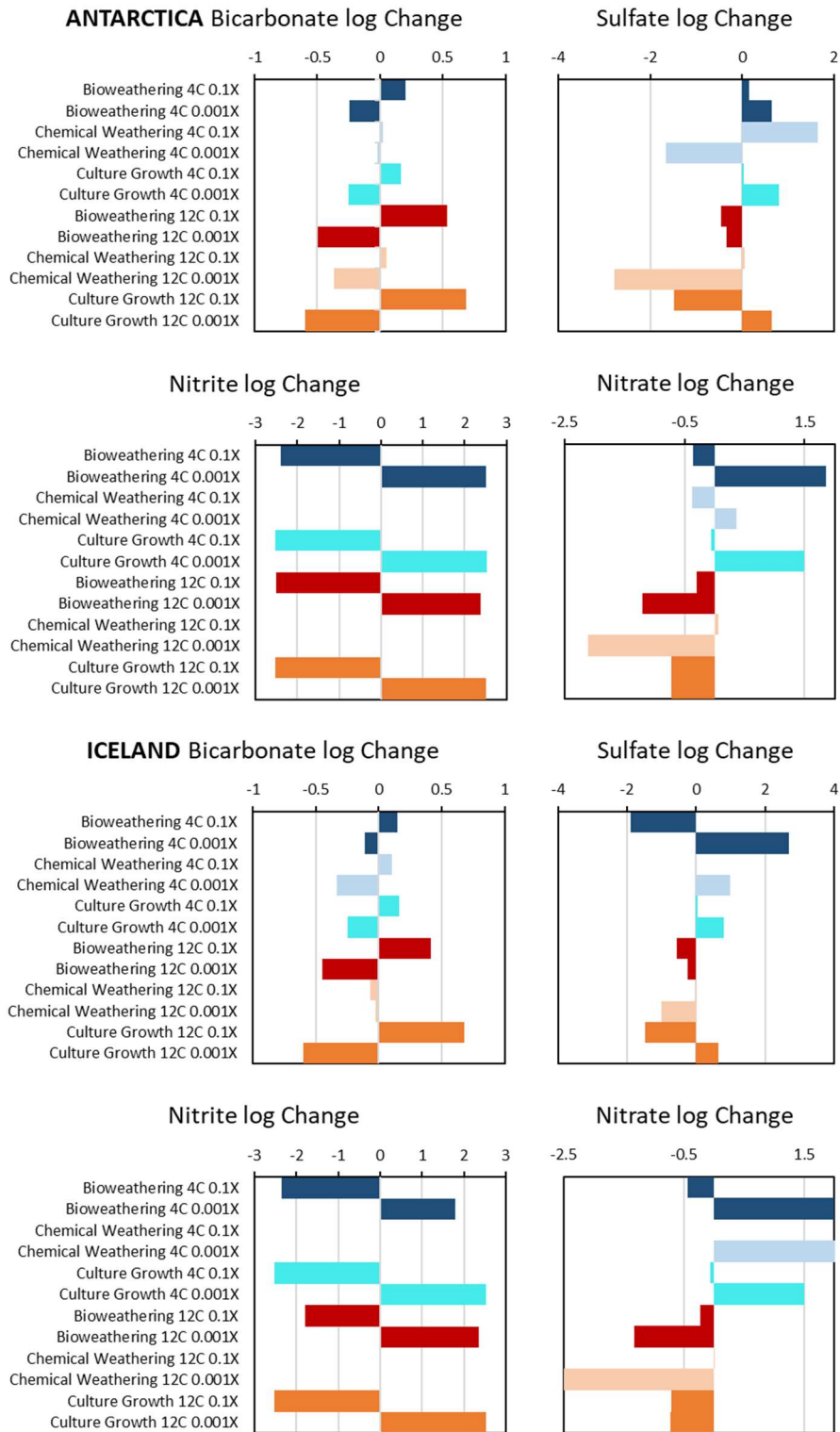


Figure 3.10. Average logarithmic major anion concentration ratios 4 weeks (average of average of $\log[\text{week 4} / \text{week 0}]$) in Antarctic and Icelandic biotic weathering, abiotic weathering, and

culture growth experiments. Shades of blue refer to cold (4°C) conditions, while red shades refer to warmer temperature (12°C) experiments. In this figure, 0 represents no change in concentrations of solutes, as compared to starting conditions. Positive bars represent net increased concentration, while negative bars represent decreased solute concentrations. The length of the bar represents the magnitude of the change.

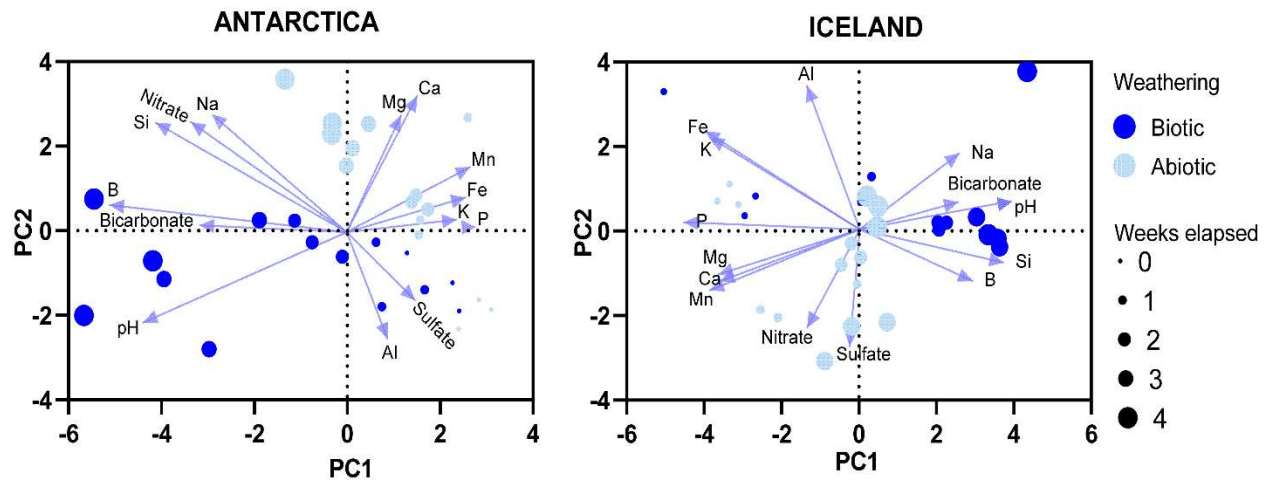


Figure 3.11. Principal Component Analysis (PCA) of the aquatic chemistry resulting from cold (4°C) biotic and abiotic weathering of Antarctica and Iceland glacial muds. Dark blue dots represent biotic reactors, whereas light blue ones represent abiotic experiments. Increasing size of the dots represents elapsed (increasing) time. Vectors represent loadings (variables) in PCA, and their magnitudes represent their relative significance in terms of the differences observed in aquatic chemistry (i.e., higher magnitudes are more significant). If the vectors are pointing towards particular data points or within the same quartile, it means that those data points significantly control the differences in concentration represented by the loading vectors. The sign of the principal components (PC) are not representative of physical differences in the sample, but are simply an artifact of the PCA analysis process.

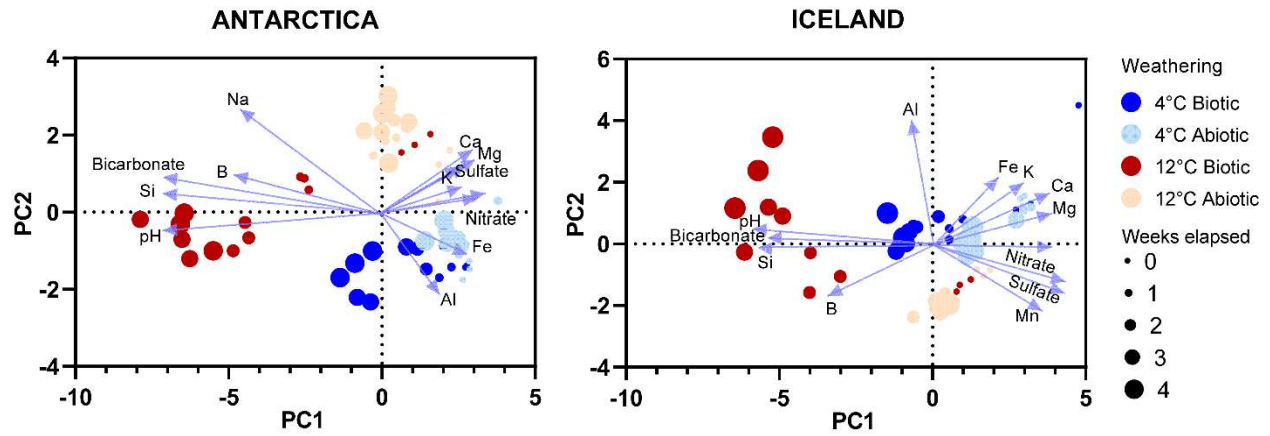


Figure 3.12. PCA of the aquatic chemistry following cold (4°C) and warm temperature (12°C, Demirel-Floyd et al. (2022)) biotic and abiotic weathering of Antarctica and Iceland glacial muds. Blue colours represent cold conditions, whereas the dark colours indicate warm weathering conditions. Increasing size of the data points refer to elapsed time.

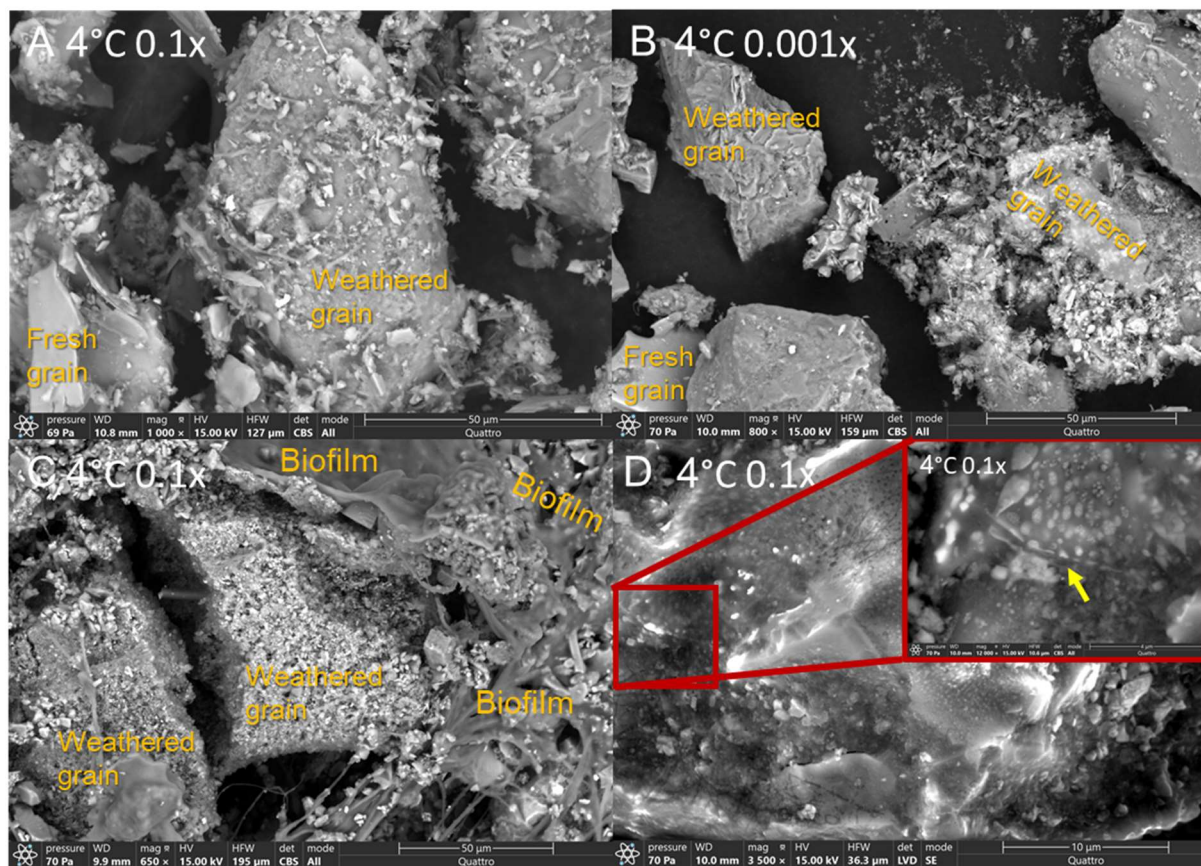


Figure 3.13. SEM images showing flaking on grain surfaces due to bioweathering (A-C) and that nano-phase precipitates (D) occur in 4°C bioweathering reactors after 4 weeks of weathering. Grains show flaky-etched surfaces and disintegration within Antarctic 4°C 0.1x (A) and 0.001x (B) reactors, as a result of biological weathering. Images from 0.1x (C) 4°C bioweathering reactors from Iceland experiments illustrate etching (weathering) of grains. We additionally detected nano-phase minerals under biofilm cover on a heavily etched grain within Icelandic 4°C 0.1x bioweathering reactors (D), resembling those observed in Demirel-Floyd et al. (2022) 12°C bioweathering reactors on the same sediments. Image on the right corner in Figure 3.13D is a magnified area on the image designated by the red square, showing the nano-sized spherical minerals forming micron-sized agglomerates. Arrow points to where a cyanobacterial filament used to attach on the grain via the biofilm.

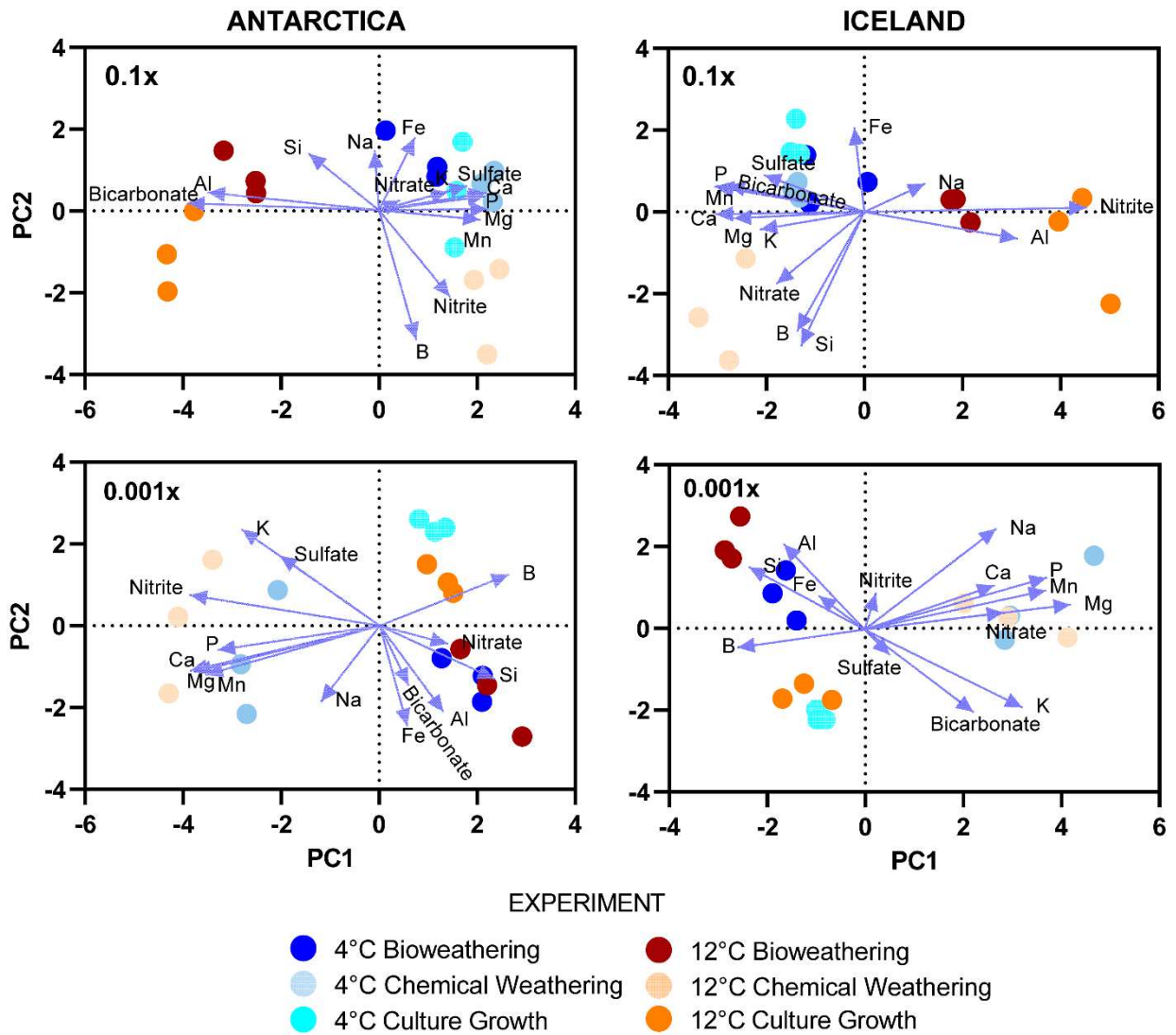


Figure 3.14. PCA of the aquatic chemistry following cold (4°C) and warm temperature (12°C, Demirel-Floyd et al. (2022) biotic and abiotic weathering of Antarctica and Iceland glacial muds. Blue colours represent cold conditions, whereas the red colours indicate warm weathering conditions. Increasing size of the data points refer to increasing weathering solute concentrations.

SUPPLEMENTARY MATERIALS

SUPPLEMENTARY MATERIALS FOR CHAPTER 1

Supplementary Text for Chapter 1

Detailed Geological Setting

Antarctica

The McMurdo Dry Valleys (MDVs) are east-west trending icesheet-free valleys in Antarctica that are located between the Trans-Antarctic Mountains and the Ross Sea. With mean annual temperature (MAT) around -18°C (within -14°C to -30°C temperature range) and mean annual precipitation (MAP; mostly snowfall) of 100 mm/yr, the MDVs are considered as polar desert environments (Fountain et al., 1999; Doran et al., 2002, 2008). These valleys only contain active fluvial systems during 4-12 weeks of the austral summer, but host liquid water in briny proglacial lakes year-round. Shallow permafrost layers hinder subsurface water flow, though there is shallow groundwater activity (McKnight et al., 1999; Gooseff et al., 2002, 2013) that is reported to be locally briny, which would allow water availability even through subzero winter conditions (Lyons et al., 1998; Lyons et al., 2005; Ball and Levy, 2015; Cuzzo et al., 2020; Lyons et al., 2021). Despite being an extremely cold and hyper-arid environment, chemical weathering still occurs within the austral summer within meltwaters, as inferred by solute fluxes in MDV meltwater streams (Gooseff et al., 2002; Stumpf et al., 2012; Lyons et al., 2015), and within rocks and soils (Guglielmin et al., 2005; Cuzzo et al., 2020).

Mechanical grinding of rocks/sediments under glaciers, as well as eolian redistribution of fine-grained glacial deposits supply fresh material available for weathering reactions (Stumpf et al., 2012; Marra et al., 2017). Though formerly thought to be a barren desert, now MDVs are known to house a diverse polyextremophilic microbial community within benthic lacustrine microbial mats, largely cyanobacterial mats in ephemeral streams, within endolithic

environments (soil and rock cracks), and in cryoconite holes (Cary et al., 2010; Cowan et al., 2010; Anesio and Laybourn-Parry, 2012). It is suggested that these communities are contributing to the nutrient fluxes within meltwater streams (i.e, Fe fluxes reaching to the Southern Ocean) via biological weathering, via in-situ microcosm studies and investigating the geochemistry of meltwaters (Maurice et al., 2002; Lyons et al., 2015). Photosynthetic microbial mats largely dominate the biogeochemical cycles, controlling C, N and P cycling (McKnight et al., 1999, 2004, 2007; Geyer et al., 2017; Smith et al., 2017), as well as providing nutrients via bioweathering of sediments with the help of heterotrophic organisms within MDV watersheds and soils (Demirel-Floyd et al., 2022).

We sampled glacial drifts, proglacial fluvial sediments, soils and water tracks within Wright Valley and Taylor Valley of MDVs, that were partially reported in previous publications (Hall et al., 1993; Hall et al., 2000; Marra et al., 2014, 2015, 2017; Levy et al., 2011). Drift deposits within the MDVs have different ages, composition, and texture due to complicated glacial histories, though both of the valleys are underlain by granitic and metamorphic bedrock (Hall et al., 1993; Hall et al. 2000, Hall and Denton, 2000; Hall and Denton, 2005; Hall, 2009; Hall et al. 2013).

Taylor Valley

Samples within Taylor Valley were collected from the Goldman Glacial Stream and pre-Bonney drifts the Goldman Stream is flowing over, along with Ross Sea drift and Howard Glacier Stream sediments during the 2010 austral summer field season (Stumpf et al., 2012; Marra et al., 2014, 2015, 2017). We additionally collected soil profile samples from one location,

with 10 cm depth intervals, until reaching the permafrost at 40 cm. See Marra et al. (2017) for geology and sample location maps.

Eastern Taylor Valley deposits are largely affected by the encroachment of the Ross Sea Ice within the Taylor Valley, which introduced partially wet-based glacial conditions in a cold-based glacial setting, due to East Antarctic Ice Sheet movement during Last Glacial Maximum (LGM; Hall et al., 2000). The drift deposits emplaced during this LGM glacial event within Taylor Valley are called Ross Sea drift, which also includes marine sediments. Delta Stream (Hall et al., 2000), also referred as Howard Glacier Stream (Marra et al., 2017), flows on the Ross Sea drift deposits that contain clasts from the underlying granite and biotite orthogenesis, as well as kenyte, basalt, sandstone, and dolerite clasts that are sourced out of the valley (Hall et al., 2000). The western portion of the valley is covered by undifferentiated pre-Bonney drifts that are also reworked by proglacial fluvial stream systems (Hall et al., 2000). Proglacial lakes, meltwater ponds and paleo-lake beds introduce salt to glacial deposits, as well as eolian sources and weathering processes (Bisson et al., 2005). Taylor Valley also hosts heterogenous dry-frozen and shallow ice-cemented, poorly developed salty soils developing on late-Quaternary, Pliocene and Holocene-aged glacial drifts, marine sediments and paleo-lake beds (Campbell and Claridge, 2006; Bockheim and McLeod, 2008; Ugolini and Bockheim, 2008; Bockheim and McLeod, 2015). In austral summer, the upper 10-60 cm of the permafrost thaws, providing either a dry or melt-saturated active layer (Campbell et al., 1997; Bockheim et al., 2007). We refer to previous studies for further details about the drift deposits, soils and the glacial history of Taylor Valley (Hall et al. 2000; Hall and Denton, 2000; Campbell and Claridge, 2006; Bockheim and McLeod, 2008).

Water tracks

Water track samples were collected from water tracks observed in Taylor Valley, around Lake Hoare, Lake Fryxell, and Lake Bonney basins, sampled during a 2009-2010 field campaign and mapped by Levy et al. (2011). Water tracks are gully-like features that have darker toned surfaces, which are observed on gentle to steep slopes of soils with high moisture (Levy et al., 2008, 2011). Water track soils show the typical characteristics of sandy Antarctic soils with poorly developed profiles, but are generally saltier in composition, inferred by their electrical conductivity (Liu et al., 2002; Bockheim et al., 2008). Water tracks may be similar to those on Mars known as recurrent slope lineae, which are attributed to briny groundwater activity (Levy et al., 2011; McEwen et al., 2011), which is potentially causing seasonal bright salt efflorescences on Taylor Valley soils (Liu et al., 2002). Besides their association with groundwater seeps, water tracks are observed within dry ephemeral stream channels. Water tracks also contribute to proglacial lake nutrient budgets by transporting weathering solutes. Therefore, water tracks are considered to be the intermediate medium connecting hydrological cycles within Taylor Valley (Levy et al., 2011). See Levy et al. (2011) for further details about the water track sediments of Taylor Valley.

Wright Valley

Wright Valley sediments include multiple drift samples collected by Hall et al. (1993), and Onyx River, Denton Glacial Stream and Clark Glacial Stream samples collected during 2010 austral summer field campaign within the Wright Valley (Stumpf et al., 2012; Marra et al., 2014, 2015, 2017). We additionally collected soil samples from two soil profiles around Clark Glacier and upper Onyx River region, with 10 cm depth intervals, until reaching the permafrost at 30 cm. See Stumpf et al. (2012) and Marra et al. (2017) for geology and sampling maps.

The eastern end of the Wright Valley is underlain by a bedrock composition of granite, quartz monzonite and granodiorite (Brownworth and Denton plutons) and filled with pre-LGM drifts dating as old as Miocene that contain heterogeneously sample clasts from these bedrocks (Hall and Denton, 2005). Clark Glacier Stream (Marra et al., 2017) emanates from the Clark Glacier and drains into the Onyx River, flowing primarily over the Quaternary-aged Brownworth drift and potentially eroding clast from the underlying mid-Quaternary-aged Trilogy and Quaternary-aged Loke drifts. The Onyx River drains from Lake Brownworth and transects the whole valley, eroding additional sediment from Valkyrie, Loop, Peleus and various Alpine drifts. Poorly developed soils of Wright Valley are mainly located around the Wright Lower Glacier and Onyx River flood plains of, consisting of all of these drift deposits, as well as bedrocks clasts of Ferrar dolerite, Olympus granite gneiss, Vida granite, and microdiorite (Hall and Denton, 2005; Campbell and Claridge, 2006; Bockheim and McLeod, 2008). See previous studies for further details about the drift deposits, soils and the glacial history of Wright Valley (Hall et al., 1993; Hall and Denton, 2005; Campbell and Claridge, 2006; Bockheim and McLeod, 2008).

Peru

Our fluvial, glacial drift, and lacustrine samples were collected during January 2016 field season from two NE-SW trending proglacial valleys (Llanganuco and Paron) of the Cordillera Blanca Mountain range, that generally exhibit a cold and semi-arid climate regime with highly seasonal precipitation (MAT= 0-9°C; MAP= 800-1200 mm/yr), due to high elevation and El Niño– La Niña oscillations (Kaser et al., 1990, 2003; Vuille et al., 2008; Bury et al., 2011), despite its location near the equator. The hydrological cycle during the dry season (austral winter from June to September) consists of glacial streams and groundwater, and the water budget is reduced by sublimation processes (Vuille et al., 2008; Gordon et al. 2015). However, abundant

rainfall during austral summer (from October to May) may result in lake outburst events (Kaser, 2001). The wet season allows the western Cordillera Blanca glacial region to host meadows that are defined by swampy plains with grass, sedge, and wetland plants in high-moisture soils that are underlain by lacustrine sediments and glacial till (Kaser et al., 2003; Baraer et al., 2014; Gordon et al., 2015).

Cordillera Blanca is the region with the most glacier cover of the Peruvian Andes at high-elevation terrain, with peaks reaching up to 6768 m (Iturrizaga, 2014). Bedrock and sediment cover in Cordillera Blanca valleys are affected by the glacial history of the region, including substantial glacial retreat in the Little Ice Age (LIA) that exposed polished bedrock and formed proglacial lakes (Racoviteanu et al., 2008; Iturrizaga, 2014). Geomorphological landforms and the glacial sediment budget of the Cordillera Blanca valleys are additionally affected by erosion resulting from uplift and large earthquakes triggering catastrophic mass movements. Cordillera Blanca region is located within an active fault zone of the Callejon de Huaylas basin, that is largely normal faulted and designated by the Andean fold-thrust belt on the east. The Cordillera Blanca fault defines the boundary between Miocene aged granodioritic batholith and Mesozoic schist and sandstones, while cutting through the Rio Santa Valley Pleistocene moraines (Siame et al., 2006; Giovanni et al., 2010). A major mass movement triggered by an offshore subduction zone earthquake with the magnitude of 7.8 in 1970, filling up the glacial valleys and settlements with glacial muds and moraine deposits dramatically examples the effects of active tectonics on the Cordillera Blanca valley systems (Cluff 1971; Evans et al. 2009; Iturrizaga, 2008).

Llanganuco Valley

Llanganuco valley is largely underlain by the granodioritic and tonalitic Cordillera Blanca batholith and locally by pyrite and sulfide mineral-rich marine black shales of the Upper Jurassic Chicama formation, which is under ice cover (Wilson et al., 1995; Love et al., 2004). Llanganuco valley slopes are susceptible to small and large-scale rockslides that feed the debris-dammed lakes (Iturrizaga, 2014). Llanganuco sediment budget was affected by a Huascaran debris avalanche, followed by the big Yungay mass movement event in 1970, majorly filling the Llanganuco Canyon and stopping at Ranrahirca village (Cluff, 1971). The debris thickness is reported to range between 10-40 ft locally, which contained massive boulders, gravel, mud ice and water, blocking the Llanganuco River and resulting in glacial lake level rises (Cluff 1971; Evans et al., 2009). We sampled fluvial sediments along the Llanganuco River throughout the Llanganuco Valley, extending down to Ranrahirca at the distal sampling point.

Paron Valley

Paron valley is a 15 km-long northern Cordillera Blanca glacial valley, extends towards the east of Caraz. Paron River draining through the Valley is a segment of the Lullan River catchment area that drains into the Pacific Ocean (Iturrizaga, 2018). The majority of the Paron valley is underlain by the Miocene batholith granodiorite complexes (Siame et al., 2006). Glacier-dammed lakes in this valley were suggested to be more frequent during LGM when glaciers were larger (Iturrizaga, 2018). We collected samples from the only remaining large glacier-dammed lake, Laguna Paron, as well as fluvial slackwater bar sediments from the Paron River throughout the Valley.

Other Peruvian Sites

We additionally carried out a sampling campaign on the NE of Huaraz, sampling glacial lake debris from the Llaka Lake (~14 km NE of Huaraz) and soil from Zona de Pitek (~7 km NE of Huaraz). The silty Llaka Lake debris contains modern drift deposits on granitic bedrock (with local metasediments) from a glacier bounded by 5000-6100 m high peaks (Vallunaraju, Ocshapalca, and Ranrapalca) of Toclaraju mountain. Soil samples of Zona da Pitek were collected 20 cm and 60 cm down the soil profile, at the road junction out of the same glacial valley where the Llaka Lake is located.

Norway

Our glacial drift, soil, proglacial lake and fluvial sediment samples from Norway are collected from Austerdalen and Langedalen valleys of the the Jostedalsbreen glacial region during August-September 2014 field campaign (Joo et al., 2018b); the watersheds are underlain by mainly on quartz monzonite, granitic gneiss and granodiorite bedrock (Lutro and Tveten, 1996).

Josteldalsbreen ice cap is located between the east of the Nordfjord region and north of Sognefjord in the southwest cost of Norway, feeding S-NNW and N-S trending glacial valley streams draining into lakes and fjords. Nordfjord region is a part of Norwegian Caledonides, generally underlain by Precambrian acidic gneiss (granite to granodiorite composition) at the western section (Josteldalsbreen watershed) and dominated by basic pyroxene-granulite gneiss towards the east (Jotunheimen watershed; Mellor, 1987). The bedrock composition and structure are affected by Precambrian and Caledonian orogenies, as well as varying grades of metamorphism (Rye et al., 1997). The gneiss dominated bedrock has undergone ultrahigh and high-pressure metamorphism during continental subduction and is referred to generally as The Western Gneiss Region (Root et al., 2005; Butler et al., 2015).

Josteldalsbreen region has a cold and humid climate, determined by the MAT of 4.5° and MAP of 1769 mm/yr. The glaciomorphological sediment and landforms of the western Norway has imprints from the Little Ice Age (LIA) maxima of the late Holocene (Bickerton and Matthews, 1993; Lewis and Bernie, 2001). Non-glacial landforms were also changing during late LIA in the Josteldalsbreen area, recorded by a substantial increase in mass movements (Grove, 1972; Lewis and Bernie, 2001). Today, glacial valleys in the region are dominated by the fluvial fans, that hosts limited vegetation (grass, herbs, willows) in the active parts and well-developed scrubs and woodlands in the inactive sections (Innes, 1984).

Austerdalen Valley

Austerdalsbreen foreland (elevation of 350 m) has MAT of 5°C and MAP of 2250 mm/yr (Green and Harding, 1980; Ostrem and Ziegler, 1969). The glacial meltwater stream in the Austerdalen valley joins with Langedalen valley proglacial stream and is named Storelvi river at the junction, which flows into the proglacial Veitastrond lake (King, 1959; Joo et al., 2022). We sampled fluvial sediment along a 16 km transect starting from the Austerdalen proglacial stream starting at glacier terminus and through the entire Storelvi river (~5 km segment), ending at the Veitastrond lake with a proglacial lake sample, as well as a distal and proximal glacial drift, and a soil profile (at 10, 20, 30, 50 and 100 cm depths) within the valley (Joo et al., 2018b, 2022).

Austerdalen Valley passes through a granitic basement (Lutro and Tveten, 1996), though we noticed that the valley is filled with banded gneiss and granitic gneiss boulders during our field observations (Soreghan et al., 2016; Joo et al., 2018b). The granite bedrock has contacts with monzonite at higher elevations of the glacier, migmatite towards the west in the Langedalen valley and a thrustbed phyllite at the SE of the Veitastrond lake (Lutro and Tveten, 1996).

Terminal and lateral moraines in Austerdalen valley contains glacial deposits that record the

glacial retreat after the maximum glacial advance in LIA. The Austerdalsbreen glacier is reported to have reached its maximum extent in recorded history in 1750, resulting in ten phases of moraine deposition (King, 1959).

Langedalen Valley

Langedalen valley is an approximately ~6 km-long valley trending from NW from the Langedalsbreen glacier to SE, joining the Austerdalen valley at the main channel of the Storelvi river. Langedalen valley is underlain by monzonite in the NE and approximately 20% of the transect is of granitic bedrock towards the valley exit on the SE (Lutro and Tveten, 1996). We sampled fluvial sediments approximately a ~4.5-km transect of the meltwater stream, starting at ~1.5 km distance from the source, and ending at the Austerdalen junction, as well as a proximal drift sample (Joo et al., 2018b).

Iceland

Iceland is a volcanic island in the South Atlantic Circle, underlain by volcanic rocks of 13 Ma-recent age and that has been experiencing silica-rich basaltic tephra ejections for the last 12,000 years (Andrews and Eberl, 2007). Climate isn't harsh due to the warm waters brought by the North Atlantic Current, though still cold with MAT ranging between 0-4°C, and humid with MAP >600 mm/year that supports vegetation (Olafsson et al., 2007). Low pressure regions commonly produce 5-15 m/s winds that can go up to 50 m/s during storm events; thus, aeolian processes contribute to landform evolution and sediment budgets of the fluvial catchments (Arnalds et al. 2016).

Icelandic glacial landforms are affected the late 19th century warming of the climate. Retreat of the Iceland ice caps exposed vegetated (largely birch) subglacial landscapes and

produced substantial dust, post glacial advance ~5000-4000 ago due to climatic shift (Hannesdottir et al., 2014; Arnalds et al. 2016). Glacial diamictons are formed through the erosion Tertiary and Quaternary volcanic sequences (Andrews and Helgadottir 2003). The Eyjafjallajökull volcanic eruption in 2010 (Sigmundsson et al. 2010) caused a catastrophic glacial outburst flood, which are common in the regions. These floods also contribute to the dust and sediment budgets as well as the landform development, as they rework former deposits and transport large amounts of fresh sediments (Prospero et al. 2012). Recharge of the Eyjafjallajökull volcano basaltic magma opened a short effusive fissure, potentially triggering the initial eruption of basaltic lava with SiO₂ content of 48% (Sigmundsson et al., 2010). Magma-ice interactions resulted in a secondary eruption within the ice-capped caldera of the volcano, resulting in a glacial outwash event (Sigmundsson et al., 2010).

We collected glacial outwash sediments from one of the S-N trending tributaries flowing over the Eyjafjallajökull glacial outwash deposits in a May 2016 field campaign. 3 fluvial sediment samples were collected from ~2 km segment of the glacial outwash tributary, starting ~1.3 km away from the source and ending at the junction to the river flowing on Katla glaciovolcanic outwash flood plains that drains into the ocean towards the SW.

Washington

We sampled fluvial sediments from Mountaineer Creek within Stuart Lake and Colchuck Lake catchment area at intervals until the junction with the Eightmile Creek at Mt. Stuart (at 3600-4800 m elevation), Washington State during A. June 2019 sampling campaign. We additionally sampled 2 glacial drifts (Mt. Stuart drift and Horseshoe Lake debris drift) on the slopes of Mt. Stuart (at 7200 and 5900 m elevation, respectively), as well as a topsoil on the lower banks of Mountaineer Creek.

Mt. Stuart is as a glaciated part of Washington Cascades that has a climate heavily affected by the topography, where high peaks act as a barrier for moist air masses (Reiners et al., 2003). MAP in the Northern Cascades region around Mt. Stuart is 1500-2000 mm/yr and MAT is ~8-10°C around Mt. Stuart (according to PRISM group 30-yr annual precipitation and temperature maps, Daly et al., 1994; Daly et al., 2008). Erosion rates across the Cascades are reported to show similar trends with precipitation profiles, reaching a maximum of 0.33 mm/yr, which is also associated with fluvial discharge (Reiners et al., 2003).

Our sampling site is located on the granitic bedrock of the Late Cretaceous calc-alkaline pluton that intruded the metamorphic basement (pre-Cretaceous Chiwaukum Schist) of the Cascades, which is called the Mt. Stuart Batholith (Erikson, 1977; Brown and Walker, 1993). Locally, lithology within the batholith might change between tonalite, quartz diorite, granodiorite, granite, gabbro, and ultramafite, and may be intruded by mafic Tertiary dikes. Mt. Stuart Batholith borderlines a NW trending horst, which is surrounded by the Deception-Straight Creek Fault, Leavenworth fault and Chiwaukum Graben (Erikson, 1977).

Puerto Rico

We collected fluvial sediment, saprolite and soil samples during May 2014 and 2018 from the Rio Guayanés and Rio Guayabo watersheds in southeastern Puerto Rico, which were heavily affected by Hurricane Maria in 2017 (Joo et al., 2018a, 2018b; Webb et al., 2022). These watersheds are largely underlain by Late Cretaceous San Lorenzo granodiorite, as well as quartz diorite, and minor metavolcanics (Rogers et al., 1979). The granodioritic bedrock hosts thick layers of soil and saprolite (up to 1m and 8m, respectively, Fletcher et al., 2006; Murphy et al., 2012). In a larger scale, the field site is within the Cordillera Central Mountain range, largely underlain by igneous rocks aged Jurassic to Eocene (Monroe, 1980). The region is also

tectonically active along the Puerto Rico Trench, which affects the landforms by 1 mm/yr uplift rates and moderate earthquakes (Mann et al., 2005).

Puerto Rico exhibits a hot and humid, tropical climate defined by MAT of 22°C and MAP of 4200 mm/yr (Joo et al., 2018a, 2018b). Puerto Rico is generally on the route of tropical storms and hurricanes, which are known to induce landslides (Lepore et al., 2012; Besette-Kirton et al., 2019). Increased deforestation due to anthropogenic activity additionally increases the susceptibility to landslides via destabilizing the water-saturated slopes (Larsen & Parks, 1997). Therefore, sediment budget within the watersheds is likely affected by anthropogenic erosion, chemical weathering, hurricane deposits, as well as storm induced landslides.

Anza Borrego

We collected fluvial sediment and soil samples from the Anza Borrego Desert, which is a 2400 km² section of the Sonoran Desert region, in December 2013. Anza Borrego has a hot and dry desert climate with MAT of 23°C and MAP of 150 mm/yr (Geiger & Pohl, 1953; Joo et al., 2016). There is limited fluvial transport within the watershed, but rare, intense precipitation events result in stream and overland flow (Joo et al., 2016; 2018b). This watershed is largely underlain by tonalitic bedrock, within a region that contains Jurassic metamorphic and Cretaceous plutonic units (Remeika & Lindsay, 1992).

Anza Borrego is largely affected by active tectonics due to activity along the Elsinore fault zones (Dorsey et al., 2011). Uplift of the Peninsular Ranges batholith may have been generating sediments via erosion since the Pliocene and early Pleistocene, forming Quaternary alluvial fans and filling up the “wineglass canyon”, where our study site is located (Remeika & Lindsay, 1992; Axen & Fletcher, 1998).

Detailed Mineralogic Descriptions

Felsic minerals

Quartz and feldspar combined compose the majority of all the mud-sized sediments examined, with feldspars being the most abundant phase (Table 1.3). Quartz + feldspar within most of the field sites are ~40-45%, except for significantly higher primary felsic mineral content in Peru (~83%) and Anza Borrego (~77%). The mud fractions with high felsic mineral content in Peru and Anza Borrego are composed of ~55% and ~60% feldspar and ~28% and ~16% quartz, respectively.

All field sites contain a range of calcic-sodic plagioclases and sodic-potassic alkali feldspars. Antarctica, Iceland, Norway and Puerto Rico are dominated by calcic plagioclases (labradorite>bytownite>anorthite), whereas Peru, Washington and Anza Borrego have higher sodic plagioclase content (albite dominated Washington and Anza Borrego; oligoclase dominated in Peru). K-feldspars (microcline and orthoclase) represent the alkali feldspar content in a majority of the sediments with occasional anorthoclase occurrences in Antarctic, Washington, and Peru samples. Plagioclase dominates the feldspar fraction in all field sites. Antarctica, Peru and Norway sediments have lower plagioclase/alkali feldspar ratios on average (2.7-3.5), compared to Anza Borrego, Puerto Rico and Washington sediments (8.3-9.3) that have significantly lower alkali feldspars abundances. Felsic mineral content of basaltic Iceland sediments, as they only contain 1.1% cristobalite and 0.6% alkali feldspar in average.

Mafic minerals

Mafic primary mineral concentrations are significantly lower in the mud fractions from Peru (0.7%) and Norway (1.7%) sediments, whereas mafic mineral concentrations are highest in Iceland sediments (62.1%), as expected. Antarctica, Washington and Puerto Rico sediments have

similar mafic primary mineral contents on average (10%, 15%, and 11%, respectively).

Amongst the mafic minerals observed, mud-sized sediments from Iceland and Antarctica contain higher pyroxene contents, while amphibole dominates in Puerto Rico, Washington and Norway sediments, and Peru sediments contain almost equal concentrations of both. Anza Borrego sediments do not contain any mafic minerals (other than biotite) and Iceland sediments are the only samples containing olivine (forsterite).

Iceland sediments have the highest pyroxene content (18.6%), followed by Antarctic samples (6.7%). Other field sites contain less than 1% pyroxene on average with some local enrichments (Table 1.3). Overall, pyroxene compositions are dominated by clinopyroxenes (augite>diopside>hedenbergite). However, orthopyroxene (enstatite) also occurs in muds collected in Iceland and Wright Valley (Antarctica) in lower abundance.

Washington and Puerto Rico muds have higher amphibole contents on average (15% and 11%, respectively), followed by Antarctica (3.6%), Norway (1.7%) and Peru sediments (0.3%). Icelandic muds do not contain amphiboles. Actinolite dominates the amphibole content of most of the muds, with tremolite content higher in Antarctic sediments and only hornblende observed in Puerto Rico muds. Occasional edenite (Antarctic Wright Valley, Washington), richterite (Peru) and ferri-clinoholmquistite (Washington) were also observed. Note that the Washington field area is partially underlain by bedrock that includes amphibolite facies accompanied by epidote occurrences, resulting in the highest diversity in amphibole content as compared to other field sites.

Mica

Overall, mica content is (muscovite + biotite + phlogopite; Table 1.3) is highest in Peru and Antarctica sediments (~11% on average), followed by Anza Borrego (8%), Washington

(6.1%), Puerto Rico (4.5%) and Norway (2.5%). Iceland muds do not contain any mica minerals. Puerto Rico mica content is exclusively biotite, which generally predominates in muds from all the other field sites except Norway. Norway muds contain muscovite, except for one drift sample with biotite. Muscovite was also observed commonly in Peru and Antarctic muds where it can locally dominate the mica content or is present in equal abundance to biotite. Phlogopite was also observed in Washington and Anza Borrego muds. It is also important to note that most of the Antarctic sampling locations are underlain by biotite orthogneiss (Hall et al., 2000; Marra et al., 2017), resulting in the higher biotite content of Antarctic sediments.

Accessory minerals

Accessory mineral phases are generally Fe- and Ti-oxides, as well as rare apatite occurrences observed the within muds from all field sites. Antarctic sediments also commonly contained cordierite group minerals which were not observed in the other sites. Abundances of accessory minerals are reported in Table 1.3 as the sum of all accessory minerals within each sample.

Antarctic muds contain birnessite (Taylor Valley), magnetite (Wright Valley), as well as apatite (Wright Valley). Iceland muds contain ilmenite and magnetite, whereas we detected hematite in only Norway soils, and Washington muds contain titanite and anatase as accessory oxides. Joo et al. (2018) reported up to 1.4% Fe-oxides in Anza Borrego muds, though we did not detect any in our analyses, potentially due to falling below detection limit of 1%.

Note that wet sieving and treating the muds with acetic acid and hydrogen peroxide like removed any salts, carbonates, and sulfide species, respectively. We also noted individual occurrences of apatite within Taylor Valley and Washington. However, these occurrences were modeled below 1% by the Jade software, therefore, we did not take them into account, using a

detection limit of 1%. However, apatite can dissolve with washing and acid treatments and could be more concentrated in higher grain sizes.

Zeolites

Zeolites were only observed within glacial settings, where the highest concentrations are observed within Washington muds (8.5% on average), followed by Norway (0.9%), Antarctica (0.7%), Iceland (0.7%), and Peru (0.2%). Washington sediments show the highest abundances of zeolites within the mud fraction, with laumontite concentrations reach up to 21% within glaciofluvial muds with rest of the zeolite composition generally consisting of stilbite and analcime. Zeolite concentrations within Norway muds reach up to 5%, mostly composed of heulandite and babingtonite. Though the average concentration of zeolite is low in Antarctic muds, zeolite occurrences are more frequent and diverse, ranging between 1-8.7%, where chabazite, babingtonite, heulandite and clinoptilolite. Iceland and Peru muds had only one detectable zeolite occurrence each, with 2% and 2.6% abundance, respectively.

Amorphous phases

Based on the XRD data, amorphous phases are likely common in both the Icelandic and Antarctic sediment samples. We infer from the hump-shaped background observed within the XRD pattern (Figure S1.1) is due to amorphous silica-rich phases. Therefore, we did further modeling analysis of the mineralogy observed within an Antarctic glacial drift (T10-HOW-9Drift) with ClaySIM to elucidate potential amorphous phases. Our analysis indicated that up to 7-8% of the clay-sized fraction was composed of amorphous smectite within the Antarctic drift. Total amorphous content within Icelandic sediments were comparable between Jade and ClaySIM (20-38%, Table 1.3). According to the representative ClaySIM modeling of Icelandic glacial outwash meltwater stream sample (EYF-2-IS), 4-8% of the amorphous phases are likely

amorphous smectites, with the rest being composed of volcanic glass. Jade analyses also included 2-4% Opal-A within the Icelandic amorphous phases. In Table 1.3, we report the total amorphous content (Opal-A + other amorphous silica) modeled by the Jade software.

Supplementary Figures for Chapter 1

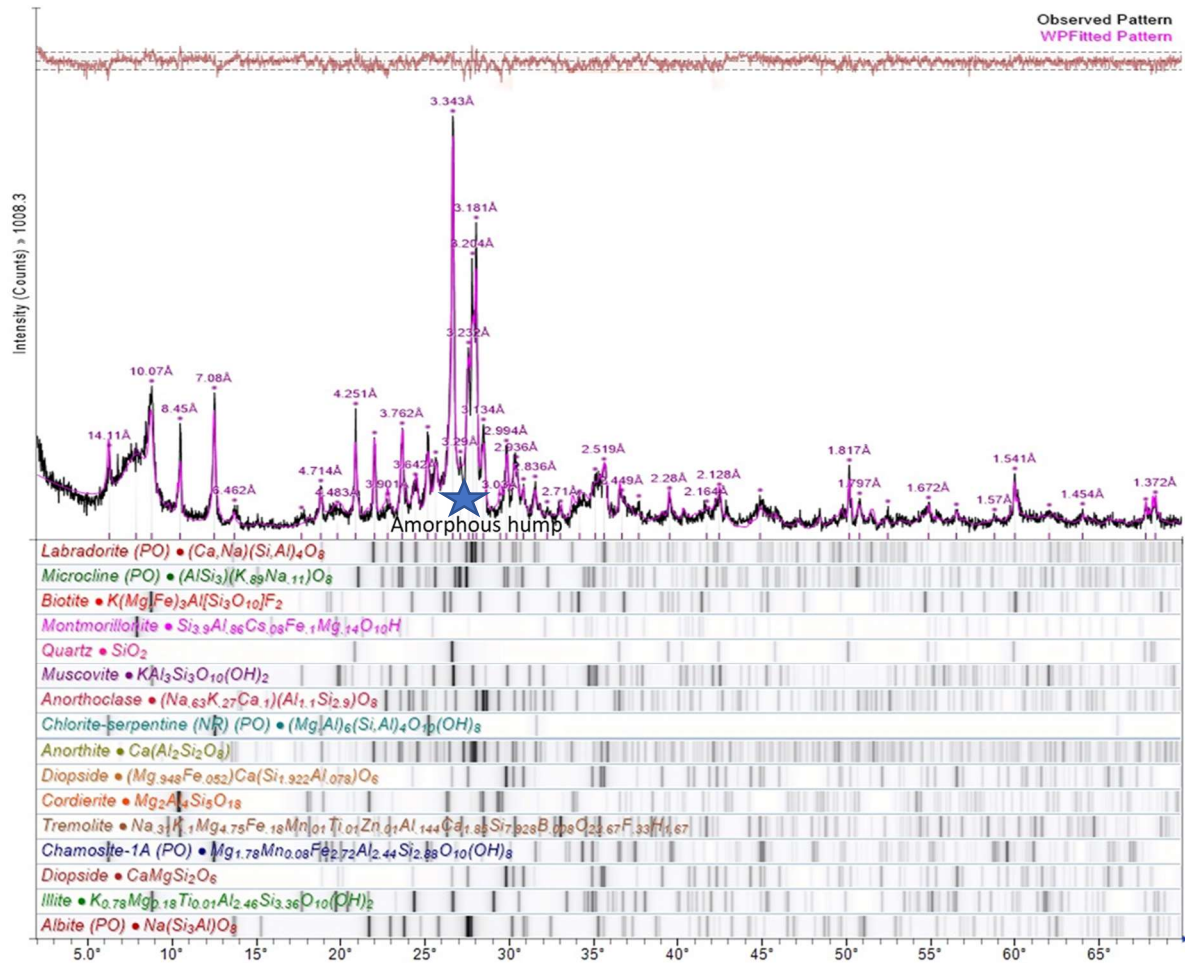


Figure S1.1. Example XRD pattern fitting with JADE software on an Antarctic Taylor Valley drift sample (T10-HOW-9Drift). Blue star demonstrates the location of the “amorphous hump” that shows there are amorphous phases in Antarctic samples.

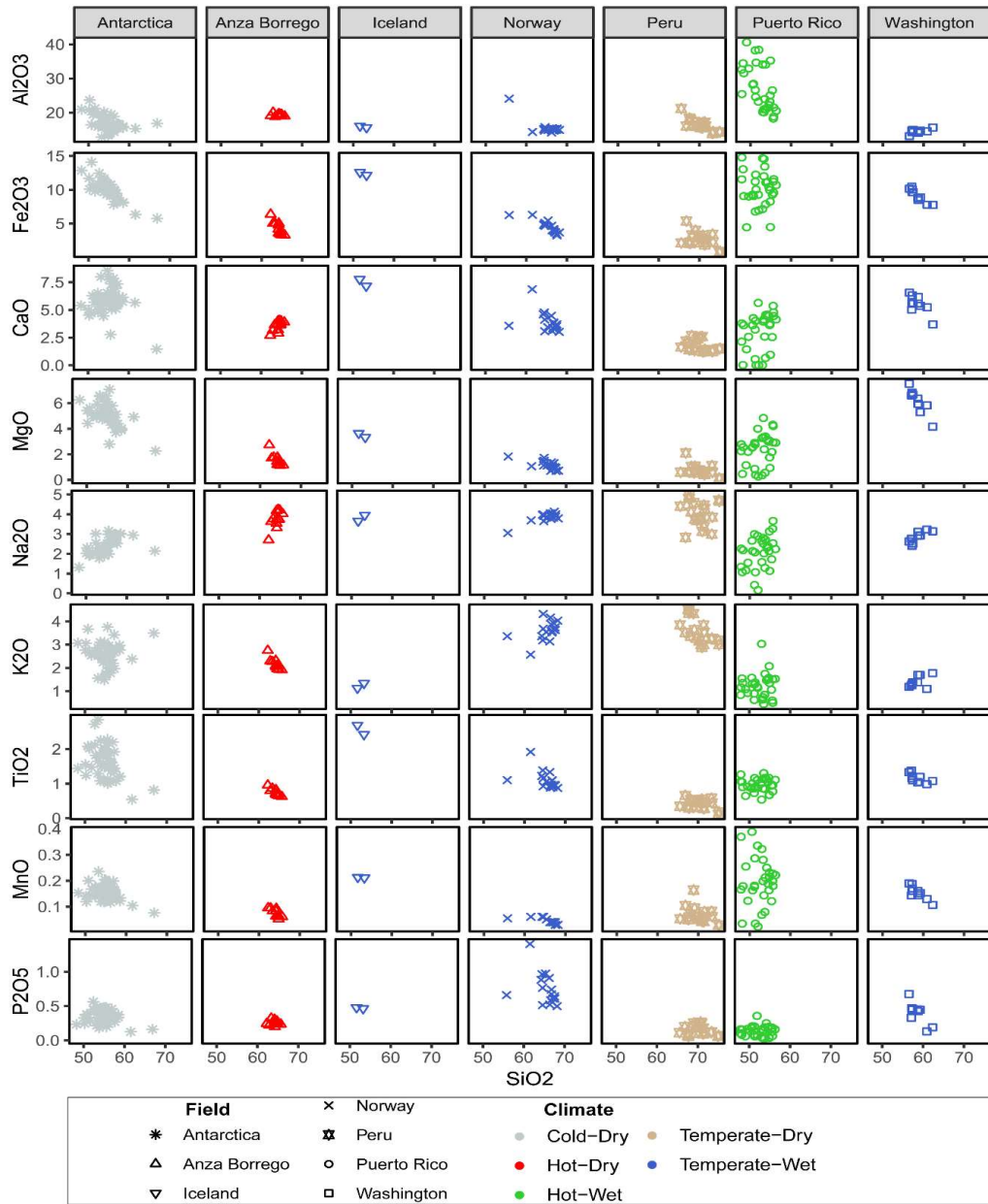


Figure S1.2. Selected major oxides plotted against SiO_2 for all field sites. All concentrations are in wt %, and data points are colored with respect to climatic regime, as illustrated in the legend.

The most obvious trends suggestive of weathering are the decreasing of Al₂O₃ concentrations with increasing SiO₂ within Antarctica, Peru, and Puerto Rico muds.

Supplementary Tables for Chapter 1

Table S1.1. Meta data of all samples

Sample Number	Field	Location	Latitude (decimal)	Longitude (decimal)	Elevation (m)
122612-2	Antarctica	Taylor Valley	-77.6234	162.8978	108
122612-1	Antarctica	Taylor Valley	-77.6232	162.8977	
011213-12	Antarctica	Taylor Valley	-77.6380	162.8848	
122512-13	Antarctica	Taylor Valley	-77.5757	163.4922	
122412-1	Antarctica	Taylor Valley	-77.5783	163.5416	
123012-12	Antarctica	Taylor Valley	-77.7330	162.3227	
122412-5	Antarctica	Taylor Valley	-77.5789	163.5404	
123012-5	Antarctica	Taylor Valley	-77.7428	162.3470	520
122512-12	Antarctica	Taylor Valley	-77.5755	163.4928	20
122412-7	Antarctica	Taylor Valley	-77.5791	163.5395	424
122412-2	Antarctica	Taylor Valley	-77.5782	163.5414	389
010213-2	Antarctica	Taylor Valley	-77.7286	162.3435	389
011213-13	Antarctica	Taylor Valley	-77.5819	163.4934	389
122312-6	Antarctica	Taylor Valley	-77.7288	162.3447	389
010213-1	Antarctica	Taylor Valley	-77.5790	163.5392	6
122312-8	Antarctica	Taylor Valley	-77.5817	163.4928	
122412-8	Antarctica	Taylor Valley	-77.5790	163.5392	
123012-11	Antarctica	Taylor Valley	-77.7330	162.3215	297
Whillans	Antarctica	Whillans Ice Sheet	-83.4783	-138.2461	334
T10-GOLD-10Drift	Antarctica	Taylor Valley	-77.6518	162.9331	447
T10-GOLD-12Drift	Antarctica	Taylor Valley	-77.6518	162.9331	371
T10-GOLD-9Drift	Antarctica	Taylor Valley	-77.6654	162.9106	492
T10-GOLD-1	Antarctica	Taylor Valley	-77.6865	162.8721	611
T10-Gold 2	Antarctica	Taylor Valley	-77.6861	162.8768	608
T10-Gold 4	Antarctica	Taylor Valley	-77.6842	162.8731	577
T10-Gold 5	Antarctica	Taylor Valley	-77.6823	162.8765	577
T10-Gold 6	Antarctica	Taylor Valley	-77.6804	162.8814	554
T10-GOLD-7	Antarctica	Taylor Valley	-77.6788	162.8892	536
T10-GOLD-9	Antarctica	Taylor Valley	-77.6738	162.6738	491
T10-Gold 10	Antarctica	Taylor Valley	-77.6693	162.9055	452
T10-Gold 11	Antarctica	Taylor Valley	-77.6653	162.9128	400
T10-Gold 12	Antarctica	Taylor Valley			
T10-Gold 13	Antarctica	Taylor Valley	-77.6592	162.9309	343
T10-GOLD-14	Antarctica	Taylor Valley	-77.6561	162.9203	352

T10-Gold 15	Antarctica	Taylor Valley	-77.6235	163.1093	339
T10-HOW-8Drift	Antarctica	Taylor Valley	-77.6570	163.0967	
T10-HOW-9Drift	Antarctica	Taylor Valley	-77.6598	163.0843	255
T10-HOW-10Drift	Antarctica	Taylor Valley	-77.6619	163.0692	279
T10-HOW-12Drift	Antarctica	Taylor Valley	-77.6729	162.8951	297
HOW-1	Antarctica	Taylor Valley	-77.6272	163.1150	24
HOW-2	Antarctica	Taylor Valley	-77.6313	163.1110	41
HOW-3	Antarctica	Taylor Valley	-77.6344	163.1193	69
HOW-4	Antarctica	Taylor Valley	-77.6379	163.1287	89
HOW-5	Antarctica	Taylor Valley	-77.6423	163.1260	127
HOW-6	Antarctica	Taylor Valley	-77.6467	163.1228	158
T10-HOW-7	Antarctica	Taylor Valley	-77.6503	163.1103	190
T10-HOW-8	Antarctica	Taylor Valley	-77.6570	163.0967	
T10-HOW-9	Antarctica	Taylor Valley	-77.6598	163.0843	255
HOW-10	Antarctica	Taylor Valley	-77.6619	163.0692	279
HOW-11	Antarctica	Taylor Valley	-77.6622	163.0746	286
HOW-12	Antarctica	Taylor Valley	-77.6729	162.8951	297
HOW-13	Antarctica	Taylor Valley	-77.6728	162.9023	287
D7	Antarctica	Taylor Valley			
T10-CAMP-SP-0cm	Antarctica	Taylor Valley	-77.6518	162.9331	374
T10-CAMP-SP-10cm	Antarctica	Taylor Valley	-77.6518	162.9331	374
T10-CAMP-SP-20cm	Antarctica	Taylor Valley	-77.6518	162.9331	374
T10-CAMP-SP-30cm	Antarctica	Taylor Valley	-77.6518	162.9331	374
BHS-90-115	Antarctica	Wright Valley			
BHS-93-36	Antarctica	Wright Valley			
BHS-93-34	Antarctica	Wright Valley			
BHS-93-20	Antarctica	Wright Valley			
BHS-90-027z	Antarctica	Wright Valley			
BHS-93-19	Antarctica	Wright Valley			
BHS-93-23	Antarctica	Wright Valley			
BHS-93-29	Antarctica	Wright Valley			
BHS-93-28	Antarctica	Wright Valley			
10-OR-14	Antarctica	Wright Valley	-77.4501	162.4976	264
10-OR-16	Antarctica	Wright Valley	-77.4553	162.4764	255
10-OR-19	Antarctica	Wright Valley	-77.4631	162.4428	252
UOR-SP-10cm	Antarctica	Wright Valley	-77.4332	162.4054	336
UOR-SP-20cm	Antarctica	Wright Valley	-77.4332	162.4054	
UOR-SP-30cm	Antarctica	Wright Valley	-77.4332	162.4054	
<i>UOR-SP-Merged</i>	Antarctica	Wright Valley	-77.4332	162.4054	336
10-CG-1	Antarctica	Wright Valley	-77.4176	162.5365	460-470
W10-CG-2	Antarctica	Wright Valley	-77.4180	162.5532	455
W10-CG-3	Antarctica	Wright Valley	-77.4178	162.5689	450
W10-CG-4	Antarctica	Wright Valley	-77.4189	162.5918	443
W10-CG-5	Antarctica	Wright Valley	-77.4193	162.6103	430
10-CG-6	Antarctica	Wright Valley	-77.4211	162.6280	402

W10-CG-7	Antarctica	Wright Valley	-77.4272	162.6559	317
W10-CG-8	Antarctica	Wright Valley	-77.4315	162.6604	297
W10-CG-9	Antarctica	Wright Valley	-77.4357	162.6613	289
W10-CG-10	Antarctica	Wright Valley	-77.4395	162.6493	284
10-CG-12	Antarctica	Wright Valley	-77.4444	162.6327	275
10-DG-1	Antarctica	Wright Valley	-77.4619	162.6126	539
W10-DG-2	Antarctica	Wright Valley	-77.4627	162.6160	544
W10-DG-3	Antarctica	Wright Valley	-77.4614	162.6190	520
W10-DG-4	Antarctica	Wright Valley	-77.4588	162.6196	447
W10-DG-5	Antarctica	Wright Valley	-77.4568	162.6155	420
W10-DG-6	Antarctica	Wright Valley	-77.4547	162.6167	379
W10-DG-7	Antarctica	Wright Valley	-77.4524	162.6159	328
W10-DG-8	Antarctica	Wright Valley	-77.4500	162.6130	286
10-DG-9	Antarctica	Wright Valley	-77.4485	162.6065	284
10-DG-10	Antarctica	Wright Valley	-77.4478	162.5981	285
W10-DG-11	Antarctica	Wright Valley	-77.4456	162.5993	272
W10-DWG-1	Antarctica	Wright Valley	-77.4709	162.5429	600
W10-DWG-3	Antarctica	Wright Valley	-77.4693	162.5266	480
W10-DWG-4	Antarctica	Wright Valley	-77.4686	162.5178	425
W10-DWG-5	Antarctica	Wright Valley	-77.4681	162.5088	393
W10-DWG-7	Antarctica	Wright Valley	-77.4664	162.4931	309
W10-DWG-8	Antarctica	Wright Valley	-77.4649	162.4859	266
T10-MAG-2	Antarctica	Taylor Valley	-77.6956	162.7449	704
10-LWG-1	Antarctica	Wright Valley	-77.4116	162.8083	
W10-CG-SP1-10cm	Antarctica	Wright Valley	-77.4179	162.5560	453
W10-CG-SP1-20cm	Antarctica	Wright Valley	-77.4179	162.5560	453
W10-CG-SP1-30cm	Antarctica	Wright Valley	-77.4179	162.5560	453
LP-16-1	Peru	Lake Paron	-8.9889	-77.6697	4177
LP-16-2	Peru	Lake Paron	-8.9991	-77.6841	4179
RL-16-1	Peru	Rio Llanganuco	-9.0513	-77.6170	3855
RL-16-2	Peru	Rio Llanganuco	-9.0682	-77.6395	3852
RL-16-3	Peru	Rio Llanganuco	-9.0809	-77.6534	3781
RL-16-4	Peru	Rio Llanganuco	-9.0870	-77.6593	3657
RL-16-5	Peru	Rio Llanganuco	-9.0931	-77.6680	3562
RL-16-6	Peru	Rio Llanganuco	-9.0994	-77.6746	3469
RL-16-7	Peru	Rio Llanganuco	-9.1450	-77.7041	2775
RL-16-8	Peru	Rio Llanganuco	-9.1542	-77.7150	2635
RL-16-Distal	Peru	Rio Llanganuco	-9.1691	-77.7257	2499
Llaka Lake Debris	Peru	Lake Paron	-9.4344	-77.4436	4473
RP-16-1D	Peru	Rio Paron	-9.0036	-77.6874	4100
RP-16-2	Peru	Rio Paron	-9.0082	-77.6944	
RP-16-3	Peru	Rio Paron	-9.0126	-77.7000	3958
RP-16-4D	Peru	Rio Paron	-9.0181	-77.7069	
RP-16-5	Peru	Rio Paron	-9.0240	-77.7159	3735
RP-16-6	Peru	Rio Paron	-9.0392	-77.7328	3290

RP-16-7	Peru	Rio Paron	-9.0287	-77.7237	
RP-16-8	Peru	Rio Paron	-9.0504	-77.7466	3016
Zona de Pitek 20 cm	Peru	Unchus	9.4917	77.4726	3704
Zona de Pitek 60 cm	Peru	Unchus	9.4917	77.4726	3704
MS Glacial Drift	Washington	Mount Stuart	47.4868	-120.9003	411
MS B1 SED Horshoe	Washington	Mount Stuart	47.4890	-120.9008	1660
MSA-1	Washington	Mount Stuart	47.5021	-120.8497	1400
MSA-2	Washington	Mount Stuart	47.5046	-120.8426	1390
MSA-3	Washington	Mount Stuart	47.5092	-120.8304	1220
MSA-5	Washington	Mount Stuart	47.5336	-120.8155	1070
MSB-4 SED	Washington	Mount Stuart	47.4979	-120.86079	
MSB-5 Sed-1	Washington	Mount Stuart	47.5041	-120.84012	
MSB-5 Sed-2	Washington	Mount Stuart	47.5041	-120.84012	
MSB-5 Soil	Washington	Mount Stuart	47.5041	-120.84005	1380
MSc A1	Washington	Mount Stuart	47.5020	-120.8423	1410
AUS Drift PROX	Norway	Austerdalsbreen	61.5840	7.0010	407
AUS Drift Distal	Norway	Austerdalsbreen	61.5630	6.9920	318
AUS-1	Norway	Austerdalsbreen	61.5890	6.9940	
AUS-SED-2	Norway	Austerdalsbreen	61.5830	7.0030	385
AUS-3	Norway	Austerdalsbreen	61.5790	6.9960	360
AUS-SED-4	Norway	Austerdalsbreen	61.5730	6.9930	340
AUS-5	Norway	Austerdalsbreen	61.5630	6.9930	317
AUS-SED-6	Norway	Austerdalsbreen	61.5570	6.9900	329
AUS-7	Norway	Austerdalsbreen	61.5440	6.9770	288
AUS-SED-8	Norway	Austerdalsbreen	61.5413	6.9703	251
AUS-SED-Lake	Norway	Austerdalsbreen	61.5860	6.9990	427
AUS-PED-10CM	Norway	Austerdalsbreen	61.5413	6.9703	253
AUS-PED-20CM	Norway	Austerdalsbreen	61.5413	6.9703	253
AUS-PED-30CM	Norway	Austerdalsbreen	61.5413	6.9703	253
AUS-PED-50CM	Norway	Austerdalsbreen	61.5413	6.9703	253
AUS-PED-1M	Norway	Austerdalsbreen	61.5413	6.9703	253
<i>AUS-PED-Merged</i>	Norway	Austerdalsbreen	61.5413	6.9703	252
LANG Drift Prox	Norway	Langedalsbreen	61.5577	6.9139	278
LANG5	Norway	Langedalsbreen	61.5501	6.9391	
LANG7	Norway	Langedalsbreen	61.5455	6.9583	256
LANG9	Norway	Langedalsbreen	61.5371	6.9666	
ELVA-1	Norway	Elvabakkane	61.5350	6.9690	248
ELVA-3	Norway	Elvabakkane	61.5200	6.9790	236
ELVA-5	Norway	Elvabakkane	61.5078	6.9836	
ELVA-7	Norway	Elvabakkane	61.4966	6.9851	
ELVA-9	Norway	Elvabakkane	61.4861	6.9993	
ELVA-11	Norway	Elvabakkane	61.4805	7.0196	
ELVA-13	Norway	Elvabakkane	61.4688	7.0358	170

VEITASTROND-LAKE-SED	Norway	Veitastrond	61.4634	7.0368	172
EYF-1-IS	Iceland	South, Ásólfsskáli	63.6810	-19.6339	
EYF-2-IS	Iceland	South, Ásólfsskáli	63.6829	-19.6361	173
EYF-3-IS	Iceland	South, Ásólfsskáli	63.6696	-19.6251	364
PM-RG-SED-1	Puerto Rico	Rio Guayanes	18.0674	-65.9912	
PM-RG-SED-2	Puerto Rico	Rio Guayanes	18.0691	-65.9957	
PM-RG-SED-3	Puerto Rico	Rio Guayanes	18.0747	-65.9896	
PM-RG-SED-4	Puerto Rico	Rio Guayanes	18.0806	-65.9838	
PM-RG-SED-5	Puerto Rico	Rio Guayanes	18.0813	-65.9749	
PM-RG-SED-6	Puerto Rico	Rio Guayanes	18.0794	-65.9596	
PM-RG-SED-7	Puerto Rico	Rio Guayanes	18.0577	-65.9220	
PM-RG-SED-8	Puerto Rico	Rio Guayanes	18.0528	-65.9115	
PM-RG-SED-9	Puerto Rico	Rio Guayanes	18.0597	-65.8753	
PM-RG-SED-10	Puerto Rico	Rio Guayanes	18.0569	-65.8999	
PM-RG-SAP-1	Puerto Rico	Rio Guayanes	18.0648	-65.9950	
PM-RG-SAP-2	Puerto Rico	Rio Guayanes	18.0682	-65.9922	
PM-RG-SAP-3	Puerto Rico	Rio Guayanes	18.0747	-65.9896	
PM-RG-SAP-4Red	Puerto Rico	Rio Guayanes	18.0735	-65.9883	
PM-RG-SAP-5A	Puerto Rico	Rio Guayanes	18.0753	-65.9338	
PM-RG-SAP-5B	Puerto Rico	Rio Guayanes	18.0753	-65.9338	
PM-RG-SAP-6A-Red	Puerto Rico	Rio Guayanes	18.0781	-65.9387	
PM-RG-SAP-6B-Yellow	Puerto Rico	Rio Guayanes	18.0781	-65.9387	
PM-RG-SAP-6C-Brown	Puerto Rico	Rio Guayanes	18.0781	-65.9387	
PM-RB-SED-1	Puerto Rico	Rio Guayoba	18.0545	-65.9451	
PM-RB-SED-2	Puerto Rico	Rio Guayoba	18.0524	-65.9389	
PM-RB-SED-3	Puerto Rico	Rio Guayoba	18.0503	-65.9292	
PM-RB-SED-4	Puerto Rico	Rio Guayoba	18.0491	-65.9228	
RG-14-SOIL-2	Puerto Rico	Rio Guayanes			
RG-14-SOIL-4	Puerto Rico	Rio Guayanes			
RG-14-SOIL-6	Puerto Rico	Rio Guayanes			
RB-14-SED-1	Puerto Rico	Rio Guayoba	18.0490	-65.9233	
RB-14-SED-2	Puerto Rico	Rio Guayoba	18.0508	-65.9300	
RB-14-SED-3	Puerto Rico	Rio Guayoba	18.0523	-65.9389	
RB-14-SED-4	Puerto Rico	Rio Guayoba	18.0544	-65.9454	
RB-14-SED-5	Puerto Rico	Rio Guayoba	18.0603	-65.9518	
IGNF-13-SOIL-1	South California	Anza Borrego	32.8540	-116.2880	
IGNF-13-SOIL-2	South California	Anza Borrego	32.8540	-116.2880	
IGNF-13-SOIL-3	South California	Anza Borrego	32.8540	-116.2880	
IGNF-13-SOIL-4	South California	Anza Borrego	32.8540	-116.2880	

IGNF-13-SOIL-5	South California	Anza Borrego	32.8540	-116.2880
IGNF-13-SOIL-6	South California	Anza Borrego	32.8540	-116.2880
IGNF-13-SOIL-7	South California	Anza Borrego	32.8540	-116.2880
IGNF-13-SED-1	South California	Anza Borrego	32.8537	-116.2886
IGNF-13-SED-5	South California	Anza Borrego	32.8573	-116.2731
IGNF-13-SED-7	South California	Anza Borrego	32.8595	-116.2632
IGNF-13-SED-11	South California	Anza Borrego	32.8637	-116.2444
IGNF-13-SED-13	South California	Anza Borrego	32.8685	-116.2383
IGNF-13-SED-15	South California	Anza Borrego	32.8718	-116.2187

Table S1.1. (Continued)

Sample Number	Field	Age	Sediment type	Ice basal regime
122612-2	Antarctica	Modern	Water track	
122612-1	Antarctica	Modern	Water track	
011213-12	Antarctica	Modern	Water track	
122512-13	Antarctica	Modern	Water track	
122412-1	Antarctica	Modern	Water track	
123012-12	Antarctica	Modern	Water track	
122412-5	Antarctica	Modern	Water track	
123012-5	Antarctica	Modern	Water track	
122512-12	Antarctica	Modern	Water track	
122412-7	Antarctica	Modern	Water track	
122412-2	Antarctica	Modern	Water track	
010213-2	Antarctica	Modern	Water track	
011213-13	Antarctica	Modern	Water track	
122312-6	Antarctica	Modern	Water track	
010213-1	Antarctica	Modern	Water track	
122312-8	Antarctica	Modern	Water track	
122412-8	Antarctica	Modern	Water track	
123012-11	Antarctica	Modern	Water track	
Whillans	Antarctica	Modern	Subglacial drift	wet-based ice
T10-GOLD-10Drift	Antarctica	LP-LGM	Drift	partly wet-based
T10-GOLD-12Drift	Antarctica	LP-LGM	Drift	partly wet-based
T10-GOLD-9Drift	Antarctica	LP-LGM	Drift	partly wet-based

T10-GOLD-1	Antarctica	Modern	Proglacial fluvial	
T10-Gold 2	Antarctica	Modern	Proglacial fluvial	
T10-Gold 4	Antarctica	Modern	Proglacial fluvial	
T10-Gold 5	Antarctica	Modern	Proglacial fluvial	
T10-Gold 6	Antarctica	Modern	Proglacial fluvial	
T10-GOLD-7	Antarctica	Modern	Proglacial fluvial	
T10-GOLD-9	Antarctica	Modern	Proglacial fluvial	
T10-Gold 10	Antarctica	Modern	Proglacial fluvial	
T10-Gold 11	Antarctica	Modern	Proglacial fluvial	
T10-Gold 12	Antarctica	Modern	Proglacial fluvial	
T10-Gold 13	Antarctica	Modern	Proglacial fluvial	
T10-GOLD-14	Antarctica	Modern	Proglacial fluvial	
T10-Gold 15	Antarctica	Modern	Proglacial fluvial	
T10-HOW-8Drift	Antarctica	LP-LGM	Drift	partly wet-based
T10-HOW-9Drift	Antarctica	LP-LGM	Drift	partly wet-based
T10-HOW-10Drift	Antarctica	LP-LGM	Drift	partly wet-based
T10-HOW-12Drift	Antarctica	LP-LGM	Drift	partly wet-based
HOW-1	Antarctica	Modern	Proglacial fluvial	
HOW-2	Antarctica	Modern	Proglacial fluvial	
HOW-3	Antarctica	Modern	Proglacial fluvial	
HOW-4	Antarctica	Modern	Proglacial fluvial	
HOW-5	Antarctica	Modern	Proglacial fluvial	
HOW-6	Antarctica	Modern	Proglacial fluvial	
T10-HOW-7	Antarctica	Modern	Proglacial fluvial	
T10-HOW-8	Antarctica	Modern	Proglacial fluvial	
T10-HOW-9	Antarctica	Modern	Proglacial fluvial	
HOW-10	Antarctica	Modern	Proglacial fluvial	
HOW-11	Antarctica	Modern	Proglacial fluvial	
HOW-12	Antarctica	Modern	Proglacial fluvial	
HOW-13	Antarctica	Modern	Proglacial fluvial	
D7	Antarctica	Modern	Proglacial fluvial	
T10-CAMP-SP-0cm	Antarctica	LP-LGM	Soil	
T10-CAMP-SP-10cm	Antarctica	LP-LGM	Soil	
T10-CAMP-SP-20cm	Antarctica	LP-LGM	Soil	
T10-CAMP-SP-30cm	Antarctica	LP-LGM	Soil	
BHS-90-115	Antarctica	EQ_Pliocene	Drift	cold-based ice
BHS-93-36	Antarctica	E-M Q	Drift	cold-based ice
BHS-93-34	Antarctica	E-M Q	Drift	cold-based ice
BHS-93-20	Antarctica		Drift	
BHS-90-027z	Antarctica	Miocene	Drift	wet-based ice
BHS-93-19	Antarctica		Drift	
BHS-93-23	Antarctica	E-M Q	Drift	cold-based ice

BHS-93-29	Antarctica	LQ	Drift	cold-based ice
BHS-93-28	Antarctica		Drift	cold-based ice
10-OR-14	Antarctica	Modern	Proglacial fluvial	
10-OR-16	Antarctica	Modern	Proglacial fluvial	
10-OR-19	Antarctica	Modern	Proglacial fluvial	
UOR-SP-10cm	Antarctica	LQ	Soil	
UOR-SP-20cm	Antarctica	LQ	Soil	
UOR-SP-30cm	Antarctica	LQ	Soil	
<i>UOR-SP-Merged</i>	Antarctica	LQ	Soil	
10-CG-1	Antarctica	Modern	Proglacial fluvial	
W10-CG-2	Antarctica	Modern	Proglacial fluvial	
W10-CG-3	Antarctica	Modern	Proglacial fluvial	
W10-CG-4	Antarctica	Modern	Proglacial fluvial	
W10-CG-5	Antarctica	Modern	Proglacial fluvial	
10-CG-6	Antarctica	Modern	Proglacial fluvial	
W10-CG-7	Antarctica	Modern	Proglacial fluvial	
W10-CG-8	Antarctica	Modern	Proglacial fluvial	
W10-CG-9	Antarctica	Modern	Proglacial fluvial	
W10-CG-10	Antarctica	Modern	Proglacial fluvial	
10-CG-12	Antarctica	Modern	Proglacial fluvial	
10-DG-1	Antarctica	Modern	Proglacial fluvial	
W10-DG-2	Antarctica	Modern	Proglacial fluvial	
W10-DG-3	Antarctica	Modern	Proglacial fluvial	
W10-DG-4	Antarctica	Modern	Proglacial fluvial	
W10-DG-5	Antarctica	Modern	Proglacial fluvial	
W10-DG-6	Antarctica	Modern	Proglacial fluvial	
W10-DG-7	Antarctica	Modern	Proglacial fluvial	
W10-DG-8	Antarctica	Modern	Proglacial fluvial	
10-DG-9	Antarctica	Modern	Proglacial fluvial	
10-DG-10	Antarctica	Modern	Proglacial fluvial	
W10-DG-11	Antarctica	Modern	Proglacial fluvial	
W10-DWG-1	Antarctica	Modern	Proglacial fluvial	
W10-DWG-3	Antarctica	Modern	Proglacial fluvial	
W10-DWG-4	Antarctica	Modern	Proglacial fluvial	
W10-DWG-5	Antarctica	Modern	Proglacial fluvial	
W10-DWG-7	Antarctica	Modern	Proglacial fluvial	
W10-DWG-8	Antarctica	Modern	Proglacial fluvial	
T10-MAG-2	Antarctica	Modern	Proglacial fluvial	
10-LWG-1	Antarctica	Modern	Proglacial fluvial	
W10-CG-SP1-10cm	Antarctica		Soil	
W10-CG-SP1-20cm	Antarctica		Soil	
W10-CG-SP1-30cm	Antarctica		Soil	
LP-16-1	Peru	Modern	Proglacial lake	
LP-16-2	Peru	Modern	Proglacial lake	
RL-16-1	Peru	Modern	Proglacial fluvial	

RL-16-2	Peru	Modern	Proglacial fluvial	
RL-16-3	Peru	Modern	Proglacial fluvial	
RL-16-4	Peru	Modern	Proglacial fluvial	
RL-16-5	Peru	Modern	Proglacial fluvial	
RL-16-6	Peru	Modern	Proglacial fluvial	
RL-16-7	Peru	Modern	Proglacial fluvial	
RL-16-8	Peru	Modern	Proglacial fluvial	
RL-16-Distal	Peru	Modern	Proglacial fluvial	
Llaka Lake Debris	Peru	Modern	Drift	wet-based ice
RP-16-1D	Peru	Modern	Proglacial fluvial	
RP-16-2	Peru	Modern	Proglacial fluvial	
RP-16-3	Peru	Modern	Proglacial fluvial	
RP-16-4D	Peru	Modern	Proglacial fluvial	
RP-16-5	Peru	Modern	Proglacial fluvial	
RP-16-6	Peru	Modern	Proglacial fluvial	
RP-16-7	Peru	Modern	Proglacial fluvial	
RP-16-8	Peru	Modern	Proglacial fluvial	
Zona de Pitek 20 cm	Peru	Modern	Soil	
Zona de Pitek 60 cm	Peru	Modern	Soil	
MS Glacial Drift	Washington	Modern	Drift	wet-based ice
MS B1 SED Horshoe	Washington	Modern	Drift	wet-based ice
MSA-1	Washington	Modern	Proglacial fluvial	
MSA-2	Washington	Modern	Proglacial fluvial	
MSA-3	Washington	Modern	Proglacial fluvial	
MSA-5	Washington	Modern	Proglacial fluvial	
MSB-4 SED	Washington	Modern	Proglacial fluvial	
MSB-5 Sed-1	Washington	Modern	Proglacial fluvial	
MSB-5 Sed-2	Washington	Modern	Proglacial fluvial	
MSB-5 Soil	Washington	Recent	Soil	
MSc A1	Washington	Modern	Proglacial fluvial	
AUS Drift PROX	Norway	Little Ice Age	Drift	wet-based ice
AUS Drift Distal	Norway	Little Ice Age	Drift	wet-based ice
AUS-1	Norway	Modern	Proglacial fluvial	
AUS-SED-2	Norway	Modern	Proglacial fluvial	
AUS-3	Norway	Modern	Proglacial fluvial	
AUS-SED-4	Norway	Modern	Proglacial fluvial	
AUS-5	Norway	Modern	Proglacial fluvial	
AUS-SED-6	Norway	Modern	Proglacial fluvial	
AUS-7	Norway	Modern	Proglacial fluvial	
AUS-SED-8	Norway	Modern	Proglacial fluvial	
AUS-SED-Lake	Norway	Modern	Proglacial lake	
AUS-PED-10CM	Norway	Recent	Soil	
AUS-PED-20CM	Norway	Recent	Soil	

AUS-PED-30CM	Norway	Recent	Soil	
AUS-PED-50CM	Norway	Recent	Soil	
AUS-PED-1M	Norway	Recent	Soil	
<i>AUS-PED-Merged</i>	Norway	Recent	Soil	
LANG Drift Prox	Norway	Little Ice Age	Drift	wet-based ice
LANG5	Norway	Modern	Proglacial fluvial	
LANG7	Norway	Modern	Proglacial fluvial	
LANG9	Norway	Modern	Proglacial fluvial	
ELVA-1	Norway	Modern	Proglacial fluvial	
ELVA-3	Norway	Modern	Proglacial fluvial	
ELVA-5	Norway	Modern	Proglacial fluvial	
ELVA-7	Norway	Modern	Proglacial fluvial	
ELVA-9	Norway	Modern	Proglacial fluvial	
ELVA-11	Norway	Modern	Proglacial fluvial	
ELVA-13	Norway	Modern	Proglacial fluvial	
VEITASTROND-LAKE-SED	Norway	Modern	Proglacial lake	
EYF-1-IS	Iceland	Modern	Proglacial fluvial	
EYF-2-IS	Iceland	Modern	Proglacial fluvial	
EYF-3-IS	Iceland	Modern	Proglacial fluvial	
PM-RG-SED-1	Puerto Rico	Modern	Fluvial sediment	
PM-RG-SED-2	Puerto Rico	Modern	Fluvial sediment	
PM-RG-SED-3	Puerto Rico	Modern	Fluvial sediment	
PM-RG-SED-4	Puerto Rico	Modern	Fluvial sediment	
PM-RG-SED-5	Puerto Rico	Modern	Fluvial sediment	
PM-RG-SED-6	Puerto Rico	Modern	Fluvial sediment	
PM-RG-SED-7	Puerto Rico	Modern	Fluvial sediment	
PM-RG-SED-8	Puerto Rico	Modern	Fluvial sediment	
PM-RG-SED-9	Puerto Rico	Modern	Fluvial sediment	
PM-RG-SED-10	Puerto Rico	Modern	Fluvial sediment	
PM-RG-SAP-1	Puerto Rico		Saprolite	
PM-RG-SAP-2	Puerto Rico		Saprolite	
PM-RG-SAP-3	Puerto Rico		Saprolite	
PM-RG-SAP-4Red	Puerto Rico		Saprolite	
PM-RG-SAP-5A	Puerto Rico		Saprolite	
PM-RG-SAP-5B	Puerto Rico		Saprolite	
PM-RG-SAP-6A-Red	Puerto Rico		Saprolite	
PM-RG-SAP-6B-Yellow	Puerto Rico		Saprolite	
PM-RG-SAP-6C-Brown	Puerto Rico		Saprolite	
PM-RB-SED-1	Puerto Rico	Modern	Fluvial sediment	
PM-RB-SED-2	Puerto Rico	Modern	Fluvial sediment	
PM-RB-SED-3	Puerto Rico	Modern	Fluvial sediment	
PM-RB-SED-4	Puerto Rico	Modern	Fluvial sediment	

RG-14-SOIL-2	Puerto Rico		Soil
RG-14-SOIL-4	Puerto Rico		Soil
RG-14-SOIL-6	Puerto Rico		Soil
RB-14-SED-1	Puerto Rico	Modern	Fluvial sediment
RB-14-SED-2	Puerto Rico	Modern	Fluvial sediment
RB-14-SED-3	Puerto Rico	Modern	Fluvial sediment
RB-14-SED-4	Puerto Rico	Modern	Fluvial sediment
RB-14-SED-5	Puerto Rico	Modern	Fluvial sediment
IGNF-13-SOIL-1	California South		Soil
IGNF-13-SOIL-2	California South		Soil
IGNF-13-SOIL-3	California South		Soil
IGNF-13-SOIL-4	California South		Soil
IGNF-13-SOIL-5	California South		Soil
IGNF-13-SOIL-6	California South		Soil
IGNF-13-SOIL-7	California South		Soil
IGNF-13-SED-1	California South	Modern	Fluvial sediment
IGNF-13-SED-5	California South	Modern	Fluvial sediment
IGNF-13-SED-7	California South	Modern	Fluvial sediment
IGNF-13-SED-11	California South	Modern	Fluvial sediment
IGNF-13-SED-13	California South	Modern	Fluvial sediment
IGNF-13-SED-15	California	Modern	Fluvial sediment

Table S1.2. BET surface area values ($\text{m}^2 \text{g}^{-1}$), and LPSA (clay grain size fraction, $<4\mu\text{m}$; silt grain size fraction, $4\text{-}63\mu\text{m}$) of the muds, and granulometry (mud grain size fraction, $<63\mu\text{m}$; sand grain size fraction, $63\mu\text{m}\text{-}2 \text{mm}$; gravel grain size fraction, $>2\text{mm}$) results of the bulk fraction of the sediments.

Sample Number	BET (m^2g^{-1})	Grain size mode	Clay%	Silt%	Mud%	Sand%	Gravel%
122612-2	15.7	49.4	3.7	96.3	1.0	92.8	6.2
122612-1	5.4	3.1	49.9	50.1	3.4	85.3	11.3
011213-12	8.7	31.6	15.5	84.5	0.3	82.4	17.2
122512-13	63.8	3.1	37.6	62.4	0.8	92.8	6.4

122412-1	60.4	53.9	1.8	98.2	2.0	89.8	8.2
123012-12	20.5	56.8	1.7	98.3	6.4	90.8	2.8
122412-5	47.7	57.0	5.1	94.9	2.0	73.9	24.1
123012-5	15.1	9.0	14.9	85.1	53.8	46.2	0.0
122512-12	51.0	43.0	19.5	80.5	29.9	69.9	0.2
122412-7	44.4	31.1	14.8	85.2	20.7	76.5	2.7
122412-2	44.3	45.0	25.7	74.3	4.7	95.3	0.1
010213-2	29.5	62.1	7.6	92.4	11.7	88.3	0.0
011213-13	20.7	51.8	15.5	84.5	1.1	98.8	0.1
122312-6	28.8	56.6	5.3	94.7	11.5	88.5	0.0
010213-1	23.3	41.8	21.5	78.5	6.4	93.6	0.0
122312-8	28.5	56.9	13.2	86.8	2.8	97.2	0.0
122412-8	34.2	47.1	20.0	80.0	7.8	92.2	0.0
123012-11	49.7	50.7	14.9	85.1	9.9	90.1	0.0
Whillans	13.7						
T10-GOLD-10Drift	11.0	13.5	15.6	84.4	1.5	85.4	13.1
T10-GOLD-12Drift	30.1	2.8	73.1	26.9	5.8	65.7	28.6
T10-GOLD-9Drift	27.8	30.2	10.7	89.3	2.0	64.4	33.5
T10-GOLD-1	32.4	67.1	8.5	91.5	5.7	63.1	31.3
T10-Gold 2	39.8	43.7	33.7	66.3	6.4	79.4	14.2
T10-Gold 4	38.3	75.4	2.9	97.1	2.4	60.2	37.4
T10-Gold 5	15.0	23.7	4.7	95.3	2.5	63.8	33.7
T10-Gold 6	40.9	40.8	30.3	69.7	2.2	81.4	16.4
T10-GOLD-7	39.6	48.3	18.5	81.5	0.6	83.3	16.1
T10-GOLD-9	33.5	54.7	6.6	93.4	0.5	47.0	52.5
T10-Gold 10	24.7	38.6	12.5	87.5	0.6	59.9	39.5
T10-Gold 11	23.9	54.2	9.1	90.9	1.1	69.7	29.2
T10-Gold 12	33.6	50.2	31.0	69.0	1.2	62.6	36.2
T10-Gold 13	23.9	56.7	5.2	94.8	1.1	48.0	50.9
T10-GOLD-14	24.8	55.9	1.2	98.8	5.7	39.6	54.7
T10-Gold 15	66.3	3.7	37.6	62.4	6.4	79.5	14.1
T10-HOW-8Drift	32.4	45.8	15.4	84.6	1.5	75.9	22.6
T10-HOW-9Drift	51.0	8.7	29.6	70.4	4.5	59.6	35.9
T10-HOW-10Drift	9.8	13.7	13.8	86.2	1.2	73.0	25.8
T10-HOW-12Drift	32.1	60.1	18.9	81.1	5.3	59.6	35.1
HOW-1	36.3	43.7	29.2	70.8	2.0	83.5	14.5
HOW-2	70.6	2.0	47.3	52.7	8.5	91.5	0.0
HOW-3	29.9	39.8	34.6	65.4	6.9	93.1	0.0
HOW-4	54.0	39.8	34.4	65.6	4.4	61.9	33.7
HOW-5	34.5	43.7	43.1	56.9	6.4	80.9	12.7
HOW-6	50.5	6.2	44.1	55.9	13.9	86.1	0.0
T10-HOW-7	34.3	5.8	34.5	65.5	1.4	59.9	38.7
T10-HOW-8	41.8	2.3	33.0	67.0	0.9	76.3	22.8
T10-HOW-9	32.3	5.4	32.7	67.3	5.8	90.9	3.3
HOW-10	64.8	6.5	45.5	54.5	12.7	62.9	24.5

HOW-11	20.3	43.7	26.6	73.4	11.0	89.0	0.0
HOW-12	64.6	26.2	34.9	65.1	4.8	74.1	21.2
HOW-13	22.9	43.7	28.8	71.2	25.7	74.3	0.0
D7	67.4	4.5	37.5	62.5	49.4	10.1	40.5
T10-CAMP-SP-0cm	57.1	41.9	22.6	77.4	3.7	72.4	23.9
T10-CAMP-SP-10cm	67.2	61.5	5.3	94.7	2.3	72.0	25.7
T10-CAMP-SP-20cm	66.0	46.3	10.4	89.6	7.1	72.1	20.8
T10-CAMP-SP-30cm	64.2	60.3	2.5	97.5	5.6	68.6	25.9
BHS-90-115	28.3	57.4	10.3	89.7	1.6	83.8	14.6
BHS-93-36	19.2	59.3	9.8	90.2	2.5	70.1	27.4
BHS-93-34	10.6	54.0	12.8	87.2	0.7	63.5	35.8
BHS-93-20	19.3	52.1	13.9	86.1	29.1	65.8	5.2
BHS-90-027z	27.8	27.5	33.1	66.9	39.5	36.4	24.1
BHS-93-19	9.2	64.6	16.9	83.0	0.2	74.6	25.2
BHS-93-23	14.2	48.0	19.2	80.8	1.0	62.5	36.4
BHS-93-29	6.7	29.8	9.8	90.2	0.1	10.4	89.5
BHS-93-28	10.1	61.4	3.7	96.3	2.1	50.7	47.2
10-OR-14	14.6	51.0	13.4	86.6	0.8	97.2	2.0
10-OR-16	9.3	60.3	5.6	94.4	1.0	95.2	3.8
10-OR-19	9.1	56.3	4.9	95.1	7.8	87.3	4.9
UOR-SP-10cm	11.8	40.5	28.0	72.0	0.2	98.8	1.0
UOR-SP-20cm	23.3	45.0	26.4	73.6	1.2	85.6	13.2
UOR-SP-30cm	26.3	58.8	25.4	74.6	3.2	71.5	25.3
<i>UOR-SP-Merged</i>	20.5	48.1	26.6	73.4	1.5	83.9	14.6
10-CG-1	15.1	50.2	19.4	80.6	2.4	92.1	5.5
W10-CG-2	29.0						
W10-CG-3	24.0	60.5	26.1	73.9	0.6	92.5	6.9
W10-CG-4	12.6	66.4	19.3	80.7	0.3	98.9	0.8
W10-CG-5	10.8	60.5	22.6	77.4	0.2	94.8	5.0
10-CG-6	9.9	60.5	15.3	84.7	0.4	98.2	1.5
W10-CG-7	8.3	60.5	19.9	80.1	0.2	99.8	0.0
W10-CG-8	5.9	66.4	13.9	86.1	0.3	99.2	0.5
W10-CG-9	6.9	66.4	12.5	87.5	0.1	98.5	1.3
W10-CG-10	2.5	63.4	13.2	86.8	0.1	99.0	0.9
10-CG-12	8.4	60.5	18.2	81.8	0.1	99.3	0.7
10-DG-1	11.1	8.4	26.0	74.0	49.3	46.1	4.6
W10-DG-2	16.2						
W10-DG-3	19.0						
W10-DG-4	24.5						
W10-DG-5	15.7						
W10-DG-6	17.9						
W10-DG-7	14.6						
W10-DG-8	10.1						
10-DG-9	6.3	49.9	9.1	90.9	12.4	52.2	35.3
10-DG-10	12.0	3.9	52.3	47.7	13.0	62.5	24.5

W10-DG-11	14.4						
W10-DWG-1	12.3	67.5	5.5	94.5	2.5	63.8	33.7
W10-DWG-3	19.6	52.6	5.7	94.3	1.1	48.0	50.9
W10-DWG-4	14.6	5.2	46.7	53.3	1.1	42.4	56.5
W10-DWG-5	16.9	8.4	21.1	78.9	1.8	42.4	55.8
W10-DWG-7	15.0	21.5	18.7	81.3	1.6	36.0	62.4
W10-DWG-8	12.1	17.3	20.8	79.2	1.0	71.8	27.2
T10-MAG-2	45.8	4.0	55.6	44.4	7.7	64.5	27.8
10-LWG-1	9.6	59.9	14.0	86.0	0.1	92.4	7.5
W10-CG-SP1-10cm	33.1	4.0	37.5	62.5	1.0	84.7	14.2
W10-CG-SP1-20cm	11.0	25.1	18.4	81.6	0.2	32.6	67.2
W10-CG-SP1-30cm	25.7						
LP-16-1	7.0	3.6	55.9	44.1	92.5	6.8	0.6
LP-16-2	4.0	5.0	38.3	61.7	97.1	2.9	0.0
RL-16-1	2.8	38.4	6.6	93.4	35.0	60.8	4.2
RL-16-2	11.5	16.6	18.9	81.1	39.8	41.1	19.1
RL-16-3	4.2	57.0	9.7	90.3	2.1	69.7	28.2
RL-16-4	8.4	5.8	29.2	70.8	2.8	53.8	43.5
RL-16-5	2.8	61.7	5.8	94.2	10.1	76.5	13.4
RL-16-6	4.5	48.4	16.4	83.6	9.3	68.6	22.1
RL-16-7	3.6	45.8	3.6	96.4	40.5	48.4	11.1
RL-16-8	1.9	49.5	3.0	97.0	41.0	58.3	0.7
RL-16-Distal	3.9	50.7	3.2	96.8	32.8	52.4	14.8
Llaka Lake Debris	6.2	41.0	27.5	72.5	18.0	36.4	45.6
RP-16-1D	6.1	6.6	28.4	85.0	69.1	30.8	0.1
RP-16-2	6.7	8.5	26.8	73.2	56.9	43.1	0.1
RP-16-3	0.7	53.3	2.4	97.6	27.5	72.2	0.3
RP-16-4D	1.5	42.9	3.5	96.5	15.0	82.9	2.1
RP-16-5	9.5	7.9	26.5	73.5	29.5	63.3	7.2
RP-16-6	3.1	37.1	11.2	88.8	3.5	37.4	59.1
RP-16-7	7.4	9.4	22.3	77.7	7.7	47.2	45.1
RP-16-8	1.5				3.6	69.5	26.9
Zona de Pitek 20 cm	5.2	50.5	7.8	92.2	64.2	35.4	0.3
Zona de Pitek 60 cm	4.8	51.2	8.5	91.5	70.9	29.0	0.1
MS Glacial Drift	5.0	30.9	10.9	89.1	10.9	62.5	26.6
MS B1 SED Horshoe	6.4	9.3	21.7	78.3	6.2	83.1	10.7
MSA-1	6.5	62.1	2.8	97.2	4.4	95.6	0.0
MSA-2	4.6	56.4	3.4	96.6	4.8	95.1	0.2
MSA-3	9.6	57.9	5.9	94.1	2.2	97.6	0.2
MSA-5	6.9	47.5	5.1	94.9	3.8	75.2	20.9
MSB-4 SED	5.6	37.8	8.9	91.1	1.3	86.9	11.8
MSB-5 Sed-1	5.4	47.3	5.0	95.0	8.5	87.8	3.8
MSB-5 Sed-2	7.2	57.0	4.2	95.8	4.8	93.4	1.8
MSB-5 Soil	3.2	40.1	7.4	92.6	19.6	80.0	0.4
MSc A1	2.0	47.6	3.5	96.5	18.0	79.8	2.2

AUS Drift PROX	1.0	34.2	6.5	93.5	1.9	29.7	68.4
AUS Drift Distal	2.9	56.1	2.1	97.9	6.9	49.2	44.0
AUS-1	1.2	70.7	0.6	99.4	1.9	65.8	32.3
AUS-SED-2	1.1	48.9	1.8	98.2	69.5	30.5	0.0
AUS-3	0.9	41.2	3.2	96.8	50.4	34.1	15.5
AUS-SED-4	0.9	50.6	1.8	98.2	28.3	68.9	2.8
AUS-5	0.8	38.1	4.0	96.0	10.0	50.6	39.4
AUS-SED-6	2.0	50.2	1.1	98.9	38.9	60.1	1.0
AUS-7	0.3	46.3	2.8	97.2	21.4	70.4	8.1
AUS-SED-8	1.2	49.6	1.4	98.6	45.6	53.7	0.7
AUS-SED-Lake	0.9	58.6	1.0	99.0	33.5	66.3	0.2
AUS-PED-10CM	7.4	51.9	4.1	95.9	0.8	46.8	52.3
AUS-PED-20CM	3.3	49.3	3.8	96.2	0.3	45.9	53.8
AUS-PED-30CM	3.6	47.9	3.4	96.6	1.1	43.6	55.3
AUS-PED-50CM	8.6	59.0	1.0	99.0	1.0	44.2	54.8
AUS-PED-1M	9.0	56.4	4.2	95.8	0.5	66.5	33.0
<i>AUS-PED-Merged</i>	6.4	52.9	3.3	96.7	0.8	30.0	69.2
LANG Drift Prox	3.1	9.6	13.7	86.3	1.3	25.2	73.5
LANG5	0.5						
LANG7	0.5						
LANG9	0.5						
ELVA-1	1.4	56.7	3.5	96.5	8.0	90.4	1.7
ELVA-3	1.4	33.2	3.6	96.4	26.0	71.4	2.6
ELVA-5	1.0	46.4	2.9	97.2	9.2	90.8	0.0
ELVA-7	1.2	40.5	3.2	96.8	31.1	50.9	18.0
ELVA-9	1.7	39.9	4.6	95.4	18.3	66.8	14.8
ELVA-11	1.2	57.4	3.2	96.8	7.5	91.5	1.0
ELVA-13	0.9	43.0	3.2	96.8	26.4	71.5	2.0
VEITASTROND-LAKE-SED	4.3	21.9	8.7	91.3	93.5	6.4	0.1
EYF-1-IS	13.0	4.9	29.7	70.3	0.9	44.1	55.1
EYF-2-IS	12.5	52.0	7.1	92.9	36.0	62.8	1.2
EYF-3-IS	15.7	38.2	23.1	76.9	14.8	69.4	15.8
PM-RG-SED-1	11.3		2.9	97.1	17.9	64.3	17.8
PM-RG-SED-2	22.3		4.1	95.9	8.9	89.7	1.5
PM-RG-SED-3	35.2		46.8	53.2	14.0	84.2	1.8
PM-RG-SED-4	22.7		13.1	86.9	4.9	93.7	1.4
PM-RG-SED-5	21.2		18.4	81.6	4.7	92.5	2.9
PM-RG-SED-6	22.6		5.2	94.8	7.6	92.4	0.0
PM-RG-SED-7	19.7		6.4	93.6	1.9	98.0	0.1
PM-RG-SED-8	27.3		10.9	89.1	2.0	89.7	8.3
PM-RG-SED-9	20.2						
PM-RG-SED-10	26.9						
PM-RG-SAP-1	8.2		0.8	99.2	27.3	59.5	13.2
PM-RG-SAP-2	16.8		4.7	95.3	71.0	24.9	4.1
PM-RG-SAP-3	16.7		3.3	96.7	17.8	72.8	9.5

PM-RG-SAP-4Red	25.3		10.4	89.7	33.7	66.3	0.0
PM-RG-SAP-5A	9.0		12.9	87.1	11.6	84.1	4.4
PM-RG-SAP-5B	11.0		13.3	86.7	27.9	68.7	3.4
PM-RG-SAP-6A-Red	21.9		9.1	90.9	52.1	47.4	0.5
PM-RG-SAP-6B-Yellow	17.5		9.0	91.0	36.3	58.5	5.2
PM-RG-SAP-6C-Brown	30.5		11.5	88.5	51.7	48.2	0.1
PM-RB-SED-1	15.7		5.7	94.3	7.1	91.5	1.4
PM-RB-SED-2	14.2		1.0	99.1	3.7	93.7	2.6
PM-RB-SED-3	16.0		4.1	95.9	2.9	94.6	2.5
PM-RB-SED-4	13.7		3.9	96.1	29.4	70.6	0.0
RB-14-SED-1	15.4						
RB-14-SED-2	15.7						
RB-14-SED-3	32.0						
RB-14-SED-5	24.6						
IGNF-13-SOIL-1			7.3	92.7	4.7	62.1	33.1
IGNF-13-SOIL-2			8.2	91.8	5.5	66.9	27.5
IGNF-13-SOIL-3			8.7	91.3	5.6	63.7	30.7
IGNF-13-SOIL-4			7.2	92.8	3.0	78.8	18.2
IGNF-13-SOIL-5			8.3	91.7	1.4	68.6	30.0
IGNF-13-SOIL-6			6.6	93.4	3.9	69.6	26.5
IGNF-13-SOIL-7			7.6	92.4	1.2	70.4	28.4
IGNF-13-SED-1	15.9	34.6	21.0	79.0	3.2	57.9	38.8
IGNF-13-SED-5	19.1	41.7	28.5	71.5	2.5	70.7	26.9
IGNF-13-SED-7	17.6	55.1	15.7	84.3	3.9	57.6	38.5
IGNF-13-SED-11	14.2	41.7	21.9	78.1	3.6	60.7	35.7
IGNF-13-SED-13	11.0	50.2	17.9	82.1	4.1	67.4	28.4
IGNF-13-SED-15	17.6	50.2	23.1	76.9	3.2	71.3	25.6

Table S1.3. Quantitative mineralogy (%) of the muds.

Sample Number	Plagioclase	K-spar	Quartz	Pyroxene	Amphibole	Epidote
122612-2	24.60	5.30	8.50	13.30	4.90	0.00
122612-1	22.58	4.84	7.46	5.85	4.33	0.00
011213-12	29.27	7.29	9.79	15.78	2.50	0.00
122512-13	29.97	9.29	6.49	4.80	1.40	0.00
122412-1	34.63	20.92	6.51	5.71	4.10	0.00
123012-12	48.65	5.41	10.91	6.11	3.50	0.00
122412-5	27.27	14.89	10.79	5.39	3.40	0.00
010213-1	26.96	3.12	9.46	10.97	3.92	0.00
122312-8	37.79	7.80	9.12	2.03	9.32	0.00
122412-8	45.25	2.90	10.69	8.59	2.70	0.00
123012-11	19.74	1.10	6.81	4.01	3.21	0.00
Whillans	23.90	0.00	22.00	0.00	3.30	0.00
T10-GOLD-10Drift	13.60	3.32	4.23	0.00	0.00	0.00

T10-GOLD-12Drift	22.20	6.80	7.90	5.90	1.40	0.00
T10-GOLD-9Drift	27.20	3.10	6.41	5.38	2.38	0.00
T10-GOLD-1	15.08	2.90	5.00	5.29	2.40	0.00
T10-GOLD-7	16.48	1.41	7.04	5.23	3.42	0.00
T10-GOLD-9	19.70	4.40	10.80	12.10	3.40	0.00
T10-GOLD-14	21.45	2.32	7.15	3.63	2.72	0.00
T10-HOW-8Drift	22.64	5.33	5.53	4.93	3.12	0.00
T10-HOW-9Drift	26.25	9.98	5.09	3.49	4.39	0.00
T10-HOW-10Drift	24.27	16.25	8.43	3.41	3.61	0.00
T10-HOW-12Drift	30.57	7.89	9.09	5.19	1.90	0.00
T10-HOW-7	20.90	6.60	4.00	6.80	2.20	0.00
T10-HOW-9	20.98	5.69	4.00	1.80	3.10	0.00
D7	26.97	14.49	6.99	3.80	1.50	0.00
T10-CAMP-SP-0cm	24.60	4.40	5.20	4.40	2.00	0.00
T10-CAMP-SP-10cm	19.70	6.80	4.50	5.00	4.30	0.00
T10-CAMP-SP-20cm	27.22	8.67	7.46	7.76	1.71	0.00
T10-CAMP-SP-30cm	33.40	7.50	7.40	5.80	2.20	0.00
BHS-90-115	20.42	9.61	5.81	4.70	3.00	0.00
BHS-93-36	17.60	2.60	5.20	4.10	3.90	0.00
BHS-93-34	33.00	6.80	10.70	5.60	4.50	0.00
BHS-93-20	22.02	6.61	8.51	4.10	3.70	0.00
BHS-90-027z	41.92	11.78	19.06	11.38	2.50	0.00
BHS-93-19	41.78	8.17	12.61	9.28	3.83	0.00
BHS-93-23	20.24	7.35	6.34	5.34	5.74	0.00
BHS-93-29	45.38	19.78	14.36	4.62	2.81	0.00
BHS-93-28	26.51	6.35	6.65	6.15	3.43	0.00
10-OR-14	25.13	6.53	7.84	9.15	5.33	0.00
10-OR-16	37.70	8.40	11.80	14.20	7.00	0.00
10-OR-19	23.12	7.64	7.94	4.02	12.86	0.00
UOR-SP-10cm	23.26	6.57	7.38	7.38	0.00	0.00
UOR-SP-20cm	19.70	3.84	6.36	7.07	2.02	0.00
UOR-SP-30cm	23.24	4.02	7.04	6.14	2.41	0.00
<i>UOR-SP-Merged</i>	22.06	4.81	6.93	6.86	1.48	0.00
10-CG-1	36.16	7.69	11.19	6.59	3.30	0.00
10-CG-6	28.77	11.99	14.29	27.67	5.89	0.00
10-CG-12	33.97	18.59	14.37	21.71	6.13	0.00
10-DG-1	20.18	2.90	8.59	3.10	4.10	0.00
10-DG-9	22.22	15.12	7.21	4.80	7.41	0.00
10-DG-10	17.50	13.90	5.10	2.20	7.10	0.00
W10-DWG-1	16.78	3.90	5.79	2.40	4.70	0.00
T10-MAG-2	15.11	21.35	5.64	2.42	0.00	0.00
W10-CG-SP1-10cm	30.76	12.02	11.32	13.43	3.61	0.00
W10-CG-SP1-20cm	42.14	6.41	13.81	10.41	2.90	0.00
W10-CG-SP1-30cm	23.82	5.31	7.61	12.41	4.00	0.00
LP-16-1	46.90	16.70	16.10	0.00	0.00	0.00

LP-16-2	44.30	18.50	22.50	0.00	0.00	0.00
RL-16-1	47.78	12.02	25.96	0.00	0.00	0.00
RL-16-2	38.20	11.60	20.50	0.00	1.70	0.00
RL-16-3	43.36	13.99	26.67	4.90	0.00	0.00
RL-16-4	49.60	6.50	31.10	0.00	0.00	0.00
RL-16-5	39.90	12.90	37.40	0.00	0.00	0.00
RL-16-6	28.90	24.10	34.10	0.00	0.00	0.00
RL-16-7	30.80	14.80	32.60	0.00	1.10	0.00
RL-16-8	43.54	10.01	27.93	0.00	1.10	0.00
RL-16-Distal	34.44	19.29	31.82	0.00	0.00	0.00
Llaka Lake Debris	30.07	27.87	24.98	0.00	0.00	0.00
Zona de Pitek 20 cm	40.56	4.80	32.37	0.00	0.00	0.00
Zona de Pitek 60 cm	41.26	17.38	27.97	0.00	0.60	0.00
MS Glacial Drift	40.65	2.13	9.86	0.00	17.99	4.37
MS B1 SED Horshoe	42.57	1.89	6.78	0.00	13.86	0.00
MSA-1	22.95	0.00	5.41	0.00	12.22	0.00
MSA-2	27.98	2.91	9.33	0.00	23.07	0.00
MSA-3	24.42	6.41	7.31	0.00	20.12	0.00
MSA-5	29.57	0.00	8.39	0.00	13.69	0.00
MSB-4 SED	38.50	4.10	11.40	0.00	23.20	0.00
MSB-5 Sed-1	34.60	1.00	9.60	0.00	18.20	0.00
MSB-5 Sed-2	21.80	2.60	5.60	1.20	9.70	0.00
MSB-5 Soil	38.30	5.90	7.90	0.00	8.70	0.00
MSc A1	24.02	10.21	6.71	0.00	4.30	0.00
AUS Drift PROX	21.74	8.00	10.05	0.00	0.00	0.00
AUS Drift Distal	34.24	9.29	15.96	0.00	0.00	0.00
AUS-SED-2	46.39	6.71	6.71	0.00	0.00	0.00
AUS-SED-4	37.16	12.29	22.48	0.00	7.79	0.00
AUS-SED-6	28.96	6.86	13.82	0.00	0.00	0.00
AUS-SED-8	28.13	9.48	17.84	0.00	1.41	0.00
AUS-SED-Lake	38.66	21.28	19.08	0.00	1.80	0.00
AUS-PED-10CM	34.98	18.85	13.91	0.00	2.52	0.00
AUS-PED-20CM	32.96	8.16	17.86	0.00	2.45	0.00
AUS-PED-30CM	27.74	13.67	15.68	0.00	1.21	0.00
AUS-PED-50CM	20.54	4.11	8.72	0.00	1.00	0.00
AUS-PED-1M	19.96	6.11	8.86	0.00	0.00	0.00
<i>AUS-PED-Merged</i>	27.24	10.18	13.00	0.00	1.44	0.00
LANG Drift Prox	18.98	11.59	7.99	0.00	1.90	0.00
VEITASTROND-LAKE- SED	19.80	6.50	9.80	0.00	4.10	0.00
EYF-1-IS	43.95	1.71	0.00	17.74	0.00	0.00
EYF-2-IS	39.25	0.00	0.00	22.60	0.00	0.00
EYF-3-IS	37.90	0.00	0.00	15.40	0.00	0.00
PM-RG-SED-1	43.90	0.00	6.20	0.00	16.20	0.00
PM-RG-SED-2	41.30	0.00	9.50	0.00	14.40	0.00

PM-RG-SED-3	24.10	0.00	21.20	0.00	19.80	0.00
PM-RG-SED-4	38.80	0.00	12.10	0.00	13.40	0.00
PM-RG-SED-5	32.30	0.00	7.20	0.00	17.20	0.00
PM-RG-SED-6	28.40	0.00	11.50	0.00	8.80	0.00
PM-RG-SED-7	51.10	0.00	14.50	0.00	8.40	0.00
PM-RG-SED-8	34.90	0.00	14.10	0.00	9.30	0.00
PM-RG-SED-9	40.40	0.00	11.40	0.00	7.50	0.00
PM-RG-SED-10	50.10	0.00	10.50	0.00	14.40	0.00
PM-RG-SAP-1	72.20	0.00	9.20	0.00	11.00	0.00
PM-RG-SAP-2	35.90	5.00	0.00	0.00	28.50	0.00
PM-RG-SAP-3	22.90	0.00	2.70	0.00	3.30	0.00
PM-RG-SAP-4Red	1.30	0.00	0.10	0.00	1.70	0.00
PM-RG-SAP-5A	24.50	5.40	1.30	1.80	14.70	0.00
PM-RG-SAP-5B	25.10	0.00	3.10	0.00	0.00	0.00
PM-RG-SAP-6A-Red	0.00	3.50	2.10	0.00	0.00	0.00
PM-RG-SAP-6B-Yellow	0.00	17.80	0.80	0.00	9.50	0.00
PM-RG-SAP-6C-Brown	6.00	13.90	0.70	0.00	7.10	0.00
PM-RB-SED-1	25.70	0.00	8.40	0.00	11.60	0.00
PM-RB-SED-2	23.20	21.20	7.60	0.00	8.90	0.00
PM-RB-SED-3	32.40	4.60	7.80	0.00	16.30	0.00
PM-RB-SED-4	28.30	2.30	8.10	0.00	11.90	0.00
IGNF-13-SED-1	54.80	11.10	16.60	0.00	0.00	0.00
IGNF-13-SED-7	59.40	5.70	14.00	0.00	0.00	0.00
IGNF-13-SED-11	55.20	4.60	17.90	0.00	0.00	0.00
IGNF-13-SED-13	62.90	4.50	17.70	0.00	0.00	0.00
IGNF-13-SED-15	39.40	6.60	16.00	0.00	0.00	0.00

Table S1.3. (Continued)

Sample Number	Cordierite	Mica	Illite	Chlorite	Smectite	Vermiculite
122612-2	5.40	11.20	10.10	7.00	9.70	0.00
122612-1	3.93	0.00	34.58	8.06	5.95	0.00
011213-12	0.00	14.39	11.19	7.69	2.10	0.00
122512-13	2.30	19.78	12.79	7.89	5.29	0.00
122412-1	3.60	14.91	8.01	1.60	0.00	0.00
123012-12	0.00	12.01	5.61	7.81	0.00	0.00
122412-5	0.00	25.07	3.60	5.99	2.50	0.00
010213-1	0.00	14.39	8.75	22.43	0.00	0.00
122312-8	0.00	13.78	2.74	7.90	9.52	0.00
122412-8	0.00	16.48	0.00	13.39	0.00	0.00
123012-11	0.00	35.77	3.61	18.04	3.21	0.00
Whillans	0.00	20.80	26.00	4.00	0.00	0.00
T10-GOLD-10Drift	0.00	7.55	61.33	5.84	3.02	0.00
T10-GOLD-12Drift	1.70	9.30	35.10	8.60	1.10	0.00
T10-GOLD-9Drift	1.34	6.10	25.03	15.72	7.34	0.00

T10-GOLD-1	0.00	4.80	28.07	10.79	18.78	2.30
T10-GOLD-7	0.00	7.64	20.50	8.44	21.21	8.64
T10-GOLD-9	2.30	14.20	17.80	6.50	1.80	4.60
T10-GOLD-14	0.00	3.93	28.70	8.96	21.15	0.00
T10-HOW-8Drift	0.00	12.78	16.90	13.28	15.49	0.00
T10-HOW-9Drift	0.00	14.27	22.46	8.38	5.69	0.00
T10-HOW-10Drift	0.00	12.84	21.67	7.42	2.11	0.00
T10-HOW-12Drift	1.30	10.19	10.19	12.79	10.89	0.00
T10-HOW-7	0.00	14.90	25.30	11.60	3.20	0.00
T10-HOW-9	0.00	11.29	32.17	13.19	3.40	1.50
D7	0.00	12.39	9.49	4.90	18.48	0.00
T10-CAMP-SP-0cm	1.20	20.30	14.40	8.40	15.10	0.00
T10-CAMP-SP-10cm	2.20	20.90	4.10	11.40	17.80	0.00
T10-CAMP-SP-20cm	2.12	6.25	24.60	6.25	7.96	0.00
T10-CAMP-SP-30cm	1.70	16.60	15.80	6.00	3.60	0.00
BHS-90-115	1.70	17.42	24.12	13.21	0.00	0.00
BHS-93-36	0.00	14.50	38.60	10.00	3.50	0.00
BHS-93-34	2.70	4.80	20.40	11.50	0.00	0.00
BHS-93-20	2.20	0.00	31.53	15.12	3.40	0.00
BHS-90-027z	0.00	0.00	0.00	3.49	1.20	0.00
BHS-93-19	1.82	5.65	10.39	6.46	0.00	0.00
BHS-93-23	0.00	8.46	17.93	13.29	15.31	0.00
BHS-93-29	0.00	0.00	3.21	9.84	0.00	0.00
BHS-93-28	0.00	0.00	41.43	6.75	0.00	0.00
10-OR-14	0.00	0.00	20.30	12.56	10.95	2.21
10-OR-16	0.00	1.00	5.30	4.20	1.50	8.90
10-OR-19	0.00	5.93	33.27	5.23	0.00	0.00
UOR-SP-10cm	2.73	9.71	31.45	1.72	6.88	2.93
UOR-SP-20cm	0.00	12.73	37.17	9.19	1.92	0.00
UOR-SP-30cm	2.41	17.30	24.25	11.07	2.11	0.00
<i>UOR-SP-Merged</i>	1.71	13.25	30.95	7.33	3.64	0.98
10-CG-1	1.80	3.00	19.58	3.40	6.29	0.00
10-CG-6	0.00	3.40	0.00	4.00	0.00	1.20
10-CG-12	0.00	1.71	0.00	3.52	0.00	0.00
10-DG-1	0.00	6.49	38.76	7.59	6.79	0.00
10-DG-9	2.50	10.91	24.62	3.70	1.50	0.00
10-DG-10	0.00	4.90	41.70	5.30	2.30	0.00
W10-DWG-1	1.70	15.48	31.47	6.39	11.39	0.00
T10-MAG-2	0.00	19.94	20.54	12.59	2.42	0.00
W10-CG-SP1-10cm	0.00	25.15	0.00	3.71	0.00	0.00
W10-CG-SP1-20cm	0.00	15.12	2.60	5.01	0.00	0.00
W10-CG-SP1-30cm	0.00	3.70	19.82	12.51	10.81	0.00
LP-16-1	0.00	10.90	0.00	3.90	0.00	0.00
LP-16-2	0.00	12.30	0.00	2.40	0.00	0.00
RL-16-1	0.00	10.91	0.00	3.33	0.00	0.00

RL-16-2	0.00	16.40	0.00	9.00	0.00	0.00
RL-16-3	0.00	11.09	0.00	0.00	0.00	0.00
RL-16-4	0.00	8.10	0.00	4.70	0.00	0.00
RL-16-5	0.00	6.10	0.00	3.70	0.00	0.00
RL-16-6	0.00	10.60	0.00	2.30	0.00	0.00
RL-16-7	0.00	14.70	0.00	6.00	0.00	0.00
RL-16-8	0.00	9.51	0.00	7.91	0.00	0.00
RL-16-Distal	0.00	11.31	0.00	3.13	0.00	0.00
Llaka Lake Debris	0.00	14.29	0.00	2.80	0.00	0.00
Zona de Pitek 20 cm	0.00	13.59	1.40	7.29	0.00	0.00
Zona de Pitek 60 cm	0.00	9.99	0.00	2.80	0.00	0.00
MS Glacial Drift	0.00	9.55	0.00	5.79	0.00	0.00
MS B1 SED Horshoe	0.00	7.78	0.00	7.88	5.58	0.00
MSA-1	0.00	11.52	0.00	9.52	11.82	15.83
MSA-2	0.00	5.92	0.00	10.53	8.73	2.91
MSA-3	0.00	2.10	0.00	15.72	8.01	1.80
MSA-5	0.00	9.19	0.00	13.29	11.39	4.80
MSB-4 SED	0.00	0.50	0.00	17.20	2.10	0.00
MSB-5 Sed-1	0.00	0.00	0.00	14.40	6.30	6.90
MSB-5 Sed-2	0.00	8.10	0.00	8.60	18.40	16.00
MSB-5 Soil	0.00	4.50	0.00	13.70	8.20	9.10
MSc A1	0.00	8.01	0.00	5.51	13.81	0.00
AUS Drift PROX	0.00	0.00	58.77	1.43	0.00	0.00
AUS Drift Distal	0.00	2.73	37.78	0.00	0.00	0.00
AUS-SED-2	0.00	0.00	40.18	0.00	0.00	0.00
AUS-SED-4	0.00	8.59	11.69	0.00	0.00	0.00
AUS-SED-6	0.00	3.73	46.62	0.00	0.00	0.00
AUS-SED-8	0.00	1.92	41.23	0.00	0.00	0.00
AUS-SED-Lake	0.00	1.50	17.68	0.00	0.00	0.00
AUS-PED-10CM	0.00	1.31	19.96	0.00	4.64	0.00
AUS-PED-20CM	0.00	3.98	29.90	0.00	3.16	0.00
AUS-PED-30CM	0.00	0.00	34.57	0.00	2.01	0.00
AUS-PED-50CM	0.00	0.00	59.72	1.50	1.70	0.00
AUS-PED-1M	0.00	1.32	60.69	1.53	1.53	0.00
<i>AUS-PED-Merged</i>	0.00	1.32	40.97	0.61	2.61	0.00
LANG Drift Prox	0.00	5.89	45.75	3.30	4.60	0.00
VEITASTROND-LAKE- SED	0.00	4.60	53.80	1.40	0.00	0.00
EYF-1-IS	0.00	0.00	0.00	0.00	8.27	0.00
EYF-2-IS	0.00	0.00	0.00	0.00	4.44	0.00
EYF-3-IS	0.00	0.00	0.00	0.00	2.40	0.00
PM-RG-SED-1	0.00	0.00	5.00	0.00	0.00	0.00
PM-RG-SED-2	0.00	0.00	10.80	0.00	0.00	0.00
PM-RG-SED-3	0.00	0.00	0.00	0.00	0.00	0.00
PM-RG-SED-4	0.00	0.00	0.00	0.00	0.00	0.00

PM-RG-SED-5	0.00	2.30	0.00	0.00	0.00	0.00
PM-RG-SED-6	0.00	0.00	0.00	0.00	0.00	0.00
PM-RG-SED-7	0.00	0.00	0.00	0.00	0.00	0.00
PM-RG-SED-8	0.00	0.00	0.00	0.00	0.00	0.00
PM-RG-SED-9	0.00	0.00	0.00	0.00	0.00	0.00
PM-RG-SED-10	0.00	0.00	0.00	0.00	0.00	0.00
PM-RG-SAP-1	0.00	0.00	0.00	0.00	0.00	2.20
PM-RG-SAP-2	0.00	5.80	0.00	0.00	0.00	3.30
PM-RG-SAP-3	0.00	3.20	0.00	0.00	0.00	0.00
PM-RG-SAP-4Red	0.00	6.60	0.00	0.00	0.00	0.00
PM-RG-SAP-5A	0.00	1.50	0.00	25.20	0.00	0.00
PM-RG-SAP-5B	0.00	26.00	1.10	1.30	0.00	1.40
PM-RG-SAP-6A-Red	0.00	1.40	0.00	0.00	0.00	0.00
PM-RG-SAP-6B-Yellow	0.00	0.00	0.00	0.00	0.00	0.00
PM-RG-SAP-6C-Brown	0.00	2.90	1.60	0.00	0.00	0.00
PM-RB-SED-1	0.00	19.70	3.80	0.00	0.00	0.00
PM-RB-SED-2	0.00	0.00	0.00	0.00	0.00	0.00
PM-RB-SED-3	0.00	7.60	1.90	0.00	0.00	0.00
PM-RB-SED-4	0.00	26.50	0.00	0.00	0.00	0.00
IGNF-13-SED-1	0.00	4.20	9.10	0.00	0.00	0.00
IGNF-13-SED-7	0.00	5.00	11.20	0.00	0.00	0.00
IGNF-13-SED-11	0.00	12.10	2.50	0.00	4.30	0.00
IGNF-13-SED-13	0.00	6.80	7.50	0.00	0.00	0.00
IGNF-13-SED-15	0.00	11.60	22.40	0.00	0.00	0.00

Table S1.3. (Continued)

Sample Number	Palygorskite	Serpentine	Zeolite	Kaolinite	Accessory
122612-2	0.00	0.00	0.00	0.00	0.00
122612-1	0.00	0.00	2.42	0.00	0.00
011213-12	0.00	0.00	0.00	0.00	0.00
122512-13	0.00	0.00	0.00	0.00	0.00
122412-1	0.00	0.00	0.00	0.00	0.00
123012-12	0.00	0.00	0.00	0.00	0.00
122412-5	0.00	0.00	0.00	0.00	1.10
010213-1	0.00	0.00	0.00	0.00	0.00
122312-8	0.00	0.00	0.00	0.00	0.00
122412-8	0.00	0.00	0.00	0.00	0.00
123012-11	0.00	0.00	4.51	0.00	0.00
Whillans	0.00	0.00	0.00	0.00	0.00
T10-GOLD-10Drift	0.00	0.00	1.11	0.00	0.00
T10-GOLD-12Drift	0.00	0.00	0.00	0.00	0.00
T10-GOLD-9Drift	0.00	0.00	0.00	0.00	0.00
T10-GOLD-1	0.00	0.00	4.60	0.00	0.00
T10-GOLD-7	0.00	0.00	0.00	0.00	0.00

T10-GOLD-9	0.00	0.00	0.00	0.00	2.40
T10-GOLD-14	0.00	0.00	0.00	0.00	0.00
T10-HOW-8Drift	0.00	0.00	0.00	0.00	0.00
T10-HOW-9Drift	0.00	0.00	0.00	0.00	0.00
T10-HOW-10Drift	0.00	0.00	0.00	0.00	0.00
T10-HOW-12Drift	0.00	0.00	0.00	0.00	0.00
T10-HOW-7	0.00	0.00	4.50	0.00	0.00
T10-HOW-9	0.00	0.00	2.90	0.00	0.00
D7	0.00	0.00	1.00	0.00	0.00
T10-CAMP-SP-0cm	0.00	0.00	0.00	0.00	0.00
T10-CAMP-SP-10cm	0.00	0.00	3.30	0.00	0.00
T10-CAMP-SP-20cm	0.00	0.00	0.00	0.00	0.00
T10-CAMP-SP-30cm	0.00	0.00	0.00	0.00	0.00
BHS-90-115	0.00	0.00	0.00	0.00	0.00
BHS-93-36	0.00	0.00	0.00	0.00	0.00
BHS-93-34	0.00	0.00	0.00	0.00	0.00
BHS-93-20	0.00	0.00	2.80	0.00	0.00
BHS-90-027z	0.00	0.00	8.68	0.00	0.00
BHS-93-19	0.00	0.00	0.00	0.00	0.00
BHS-93-23	0.00	0.00	0.00	0.00	0.00
BHS-93-29	0.00	0.00	0.00	0.00	0.00
BHS-93-28	0.00	0.00	2.72	0.00	0.00
10-OR-14	0.00	0.00	0.00	0.00	0.00
10-OR-16	0.00	0.00	0.00	0.00	0.00
10-OR-19	0.00	0.00	0.00	0.00	0.00
UOR-SP-10cm	0.00	0.00	0.00	0.00	0.00
UOR-SP-20cm	0.00	0.00	0.00	0.00	0.00
UOR-SP-30cm	0.00	0.00	0.00	0.00	0.00
<i>UOR-SP-Merged</i>	0.00	0.00	0.00	0.00	0.00
10-CG-1	0.00	0.00	1.00	0.00	0.00
10-CG-6	0.00	0.00	0.00	0.00	1.20
10-CG-12	0.00	0.00	0.00	0.00	0.00
10-DG-1	0.00	0.00	1.50	0.00	0.00
10-DG-9	0.00	0.00	0.00	0.00	0.00
10-DG-10	0.00	0.00	0.00	0.00	0.00
W10-DWG-1	0.00	0.00	0.00	0.00	0.00
T10-MAG-2	0.00	0.00	0.00	0.00	0.00
W10-CG-SP1-10cm	0.00	0.00	0.00	0.00	0.00
W10-CG-SP1-20cm	0.00	0.00	1.60	0.00	0.00
W10-CG-SP1-30cm	0.00	0.00	0.00	0.00	0.00
LP-16-1	3.60	1.90	0.00	0.00	0.00
LP-16-2	0.00	0.00	0.00	0.00	0.00
RL-16-1	0.00	0.00	0.00	0.00	0.00
RL-16-2	0.00	0.00	2.60	0.00	0.00
RL-16-3	0.00	0.00	0.00	0.00	0.00

RL-16-4	0.00	0.00	0.00	0.00	0.00
RL-16-5	0.00	0.00	0.00	0.00	0.00
RL-16-6	0.00	0.00	0.00	0.00	0.00
RL-16-7	0.00	0.00	0.00	0.00	0.00
RL-16-8	0.00	0.00	0.00	0.00	0.00
RL-16-Distal	0.00	0.00	0.00	0.00	0.00
Llaka Lake Debris	0.00	0.00	0.00	0.00	0.00
Zona de Pitek 20 cm	0.00	0.00	0.00	0.00	0.00
Zona de Pitek 60 cm	0.00	0.00	0.00	0.00	0.00
MS Glacial Drift	0.00	0.00	9.65	0.00	0.00
MS B1 SED Horshoe	1.20	0.00	12.46	0.00	0.00
MSA-1	0.00	0.00	10.72	0.00	0.00
MSA-2	0.00	0.00	4.61	0.00	0.00
MSA-3	0.00	0.00	8.11	0.00	6.01
MSA-5	0.00	0.00	3.80	0.00	5.89
MSB-4 SED	0.00	0.00	3.00	0.00	0.00
MSB-5 Sed-1	0.00	0.00	1.80	0.00	7.20
MSB-5 Sed-2	0.00	0.00	8.00	0.00	0.00
MSB-5 Soil	0.00	0.00	3.70	0.00	0.00
MSc A1	0.00	0.00	27.43	0.00	0.00
AUS Drift PROX	0.00	0.00	0.00	0.00	0.00
AUS Drift Distal	0.00	0.00	0.00	0.00	0.00
AUS-SED-2	0.00	0.00	0.00	0.00	0.00
AUS-SED-4	0.00	0.00	0.00	0.00	0.00
AUS-SED-6	0.00	0.00	0.00	0.00	0.00
AUS-SED-8	0.00	0.00	0.00	0.00	0.00
AUS-SED-Lake	0.00	0.00	0.00	0.00	0.00
AUS-PED-10CM	0.00	0.00	2.32	0.00	1.50
AUS-PED-20CM	0.00	0.00	1.53	0.00	0.00
AUS-PED-30CM	0.00	0.00	5.13	0.00	0.00
AUS-PED-50CM	0.00	0.00	2.71	0.00	0.00
AUS-PED-1M	0.00	0.00	0.00	0.00	0.00
<i>AUS-PED-Merged</i>	0.00	0.00	2.34	0.00	0.30
LANG Drift Prox	0.00	0.00	0.00	0.00	0.00
VEITASTROND-LAKE- SED	0.00	0.00	0.00	0.00	0.00
EYF-1-IS	0.00	0.00	0.00	0.00	4.94
EYF-2-IS	0.00	0.00	0.00	0.00	3.03
EYF-3-IS	0.00	0.00	2.00	0.00	1.90
PM-RG-SED-1	0.00	0.00	0.00	28.80	0.00
PM-RG-SED-2	0.00	0.00	0.00	24.10	0.00
PM-RG-SED-3	0.00	0.00	0.00	34.90	0.00
PM-RG-SED-4	0.00	0.00	0.00	35.70	0.00
PM-RG-SED-5	0.00	0.00	0.00	40.90	0.00
PM-RG-SED-6	0.00	0.00	0.00	51.20	0.00

PM-RG-SED-7	0.00	0.00	0.00	26.00	0.00
PM-RG-SED-8	0.00	0.00	0.00	41.80	0.00
PM-RG-SED-9	0.00	0.00	0.00	40.80	0.00
PM-RG-SED-10	0.00	0.00	0.00	25.10	0.00
PM-RG-SAP-1	0.00	0.00	0.00	5.40	0.00
PM-RG-SAP-2	0.00	0.00	0.00	21.50	0.00
PM-RG-SAP-3	0.00	0.00	0.00	67.90	0.00
PM-RG-SAP-4Red	0.00	0.00	0.00	81.30	0.00
PM-RG-SAP-5A	0.00	0.00	0.00	21.00	0.00
PM-RG-SAP-5B	0.00	0.00	0.00	35.50	0.00
PM-RG-SAP-6A-Red	0.00	0.00	0.00	93.00	0.00
PM-RG-SAP-6B-Yellow	0.00	0.00	0.00	72.00	0.00
PM-RG-SAP-6C-Brown	0.00	0.00	0.00	67.70	0.00
PM-RB-SED-1	0.00	0.00	0.00	30.80	0.00
PM-RB-SED-2	0.00	0.00	0.00	39.10	0.00
PM-RB-SED-3	0.00	0.00	0.00	29.40	0.00
PM-RB-SED-4	0.00	0.00	0.00	22.90	0.00
IGNF-13-SED-1	0.00	0.00	0.00	4.20	0.00
IGNF-13-SED-7	0.00	0.00	0.00	4.60	0.40
IGNF-13-SED-11	0.00	0.00	0.00	2.60	0.90
IGNF-13-SED-13	0.00	0.00	0.00	0.60	0.00
IGNF-13-SED-15	0.00	0.00	0.00	3.00	1.10

Table S1.3. (Continued)

Sample Number	Pyrophyllite	Clinozoisite	Olivine	Cristobalite	Amorphous
122612-2	0.00	0.00	0.00	0.00	0.00
122612-1	0.00	0.00	0.00	0.00	0.00
011213-12	0.00	0.00	0.00	0.00	0.00
122512-13	0.00	0.00	0.00	0.00	0.00
122412-1	0.00	0.00	0.00	0.00	0.00
123012-12	0.00	0.00	0.00	0.00	0.00
122412-5	0.00	0.00	0.00	0.00	0.00
010213-1	0.00	0.00	0.00	0.00	0.00
122312-8	0.00	0.00	0.00	0.00	0.00
122412-8	0.00	0.00	0.00	0.00	0.00
123012-11	0.00	0.00	0.00	0.00	0.00
Whillans	0.00	0.00	0.00	0.00	0.00
T10-GOLD-10Drift	0.00	0.00	0.00	0.00	0.00
T10-GOLD-12Drift	0.00	0.00	0.00	0.00	0.00
T10-GOLD-9Drift	0.00	0.00	0.00	0.00	0.00
T10-GOLD-1	0.00	0.00	0.00	0.00	0.00
T10-GOLD-7	0.00	0.00	0.00	0.00	0.00
T10-GOLD-9	0.00	0.00	0.00	0.00	0.00
T10-GOLD-14	0.00	0.00	0.00	0.00	0.00

T10-HOW-8Drift	0.00	0.00	0.00	0.00	0.00
T10-HOW-9Drift	0.00	0.00	0.00	0.00	0.00
T10-HOW-10Drift	0.00	0.00	0.00	0.00	0.00
T10-HOW-12Drift	0.00	0.00	0.00	0.00	0.00
T10-HOW-7	0.00	0.00	0.00	0.00	0.00
T10-HOW-9	0.00	0.00	0.00	0.00	0.00
D7	0.00	0.00	0.00	0.00	0.00
T10-CAMP-SP-0cm	0.00	0.00	0.00	0.00	0.00
T10-CAMP-SP-10cm	0.00	0.00	0.00	0.00	0.00
T10-CAMP-SP-20cm	0.00	0.00	0.00	0.00	0.00
T10-CAMP-SP-30cm	0.00	0.00	0.00	0.00	0.00
BHS-90-115	0.00	0.00	0.00	0.00	0.00
BHS-93-36	0.00	0.00	0.00	0.00	0.00
BHS-93-34	0.00	0.00	0.00	0.00	0.00
BHS-93-20	0.00	0.00	0.00	0.00	0.00
BHS-90-027z	0.00	0.00	0.00	0.00	0.00
BHS-93-19	0.00	0.00	0.00	0.00	0.00
BHS-93-23	0.00	0.00	0.00	0.00	0.00
BHS-93-29	0.00	0.00	0.00	0.00	0.00
BHS-93-28	0.00	0.00	0.00	0.00	0.00
10-OR-14	0.00	0.00	0.00	0.00	0.00
10-OR-16	0.00	0.00	0.00	0.00	0.00
10-OR-19	0.00	0.00	0.00	0.00	0.00
UOR-SP-10cm	0.00	0.00	0.00	0.00	0.00
UOR-SP-20cm	0.00	0.00	0.00	0.00	0.00
UOR-SP-30cm	0.00	0.00	0.00	0.00	0.00
<i>UOR-SP-Merged</i>	0.00	0.00	0.00	0.00	0.00
10-CG-1	0.00	0.00	0.00	0.00	0.00
10-CG-6	0.00	0.00	0.00	0.00	0.00
10-CG-12	0.00	0.00	0.00	0.00	0.00
10-DG-1	0.00	0.00	0.00	0.00	0.00
10-DG-9	0.00	0.00	0.00	0.00	0.00
10-DG-10	0.00	0.00	0.00	0.00	0.00
W10-DWG-1	0.00	0.00	0.00	0.00	0.00
T10-MAG-2	0.00	0.00	0.00	0.00	0.00
W10-CG-SP1-10cm	0.00	0.00	0.00	0.00	0.00
W10-CG-SP1-20cm	0.00	0.00	0.00	0.00	0.00
W10-CG-SP1-30cm	0.00	0.00	0.00	0.00	0.00
LP-16-1	0.00	0.00	0.00	0.00	0.00
LP-16-2	0.00	0.00	0.00	0.00	0.00
RL-16-1	0.00	0.00	0.00	0.00	0.00
RL-16-2	0.00	0.00	0.00	0.00	0.00
RL-16-3	0.00	0.00	0.00	0.00	0.00
RL-16-4	0.00	0.00	0.00	0.00	0.00
RL-16-5	0.00	0.00	0.00	0.00	0.00

RL-16-6	0.00	0.00	0.00	0.00	0.00
RL-16-7	0.00	0.00	0.00	0.00	0.00
RL-16-8	0.00	0.00	0.00	0.00	0.00
RL-16-Distal	0.00	0.00	0.00	0.00	0.00
Llaka Lake Debris	0.00	0.00	0.00	0.00	0.00
Zona de Pitek 20 cm	0.00	0.00	0.00	0.00	0.00
Zona de Pitek 60 cm	0.00	0.00	0.00	0.00	0.00
MS Glacial Drift	0.00	0.00	0.00	0.00	0.00
MS B1 SED Horshoe	0.00	0.00	0.00	0.00	0.00
MSA-1	0.00	0.00	0.00	0.00	0.00
MSA-2	0.00	0.00	0.00	0.00	0.00
MSA-3	0.00	0.00	0.00	0.00	0.00
MSA-5	0.00	0.00	0.00	0.00	0.00
MSB-4 SED	0.00	0.00	0.00	0.00	0.00
MSB-5 Sed-1	0.00	0.00	0.00	0.00	0.00
MSB-5 Sed-2	0.00	0.00	0.00	0.00	0.00
MSB-5 Soil	0.00	0.00	0.00	0.00	0.00
MSc A1	0.00	0.00	0.00	0.00	0.00
AUS Drift PROX	0.00	0.00	0.00	0.00	0.00
AUS Drift Distal	0.00	0.00	0.00	0.00	0.00
AUS-SED-2	0.00	0.00	0.00	0.00	0.00
AUS-SED-4	0.00	0.00	0.00	0.00	0.00
AUS-SED-6	0.00	0.00	0.00	0.00	0.00
AUS-SED-8	0.00	0.00	0.00	0.00	0.00
AUS-SED-Lake	0.00	0.00	0.00	0.00	0.00
AUS-PED-10CM	0.00	0.00	0.00	0.00	0.00
AUS-PED-20CM	0.00	0.00	0.00	0.00	0.00
AUS-PED-30CM	0.00	0.00	0.00	0.00	0.00
AUS-PED-50CM	0.00	0.00	0.00	0.00	0.00
AUS-PED-1M	0.00	0.00	0.00	0.00	0.00
<i>AUS-PED-Merged</i>	0.00	0.00	0.00	0.00	0.00
LANG Drift Prox	0.00	0.00	0.00	0.00	0.00
VEITASTROND-LAKE- SED	0.00	0.00	0.00	0.00	0.00
EYF-1-IS	0.00	0.00	3.13	0.00	20.26
EYF-2-IS	0.00	0.00	4.14	1.11	25.43
EYF-3-IS	0.00	0.00	2.30	0.00	38.10
PM-RG-SED-1	0.00	0.00	0.00	0.00	0.00
PM-RG-SED-2	0.00	0.00	0.00	0.00	0.00
PM-RG-SED-3	0.00	0.00	0.00	0.00	0.00
PM-RG-SED-4	0.00	0.00	0.00	0.00	0.00
PM-RG-SED-5	0.00	0.00	0.00	0.00	0.00
PM-RG-SED-6	0.00	0.00	0.00	0.00	0.00
PM-RG-SED-7	0.00	0.00	0.00	0.00	0.00
PM-RG-SED-8	0.00	0.00	0.00	0.00	0.00

PM-RG-SED-9	0.00	0.00	0.00	0.00	0.00
PM-RG-SED-10	0.00	0.00	0.00	0.00	0.00
PM-RG-SAP-1	0.00	0.00	0.00	0.00	0.00
PM-RG-SAP-2	0.00	0.00	0.00	0.00	0.00
PM-RG-SAP-3	0.00	0.00	0.00	0.00	0.00
PM-RG-SAP-4Red	0.00	0.00	0.00	0.00	0.00
PM-RG-SAP-5A	4.50	0.00	0.00	0.00	0.00
PM-RG-SAP-5B	0.00	6.60	0.00	0.00	0.00
PM-RG-SAP-6A-Red	0.00	0.00	0.00	0.00	0.00
PM-RG-SAP-6B-Yellow	0.00	0.00	0.00	0.00	0.00
PM-RG-SAP-6C-Brown	0.00	0.00	0.00	0.00	0.00
PM-RB-SED-1	0.00	0.00	0.00	0.00	0.00
PM-RB-SED-2	0.00	0.00	0.00	0.00	0.00
PM-RB-SED-3	0.00	0.00	0.00	0.00	0.00
PM-RB-SED-4	0.00	0.00	0.00	0.00	0.00
IGNF-13-SED-1	0.00	0.00	0.00	0.00	0.00
IGNF-13-SED-7	0.00	0.00	0.00	0.00	0.00
IGNF-13-SED-11	0.00	0.00	0.00	0.00	0.00
IGNF-13-SED-13	0.00	0.00	0.00	0.00	0.00
IGNF-13-SED-15	0.00	0.00	0.00	0.00	0.00

Table S1.4. Major oxide (%) compositions of the muds. Note that LOI was subtracted from the total composition and rest was normalized to 100%.

Sample Number	SiO ₂	Al ₂ O ₃	Fe ₂ O ₃	CaO	MgO	Na ₂ O	K ₂ O
122612-2	54.50	18.24	9.28	6.19	6.11	1.90	2.24
123012-5	50.75	16.46	14.09	4.69	5.62	1.92	3.67
122512-12	52.39	15.90	10.88	6.53	5.06	3.01	2.60
122412-7	56.85	15.49	9.48	5.11	4.43	2.85	2.76
122412-2	52.43	19.61	10.15	4.80	4.89	2.55	2.73
010213-2	55.58	15.36	9.43	6.66	7.07	2.00	2.41
122312-6	55.50	15.21	9.62	5.75	5.16	2.98	2.66
010213-1	53.24	17.47	10.56	6.13	6.54	1.78	2.51
123012-11	48.28	20.93	12.84	5.39	6.25	1.32	3.07
Whillans	66.88	16.86	5.77	1.46	2.27	2.15	3.49
T10-GOLD-12Drift	56.27	15.54	10.04	5.53	5.03	2.57	2.74
T10-GOLD-9Drift	50.13	20.80	11.71	5.00	5.42	2.03	2.77
T10-GOLD-1	52.63	16.24	12.45	5.46	5.93	2.01	2.70
T10-Gold 5	54.51	15.53	10.83	6.12	5.55	2.41	2.52
T10-Gold 12	55.83	16.30	10.28	5.06	4.89	2.56	2.96
T10-GOLD-14	54.79	16.42	10.39	6.06	4.98	2.21	3.10
T10-HOW-8Drift	53.21	18.65	10.64	5.10	5.25	2.06	2.87
T10-HOW-9Drift	53.79	17.08	11.69	4.45	5.18	2.20	3.11
T10-HOW-12Drift	56.50	15.41	9.88	5.51	5.09	2.57	2.80

D7	57.16	16.18	8.83	5.43	3.71	2.59	3.42
T10-CAMP-SP-0cm	53.86	15.80	11.40	5.54	5.41	2.04	2.94
T10-CAMP-SP-10cm	51.11	19.43	10.72	6.28	5.19	1.95	2.64
T10-CAMP-SP-20cm	54.74	15.70	10.21	6.55	5.19	2.09	2.92
T10-CAMP-SP-30cm	54.97	15.90	10.27	6.19	4.88	2.16	2.95
BHS-90-115	50.26	23.68	10.09	4.52	4.42	2.30	3.05
BHS-93-36	54.21	17.89	9.92	6.04	5.21	2.26	2.39
BHS-93-34	57.63	16.55	8.36	6.09	4.39	2.52	2.86
BHS-93-20	55.83	16.22	9.66	6.12	4.99	2.54	2.62
BHS-90-027z	61.54	15.33	6.34	5.65	4.91	2.94	2.38
BHS-93-23	51.60	21.26	9.78	5.70	5.03	2.09	2.54
BHS-93-29	56.17	18.86	7.82	6.22	4.29	2.57	2.60
<i>UOR-SP-Merged</i>	53.81	20.23	9.63	5.00	4.75	2.20	2.92
10-CG-1	56.84	16.16	8.19	6.97	4.64	2.98	2.20
W10-CG-2	57.23	16.74	8.66	5.59	4.06	3.00	2.66
W10-CG-3	56.56	15.91	9.13	6.34	4.67	2.80	2.35
W10-CG-4	53.21	12.82	11.84	7.99	6.58	2.30	1.56
W10-CG-5	56.00	15.27	9.10	7.33	5.30	2.70	2.02
10-CG-6	55.83	15.14	9.29	7.34	5.24	2.70	1.98
W10-CG-7	55.02	13.70	10.27	8.00	6.09	2.42	1.69
W10-CG-8	56.22	14.34	9.19	7.85	5.79	2.54	1.78
W10-CG-9	55.18	13.92	10.26	7.74	5.89	2.43	1.76
W10-CG-10	54.78	13.26	10.29	8.57	6.57	2.30	1.48
10-CG-12	57.19	15.33	8.35	7.35	5.13	2.72	1.97
10-DG-1	55.19	16.16	10.76	5.62	4.72	2.52	2.80
10-DG-9	58.52	15.61	8.08	6.13	4.02	3.00	2.77
10-DG-10	58.48	15.97	8.15	5.73	3.89	3.02	2.97
T10-MAG-2	55.54	19.47	10.78	2.77	2.80	3.16	3.75
LP-16-1	67.56	18.39	2.07	1.40	0.62	4.80	4.52
LP-16-2	67.74	18.11	2.26	1.42	0.61	4.80	4.47
RL-16-1	68.18	16.33	3.33	2.68	1.05	4.12	3.36
RL-16-2	66.83	16.08	5.37	2.20	2.11	2.83	3.52
RL-16-3	65.55	21.20	2.13	1.64	0.60	4.41	3.85
RL-16-4	69.06	15.95	4.00	1.60	1.06	3.75	3.64
RL-16-5	73.37	14.48	2.27	1.41	0.59	3.85	3.28
RL-16-6	73.25	13.86	3.42	1.23	1.12	2.99	3.24
RL-16-7	69.60	16.12	3.25	2.38	0.81	3.68	3.27
RL-16-8	70.23	15.71	2.87	2.56	0.77	3.85	3.15
RL-16-Distal	70.72	15.51	2.75	2.60	0.69	3.83	3.00
Llaka Lake Debris	67.75	17.74	2.07	1.97	0.60	4.96	4.35
RP-16-1D	68.85	17.47	2.17	1.33	0.54	4.58	4.34
RP-16-3	74.97	14.43	0.76	1.48	0.14	4.72	3.19
RP-16-5	71.33	16.09	1.84	1.42	0.44	4.47	3.84
RP-16-6	71.49	16.07	2.15	1.41	0.44	4.29	3.54
RP-16-8	75.11	14.31	0.88	1.54	0.11	4.65	3.00

Zona de Pitek 20 cm	70.91	17.13	3.26	1.21	0.52	3.13	2.88
Zona de Pitek 60 cm	71.35	17.20	2.64	1.26	0.42	3.36	3.00
MS Glacial Drift	58.71	14.11	8.49	6.16	5.95	3.11	1.70
MS B1 SED Horshoe	59.24	14.67	8.88	5.36	5.29	2.92	1.70
MSA-1	56.54	13.11	10.15	6.55	7.52	2.62	1.18
MSA-2	58.65	14.53	8.78	5.59	6.36	2.92	1.38
MSA-3	57.24	14.44	9.64	6.30	6.83	2.40	1.25
MSA-5	57.42	14.97	9.66	5.55	6.66	2.51	1.37
MSB-5 Sed-1	57.12	14.78	10.45	5.03	6.61	2.77	1.25
MSB-5 Sed-2	57.23	14.25	10.04	5.64	6.77	2.75	1.31
MSB-5 Soil	60.91	14.55	7.79	5.23	5.82	3.22	1.10
MSc A1	62.32	15.64	7.75	3.69	4.17	3.14	1.78
AUS Drift PROX	66.59	15.24	4.12	3.37	1.06	3.87	3.87
AUS Drift Distal	68.15	14.93	3.68	3.02	0.72	3.79	4.03
AUS-SED-2	67.00	15.21	3.70	3.22	1.31	3.83	3.95
AUS-3	66.75	14.73	4.15	3.77	0.93	4.04	3.53
AUS-SED-4	66.78	14.97	3.90	3.87	0.85	3.88	3.58
AUS-5	67.18	14.94	3.69	3.52	1.00	4.13	3.66
AUS-SED-6	66.37	15.47	4.01	3.10	1.37	3.77	4.17
AUS-7	66.22	14.18	4.66	4.47	0.71	4.05	3.14
AUS-SED-8	67.50	15.05	3.45	3.52	0.93	3.89	3.74
AUS-SED-Lake	67.54	15.31	3.24	3.70	0.70	4.00	3.63
<i>AUS-PED-Merged</i>	65.34	14.90	5.45	3.44	1.12	3.84	3.54
LANG Drift Prox	55.79	24.09	6.26	3.58	1.83	3.05	3.36
LANG7	61.51	14.35	6.29	6.87	1.07	3.69	2.57
ELVA-1	64.26	15.14	4.80	4.60	1.41	3.97	3.37
ELVA-3	64.60	15.26	4.65	4.12	1.50	3.92	3.68
ELVA-13	64.48	14.76	5.00	4.77	1.13	3.99	3.19
VEITASTROND-LAKE-SED	64.60	15.74	5.10	3.07	1.73	3.65	4.32
EYF-2-IS	51.65	16.10	12.58	7.77	3.65	3.66	1.13
EYF-3-IS	53.25	15.63	12.15	7.16	3.33	3.95	1.34
PM-RG-SED-1	55.63	18.28	11.21	5.36	4.32	3.27	0.60
PM-RG-SED-2	51.18	26.65	11.21	3.22	2.90	2.99	0.62
PM-RG-SED-3	53.51	23.99	13.43	2.59	2.39	2.02	0.44
PM-RG-SED-4	53.00	20.21	14.67	3.99	3.27	2.66	0.63
PM-RG-SED-5	53.31	20.07	14.57	3.93	3.33	2.53	0.64
PM-RG-SED-6	47.87	32.62	11.54	2.14	2.25	1.34	0.84
PM-RG-SED-7	47.91	25.44	14.79	3.78	2.79	2.26	1.17
PM-RG-SED-8	49.57	32.91	9.01	2.57	2.20	1.55	0.92
PM-RG-SED-9	55.39	26.53	9.28	2.54	2.18	1.72	1.06
PM-RG-SED-10	50.57	28.21	9.28	3.62	2.52	2.66	1.58
PM-RG-SAP-1	55.72	18.84	11.57	4.45	4.21	3.66	0.50
PM-RG-SAP-2	53.31	20.98	12.01	4.14	4.84	2.81	0.74
PM-RG-SAP-3	49.06	40.59	4.45	1.44	1.15	1.16	1.09
PM-RG-SAP-4Red	51.18	38.24	6.78	0.55	0.86	0.42	0.89

PM-RG-SAP-5A	51.93	23.21	9.25	5.63	4.00	2.91	1.19
PM-RG-SAP-5B	54.85	25.05	8.25	3.75	1.75	3.13	2.07
PM-RG-SAP-6A-Red	52.04	38.39	6.95	0.01	0.27	0.16	1.14
PM-RG-SAP-6B-Yellow	54.91	35.24	4.48	0.94	0.93	1.14	1.35
PM-RG-SAP-6C-Brown	53.72	34.06	7.85	0.66	0.56	1.29	0.85
PM-RB-SED-1	50.73	28.44	9.05	4.26	2.58	2.14	1.33
PM-RB-SED-2	48.36	31.56	9.05	3.62	2.56	2.18	1.35
PM-RB-SED-3	53.82	21.01	11.06	4.55	3.39	2.72	1.74
PM-RB-SED-4	54.75	23.23	9.95	3.63	3.09	2.14	1.57
RG-14-SOIL-2	48.18	34.45	13.03	0.02	0.47	1.07	1.55
RG-14-SOIL-4	51.40	34.65	10.05	0.01	0.40	1.07	1.37
RG-14-SOIL-6	52.99	34.11	7.14	0.01	0.35	1.58	3.03
RB-14-SED-1	54.19	21.44	11.15	4.56	3.13	2.30	1.47
RB-14-SED-2	55.70	21.51	9.55	4.79	2.93	2.54	1.51
RB-14-SED-3	54.55	22.17	10.41	4.46	2.99	2.36	1.52
RB-14-SED-4	56.34	20.55	10.69	4.14	2.90	2.24	1.53
RB-14-SED-5	51.28	24.59	12.23	4.01	2.77	2.07	1.29
IGNF-13-SOIL-1	64.82	19.37	3.81	3.69	1.34	3.75	2.07
IGNF-13-SOIL-2	64.78	19.30	3.86	3.71	1.35	3.72	2.08
IGNF-13-SOIL-3	64.69	19.44	3.88	3.62	1.39	3.76	2.11
IGNF-13-SOIL-4	64.53	19.53	3.42	4.04	1.17	4.23	1.96
IGNF-13-SOIL-5	64.92	19.44	3.31	3.99	1.12	4.22	1.94
IGNF-13-SOIL-6	64.19	19.63	3.58	4.02	1.19	4.18	2.05
IGNF-13-SOIL-7	65.69	18.98	3.29	3.90	1.16	4.02	1.91
IGNF-13-SED-1	64.15	19.41	4.16	3.76	1.45	3.73	2.09
IGNF-13-SED-5	64.24	19.20	5.04	2.90	1.76	3.31	2.30
IGNF-13-SED-7	62.84	20.10	5.03	3.14	1.70	3.63	2.30
IGNF-13-SED-11	64.18	19.00	4.75	3.20	1.72	3.54	2.32
IGNF-13-SED-13	63.35	18.78	5.00	3.65	1.77	3.77	2.27
IGNF-13-SED-15	62.24	19.06	6.37	2.70	2.73	2.70	2.75
W10-CG-1-BR	55.78	18.34	7.41	6.28	2.85	3.41	3.71
W10-CG-2-BR	74.61	13.05	2.58	1.16	0.27	3.05	4.98
W10-CG-10-BR	64.54	16.19	5.45	4.13	1.50	3.27	3.98
W10-CG-14-BR	41.02	13.72	15.40	11.70	8.86	3.18	1.32
W10-CG-15-BR	75.81	13.34	2.61	3.58	0.27	3.42	0.66
W10-DG-1-BR	66.39	16.06	4.91	3.21	1.00	3.50	3.93
W10-GG-1-BR	55.34	16.12	9.37	7.29	4.70	3.01	2.44
W10-GG-2-BR	53.09	16.79	10.37	8.31	4.43	2.97	2.21
T10-MG-1-BR	68.15	14.54	3.98	3.22	0.86	2.38	5.87
T10-MS-1-BR	61.62	16.80	7.44	3.03	3.78	2.56	3.35
T10-MS-2-BR	72.28	14.97	1.47	3.24	0.37	4.21	3.13
T10-RD-1-BR	43.13	14.17	13.54	13.18	7.97	2.42	1.01
T10-RD-2-BR	44.95	15.84	11.74	9.02	5.89	5.14	2.75
T10-DK-1-BR	71.04	14.45	3.30	2.06	0.52	3.17	4.81
T10-DK-2-BR	70.55	14.49	3.63	2.14	0.52	3.13	4.88

T10-GOLD-1-BR	74.49	14.02	1.26	1.17	0.05	2.85	5.96
T10-GOLD-2-BR	58.54	16.58	7.40	5.49	2.80	3.48	3.89
T10-GOLD-4-BR	61.83	15.77	7.16	5.35	2.17	3.29	2.94
T10-GOLD-6-BR	79.36	8.06	5.55	1.82	1.52	1.28	1.71
T10-CC-1-BR	45.54	14.23	14.28	9.04	8.46	3.45	1.21
RB-14-BDRK-#2A	61.63	15.61	7.57	6.00	2.77	3.20	2.07
RG-14-BDRK-13	61.24	15.66	8.53	6.53	2.52	4.09	0.35
RG-14-BDRK-13amp	48.36	14.65	13.22	10.91	8.16	2.78	0.43
IGNF-13-BDRK-1B Float	73.57	13.52	2.87	3.32	0.87	3.53	1.55
IGNF-13-BDRK-1	72.69	13.85	2.91	3.98	1.04	3.47	1.11
IGNF-13-BDRK2	63.87	16.99	5.16	4.05	1.68	4.00	2.79
BDRK-Weathered-O	69.82	15.65	3.20	3.66	0.97	3.90	1.92
BDRK-Weathered-1	72.45	14.86	2.24	3.47	0.67	3.85	1.77
BDRK-Fresh	68.21	16.78	2.94	4.72	1.01	4.24	1.22
PERU-GR BDRK	72.75	15.02	1.30	1.77	0.32	4.39	3.98
Gordon et al. 2013 granitic leucosome	76.48	13.43	0.59	1.80	0.23	2.92	4.42
Gorgon et al. 2013 granodioritic leucosome	63.00	23.34	0.06	4.42	0.00	8.94	0.23
Gordon et al. 2013 eclogite-margin	71.04	15.68	2.45	3.11	1.22	4.19	1.91
Gordon et al. 2013 granodioritic leucosome	72.58	16.54	0.72	3.42	0.36	5.49	0.81
Gordon et al. 2013 granitic pegmatite	63.88	17.59	4.65	3.48	2.58	5.08	2.05
Kelly et al. 2014 Fimmvörðuháls lava flow	47.28	14.85	13.27	9.48	8.10	2.82	0.72
USGS Mount Stuart granodiorite	64.67	15.73	4.52	4.55	3.26	4.05	2.24
USGS acidic dike W Mount Stuart	65.12	16.73	3.96	4.16	3.34	3.92	2.07

Table S1.4. (Continued)

Sample Number	Cr2O3	TiO2	MnO	P2O5	SrO	BaO
122612-2	0.02	1.09	0.12	0.26	0.02	0.04
123012-5	0.01	2.08	0.20	0.38	0.03	0.09
122512-12	0.02	2.72	0.18	0.56	0.08	0.06
122412-7	0.03	2.20	0.20	0.46	0.07	0.06
122412-2	0.02	2.12	0.14	0.45	0.06	0.06
010213-2	0.03	1.00	0.16	0.20	0.04	0.05
122312-6	0.03	2.28	0.18	0.48	0.07	0.06
010213-1	0.03	1.29	0.15	0.21	0.01	0.05
123012-11	0.02	1.44	0.15	0.23	0.02	0.05
Whillans	0.01	0.82	0.08	0.16	0.02	0.05
T10-GOLD-12Drift	0.02	1.64	0.16	0.34	0.04	0.06
T10-GOLD-9Drift	0.02	1.56	0.14	0.33	0.04	0.06
T10-GOLD-1	0.02	1.82	0.17	0.41	0.04	0.10
T10-Gold 5	0.02	1.78	0.16	0.46	0.04	0.08
T10-Gold 12	0.02	1.51	0.16	0.31	0.04	0.07
T10-GOLD-14	0.02	1.49	0.12	0.30	0.05	0.08
T10-HOW-8Drift	0.02	1.65	0.16	0.29	0.04	0.06
T10-HOW-9Drift	0.02	1.83	0.17	0.37	0.04	0.09
T10-HOW-12Drift	0.02	1.60	0.18	0.33	0.04	0.07

D7	0.01	1.92	0.16	0.41	0.10	0.08
T10-CAMP-SP-0cm	0.02	2.25	0.17	0.45	0.05	0.05
T10-CAMP-SP-10cm	0.02	2.02	0.14	0.37	0.06	0.06
T10-CAMP-SP-20cm	0.03	1.89	0.15	0.39	0.07	0.07
T10-CAMP-SP-30cm	0.02	1.95	0.15	0.41	0.06	0.08
BHS-90-115	0.01	1.24	0.12	0.24	0.02	0.06
BHS-93-36	0.02	1.51	0.14	0.32	0.04	0.06
BHS-93-34	0.01	1.08	0.13	0.27	0.04	0.06
BHS-93-20	0.02	1.45	0.14	0.32	0.04	0.06
BHS-90-027z	0.02	0.54	0.10	0.13	0.05	0.05
BHS-93-23	0.01	1.47	0.17	0.29	0.02	0.05
BHS-93-29	0.01	1.05	0.12	0.24	0.02	0.06
<i>UOR-SP-Merged</i>	0.01	1.08	0.12	0.18	0.02	0.06
10-CG-1	0.02	1.39	0.15	0.35	0.05	0.06
W10-CG-2	0.01	1.44	0.15	0.33	0.05	0.07
W10-CG-3	0.02	1.61	0.16	0.36	0.04	0.06
W10-CG-4	0.04	2.85	0.24	0.49	0.04	0.04
W10-CG-5	0.02	1.60	0.17	0.39	0.04	0.05
10-CG-6	0.02	1.81	0.17	0.39	0.04	0.05
W10-CG-7	0.03	2.01	0.20	0.48	0.04	0.04
W10-CG-8	0.03	1.60	0.18	0.38	0.04	0.05
W10-CG-9	0.03	2.10	0.20	0.41	0.04	0.05
W10-CG-10	0.03	1.97	0.20	0.47	0.03	0.04
10-CG-12	0.02	1.35	0.16	0.35	0.04	0.05
10-DG-1	0.02	1.57	0.16	0.36	0.04	0.08
10-DG-9	0.01	1.21	0.13	0.37	0.05	0.08
10-DG-10	0.02	1.20	0.12	0.34	0.05	0.08
T10-MAG-2	0.01	1.14	0.17	0.30	0.02	0.08
LP-16-1	0.00	0.35	0.05	0.07	0.06	0.10
LP-16-2	0.00	0.30	0.06	0.06	0.06	0.10
RL-16-1	0.00	0.54	0.07	0.20	0.06	0.07
RL-16-2	0.00	0.66	0.10	0.20	0.04	0.06
RL-16-3	0.00	0.35	0.05	0.11	0.05	0.05
RL-16-4	0.01	0.47	0.09	0.25	0.04	0.06
RL-16-5	0.00	0.45	0.06	0.12	0.05	0.06
RL-16-6	0.00	0.58	0.08	0.11	0.04	0.06
RL-16-7	0.00	0.51	0.06	0.21	0.05	0.06
RL-16-8	0.00	0.46	0.05	0.24	0.05	0.06
RL-16-Distal	0.00	0.47	0.05	0.27	0.06	0.06
Llaka Lake Debris	0.00	0.29	0.06	0.08	0.06	0.07
RP-16-1D	0.01	0.31	0.16	0.10	0.05	0.10
RP-16-3	0.01	0.11	0.03	0.06	0.04	0.07
RP-16-5	0.01	0.28	0.06	0.09	0.05	0.08
RP-16-6	0.01	0.28	0.08	0.12	0.04	0.08
RP-16-8	0.01	0.18	0.03	0.07	0.05	0.07

Zona de Pitek 20 cm	0.00	0.55	0.04	0.25	0.04	0.05
Zona de Pitek 60 cm	0.00	0.45	0.04	0.18	0.04	0.05
MS Glacial Drift	0.03	1.04	0.14	0.42	0.05	0.07
MS B1 SED Horshoe	0.03	1.20	0.15	0.45	0.04	0.07
MSA-1	0.04	1.33	0.19	0.68	0.03	0.05
MSA-2	0.03	1.04	0.16	0.45	0.04	0.06
MSA-3	0.04	1.15	0.17	0.45	0.03	0.05
MSA-5	0.04	1.09	0.16	0.46	0.03	0.06
MSB-5 Sed-1	0.04	1.38	0.14	0.33	0.03	0.07
MSB-5 Sed-2	0.04	1.22	0.19	0.47	0.04	0.06
MSB-5 Soil	0.03	0.98	0.13	0.13	0.04	0.05
MSc A1	0.04	1.07	0.11	0.19	0.04	0.07
AUS Drift PROX	0.00	0.97	0.04	0.58	0.12	0.16
AUS Drift Distal	0.00	0.87	0.03	0.50	0.11	0.16
AUS-SED-2	0.00	0.90	0.04	0.55	0.12	0.16
AUS-3	0.01	1.09	0.04	0.67	0.13	0.16
AUS-SED-4	0.00	1.10	0.04	0.74	0.13	0.16
AUS-5	0.01	0.96	0.04	0.61	0.12	0.16
AUS-SED-6	0.00	0.89	0.04	0.52	0.11	0.17
AUS-7	0.01	1.33	0.04	0.91	0.13	0.15
AUS-SED-8	0.00	0.96	0.04	0.64	0.12	0.16
AUS-SED-Lake	0.00	0.95	0.03	0.61	0.12	0.16
<i>AUS-PED-Merged</i>	0.01	1.05	0.05	0.97	0.12	0.16
LANG Drift Prox	0.00	1.10	0.06	0.66	0.10	0.14
LANG7	0.01	1.92	0.06	1.40	0.13	0.13
ELVA-1	0.01	1.22	0.06	0.88	0.13	0.15
ELVA-3	0.01	1.15	0.06	0.77	0.12	0.16
ELVA-13	0.01	1.38	0.06	0.96	0.13	0.14
VEITASTROND-LAKE-SED	0.00	0.93	0.06	0.51	0.11	0.17
EYF-2-IS	0.01	2.69	0.21	0.48	0.05	0.03
EYF-3-IS	0.01	2.42	0.21	0.46	0.04	0.03
PM-RG-SED-1	0.01	0.96	0.20	0.13	0.02	0.02
PM-RG-SED-2	0.01	0.87	0.18	0.14	0.02	0.02
PM-RG-SED-3	0.01	1.30	0.14	0.14	0.01	0.02
PM-RG-SED-4	0.01	1.01	0.32	0.16	0.02	0.04
PM-RG-SED-5	0.01	1.14	0.28	0.14	0.02	0.03
PM-RG-SED-6	0.01	1.07	0.17	0.10	0.02	0.04
PM-RG-SED-7	0.01	1.27	0.37	0.16	0.02	0.06
PM-RG-SED-8	0.01	0.91	0.12	0.17	0.02	0.04
PM-RG-SED-9	0.00	0.94	0.12	0.17	0.02	0.04
PM-RG-SED-10	0.01	0.87	0.39	0.18	0.04	0.08
PM-RG-SAP-1	0.00	0.77	0.18	0.06	0.02	0.01
PM-RG-SAP-2	0.03	0.86	0.20	0.03	0.03	0.02
PM-RG-SAP-3	0.01	0.65	0.26	0.06	0.01	0.08
PM-RG-SAP-4Red	0.02	0.73	0.18	0.08	0.01	0.06

PM-RG-SAP-5A	0.01	1.10	0.34	0.36	0.04	0.04
PM-RG-SAP-5B	0.01	0.67	0.23	0.04	0.06	0.11
PM-RG-SAP-6A-Red	0.02	0.88	0.02	0.07	0.01	0.04
PM-RG-SAP-6B-Yellow	0.02	0.67	0.22	0.03	0.01	0.06
PM-RG-SAP-6C-Brown	0.02	0.85	0.08	0.02	0.01	0.03
PM-RB-SED-1	0.01	1.01	0.16	0.21	0.04	0.06
PM-RB-SED-2	0.01	0.90	0.18	0.16	0.02	0.06
PM-RB-SED-3	0.01	1.17	0.21	0.19	0.03	0.09
PM-RB-SED-4	0.01	1.17	0.16	0.20	0.03	0.08
RG-14-SOIL-2	0.02	1.05	0.03	0.08	0.01	0.03
RG-14-SOIL-4	0.02	0.91	0.03	0.06	0.01	0.03
RG-14-SOIL-6	0.02	0.54	0.07	0.05	0.01	0.10
RB-14-SED-1	0.01	1.13	0.25	0.25	0.04	0.08
RB-14-SED-2	0.01	0.95	0.23	0.18	0.04	0.08
RB-14-SED-3	0.01	1.04	0.19	0.19	0.03	0.08
RB-14-SED-4	0.01	1.11	0.22	0.16	0.04	0.08
RB-14-SED-5	0.00	1.16	0.29	0.20	0.04	0.06
IGNF-13-SOIL-1	0.00	0.69	0.05	0.27	0.05	0.07
IGNF-13-SOIL-2	0.00	0.72	0.06	0.28	0.05	0.08
IGNF-13-SOIL-3	0.00	0.67	0.06	0.24	0.05	0.07
IGNF-13-SOIL-4	0.00	0.67	0.06	0.26	0.05	0.07
IGNF-13-SOIL-5	0.00	0.65	0.06	0.24	0.05	0.07
IGNF-13-SOIL-6	0.00	0.69	0.06	0.28	0.06	0.07
IGNF-13-SOIL-7	0.00	0.62	0.06	0.24	0.05	0.07
IGNF-13-SED-1	0.01	0.72	0.08	0.31	0.05	0.08
IGNF-13-SED-5	0.01	0.82	0.09	0.20	0.04	0.07
IGNF-13-SED-7	0.01	0.79	0.10	0.22	0.05	0.08
IGNF-13-SED-11	0.01	0.82	0.08	0.25	0.05	0.08
IGNF-13-SED-13	0.01	0.86	0.08	0.32	0.05	0.08
IGNF-13-SED-15	0.01	0.96	0.10	0.24	0.04	0.10
W10-CG-1-BR	0.01	1.31	0.12	0.48	0.11	0.20
W10-CG-2-BR	0.01	0.13	0.05	0.02	0.03	0.05
W10-CG-10-BR	0.01	0.50	0.09	0.14	0.06	0.14
W10-CG-14-BR	0.03	3.97	0.20	0.48	0.08	0.04
W10-CG-15-BR	0.01	0.16	0.04	0.01	0.07	0.02
W10-DG-1-BR	0.01	0.55	0.06	0.16	0.05	0.16
W10-GG-1-BR	0.05	1.04	0.13	0.29	0.08	0.13
W10-GG-2-BR	0.01	1.26	0.17	0.22	0.07	0.08
T10-MG-1-BR	0.01	0.47	0.06	0.09	0.07	0.30
T10-MS-1-BR	0.01	1.01	0.17	0.08	0.04	0.10
T10-MS-2-BR	0.01	0.17	0.02	0.02	0.08	0.04
T10-RD-1-BR	0.03	3.30	0.20	0.89	0.11	0.05
T10-RD-2-BR	0.01	3.39	0.21	0.86	0.12	0.06
T10-DK-1-BR	0.01	0.35	0.05	0.07	0.04	0.12
T10-DK-2-BR	0.01	0.35	0.05	0.07	0.04	0.13

T10-GOLD-1-BR	0.01	0.04	0.05	0.01	0.04	0.05		
T10-GOLD-2-BR	0.01	1.06	0.10	0.36	0.11	0.16		
T10-GOLD-4-BR	0.01	0.96	0.10	0.21	0.07	0.15		
T10-GOLD-6-BR	0.01	0.47	0.06	0.07	0.02	0.07		
T10-CC-1-BR	0.04	2.87	0.21	0.54	0.09	0.04		
RB-14-BDRK-#2A	0.02	0.62	0.16	0.18	0.05	0.10		
RG-14-BDRK-13	0.02	0.68	0.21	0.11	0.03	0.02		
RG-14-BDRK-13amp	0.02	1.01	0.23	0.17	0.03	0.03		
IGNF-13-BDRK-1B Float	0.03	0.43	0.04	0.14	0.05	0.08		
IGNF-13-BDRK-1	0.03	0.55	0.04	0.19	0.06	0.07		
IGNF-13-BDRK2	0.03	0.87	0.08	0.27	0.06	0.14		
BDRK-Weathered-O	0.01	0.49	0.06	0.16	0.06	0.10		
BDRK-Weathered-1	0.01	0.36	0.04	0.13	0.06	0.09		
BDRK-Fresh	0.01	0.50	0.05	0.17	0.07	0.09		
PERU-GR BDRK	0.01	0.17	0.03	0.05	0.07	0.15		
Gordon et al. 2013 granitic leucosome		0.08	0.01	0.02				
Gorgon et al. 2013 granodioritic leucosome		0.01	0.00	0.00				
Gordon et al. 2013 eclogite-margin		0.27	0.07	0.06				
Gordon et al. 2013 granodioritic leucosome		0.03	0.03	0.01				
Gordon et al. 2013 granitic pegmatite		0.56	0.08	0.04				
Kelly et al. 2014 Fimmvörðuháls lava flow		2.89	0.19	0.39				
USGS Mount Stuart granodiorite		0.70	0.00	0.16		0.11		
USGS acidic dike W Mount Stuart		0.45	0.05	0.11		0.08		

Table S1.5. Heavy metal compositions of the muds (ppm).

Sample Number	As	Co	Cu	Li	Mo	Ni	Pb	Zn
122612-2	7.50	35.50	187.00	30.00	3.50	107.50	61.00	133.00
123012-5	4.13	33.00	136.00	60.00	2.00	48.00	38.00	184.00
122512-12	3.32	31.00	113.00	30.00	1.00	56.00	24.00	138.00
122412-7	3.32	27.00	131.00	30.00	1.00	63.00	34.00	141.00
122412-2	3.83	31.50	279.00	30.00	5.50	81.50	87.00	215.00
010213-2	6.00	36.00	197.00	30.00	2.00	109.00	54.00	147.00
122312-6	2.95	29.00	207.00	30.00	2.00	70.00	36.00	140.00
010213-1	4.30	39.45	222.72	29.97	7.49	119.35	42.95	158.80
123012-11	3.47	37.55	324.12	48.00	5.25	102.16	29.50	198.61
Whillans	3.89	12.51	27.02	36.69	0.33	23.18	27.69	97.07
T10-GOLD-12Drift	5.00	32.00	84.00	30.00	4.00	74.00	18.00	126.00
T10-GOLD-9Drift	4.46	35.50	153.00	30.00	11.50	111.50	37.00	171.00
T10-GOLD-1	4.42	37.00	194.00	50.00	4.00	84.00	64.00	186.00
T10-Gold 5	6.68	34.20	159.00	39.59	2.00	79.00	123.00	192.00
T10-Gold 12	6.59	29.70	217.00	39.01	2.00	64.00	175.00	192.00
T10-GOLD-14	4.03	29.00	105.00	50.00	2.00	64.00	27.00	151.00
T10-HOW-8Drift	3.67	33.50	267.00	30.00	3.50	77.50	71.00	187.00
T10-HOW-9Drift	4.26	31.00	109.00	50.00	3.00	64.00	34.00	169.00
T10-HOW-12Drift	4.54	32.00	119.00	40.00	2.00	65.00	92.00	143.00

D7	7.00	26.00	79.00	40.00	4.00	42.00	18.00	142.00
T10-CAMP-SP-0cm	3.72	34.00	136.00	40.00	3.00	67.00	20.00	172.00
T10-CAMP-SP-10cm	3.51	33.50	115.00	30.00	1.50	67.50	19.00	159.00
T10-CAMP-SP-20cm	3.96	32.00	72.00	40.00	1.00	67.00	14.00	138.00
T10-CAMP-SP-30cm	5.00	33.00	84.00	40.00	1.00	63.00	21.00	140.00
BHS-90-115	4.08	27.50	147.00	50.00	1.50	49.50	77.00	191.00
BHS-93-36	4.17	31.60	125.39	30.06	5.52	89.78	23.07	161.51
BHS-93-34	6.00	28.00	93.00	30.00	1.00	186.00	29.00	129.00
BHS-93-20	4.14	34.00	92.00	40.00	3.00	68.00	18.00	147.00
BHS-90-027z	3.00	25.00	99.00	20.00	2.00	68.00	12.00	102.00
BHS-93-23	4.30	38.00	135.00	40.00	2.00	62.00	46.00	199.00
BHS-93-29	3.66	25.50	81.00	30.00	1.50	45.50	27.00	113.00
<i>UOR-SP-Merged</i>	3.37	27.50	125.00	30.00	3.50	67.50	15.00	177.00
10-CG-1	7.37	29.80	82.00	43.63	0.28	64.00	33.00	114.00
W10-CG-2	6.72	27.60	193.00	39.83	0.58	53.00	130.00	156.00
W10-CG-3	6.90	30.50	153.00	40.87	0.94	65.00	68.00	144.00
W10-CG-4	6.86	44.60	104.00	40.62	2.00	101.00	45.00	184.00
W10-CG-5	6.58	33.80	341.00	38.97	2.00	75.00	82.00	153.00
10-CG-6	6.73	33.20	250.00	39.84	0.95	73.00	57.00	145.00
W10-CG-7	7.21	36.30	80.00	42.70	0.68	83.00	27.00	131.00
W10-CG-8	6.74	34.30	257.00	39.93	0.94	78.00	41.00	138.00
W10-CG-9	6.56	37.20	364.00	38.86	2.00	84.00	55.00	166.00
W10-CG-10	6.77	39.60	204.00	40.08	2.00	95.00	43.00	148.00
10-CG-12	6.93	30.00	179.00	41.01	2.00	70.00	38.00	131.00
10-DG-1	3.17	29.00	81.00	40.00	3.00	50.00	14.00	149.00
10-DG-9	5.00	25.00	61.00	30.00	3.00	45.00	19.00	126.00
10-DG-10	3.24	24.00	63.00	30.00	3.00	44.00	18.00	129.00
T10-MAG-2	3.61	23.00	175.00	40.00	7.00	55.00	38.00	195.00
LP-16-1	3.49	3.00	18.00	70.00	3.00	4.00	40.00	127.00
LP-16-2	3.29	1.00	16.00	60.00	1.00	1.00	34.00	108.00
RL-16-1	2.96	5.00	47.00	50.00	3.00	9.00	40.00	77.00
RL-16-2	3.64	10.00	69.00	110.00	4.00	15.00	53.00	181.00
RL-16-3	3.81	1.50	61.00	90.00	1.50	15.50	117.00	127.00
RL-16-4	5.00	4.00	86.00	90.00	5.00	24.00	127.00	137.00
RL-16-5	3.73	3.00	60.00	80.00	4.00	20.00	101.00	110.00
RL-16-6	7.00	5.00	64.00	100.00	3.00	22.00	112.00	133.00
RL-16-7	17.00	4.00	30.00	60.00	4.00	9.00	177.00	149.00
RL-16-8	14.00	4.00	31.00	60.00	2.00	9.00	101.00	111.00
RL-16-Distal	12.00	4.00	19.00	50.00	3.00	8.00	80.00	97.00
Llaka Lake Debris	2.74	2.00	16.00	80.00	1.00	2.00	27.00	87.00
RP-16-1D	3.52	2.00	33.00	50.00	5.00	0.85	59.00	155.00
RP-16-3	1.81	0.76	5.00	20.00	0.42	1.00	20.00	31.00
RP-16-5	2.75	2.00	57.00	40.00	1.00	2.00	35.00	100.00
RP-16-6	2.96	2.00	131.00	50.00	2.00	2.00	44.00	113.00
RP-16-8	1.24	1.00	4.00	10.00	0.42	1.00	24.00	35.00

Zona de Pitek 20 cm	26.00	3.00	53.00	50.00	3.00	11.00	87.00	88.00
Zona de Pitek 60 cm	12.00	3.00	59.00	50.00	3.00	10.00	50.00	73.00
MS Glacial Drift	13.00	25.00	113.00	40.00	1.00	68.00	59.00	130.00
MS B1 SED Horshoe	10.00	23.00	116.00	50.00	3.00	69.00	230.00	157.00
MSA-1	5.00	28.00	95.00	40.00	5.00	90.00	15.00	154.00
MSA-2	8.00	26.00	87.00	50.00	5.00	82.00	20.00	145.00
MSA-3	7.00	30.00	122.00	60.00	7.00	100.00	12.00	168.00
MSA-5	5.00	27.00	73.00	70.00	3.00	94.00	35.00	170.00
MSB-5 Sed-1	8.00	26.00	81.00	50.00	11.00	115.00	15.00	152.00
MSB-5 Sed-2	9.00	27.00	73.00	50.00	8.00	92.00	15.00	149.00
MSB-5 Soil	8.00	22.00	53.00	40.00	4.00	69.00	13.00	123.00
MSc A1	7.00	18.00	72.00	80.00	17.00	125.00	117.00	121.00
AUS Drift PROX	3.11	8.00	14.00	10.00	1.00	14.00	34.00	58.00
AUS Drift Distal	2.94	5.00	44.00	10.00	2.00	14.00	35.00	38.00
AUS-SED-2	2.93	9.00	25.00	20.00	1.00	17.00	28.00	69.00
AUS-3	6.00	5.00	12.00	10.00	1.00	12.00	32.00	44.00
AUS-SED-4	3.09	7.00	17.00	10.00	1.00	12.00	36.00	43.00
AUS-5	3.12	5.00	12.00	10.00	0.59	13.00	30.00	47.00
AUS-SED-6	3.05	8.00	24.00	20.00	1.00	16.00	32.00	67.00
AUS-7	3.45	4.00	13.00	10.00	1.00	12.00	34.00	37.00
AUS-SED-8	6.00	6.00	17.00	10.00	1.00	13.00	33.00	48.00
AUS-SED-Lake	6.00	5.00	13.00	10.00	1.00	13.00	31.00	37.00
<i>AUS-PED-Merged</i>	3.27	11.00	59.00	10.00	2.00	21.00	53.00	64.00
LANG Drift Prox	2.94	17.31	62.32	10.00	1.49	31.15	34.62	95.92
LANG7	3.46	8.00	16.00	10.00	0.59	19.00	37.00	48.00
ELVA-1	6.00	9.00	21.00	10.00	0.72	20.00	32.00	64.00
ELVA-3	3.32	9.00	18.00	10.00	0.69	20.00	41.00	69.00
ELVA-13	3.32	7.00	15.00	10.00	0.63	17.00	34.00	54.00
VEITASTROND-LAKE-SED	3.04	12.00	20.00	20.00	1.00	20.00	34.00	88.00
EYF-2-IS	5.00	32.00	73.00	10.00	2.00	27.00	4.00	152.00
EYF-3-IS	5.00	28.00	53.00	10.00	4.00	36.00	3.00	164.00
PM-RG-SED-1	6.00	24.00	120.00	10.00	0.84	34.00	8.00	111.00
PM-RG-SED-2	3.96	35.46	162.80	10.00	1.50	29.46	8.99	90.89
PM-RG-SED-3	6.00	22.00	163.00	10.00	1.00	24.00	9.00	98.00
PM-RG-SED-4	6.00	46.00	213.00	10.00	3.00	43.00	19.00	155.00
PM-RG-SED-5	4.43	39.00	190.00	10.00	1.00	27.00	14.00	143.00
PM-RG-SED-6	4.09	29.50	161.02	10.00	0.70	15.50	5.00	99.01
PM-RG-SED-7	3.82	37.57	199.35	10.00	5.51	39.57	17.03	127.23
PM-RG-SED-8	7.50	15.50	132.99	10.00	0.70	13.50	11.00	102.99
PM-RG-SED-9	6.00	17.00	108.00	10.00	1.00	13.00	12.00	98.00
PM-RG-SED-10	9.50	33.49	220.97	10.00	5.50	47.49	19.00	124.98
PM-RG-SAP-1	5.00	29.00	154.00	10.00	0.83	24.00	7.00	107.00
PM-RG-SAP-2	7.00	33.00	137.00	10.00	0.87	91.00	2.00	99.00
PM-RG-SAP-3	7.50	85.50	269.01	10.00	0.78	7.50	17.00	101.01
PM-RG-SAP-4Red	4.02	37.00	175.00	20.00	0.56	10.00	3.00	70.00

PM-RG-SAP-5A	3.73	27.50	58.99	10.00	0.10	1.50	7.00	176.98
PM-RG-SAP-5B	3.45	17.00	43.00	20.00	0.15	2.00	8.00	119.00
PM-RG-SAP-6A-Red	5.00	5.00	54.00	10.00	0.38	5.00	15.00	91.00
PM-RG-SAP-6B-Yellow	6.00	27.00	43.00	30.00	0.55	8.00	15.00	136.00
PM-RG-SAP-6C-Brown	3.35	11.00	56.00	10.00	0.37	5.00	14.00	81.00
PM-RB-SED-1	4.22	19.50	154.97	10.00	0.77	11.50	13.00	96.98
PM-RB-SED-2	9.51	27.55	261.52	10.00	3.51	29.56	157.32	161.32
PM-RB-SED-3	4.55	26.00	261.00	20.00	9.00	58.00	156.00	142.00
PM-RB-SED-4	5.00	23.00	166.00	20.00	6.00	36.00	101.00	126.00
RG-14-SOIL-2	5.00	7.00	133.00	10.00	0.86	9.00	54.00	55.00
RG-14-SOIL-4	6.00	4.00	109.00	10.00	1.00	8.00	19.00	41.00
RG-14-SOIL-6	6.00	5.00	107.00	10.00	1.00	8.00	16.00	40.00
RB-14-SED-1	5.00	28.00	187.00	20.00	5.00	30.00	66.00	153.00
RB-14-SED-2	9.00	26.00	184.00	20.00	4.00	27.00	52.00	144.00
RB-14-SED-3	7.00	22.00	123.00	10.00	2.00	21.00	107.00	132.00
RB-14-SED-4	4.10	25.52	137.11	10.00	0.70	9.51	15.01	105.09
RB-14-SED-5	3.75	31.50	161.01	10.00	3.50	33.50	11.00	127.01
IGNF-13-SOIL-1	4.00	4.00	60.00	40.00	0.77	8.00	4.00	102.00
IGNF-13-SOIL-2	3.51	8.00	44.00	50.00	0.52	6.00	3.00	104.00
IGNF-13-SOIL-3	3.09	6.00	31.00	40.00	0.67	8.00	5.00	97.00
IGNF-13-SOIL-4	2.80	4.00	24.00	40.00	0.54	6.00	5.00	82.00
IGNF-13-SOIL-5	2.31	6.00	19.00	40.00	0.33	6.00	2.00	81.00
IGNF-13-SOIL-6	2.97	6.00	30.00	40.00	0.33	6.00	1.34	96.00
IGNF-13-SOIL-7	3.25	5.00	41.00	30.00	0.60	6.00	5.00	84.00

Table S1.6. Trace element compositions of the sediments (ppm).

Sample Number	Ba	Cr	Cs	Ga	Hf	Nb	Rb
122612-2	439.75	235.00	2.92	22.50	17.30	22.70	94.30
123012-5	785.00	90.00	6.57	27.40	12.60	33.70	259.00
122512-12	553.00	140.00	2.69	22.30	8.20	73.70	86.20
122412-7	552.00	160.00	2.88	21.60	11.70	74.20	93.40
122412-2	529.75	155.00	3.70	25.50	12.90	64.30	107.10
010213-2	425.00	210.00	2.93	19.60	12.30	19.60	95.00
122312-6	534.00	200.00	2.29	20.40	12.40	67.10	81.30
010213-1	463.16	234.71	3.88	27.50	14.68	25.67	127.34
123012-11	469.10	185.51	5.44	35.65	8.27	28.41	177.00
Whillans	482.60	45.03	10.11	25.77	6.77	16.11	156.21
T10-GOLD-12Drift	552.00	170.00	2.93	20.20	14.70	48.60	97.60
T10-GOLD-9Drift	557.75	215.00	4.16	24.30	23.70	35.90	135.30
T10-GOLD-1	852.00	170.00	5.73	23.20	11.80	41.60	171.50
T10-Gold 5	595.00	180.00	4.10	22.60	24.90	36.60	135.00
T10-Gold 12	550.00	130.00	4.94	23.40	11.10	37.00	150.00
T10-GOLD-14	647.00	120.00	5.15	23.00	7.20	41.10	138.50
T10-HOW-8Drift	641.75	175.00	3.96	25.90	9.70	44.30	123.10

T10-HOW-9Drift	719.00	130.00	6.12	24.60	6.90	48.80	152.00
T10-HOW-12Drift	570.00	140.00	2.89	20.40	12.20	44.60	96.80
D7	557.00	80.00	3.99	21.60	6.60	62.50	118.00
T10-CAMP-SP-0cm	445.00	150.00	3.72	21.80	11.90	55.20	107.00
T10-CAMP-SP-10cm	533.75	135.00	3.64	22.30	11.50	48.70	105.10
T10-CAMP-SP-20cm	516.00	150.00	2.96	20.40	9.20	41.70	101.50
T10-CAMP-SP-30cm	569.00	130.00	3.12	21.60	8.40	51.10	106.50
BHS-90-115	511.75	75.00	4.14	28.10	11.90	51.50	131.90
BHS-93-36	563.54	175.54	3.33	21.68	18.36	38.22	102.63
BHS-93-34	573.00	100.00	3.21	21.20	6.90	28.70	110.00
BHS-93-20	566.00	140.00	3.38	22.60	8.00	43.60	107.00
BHS-90-027z	452.00	140.00	1.82	15.10	4.10	10.20	67.20
BHS-93-23	509.50	110.00	4.52	25.90	18.40	32.20	125.20
BHS-93-29	513.75	95.00	3.40	22.90	8.10	25.50	105.50
<i>UOR-SP-Merged</i>	525.75	115.00	5.92	25.10	5.30	23.70	160.30
10-CG-1	492.00	150.00	2.08	20.80	10.70	36.60	87.40
W10-CG-2	593.00	110.00	3.11	23.00	12.40	42.60	120.50
W10-CG-3	517.00	140.00	3.08	21.30	18.90	38.60	104.50
W10-CG-4	371.00	280.00	1.52	19.30	57.80	44.60	64.00
W10-CG-5	468.00	180.00	1.99	20.70	16.70	38.10	84.00
10-CG-6	451.00	180.00	1.78	20.40	30.20	38.20	79.10
W10-CG-7	383.00	200.00	1.48	17.90	42.70	37.40	63.10
W10-CG-8	406.00	190.00	1.41	18.30	21.20	32.50	65.40
W10-CG-9	420.00	210.00	1.55	18.80	38.60	37.50	67.40
W10-CG-10	359.00	220.00	1.27	18.20	33.10	36.20	53.60
10-CG-12	452.00	160.00	1.71	19.40	11.30	29.90	72.40
10-DG-1	417.00	70.00	2.64	14.90	4.30	23.00	79.30
10-DG-9	660.00	100.00	2.57	21.60	12.70	31.80	95.80
10-DG-10	700.00	90.00	2.96	22.00	7.60	31.70	106.50
T10-MAG-2	631.00	90.00	3.77	31.10	16.40	111.00	138.00
LP-16-1	858.00	0.00	5.88	31.40	3.20	16.60	203.00
LP-16-2	817.00	0.00	4.93	29.60	3.10	14.10	194.00
RL-16-1	611.00	10.00	6.52	23.00	12.60	10.60	125.50
RL-16-2	501.00	30.00	15.90	25.30	3.50	11.40	189.00
RL-16-3	597.75	15.00	10.48	33.90	8.30	19.10	226.90
RL-16-4	546.00	30.00	8.78	25.40	9.40	17.20	169.50
RL-16-5	514.00	20.00	7.96	22.30	10.30	13.80	148.50
RL-16-6	485.00	30.00	12.15	24.00	9.80	12.90	170.50
RL-16-7	564.00	20.00	7.36	22.90	5.50	12.30	143.00
RL-16-8	529.00	20.00	6.21	21.60	6.30	12.30	130.00
RL-16-Distal	508.00	10.00	5.96	20.80	7.50	12.20	121.00
Llaka Lake Debris	564.00	0.00	8.24	31.50	3.70	13.40	219.00
RP-16-1D	877.00	0.00	6.18	29.10	4.00	16.10	201.00
RP-16-3	618.00	0.00	1.42	20.10	3.40	7.00	116.00
RP-16-5	766.00	0.00	4.31	25.70	4.20	14.80	167.00

RP-16-6	694.00	0.00	4.66	26.80	4.80	15.60	160.00
RP-16-8	640.00	0.00	1.80	19.20	6.30	9.30	103.00
Zona de Pitek 20 cm	424.00	10.00	9.25	25.30	7.70	13.10	133.50
Zona de Pitek 60 cm	438.00	10.00	8.08	25.10	6.10	10.90	134.00
MS Glacial Drift	549.00	180.00	4.29	19.10	8.10	6.00	54.70
MS B1 SED Horshoe	481.00	170.00	5.96	21.50	8.70	7.90	61.10
MSA-1	390.00	300.00	3.83	21.20	26.60	8.10	37.00
MSA-2	477.00	230.00	4.15	21.40	7.50	6.00	43.40
MSA-3	436.00	280.00	3.81	24.90	14.80	7.10	39.70
MSA-5	520.00	300.00	4.98	24.80	12.70	7.00	53.50
MSB-5 Sed-1	468.00	290.00	4.21	25.50	10.20	8.00	41.70
MSB-5 Sed-2	457.00	250.00	4.21	21.40	9.70	6.40	43.80
MSB-5 Soil	414.00	210.00	2.52	22.80	6.30	6.20	27.80
MSc A1	479.00	240.00	5.06	23.60	7.30	7.50	60.10
AUS Drift PROX	1490.00	20.00	0.98	20.70	23.30	30.10	120.50
AUS Drift Distal	1530.00	20.00	0.81	19.60	29.80	28.60	117.00
AUS-SED-2	1520.00	30.00	1.19	21.30	10.10	26.90	134.00
AUS-3	1400.00	20.00	0.84	20.30	33.30	34.40	109.50
AUS-SED-4	1455.00	20.00	0.78	19.80	39.80	35.60	105.00
AUS-5	1440.00	20.00	0.90	20.50	23.20	30.00	115.50
AUS-SED-6	1600.00	20.00	1.37	22.40	18.80	26.00	144.00
AUS-7	1305.00	20.00	0.61	21.00	47.20	44.80	92.20
AUS-SED-8	1570.00	20.00	0.95	20.40	26.20	31.70	120.00
AUS-SED-Lake	1530.00	20.00	0.74	19.20	23.60	29.10	92.40
<i>AUS-PED-Merged</i>	1345.00	40.00	1.21	22.20	34.20	29.60	120.50
LANG Drift Prox	1247.52	54.44	0.97	25.12	27.59	20.86	100.36
LANG7	1135.00	40.00	0.48	20.90	62.30	35.00	61.00
ELVA-1	1355.00	30.00	0.77	21.20	22.00	23.80	94.50
ELVA-3	1455.00	30.00	0.93	21.40	18.20	23.80	113.00
ELVA-13	1300.00	30.00	0.70	21.20	46.20	30.70	87.10
VEITASTROND-LAKE-SED	1580.00	20.00	1.36	22.50	11.60	21.10	147.00
EYF-2-IS	277.00	50.00	0.29	25.60	9.10	45.10	24.00
EYF-3-IS	315.00	70.00	0.40	27.20	9.80	52.80	27.90
PM-RG-SED-1	218.00	70.00	0.46	18.10	6.20	2.00	11.30
PM-RG-SED-2	237.45	54.94	0.40	19.31	2.70	1.50	12.48
PM-RG-SED-3	188.00	50.00	0.82	23.50	3.90	4.30	9.80
PM-RG-SED-4	311.00	80.00	0.50	20.20	3.10	2.20	12.20
PM-RG-SED-5	288.00	70.00	0.53	20.30	4.80	2.50	14.20
PM-RG-SED-6	297.78	35.00	1.28	26.90	3.90	3.50	24.90
PM-RG-SED-7	484.62	75.13	1.02	23.89	13.12	4.71	27.55
PM-RG-SED-8	359.73	15.00	0.98	27.10	2.70	3.70	22.50
PM-RG-SED-9	388.00	20.00	1.07	24.40	3.60	3.80	25.00
PM-RG-SED-10	613.65	54.99	1.34	24.70	3.30	4.10	38.49
PM-RG-SAP-1	112.00	30.00	0.26	19.20	1.50	0.50	15.60
PM-RG-SAP-2	129.50	220.00	0.76	17.70	1.10	1.50	13.10

PM-RG-SAP-3	687.78	8.66	0.74	29.50	0.90	2.10	30.10
PM-RG-SAP-4Red	448.00	5.88	0.80	31.80	1.20	3.00	21.90
PM-RG-SAP-5A	409.71	5.88	0.86	28.50	8.70	2.90	27.30
PM-RG-SAP-5B	865.00	10.00	4.48	29.60	3.50	2.40	56.80
PM-RG-SAP-6A-Red	246.00	10.00	0.55	32.40	3.50	3.40	25.90
PM-RG-SAP-6B-Yellow	470.00	10.00	0.83	30.90	3.30	3.40	41.90
PM-RG-SAP-6C-Brown	302.00	10.00	0.61	29.80	3.00	3.10	17.70
PM-RB-SED-1	531.65	15.00	1.30	22.30	16.90	5.10	28.09
PM-RB-SED-2	727.22	55.10	2.46	23.89	5.71	6.51	47.19
PM-RB-SED-3	648.00	70.00	2.00	21.70	5.30	5.70	41.50
PM-RB-SED-4	595.00	40.00	1.99	22.50	4.80	5.20	38.90
RG-14-SOIL-2	283.00	8.89	2.43	27.60	1.50	4.00	27.00
RG-14-SOIL-4	245.00	7.03	1.50	27.40	3.00	4.80	23.10
RG-14-SOIL-6	791.00	4.48	2.41	25.90	3.00	3.80	47.40
RB-14-SED-1	650.00	40.00	1.59	22.00	8.30	5.10	32.90
RB-14-SED-2	649.00	30.00	1.42	21.60	8.60	5.00	30.70
RB-14-SED-3	601.00	40.00	1.27	21.60	14.40	4.50	27.80
RB-14-SED-4	644.29	15.01	1.78	24.70	8.91	5.70	34.73
RB-14-SED-5	613.80	35.00	1.56	23.10	11.90	5.30	31.50
IGNF-13-SOIL-1	651.00	30.00	3.14	26.60	12.70	10.70	70.70
IGNF-13-SOIL-2	666.00	30.00	3.30	27.00	16.50	11.40	71.00
IGNF-13-SOIL-3	675.00	30.00	3.53	27.30	12.30	10.90	74.90
IGNF-13-SOIL-4	642.00	30.00	2.83	26.20	14.10	10.40	65.80
IGNF-13-SOIL-5	655.00	30.00	2.71	26.10	14.50	10.40	67.70
IGNF-13-SOIL-6	619.00	20.00	2.83	25.90	11.40	10.50	66.10
IGNF-13-SOIL-7	651.00	30.00	2.67	24.90	16.20	9.70	64.00
IGNF-13-SED-1	673.00	20.00	3.34	25.40	9.50	11.50	72.80
IGNF-13-SED-5	659.00	30.00	4.35	24.50	6.80	12.70	82.90
IGNF-13-SED-7	698.00	20.00	4.25	26.90	7.00	13.10	86.50
IGNF-13-SED-11	693.00	30.00	4.19	25.80	7.90	13.40	86.80
IGNF-13-SED-13	713.00	30.00	4.03	24.90	7.90	11.50	82.80
IGNF-13-SED-15	746.00	30.00	5.62	26.80	4.20	13.10	109.00

Table S1.6. (Continued)

Sample Number	Sn	Sr	Ta	Th	U	V	W	Zr
122612-2	19.50	230.90	1.55	14.46	2.98	175.50	9.50	701.00
123012-5	11.00	242.00	1.90	16.65	3.17	172.00	2.00	545.00
122512-12	11.00	683.00	4.50	10.05	1.87	188.00	2.00	360.00
122412-7	15.00	553.00	4.60	11.55	2.40	140.00	5.00	546.00
122412-2	65.50	447.90	4.15	11.98	2.86	135.50	1.50	565.00
010213-2	33.00	232.00	1.30	13.30	3.81	156.00	2.00	522.00
122312-6	30.00	539.00	4.20	11.25	2.48	144.00	2.00	581.00
010213-1	11.49	253.58	1.35	13.88	2.47	165.29	1.50	622.21
123012-11	12.85	200.37	1.48	15.82	1.82	144.06	1.45	339.32

Whillans	12.51	129.26	1.25	12.85	2.65	89.23	4.50	221.83
T10-GOLD-12Drift	5.00	353.00	2.80	14.25	2.81	165.00	15.00	611.00
T10-GOLD-9Drift	25.50	269.90	2.15	15.90	3.30	159.50	3.50	951.00
T10-GOLD-1	40.00	360.00	2.30	14.50	2.79	170.00	2.00	484.00
T10-Gold 5	15.00	334.00	2.60	19.35	4.46	183.00	6.00	944.00
T10-Gold 12	30.00	323.00	2.70	15.60	2.54	151.00	7.00	427.00
T10-GOLD-14	6.00	396.00	2.20	13.05	2.20	138.00	3.00	290.00
T10-HOW-8Drift	15.50	381.90	2.75	12.18	2.12	151.50	73.50	397.00
T10-HOW-9Drift	8.00	379.00	2.70	13.75	2.02	153.00	2.00	294.00
T10-HOW-12Drift	38.00	367.00	2.80	13.10	2.59	142.00	2.00	513.00
D7	6.00	727.00	3.80	15.90	5.04	129.00	3.00	318.00
T10-CAMP-SP-0cm	6.00	462.00	3.60	13.75	2.64	147.00	6.00	513.00
T10-CAMP-SP-10cm	7.50	499.90	2.95	12.96	2.62	159.50	1.50	525.00
T10-CAMP-SP-20cm	4.00	527.00	2.90	13.35	2.49	136.00	1.00	408.00
T10-CAMP-SP-30cm	6.00	540.00	3.30	13.75	2.52	143.00	1.00	390.00
BHS-90-115	11.50	262.90	3.15	13.42	3.38	127.50	3.50	503.00
BHS-93-36	13.54	309.89	2.36	12.45	3.19	166.02	3.51	755.39
BHS-93-34	5.00	311.00	1.70	11.85	2.07	134.00	4.00	282.00
BHS-93-20	5.00	352.00	2.50	12.20	2.68	155.00	5.00	324.00
BHS-90-027z	3.00	402.00	0.60	7.00	1.34	121.00	2.00	162.00
BHS-93-23	8.00	276.40	2.00	13.51	3.04	172.00	2.00	813.00
BHS-93-29	5.50	318.90	1.35	12.10	1.98	143.50	1.50	335.00
<i>UOR-SP-Merged</i>	7.50	278.90	1.35	9.66	1.76	129.50	1.50	247.00
10-CG-1	6.00	351.00	2.70	13.50	2.40	172.00	2.00	395.00
W10-CG-2	37.00	349.00	3.30	16.45	2.56	152.00	3.00	474.00
W10-CG-3	39.00	334.00	3.00	16.20	2.94	183.00	4.00	696.00
W10-CG-4	17.00	307.00	3.60	24.90	8.05	351.00	3.00	2270.00
W10-CG-5	129.00	339.00	2.80	18.50	3.00	209.00	5.00	632.00
10-CG-6	125.00	327.00	2.90	16.60	4.15	224.00	4.00	1120.00
W10-CG-7	23.00	287.00	3.00	19.40	5.65	262.00	5.00	1590.00
W10-CG-8	56.00	302.00	2.40	15.60	3.31	215.00	4.00	790.00
W10-CG-9	84.00	296.00	2.80	16.85	4.92	269.00	3.00	1430.00
W10-CG-10	40.00	327.00	3.10	18.75	4.84	277.00	8.00	1320.00
10-CG-12	55.00	362.00	2.50	12.10	2.36	183.00	6.00	467.00
10-DG-1	3.00	234.00	1.40	7.25	1.52	89.00	1.00	198.00
10-DG-9	4.00	420.00	2.00	12.35	2.70	123.00	2.00	561.00
10-DG-10	4.00	418.00	2.00	10.80	2.14	112.00	2.00	349.00
T10-MAG-2	13.00	181.00	6.50	16.85	4.02	90.00	3.00	722.00
LP-16-1	9.00	492.00	1.50	14.35	8.03	21.00	2.00	110.00
LP-16-2	4.00	466.00	1.30	12.75	4.37	19.00	2.00	106.00
RL-16-1	75.00	484.00	0.90	18.70	11.10	55.00	9.00	519.00
RL-16-2	61.00	294.00	0.90	10.90	15.10	86.00	2.00	129.00
RL-16-3	175.50	425.90	2.95	25.38	75.18	23.50	1.50	273.00
RL-16-4	170.00	380.00	2.40	34.50	106.50	35.00	1.00	322.00
RL-16-5	110.00	324.00	1.60	30.30	60.60	31.00	1.00	368.00

RL-16-6	179.00	281.00	1.20	21.40	127.50	53.00	1.00	364.00
RL-16-7	35.00	431.00	1.10	11.25	4.91	50.00	1.00	199.00
RL-16-8	26.00	413.00	1.30	11.95	7.05	43.00	1.00	224.00
RL-16-Distal	14.00	413.00	1.20	12.40	5.90	40.00	1.00	282.00
Llaka Lake Debris	8.00	482.00	1.70	13.75	6.68	28.00	98.00	132.00
RP-16-1D	7.00	468.00	1.50	16.65	14.45	21.00	4.00	137.00
RP-16-3	10.00	399.00	0.70	9.30	1.59	5.00	1.00	104.00
RP-16-5	25.00	425.00	1.30	15.00	10.95	16.00	2.00	140.00
RP-16-6	34.00	388.00	1.40	20.20	30.70	16.00	3.00	158.00
RP-16-8	11.00	413.00	1.00	21.30	3.32	8.00	1.00	215.00
Zona de Pitek 20 cm	29.00	252.00	1.60	19.45	7.85	42.00	4.00	274.00
Zona de Pitek 60 cm	8.00	275.00	1.30	15.25	6.92	38.00	5.00	221.00
MS Glacial Drift	10.00	377.00	0.40	11.80	3.79	188.00	1.00	292.00
MS B1 SED Horshoe	25.00	312.00	0.50	13.15	9.41	194.00	1.00	326.00
MSA-1	8.00	289.00	0.60	16.25	6.46	217.00	2.00	963.00
MSA-2	6.00	316.00	0.40	7.06	7.82	172.00	1.00	256.00
MSA-3	7.00	256.00	0.50	7.28	4.19	199.00	1.00	562.00
MSA-5	9.00	281.00	0.50	9.54	7.58	189.00	1.00	424.00
MSB-5 Sed-1	7.00	292.00	0.60	5.11	5.53	194.00	1.00	372.00
MSB-5 Sed-2	7.00	290.00	0.40	5.89	6.24	178.00	1.00	338.00
MSB-5 Soil	6.00	337.00	0.40	4.37	4.63	162.00	1.00	224.00
MSc A1	10.00	266.00	0.50	3.22	5.36	123.00	2.00	263.00
AUS Drift PROX	8.00	1020.00	2.20	21.20	4.48	68.00	1.00	923.00
AUS Drift Distal	4.00	967.00	2.10	28.80	4.56	61.00	0.00	1150.00
AUS-SED-2	3.00	1010.00	1.90	24.50	3.34	65.00	2.00	388.00
AUS-3	7.00	1035.00	2.60	28.20	5.09	68.00	0.00	1260.00
AUS-SED-4	5.00	1075.00	2.50	30.80	5.92	69.00	0.00	1660.00
AUS-5	5.00	1025.00	2.20	25.50	4.07	65.00	0.00	881.00
AUS-SED-6	3.00	1000.00	1.90	27.80	4.09	67.00	1.00	711.00
AUS-7	6.00	1100.00	3.30	30.50	6.66	79.00	0.00	1790.00
AUS-SED-8	3.00	1100.00	2.40	28.00	5.04	65.00	0.00	1030.00
AUS-SED-Lake	3.00	1045.00	2.30	22.00	4.96	60.00	0.00	925.00
<i>AUS-PED-Merged</i>	10.00	1030.00	2.20	52.90	6.44	77.00	1.00	1410.00
LANG Drift Prox	5.44	743.42	1.34	20.74	2.53	94.45	1.49	1179.58
LANG7	7.00	1140.00	2.30	21.70	5.30	108.00	0.00	2520.00
ELVA-1	25.00	1055.00	1.50	19.40	2.96	80.00	0.00	875.00
ELVA-3	15.00	1030.00	1.60	21.90	3.05	79.00	0.00	715.00
ELVA-13	10.00	1065.00	2.20	23.70	4.94	85.00	0.00	1790.00
VEITASTROND-LAKE-SED	3.00	938.00	1.40	22.20	3.31	75.00	1.00	449.00
EYF-2-IS	5.00	409.00	2.80	3.34	1.05	223.00	1.00	366.00
EYF-3-IS	4.00	392.00	3.30	4.06	1.27	207.00	1.00	415.00
PM-RG-SED-1	3.00	154.00	0.20	1.10	0.82	275.00	1.00	235.00
PM-RG-SED-2	3.50	118.35	0.07	0.79	0.49	247.19	1.50	106.87
PM-RG-SED-3	3.00	84.50	0.30	2.06	0.99	320.00	2.00	150.00
PM-RG-SED-4	6.00	139.00	0.10	1.12	0.67	339.00	1.00	114.00

PM-RG-SED-5	7.00	125.00	0.20	1.55	0.91	363.00	1.00	191.00
PM-RG-SED-6	3.50	80.31	0.15	2.60	1.44	249.52	5.50	137.01
PM-RG-SED-7	5.51	190.84	0.35	3.74	2.18	384.19	1.50	562.01
PM-RG-SED-8	5.50	130.09	0.15	2.75	1.43	169.49	1.50	104.99
PM-RG-SED-9	3.00	134.50	0.20	3.93	1.62	164.00	1.00	129.00
PM-RG-SED-10	9.50	241.86	0.15	2.45	1.41	175.47	1.50	120.98
PM-RG-SAP-1	3.00	87.90	0.07	0.31	0.35	260.00	1.00	56.00
PM-RG-SAP-2	3.00	185.50	0.10	0.15	0.16	241.00	1.00	42.00
PM-RG-SAP-3	3.50	107.91	0.07	2.68	1.56	59.50	1.50	27.00
PM-RG-SAP-4Red	3.00	28.10	0.10	2.58	1.69	94.00	2.00	35.00
PM-RG-SAP-5A	3.50	254.87	0.15	7.03	3.99	151.49	1.50	336.97
PM-RG-SAP-5B	2.00	449.00	0.10	3.41	2.80	170.00	1.00	134.00
PM-RG-SAP-6A-Red	3.00	15.10	0.20	4.89	2.72	86.00	1.00	122.00
PM-RG-SAP-6B-Yellow	11.00	66.40	0.30	4.60	2.28	50.00	1.00	115.00
PM-RG-SAP-6C-Brown	9.00	79.90	0.20	4.74	2.53	92.00	1.00	100.00
PM-RB-SED-1	3.50	236.86	0.35	12.99	4.07	173.47	1.50	682.88
PM-RB-SED-2	41.58	243.39	0.35	6.41	2.70	256.01	1.50	193.38
PM-RB-SED-3	141.00	226.00	0.40	4.48	2.37	189.00	2.00	185.00
PM-RB-SED-4	68.00	208.00	0.40	3.40	1.89	146.00	1.00	176.00
RG-14-SOIL-2	16.00	10.90	0.30	3.08	1.46	196.00	1.00	35.00
RG-14-SOIL-4	3.00	7.50	0.50	7.21	1.73	155.00	1.00	77.00
RG-14-SOIL-6	3.00	14.30	0.40	9.28	1.74	111.00	1.00	74.00
RB-14-SED-1	52.00	251.00	0.40	5.43	2.55	197.00	1.00	309.00
RB-14-SED-2	36.00	282.00	0.40	4.53	2.07	180.00	1.00	325.00
RB-14-SED-3	41.00	248.00	0.40	4.90	2.71	180.00	1.00	599.00
RB-14-SED-4	3.50	242.10	0.35	5.14	2.60	173.64	1.50	331.28
RB-14-SED-5	5.50	225.92	0.35	4.52	2.42	235.52	1.50	479.04
IGNF-13-SOIL-1	11.00	437.00	0.90	9.15	2.24	50.00	1.00	486.00
IGNF-13-SOIL-2	8.00	446.00	0.90	9.92	2.40	53.00	1.00	623.00
IGNF-13-SOIL-3	8.00	455.00	0.80	7.86	2.01	47.00	1.00	454.00
IGNF-13-SOIL-4	7.00	484.00	0.80	7.92	2.05	49.00	1.00	528.00
IGNF-13-SOIL-5	7.00	493.00	0.80	9.08	2.19	49.00	2.00	554.00
IGNF-13-SOIL-6	5.00	450.00	0.80	8.12	2.11	44.00	1.00	436.00
IGNF-13-SOIL-7	6.00	488.00	0.80	10.30	2.36	44.00	1.00	622.00
IGNF-13-SED-1	9.00	412.00	0.70	8.67	1.97	41.00	1.00	342.00
IGNF-13-SED-5	10.00	340.00	0.90	8.92	2.07	58.00	1.00	251.00
IGNF-13-SED-7	8.00	373.00	0.80	9.03	2.00	50.00	1.00	264.00
IGNF-13-SED-11	9.00	384.00	0.80	8.29	2.03	53.00	1.00	290.00
IGNF-13-SED-13	7.00	445.00	0.90	7.21	1.86	53.00	1.00	283.00
IGNF-13-SED-15	6.00	315.00	0.60	8.03	1.81	80.00	1.00	152.00

Table S1.7. Rare Earth Element compositions of the muds (ppm).

Sample Number	Sc	Y	La	Ce	Pr	Nd	Sm	Eu
122612-2	23.50	31.75	50.95	96.35	11.19	41.95	7.85	1.15

123012-5	20.00	39.50	78.00	157.00	16.35	59.20	10.75	1.49
122512-12	17.00	31.10	60.30	120.50	13.85	51.90	10.10	2.52
122412-7	16.00	34.50	61.70	125.50	14.30	52.80	9.95	2.41
122412-2	15.50	32.95	60.35	129.55	13.73	51.35	9.77	2.09
010213-2	23.00	27.90	42.60	83.80	9.32	33.80	6.12	1.10
122312-6	16.00	35.00	60.10	120.50	14.05	51.50	10.35	2.14
010213-1	23.47	34.51	45.69	89.84	10.67	36.70	6.76	0.96
123012-11	20.45	29.04	57.16	95.54	12.43	43.09	7.19	1.34
Whillans	12.51	31.87	37.48	75.91	9.48	34.07	6.75	1.26
T10-GOLD-12Drift	19.00	33.60	60.30	118.00	13.60	50.10	9.31	1.69
T10-GOLD-9Drift	19.50	32.55	52.75	108.35	12.13	43.95	8.61	1.27
T10-GOLD-1	21.00	35.80	69.40	127.50	15.20	56.70	10.55	1.90
T10-Gold 5	19.80	43.80	63.70	131.00	14.45	51.90	9.83	1.79
T10-Gold 12	19.51	30.10	52.10	111.00	11.35	39.80	7.24	1.48
T10-GOLD-14	16.00	26.60	55.10	105.00	12.25	43.60	8.14	1.51
T10-HOW-8Drift	17.50	29.95	57.35	115.55	12.61	46.75	8.55	1.65
T10-HOW-9Drift	16.00	30.30	63.40	122.50	13.65	50.30	9.48	1.84
T10-HOW-12Drift	20.00	31.10	56.10	111.00	12.85	46.60	8.69	1.84
D7	13.00	28.60	74.30	144.50	15.15	54.40	8.49	2.03
T10-CAMP-SP-0cm	18.00	30.00	62.60	126.00	13.75	50.60	8.42	2.08
T10-CAMP-SP-10cm	17.50	31.15	60.35	118.95	13.29	46.35	8.65	1.95
T10-CAMP-SP-20cm	18.00	28.30	57.20	114.50	12.40	46.20	7.25	1.87
T10-CAMP-SP-30cm	18.00	29.90	67.10	128.50	14.40	49.90	8.67	2.04
BHS-90-115	15.50	30.15	57.95	108.75	12.21	43.75	7.41	1.45
BHS-93-36	19.56	33.66	51.51	101.47	11.92	43.49	8.07	1.41
BHS-93-34	17.00	27.00	45.30	86.00	10.00	36.70	7.05	1.29
BHS-93-20	18.00	29.30	51.80	97.70	11.50	43.30	8.57	1.58
BHS-90-027z	19.00	17.70	27.30	52.90	5.75	21.00	3.77	0.90
BHS-93-23	20.00	33.70	56.20	111.40	12.15	41.00	8.13	1.32
BHS-93-29	15.50	25.55	42.35	83.55	9.63	34.75	6.33	1.37
<i>UOR-SP-Merged</i>	17.50	23.75	38.75	76.55	7.91	31.55	5.35	1.19
10-CG-1	21.82	35.00	50.20	103.00	11.35	40.90	8.00	1.72
W10-CG-2	19.92	35.20	56.20	114.00	12.40	43.70	8.07	1.74
W10-CG-3	20.44	38.70	55.70	114.00	12.70	45.30	8.57	1.74
W10-CG-4	20.31	71.00	79.10	167.50	18.85	68.80	13.65	2.23
W10-CG-5	19.49	44.80	55.60	115.50	13.05	47.50	9.60	1.88
10-CG-6	19.92	46.80	53.80	112.50	12.85	47.00	9.45	1.86
W10-CG-7	21.35	56.70	60.90	128.00	14.60	53.60	10.95	1.87
W10-CG-8	19.96	45.10	52.00	109.50	12.40	46.00	9.31	1.75
W10-CG-9	19.43	52.00	56.30	118.50	13.60	50.30	10.15	1.86
W10-CG-10	20.04	57.10	58.60	124.50	14.30	53.30	10.70	1.85
10-CG-12	20.51	34.40	39.50	83.70	9.41	35.40	7.35	1.41
10-DG-1	17.00	19.60	36.30	67.20	7.87	28.40	4.92	1.05
10-DG-9	17.00	35.60	57.40	112.00	12.60	47.30	9.35	1.71
10-DG-10	15.00	31.40	52.10	101.00	11.70	42.40	7.94	1.66

T10-MAG-2	12.00	50.40	89.10	175.00	19.70	70.20	13.20	1.84
LP-16-1	5.00	13.00	32.60	63.20	7.49	26.90	4.99	0.87
LP-16-2	4.00	11.50	26.90	52.90	6.16	22.50	3.94	0.76
RL-16-1	5.00	16.00	33.80	65.50	7.85	28.90	5.14	0.99
RL-16-2	9.00	15.70	21.00	41.10	4.99	18.40	3.64	0.87
RL-16-3	3.50	17.35	45.55	90.95	10.77	38.75	6.83	0.83
RL-16-4	4.00	22.90	57.60	112.50	13.20	47.50	8.84	0.91
RL-16-5	4.00	20.50	50.50	98.00	11.60	43.30	7.75	0.88
RL-16-6	5.00	24.00	38.30	75.70	9.13	32.00	5.75	0.78
RL-16-7	5.00	17.20	25.30	49.50	5.88	22.10	4.28	1.03
RL-16-8	5.00	19.60	27.50	53.90	6.43	24.50	4.79	1.02
RL-16-Distal	5.00	21.10	27.90	54.80	6.64	24.80	5.05	1.00
Llaka Lake Debris	4.00	14.90	28.10	56.80	6.87	24.80	4.48	0.78
RP-16-1D	4.00	15.70	36.30	71.40	8.23	30.90	5.63	0.97
RP-16-3	2.00	11.60	24.50	49.30	5.58	19.70	4.03	0.63
RP-16-5	4.00	16.20	33.20	65.00	7.41	27.50	5.40	0.74
RP-16-6	4.00	18.50	47.50	93.50	10.70	39.40	7.09	0.86
RP-16-8	1.00	25.90	54.20	107.00	12.15	43.10	8.28	0.79
Zona de Pitek 20 cm	5.00	19.20	38.80	78.10	9.46	33.70	6.75	1.01
Zona de Pitek 60 cm	5.00	15.40	30.30	60.30	7.25	26.90	4.93	0.93
MS Glacial Drift	27.00	31.50	20.80	49.30	6.91	30.10	6.60	1.06
MS B1 SED Horshoe	24.00	31.40	22.90	53.40	7.26	32.50	7.18	1.20
MSA-1	35.00	45.10	28.80	64.60	9.67	39.50	9.00	1.23
MSA-2	26.00	30.20	18.80	43.30	6.29	27.20	6.32	1.02
MSA-3	28.00	35.60	19.70	46.70	6.95	29.50	7.37	1.15
MSA-5	31.00	38.90	24.40	60.70	8.01	34.00	7.63	1.20
MSB-5 Sed-1	24.00	27.00	19.70	41.00	6.05	25.30	5.48	0.91
MSB-5 Sed-2	26.00	29.80	19.20	42.80	6.59	27.20	5.66	0.89
MSB-5 Soil	25.00	25.10	14.40	32.10	4.71	20.90	5.11	0.81
MSc A1	14.00	17.40	15.60	32.70	4.34	18.00	3.72	0.91
AUS Drift PROX	9.00	39.90	110.00	233.00	32.10	121.00	19.65	3.30
AUS Drift Distal	7.00	38.70	125.00	265.00	34.50	125.00	19.50	3.04
AUS-SED-2	9.00	36.80	113.50	247.00	32.00	117.50	18.50	3.16
AUS-3	10.00	47.20	123.50	297.00	35.30	131.50	21.80	3.84
AUS-SED-4	10.00	49.50	141.00	312.00	40.20	153.00	24.20	4.16
AUS-5	9.00	40.60	110.50	259.00	31.40	117.50	19.15	3.32
AUS-SED-6	9.00	36.10	118.00	248.00	32.00	117.00	18.70	3.01
AUS-7	11.00	59.20	137.50	336.00	41.50	159.50	27.20	4.75
AUS-SED-8	10.00	44.00	127.50	276.00	36.10	135.00	22.00	3.65
AUS-SED-Lake	8.00	47.30	107.50	243.00	32.60	125.00	21.10	3.50
<i>AUS-PED-Merged</i>	10.00	42.10	227.00	504.00	52.30	178.00	24.50	4.22
LANG Drift Prox	9.40	38.91	142.33	267.70	35.28	125.32	17.80	3.11
LANG7	16.00	67.20	149.00	350.00	43.30	167.50	28.20	5.65
ELVA-1	11.00	42.40	110.00	257.00	30.80	117.00	19.35	3.73
ELVA-3	11.00	40.60	109.00	257.00	30.50	115.00	18.60	3.49

ELVA-13	12.00	52.60	122.50	292.00	35.50	135.00	22.80	4.30
VEITASTROND-LAKE-SED	9.00	32.00	110.00	226.00	28.70	105.00	16.95	2.56
EYF-2-IS	20.00	44.30	35.80	78.20	10.75	44.70	11.85	3.15
EYF-3-IS	19.00	49.00	41.90	91.00	12.15	51.30	12.75	3.44
PM-RG-SED-1	40.00	25.50	5.40	14.90	2.17	10.50	3.00	0.90
PM-RG-SED-2	37.45	19.73	4.54	13.73	1.80	9.14	2.64	0.84
PM-RG-SED-3	33.00	19.40	7.20	17.40	2.29	10.60	2.83	0.74
PM-RG-SED-4	37.00	22.70	6.40	18.00	2.26	11.40	3.21	0.98
PM-RG-SED-5	38.00	26.60	7.00	18.70	2.47	11.20	3.58	0.97
PM-RG-SED-6	29.50	22.95	8.75	24.35	2.95	13.55	3.83	0.81
PM-RG-SED-7	31.56	29.00	10.37	29.40	3.39	15.78	4.03	0.91
PM-RG-SED-8	29.50	23.35	10.75	25.35	3.22	13.75	4.14	0.97
PM-RG-SED-9	28.00	23.40	10.90	25.20	3.27	14.60	3.60	0.92
PM-RG-SED-10	25.50	22.15	9.55	26.35	3.00	13.95	3.48	0.80
PM-RG-SAP-1	28.00	14.00	3.30	7.40	1.11	5.60	1.68	0.75
PM-RG-SAP-2	38.00	17.20	2.50	6.10	1.18	6.20	2.04	0.67
PM-RG-SAP-3	9.50	38.35	31.75	51.15	6.87	29.15	5.91	1.67
PM-RG-SAP-4Red	20.00	117.50	75.80	346.00	33.40	150.00	39.40	7.94
PM-RG-SAP-5A	27.50	32.35	14.55	27.75	3.86	17.95	4.88	1.12
PM-RG-SAP-5B	19.00	18.90	9.00	23.60	2.36	11.00	2.71	0.77
PM-RG-SAP-6A-Red	24.00	1.60	2.00	8.50	0.31	1.40	0.31	0.12
PM-RG-SAP-6B-Yellow	13.00	33.70	28.60	44.80	7.64	30.80	7.72	2.01
PM-RG-SAP-6C-Brown	25.00	33.10	28.90	61.80	7.67	31.90	6.89	1.63
PM-RB-SED-1	29.49	37.54	13.55	34.94	4.56	21.35	5.56	0.98
PM-RB-SED-2	27.55	37.42	15.98	42.84	5.24	23.60	6.40	1.23
PM-RB-SED-3	30.00	30.90	13.80	36.50	4.42	19.40	4.70	0.98
PM-RB-SED-4	26.00	32.70	15.70	34.70	5.01	22.10	5.40	1.18
RG-14-SOIL-2	29.00	4.10	2.20	9.00	0.71	2.90	0.75	0.17
RG-14-SOIL-4	23.00	5.50	6.20	15.40	1.33	4.40	0.89	0.17
RG-14-SOIL-6	20.00	8.60	12.50	29.10	2.56	8.70	1.53	0.21
RB-14-SED-1	31.00	39.50	17.80	40.10	5.92	25.80	6.38	1.27
RB-14-SED-2	28.00	35.90	14.30	35.50	4.91	22.10	5.62	1.15
RB-14-SED-3	27.00	36.70	15.00	34.20	4.97	23.20	5.73	1.29
RB-14-SED-4	29.52	40.98	17.16	43.19	5.85	25.57	6.29	1.35
RB-14-SED-5	29.50	36.75	15.55	37.75	5.01	22.55	5.77	1.25
IGNF-13-SOIL-1	7.00	28.70	28.00	61.40	7.01	28.90	6.43	1.21
IGNF-13-SOIL-2	7.00	29.70	28.30	60.50	6.94	29.00	6.07	1.54
IGNF-13-SOIL-3	7.00	26.00	25.70	54.60	6.36	26.40	6.03	1.31
IGNF-13-SOIL-4	7.00	28.00	25.60	54.60	6.52	28.40	6.48	1.29
IGNF-13-SOIL-5	7.00	28.20	29.30	59.80	7.45	29.80	6.96	1.20
IGNF-13-SOIL-6	7.00	27.90	25.20	55.20	6.58	26.50	6.15	1.22
IGNF-13-SOIL-7	7.00	24.50	26.40	58.40	6.79	27.10	6.14	1.31
IGNF-13-SED-1		26.60	25.40	55.20	6.75	27.20	6.35	1.35
IGNF-13-SED-5		22.40	24.70	53.80	6.25	25.00	5.17	1.17
IGNF-13-SED-7		23.30	25.80	58.10	6.66	27.10	6.01	1.28

IGNF-13-SED-11	23.50	27.00	59.90	6.82	27.90	6.46	1.36
IGNF-13-SED-13	21.70	23.30	50.50	5.97	25.00	5.34	1.36
IGNF-13-SED-15	18.20	26.10	57.90	6.58	26.00	5.24	1.20

Table S1.7. (Continued)

Sample Number	Gd	Tb	Dy	Ho	Er	Tm	Yb	Lu
122612-2	6.08	1.00	6.08	1.08	3.85	0.54	3.31	0.56
123012-5	8.31	1.30	7.13	1.42	4.07	0.54	3.55	0.56
122512-12	7.91	1.13	6.20	1.20	3.34	0.47	2.98	0.44
122412-7	7.99	1.20	6.57	1.29	3.51	0.50	3.25	0.49
122412-2	7.84	1.16	6.34	1.32	3.55	0.44	3.15	0.44
010213-2	5.26	0.82	4.71	1.04	2.83	0.44	2.93	0.45
122312-6	8.27	1.21	6.69	1.33	3.88	0.55	3.50	0.53
010213-1	6.49	1.03	6.11	1.27	3.45	0.53	3.52	0.53
123012-11	6.04	0.85	5.51	0.98	2.99	0.38	2.65	0.41
Whillans	5.94	0.95	5.48	1.19	3.21	0.50	3.15	0.45
T10-GOLD-12Drift	7.50	1.13	6.55	1.19	3.39	0.50	3.29	0.50
T10-GOLD-9Drift	7.26	1.04	5.54	1.16	3.37	0.50	3.77	0.56
T10-GOLD-1	7.88	1.19	7.01	1.30	3.78	0.51	3.62	0.53
T10-Gold 5	9.89	1.51	8.12	1.64	4.82	0.68	4.59	0.73
T10-Gold 12	6.98	1.08	5.74	1.15	3.37	0.46	2.97	0.47
T10-GOLD-14	5.85	0.88	5.31	1.01	2.79	0.37	2.64	0.43
T10-HOW-8Drift	6.06	1.06	6.52	1.06	3.37	0.44	2.85	0.42
T10-HOW-9Drift	7.01	0.99	5.80	1.02	3.23	0.43	3.00	0.41
T10-HOW-12Drift	6.99	1.09	6.06	1.18	3.30	0.53	3.11	0.51
D7	7.59	1.10	6.06	1.21	2.85	0.40	2.76	0.35
T10-CAMP-SP-0cm	7.99	1.12	6.06	1.21	3.22	0.43	2.73	0.44
T10-CAMP-SP-10cm	7.74	1.18	5.94	1.28	3.29	0.42	2.85	0.44
T10-CAMP-SP-20cm	7.81	1.06	5.58	1.16	3.11	0.38	2.69	0.40
T10-CAMP-SP-30cm	7.75	1.10	5.94	1.28	3.20	0.44	2.78	0.39
BHS-90-115	6.40	0.96	5.86	0.94	3.03	0.46	3.05	0.44
BHS-93-36	7.24	1.14	6.42	1.18	3.62	0.60	3.62	0.58
BHS-93-34	5.81	0.82	5.04	0.96	2.85	0.41	2.56	0.41
BHS-93-20	6.07	0.98	5.61	1.07	3.18	0.42	2.89	0.43
BHS-90-027z	3.31	0.55	3.13	0.75	1.93	0.24	1.73	0.31
BHS-93-23	6.91	1.19	5.86	1.34	4.29	0.50	2.94	0.53
BHS-93-29	5.64	1.04	4.78	1.04	2.93	0.40	2.47	0.40
<i>UOR-SP-Merged</i>	4.66	0.84	4.40	0.96	2.37	0.32	2.35	0.36
10-CG-1	8.03	1.26	6.77	1.32	3.80	0.54	3.49	0.53
W10-CG-2	8.11	1.26	6.65	1.33	3.85	0.54	3.49	0.53
W10-CG-3	8.56	1.35	7.33	1.44	4.35	0.62	3.97	0.62

W10-CG-4	13.50	2.20	12.30	2.53	7.74	1.17	8.12	1.34
W10-CG-5	9.60	1.54	8.39	1.66	4.88	0.69	4.48	0.70
10-CG-6	9.43	1.52	8.54	1.75	5.14	0.74	5.04	0.81
W10-CG-7	10.85	1.78	10.05	2.06	6.24	0.91	6.15	0.99
W10-CG-8	9.42	1.49	8.32	1.67	4.97	0.70	4.64	0.71
W10-CG-9	10.15	1.64	9.23	1.91	5.78	0.87	5.82	0.96
W10-CG-10	10.70	1.81	10.30	2.10	6.26	0.90	6.14	0.94
10-CG-12	7.37	1.17	6.50	1.26	3.65	0.55	3.49	0.53
10-DG-1	4.74	0.74	3.79	0.82	2.13	0.26	1.74	0.25
10-DG-9	8.15	1.20	6.59	1.43	3.96	0.50	3.39	0.54
10-DG-10	7.67	1.02	6.01	1.24	3.26	0.44	2.81	0.43
T10-MAG-2	10.25	1.68	9.26	1.84	5.66	0.76	5.19	0.87
LP-16-1	3.32	0.48	2.48	0.47	1.17	0.16	1.06	0.17
LP-16-2	3.03	0.44	2.14	0.43	1.02	0.15	1.09	0.16
RL-16-1	3.86	0.48	2.81	0.53	1.63	0.27	1.67	0.29
RL-16-2	3.26	0.49	2.84	0.54	1.58	0.23	1.56	0.23
RL-16-3	4.00	0.56	3.00	0.54	1.47	0.28	1.79	0.26
RL-16-4	6.01	0.86	4.26	0.81	2.08	0.35	2.05	0.32
RL-16-5	4.96	0.73	3.74	0.72	1.95	0.29	1.97	0.32
RL-16-6	4.53	0.70	3.97	0.78	2.19	0.34	2.12	0.33
RL-16-7	3.55	0.53	2.92	0.61	1.64	0.26	1.68	0.28
RL-16-8	4.12	0.60	3.41	0.67	1.92	0.28	1.91	0.32
RL-16-Distal	4.46	0.63	3.67	0.75	2.11	0.31	2.24	0.34
Llaka Lake Debris	3.38	0.51	2.54	0.48	1.29	0.22	1.37	0.19
RP-16-1D	3.76	0.56	2.77	0.51	1.42	0.19	1.42	0.16
RP-16-3	2.55	0.39	2.09	0.39	1.18	0.15	1.02	0.14
RP-16-5	3.41	0.55	2.55	0.55	1.48	0.24	1.43	0.20
RP-16-6	4.40	0.67	3.40	0.64	1.61	0.23	1.55	0.23
RP-16-8	5.09	0.86	4.43	0.80	2.54	0.37	2.19	0.35
Zona de Pitek 20 cm	4.39	0.62	3.43	0.67	1.81	0.27	1.87	0.27
Zona de Pitek 60 cm	3.74	0.55	2.91	0.59	1.53	0.23	1.64	0.24
MS Glacial Drift	6.45	0.94	5.73	1.14	3.40	0.48	2.98	0.50
MS B1 SED Horshoe	6.66	1.00	5.42	1.17	3.19	0.48	3.14	0.50
MSA-1	8.71	1.22	7.98	1.54	4.92	0.70	4.50	0.70
MSA-2	6.09	0.82	5.44	1.16	3.33	0.45	3.10	0.45
MSA-3	6.57	1.02	6.67	1.32	3.90	0.48	3.76	0.56
MSA-5	7.95	1.13	6.95	1.33	3.98	0.54	3.93	0.56
MSB-5 Sed-1	5.50	0.82	4.58	0.89	2.80	0.38	2.77	0.34
MSB-5 Sed-2	5.86	0.84	5.17	1.02	3.12	0.42	2.60	0.46
MSB-5 Soil	4.72	0.71	4.47	0.86	2.79	0.36	2.46	0.37
MSc A1	3.37	0.51	3.03	0.61	1.81	0.25	1.70	0.26
AUS Drift PROX	12.15	1.44	7.76	1.40	4.04	0.58	3.72	0.62
AUS Drift Distal	10.90	1.40	7.76	1.43	3.90	0.57	3.83	0.60
AUS-SED-2	10.60	1.35	7.07	1.22	3.45	0.54	3.26	0.50
AUS-3	13.00	1.67	9.22	1.71	4.90	0.69	4.58	0.66

AUS-SED-4	14.10	1.82	9.98	1.72	4.99	0.71	4.99	0.80
AUS-5	11.65	1.47	7.59	1.51	4.23	0.56	3.67	0.57
AUS-SED-6	10.40	1.30	7.21	1.26	3.89	0.52	3.49	0.55
AUS-7	16.60	2.06	11.35	2.17	5.80	0.85	5.57	0.89
AUS-SED-8	12.25	1.53	8.29	1.59	4.57	0.61	3.98	0.68
AUS-SED-Lake	12.25	1.62	9.31	1.69	4.54	0.72	4.30	0.66
<i>AUS-PED-Merged</i>	14.00	1.87	8.89	1.68	4.63	0.62	4.23	0.61
LANG Drift Prox	10.93	1.42	8.00	1.38	3.69	0.57	3.64	0.61
LANG7	18.20	2.34	12.75	2.45	6.83	1.00	6.12	1.03
ELVA-1	12.60	1.58	8.43	1.53	4.47	0.60	3.66	0.60
ELVA-3	11.55	1.53	8.03	1.46	4.05	0.57	3.69	0.55
ELVA-13	14.45	1.84	10.20	1.91	5.37	0.80	4.77	0.83
VEITASTROND-LAKE-SED	9.13	1.15	6.20	1.08	3.02	0.42	2.69	0.44
EYF-2-IS	9.91	1.55	9.19	1.72	4.90	0.63	4.10	0.58
EYF-3-IS	11.25	1.67	9.72	1.87	5.17	0.72	4.71	0.69
PM-RG-SED-1	4.02	0.71	4.18	1.03	3.10	0.46	3.17	0.50
PM-RG-SED-2	3.19	0.55	3.47	0.79	2.25	0.35	2.70	0.35
PM-RG-SED-3	3.19	0.59	3.64	0.79	2.66	0.37	2.70	0.39
PM-RG-SED-4	3.98	0.68	4.41	0.96	2.80	0.42	3.00	0.49
PM-RG-SED-5	4.00	0.76	4.59	1.05	3.20	0.51	3.32	0.53
PM-RG-SED-6	3.86	0.72	4.34	1.02	2.89	0.48	3.25	0.52
PM-RG-SED-7	4.60	0.80	5.04	1.10	3.44	0.60	4.31	0.68
PM-RG-SED-8	3.73	0.64	3.93	0.94	2.77	0.40	2.88	0.44
PM-RG-SED-9	3.87	0.67	4.21	0.88	2.66	0.40	3.00	0.45
PM-RG-SED-10	3.77	0.59	4.11	0.89	2.49	0.39	2.66	0.43
PM-RG-SAP-1	2.18	0.41	2.48	0.56	1.70	0.26	1.75	0.27
PM-RG-SAP-2	2.58	0.49	3.11	0.68	1.89	0.28	1.79	0.30
PM-RG-SAP-3	6.94	1.16	6.64	1.48	4.05	0.62	4.37	0.78
PM-RG-SAP-4Red	32.70	5.04	28.10	5.61	16.15	2.58	18.40	2.58
PM-RG-SAP-5A	5.41	0.91	5.47	1.29	3.39	0.53	3.88	0.69
PM-RG-SAP-5B	3.00	0.52	3.40	0.73	2.18	0.33	2.66	0.48
PM-RG-SAP-6A-Red	0.28	0.06	0.40	0.09	0.33	0.06	0.50	0.08
PM-RG-SAP-6B-Yellow	6.83	1.16	6.93	1.50	4.35	0.78	5.91	0.89
PM-RG-SAP-6C-Brown	5.98	0.92	5.98	1.32	4.26	0.65	5.02	0.76
PM-RB-SED-1	5.69	1.05	6.41	1.43	4.75	0.67	5.16	0.87
PM-RB-SED-2	6.55	1.08	6.53	1.46	4.30	0.70	4.43	0.72
PM-RB-SED-3	4.90	0.87	5.26	1.17	3.63	0.57	3.92	0.61
PM-RB-SED-4	5.74	0.93	5.58	1.23	3.64	0.57	3.68	0.60
RG-14-SOIL-2	0.71	0.13	0.81	0.21	0.66	0.10	0.79	0.11
RG-14-SOIL-4	0.75	0.12	0.85	0.20	0.74	0.14	1.14	0.18
RG-14-SOIL-6	1.07	0.19	1.34	0.30	1.06	0.18	1.38	0.24
RB-14-SED-1	6.42	1.16	6.74	1.46	4.55	0.67	4.58	0.75
RB-14-SED-2	5.88	0.98	6.17	1.36	4.01	0.64	4.26	0.69
RB-14-SED-3	5.80	0.92	6.15	1.36	4.05	0.61	4.15	0.72
RB-14-SED-4	6.66	1.14	6.94	1.52	4.49	0.70	4.99	0.80

RB-14-SED-5	6.06	0.90	6.10	1.42	4.09	0.68	4.57	0.76
IGNF-13-SOIL-1	6.17	0.89	5.66	1.04	3.01	0.45	2.87	0.42
IGNF-13-SOIL-2	6.49	0.85	5.67	1.10	3.18	0.48	2.89	0.48
IGNF-13-SOIL-3	5.28	0.84	5.36	0.88	2.53	0.34	2.52	0.36
IGNF-13-SOIL-4	6.25	0.88	5.16	0.97	3.12	0.41	2.54	0.36
IGNF-13-SOIL-5	6.13	0.88	4.93	0.96	2.82	0.43	2.89	0.42
IGNF-13-SOIL-6	6.07	0.91	5.16	0.93	2.75	0.42	2.69	0.36
IGNF-13-SOIL-7	5.61	0.85	4.38	0.87	2.72	0.38	2.57	0.34
IGNF-13-SED-1	5.88	0.96	4.97	0.98	2.55	0.41	2.63	0.37
IGNF-13-SED-5	4.84	0.74	4.36	0.86	2.24	0.37	2.50	0.34
IGNF-13-SED-7	5.47	0.78	4.41	0.88	2.11	0.33	2.36	0.36
IGNF-13-SED-11	5.66	0.79	4.34	0.81	2.29	0.33	2.33	0.32
IGNF-13-SED-13	4.95	0.67	4.09	0.82	2.50	0.28	2.08	0.29
IGNF-13-SED-15	4.38	0.64	3.52	0.70	1.74	0.27	1.71	0.24

Table S1.8. Weathering indices calculated from the major oxide compositions of the muds.

Sample Number	R	WIP	V	CIA	CIW	PIA	STI
122612-2	5.07	67.46	0.73	54.54	58.79	55.30	78.51
123012-5	5.23	74.06	0.87	55.18	63.66	57.06	73.95
122512-12	5.59	77.15	0.71	49.45	54.20	49.33	71.58
122412-7	6.23	72.17	0.82	52.18	58.02	52.73	74.53
122412-2	4.54	69.60	1.00	59.81	65.73	61.97	73.61
010213-2	6.14	74.16	0.56	47.75	51.97	47.32	80.25
122312-6	6.19	76.14	0.71	49.79	54.98	49.74	73.94
010213-1	5.17	70.12	0.69	52.96	57.72	53.55	77.66
123012-11	3.91	67.73	0.92	60.10	66.43	62.48	74.45
Whillans	6.73	58.38	1.88	65.20	76.37	71.49	82.62
T10-GOLD-12Drift	6.15	72.93	0.74	50.53	55.93	50.66	77.05
T10-GOLD-9Drift	4.09	67.87	0.98	60.71	66.53	62.98	74.63
T10-GOLD-1	5.50	69.21	0.74	54.27	60.14	55.31	75.48
T10-Gold 5	5.96	71.76	0.69	50.71	55.67	50.87	76.09
T10-Gold 12	5.81	73.20	0.82	52.53	58.58	53.19	77.51
T10-GOLD-14	5.66	73.99	0.78	50.38	56.16	50.48	77.38
T10-HOW-8Drift	4.84	69.12	0.90	57.03	63.02	58.68	75.79
T10-HOW-9Drift	5.34	69.97	0.91	57.10	64.33	59.16	75.56
T10-HOW-12Drift	6.22	73.56	0.73	50.15	55.64	50.19	77.33
D7	5.99	74.58	0.94	51.23	58.04	51.61	75.86
T10-CAMP-SP-0cm	5.78	70.12	0.78	53.12	59.50	53.98	73.83
T10-CAMP-SP-10cm	4.46	68.44	0.87	56.03	61.07	57.22	73.70
T10-CAMP-SP-20cm	5.92	72.77	0.72	49.27	54.70	49.09	75.62
T10-CAMP-SP-30cm	5.87	71.71	0.77	50.58	56.31	50.73	75.36

BHS-90-115	3.60	69.29	1.24	63.13	69.23	65.94	74.37
BHS-93-36	5.14	68.95	0.79	53.79	58.34	54.49	76.80
BHS-93-34	5.91	73.53	0.79	49.77	54.86	49.71	79.86
BHS-93-20	5.84	73.06	0.73	50.02	54.81	50.02	77.83
BHS-90-027z	6.81	74.51	0.67	47.51	51.63	47.04	83.89
BHS-93-19	4.12	67.44	0.97	58.90	63.76	60.50	75.12
BHS-93-29	5.05	71.92	0.87	52.74	57.24	53.25	78.81
<i>UOR-SP-Merged</i>	4.51	69.79	0.99	57.81	63.54	59.53	77.54
10-CG-1	5.97	74.63	0.68	47.49	51.06	47.08	78.29
W10-CG-2	5.80	73.71	0.84	51.16	56.11	51.41	77.99
W10-CG-3	6.03	72.53	0.72	49.11	53.29	48.95	77.24
W10-CG-4	7.05	69.90	0.45	42.94	45.51	42.04	70.14
W10-CG-5	6.22	72.97	0.61	46.46	49.77	45.92	77.23
10-CG-6	6.26	72.49	0.60	46.25	49.49	45.69	76.21
W10-CG-7	6.81	70.93	0.50	43.93	46.67	43.13	74.98
W10-CG-8	6.65	72.26	0.53	44.17	46.96	43.39	77.35
W10-CG-9	6.72	70.73	0.52	44.32	47.18	43.54	74.58
W10-CG-10	7.01	70.94	0.45	42.21	44.49	41.32	75.08
10-CG-12	6.33	72.49	0.61	46.18	49.35	45.62	78.70
10-DG-1	5.79	72.08	0.80	51.53	57.03	51.89	77.13
10-DG-9	6.36	75.69	0.77	48.10	53.00	47.67	79.61
10-DG-10	6.21	76.39	0.83	49.06	54.43	48.83	79.57
T10-MAG-2	4.84	73.93	1.52	60.97	69.86	64.72	78.05
LP-16-1	6.23	87.55	2.01	55.21	64.71	57.38	84.40
LP-16-2	6.35	87.23	1.97	54.76	64.14	56.72	84.84
RL-16-1	7.09	74.98	1.53	53.75	61.05	54.92	84.49
RL-16-2	7.05	66.13	1.56	58.80	68.31	62.20	83.74
RL-16-3	5.25	78.51	2.29	60.69	68.91	64.04	82.55
RL-16-4	7.35	70.96	1.94	58.10	67.85	61.37	85.18
RL-16-5	8.60	67.80	1.87	55.30	63.97	57.27	86.53
RL-16-6	8.97	60.56	1.87	58.15	68.17	61.54	85.85
RL-16-7	7.33	68.67	1.76	56.04	63.91	58.01	84.95
RL-16-8	7.59	69.43	1.66	54.81	62.22	56.32	85.55
RL-16-Distal	7.74	67.62	1.68	55.03	62.19	56.53	85.62
Llaka Lake Debris	6.48	88.89	1.76	52.64	61.19	53.66	85.08
RP-16-1D	6.69	83.37	2.07	55.47	65.18	57.79	85.32
RP-16-3	8.82	74.45	1.71	51.56	58.83	52.07	89.04
RP-16-5	7.52	78.13	1.93	54.29	63.15	55.96	86.59
RP-16-6	7.55	73.70	1.99	55.80	64.36	57.90	86.57
RP-16-8	8.91	72.15	1.70	51.88	58.82	52.47	88.62
Zona de Pitek 20 cm	7.02	56.28	2.82	65.59	74.49	70.48	84.49
Zona de Pitek 60 cm	7.04	59.69	2.62	63.26	71.84	67.42	85.08
MS Glacial Drift	7.06	72.64	0.55	47.47	50.60	47.12	80.90
MS B1 SED Horshoe	6.85	66.84	0.65	51.69	55.26	51.94	80.00
MSA-1	7.32	67.47	0.46	49.35	51.86	49.29	78.97

MSA-2	6.85	67.61	0.57	51.38	54.25	51.54	80.82
MSA-3	6.72	64.78	0.53	50.67	53.19	50.74	79.97
MSA-5	6.51	64.42	0.58	53.64	56.66	54.08	80.19
MSB-5 Sed-1	6.56	65.05	0.57	53.08	55.79	53.42	78.65
MSB-5 Sed-2	6.81	66.51	0.54	51.61	54.39	51.80	79.61
MSB-5 Soil	7.10	67.62	0.55	48.88	50.91	48.78	81.51
MSc A1	6.76	63.73	0.83	55.28	59.32	56.11	80.93
AUS Drift PROX	7.41	76.56	1.66	53.65	62.92	55.18	82.22
AUS Drift Distal	7.75	75.91	1.83	53.27	63.10	54.76	83.07
AUS-SED-2	7.47	77.42	1.60	53.71	63.26	55.32	82.71
AUS-3	7.69	75.43	1.57	52.56	60.84	53.52	81.68
AUS-SED-4	7.57	73.95	1.70	53.83	62.55	55.31	81.60
AUS-5	7.63	77.24	1.57	52.56	61.07	53.55	82.46
AUS-SED-6	7.28	78.78	1.64	53.91	63.96	55.70	82.60
AUS-7	7.92	71.84	1.58	52.69	60.30	53.59	80.25
AUS-SED-8	7.61	75.37	1.69	53.64	62.68	55.12	82.45
AUS-SED-Lake	7.49	75.45	1.68	53.00	61.35	54.12	82.48
<i>AUS-PED-Merged</i>	7.44	71.46	1.96	58.50	68.87	62.16	81.65
LANG Drift Prox	3.93	66.75	2.28	68.25	76.11	73.00	76.17
LANG7	7.27	67.63	1.34	52.63	58.62	53.31	76.45
ELVA-1	7.20	75.58	1.43	53.34	61.20	54.50	80.53
ELVA-3	7.18	77.57	1.46	53.36	62.00	54.65	80.93
ELVA-13	7.41	73.32	1.48	53.37	60.98	54.49	79.71
VEITASTROND-LAKE- SED	6.96	79.97	1.59	54.44	64.95	56.56	82.06
EYF-2-IS	5.44	70.26	0.65	46.53	48.23	46.26	71.59
EYF-3-IS	5.78	72.47	0.68	46.22	48.29	45.86	72.96
PM-RG-SED-1	5.16	59.96	0.75	54.89	55.98	55.09	79.31
PM-RG-SED-2	3.26	48.12	1.58	71.51	72.83	72.32	74.16
PM-RG-SED-3	3.78	34.53	1.85	75.83	76.99	76.63	74.98
PM-RG-SED-4	4.45	47.94	1.10	64.06	65.49	64.70	77.61
PM-RG-SED-5	4.51	46.92	1.10	64.30	65.75	64.96	77.24
PM-RG-SED-6	2.49	30.37	3.00	83.63	85.62	85.27	69.28
PM-RG-SED-7	3.20	46.95	1.60	70.03	72.55	71.53	72.65
PM-RG-SED-8	2.56	33.49	2.88	81.99	84.07	83.66	70.09
PM-RG-SED-9	3.54	36.20	2.31	77.70	80.41	79.70	75.33
PM-RG-SED-10	3.04	52.90	1.84	70.90	74.08	72.86	73.11
PM-RG-SAP-1	5.02	60.53	0.79	56.91	57.85	57.14	79.89
PM-RG-SAP-2	4.31	55.82	0.90	62.20	63.71	62.81	77.87
PM-RG-SAP-3	2.05	26.31	5.90	88.35	90.67	90.42	66.32
PM-RG-SAP-4Red	2.27	14.62	11.60	94.62	96.94	96.86	68.28
PM-RG-SAP-5A	3.80	59.97	1.07	62.10	64.32	63.00	75.53
PM-RG-SAP-5B	3.71	60.63	1.69	64.22	68.14	66.07	76.72
PM-RG-SAP-6A-Red	2.30	12.01	41.21	96.19	99.27	99.24	68.31
PM-RG-SAP-6B-Yellow	2.64	26.69	6.40	87.91	91.25	90.90	71.30

PM-RG-SAP-6C-Brown	2.68	22.15	7.59	89.24	91.43	91.21	71.16
PM-RB-SED-1	3.03	47.54	1.80	71.26	73.92	72.91	72.70
PM-RB-SED-2	2.60	46.78	2.11	74.72	77.40	76.56	70.38
PM-RB-SED-3	4.35	59.63	1.13	60.89	64.41	62.22	76.86
PM-RB-SED-4	4.00	49.48	1.49	68.58	72.21	70.66	76.09
RG-14-SOIL-2	2.37	24.43	12.12	90.83	95.02	94.78	68.49
RG-14-SOIL-4	2.52	22.68	12.99	91.39	95.11	94.90	69.89
RG-14-SOIL-6	2.64	41.39	10.63	85.25	92.87	92.17	71.46
RB-14-SED-1	4.29	52.23	1.25	63.82	66.99	65.26	76.89
RB-14-SED-2	4.39	55.22	1.21	61.61	64.63	62.80	77.87
RB-14-SED-3	4.17	53.02	1.29	63.95	67.13	65.41	76.95
RB-14-SED-4	4.65	51.09	1.26	63.33	66.73	64.84	77.89
RB-14-SED-5	3.54	46.56	1.58	69.31	72.16	70.97	74.46
IGNF-13-SOIL-1	5.68	63.54	1.48	58.97	63.29	60.39	81.86
IGNF-13-SOIL-2	5.69	63.40	1.48	58.94	63.29	60.37	81.76
IGNF-13-SOIL-3	5.65	64.15	1.47	58.85	63.23	60.27	81.90
IGNF-13-SOIL-4	5.61	67.56	1.38	56.78	60.52	57.74	81.83
IGNF-13-SOIL-5	5.67	67.11	1.38	56.65	60.34	57.58	82.04
IGNF-13-SOIL-6	5.55	67.75	1.41	57.10	61.03	58.15	81.63
IGNF-13-SOIL-7	5.87	64.97	1.38	56.93	60.70	57.91	82.49
IGNF-13-SED-1	5.61	63.80	1.47	59.17	63.54	60.63	81.60
IGNF-13-SED-5	5.68	61.07	1.55	61.50	66.83	63.68	81.26
IGNF-13-SED-7	5.30	64.25	1.54	61.03	66.01	62.99	80.72
IGNF-13-SED-11	5.73	63.65	1.48	60.01	65.18	61.90	81.34
IGNF-13-SED-13	5.72	66.14	1.38	58.44	63.27	59.96	81.08
IGNF-13-SED-15	5.54	61.07	1.49	63.72	70.76	67.13	80.35
W10-CG-1-BR	5.16	84.05	1.05	50.27	56.49	50.35	77.81
W10-CG-2-BR	9.70	74.05	2.40	51.29	65.09	52.24	89.59
W10-CG-10-BR	6.77	77.77	1.30	49.77	57.38	49.69	84.22
W10-CG-14-BR	5.07	92.18	0.33	35.38	36.73	34.22	63.84
W10-CG-15-BR	9.64	46.88	1.10	51.08	52.51	51.15	89.35
W10-DG-1-BR	7.01	75.59	1.54	51.93	60.21	52.67	84.28
W10-GG-1-BR	5.83	78.34	0.66	45.74	49.45	44.99	79.76
W10-GG-2-BR	5.37	78.31	0.64	44.35	47.35	43.53	77.98
T10-MG-1-BR	7.95	81.84	1.83	48.27	61.17	47.01	85.66
T10-MS-1-BR	6.22	69.67	1.09	56.65	64.54	58.80	80.82
T10-MS-2-BR	8.20	74.54	1.35	48.20	54.10	47.70	87.97
T10-RD-1-BR	5.17	81.34	0.36	37.40	38.51	36.63	67.07
T10-RD-2-BR	4.81	105.79	0.54	41.13	44.58	39.51	67.53
T10-DK-1-BR	8.34	76.30	2.00	51.28	62.90	52.04	86.90
T10-DK-2-BR	8.26	76.80	1.99	51.03	62.69	51.64	86.80
T10-GOLD-1-BR	9.02	80.03	2.96	51.42	67.37	52.70	89.72
T10-GOLD-2-BR	5.99	84.79	1.01	48.32	55.09	47.78	80.09
T10-GOLD-4-BR	6.65	73.63	0.98	48.01	53.15	47.53	81.44
T10-GOLD-6-BR	16.71	34.61	1.12	54.14	61.85	55.52	88.17

T10-CC-1-BR	5.43	85.37	0.39	41.36	43.00	40.65	69.39
RB-14-BDRK-#2A	6.70	68.95	0.81	47.38	50.84	46.96	83.31
RG-14-BDRK-13	6.63	63.53	0.66	46.11	46.63	46.02	82.90
RG-14-BDRK-13amp	5.60	78.52	0.34	38.08	38.54	37.78	78.93
IGNF-13-BDRK-1B Float	9.23	55.60	1.15	51.63	55.16	51.87	87.03
IGNF-13-BDRK-1	8.91	53.16	1.04	51.59	54.01	51.74	86.01
IGNF-13-BDRK2	6.38	73.90	1.21	52.56	57.97	53.15	81.81
BDRK-Weathered-O	7.57	63.24	1.22	52.47	56.41	52.87	85.33
BDRK-Weathered-1	8.27	60.42	1.24	51.87	55.59	52.16	86.82
BDRK-Fresh	6.90	63.22	1.06	51.39	53.55	51.51	84.53
PERU-GR BDRK	8.22	79.39	1.77	50.97	59.71	51.38	88.02
Gorgon et al. 2013 granodioritic leucosome (NW10-12)	4.58	95.66	1.04	50.37	50.64	50.37	82.04
Gordon et al. 2013 eclogite- margin (NW10-36D)	7.69	65.74	1.16	52.40	56.29	52.79	86.78
Gordon et al. 2013 granodioritic leucosome (NW10-45E)	7.45	67.17	1.08	50.72	52.12	50.76	87.98
Gordon et al. 2013 granitic pegmatite (NW10-55)	6.16	80.06	0.94	51.33	54.89	51.53	83.11
Kelly et al. 2014 Fimmvörðuháls lava flow	5.40	76.33	0.39	42.22	43.17	41.86	69.74
USGS Mount Stuart granodiorite	6.97	76.01	0.82	48.96	52.96	48.78	83.34
USGS acidic dike W Mount Stuart	6.60	72.87	0.87	51.80	55.66	52.08	84.34

Table S1.9. BET surface area values ($\text{m}^2 \text{g}^{-1}$) of selected Clay Mineral Society standards adapted after Dogan et al. (2006, 2007).

Standard ID	Clay	Locality	Average BET (m ² g ⁻¹)
SCa-3 (white)	Montmorillonite	California, USA	43.2
SCa-3 (purple)	Montmorillonite	California, USA	65.25
NAu-1 (green)	Nontronite	Australia	52.8
NAu-2 (brown)	Nontronite	Australia	10.6
SYnH-1	Synthetic hectorite	United Catalysts Inc	244
IMt-1	Illite	Montana, USA	20.5
IMt-2	Illite	Montana, USA	17.5
ISMt-1	Illite-smectite (60/40 ordered)	Mancos shale, USA	0.4
ISCz-1	Illite-smectite (70/30 ordered)	Czechoslovakia	34.3
KGa-1b	Well-ordered kaolinite	Georgia, USA	13.1
KGa-2	Poorly-ordered kaolinite	Georgia, USA	21.7
SWy-2	Na-rich montmorillonite	Wyoming, USA	22.7
SYn-1	Synthetic mica-montmorillonite	NL Industries	118
PFl-1	Palygorskite	Florida, USA	173

SUPPLEMENTARY MATERIALS FOR CHAPTER 2

Supplementary Figures for Chapter 2

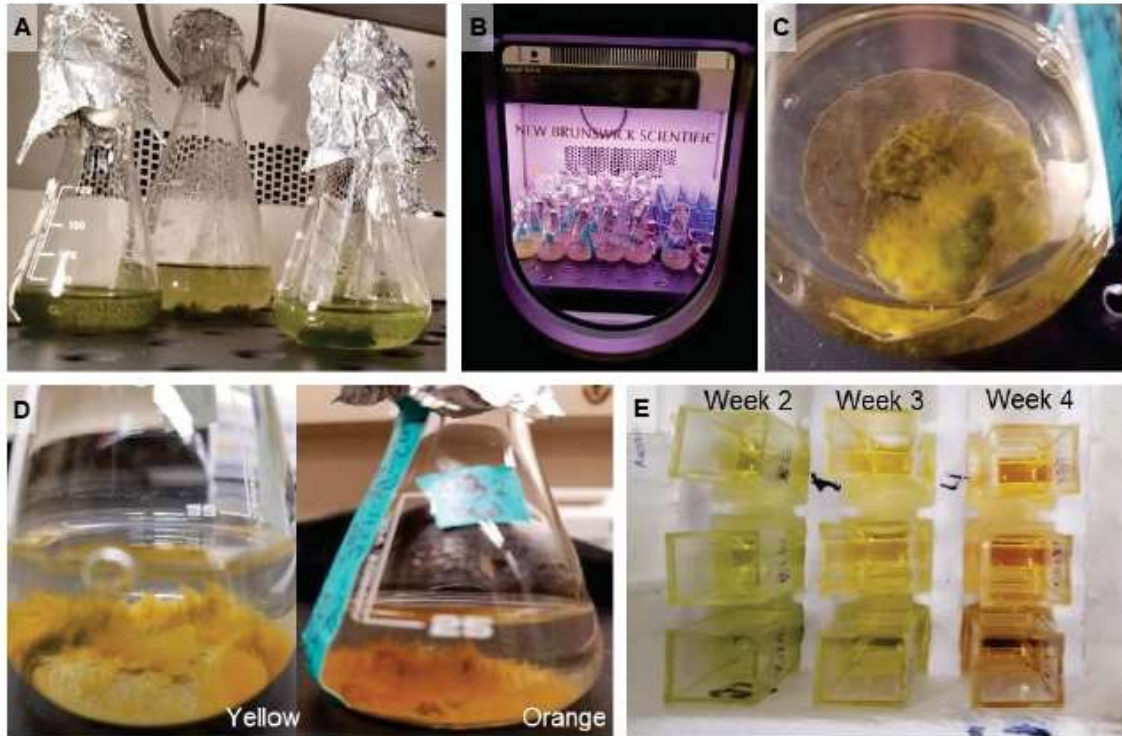


Figure S2.1. Illustration of the experimental setup and pigmentation of the microbial mat. A: Mossy green Chl-a pigment during culture growth. B: Experimental setup in the incubator. C: Green microbial mat forming on the sediments, instead of growing as planktonic cells. Notice that the solution is clear unlike Figure S2.1A. D: *L. glacialis* mat color changes to yellow and orange (carotenoids) with prolonged UV intake. E: Chl-a extracts showing the pigment change through time.

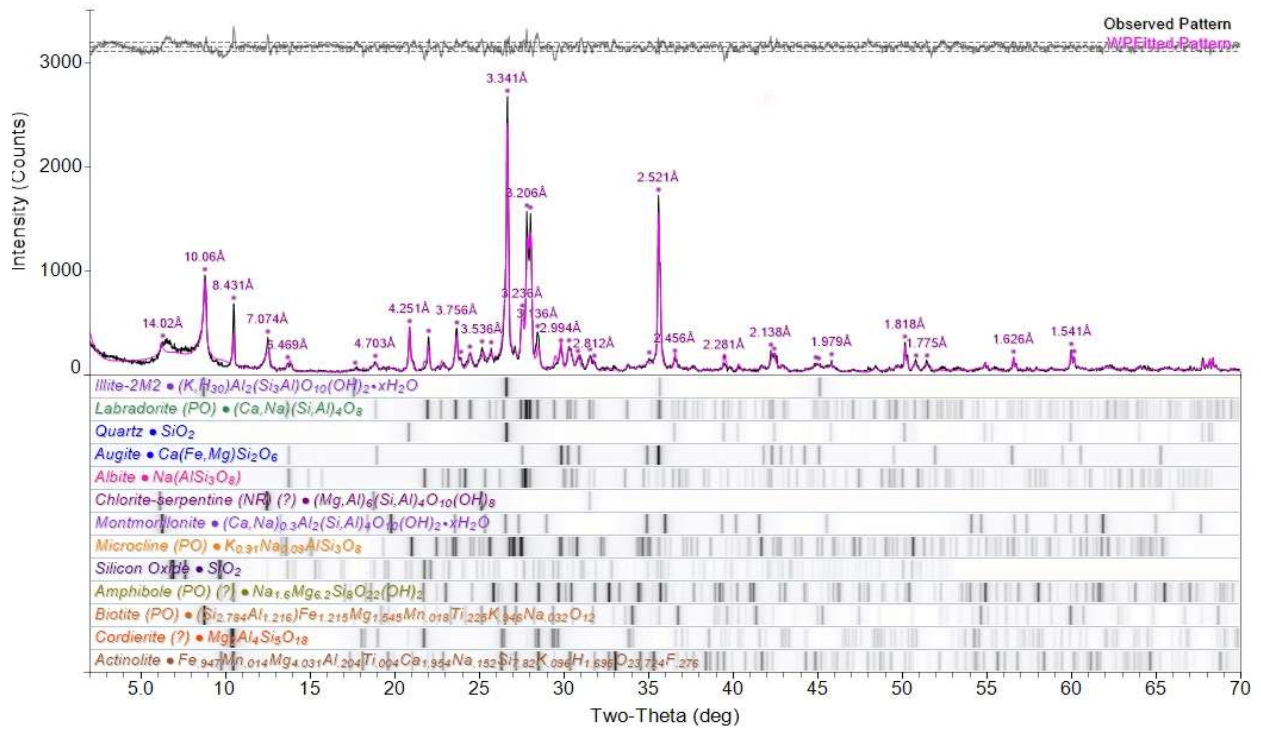


Figure S2.2. XRD pattern of the merged Onyx River (Antarctica) sediments. Quantitative results are listed in table 2.2.

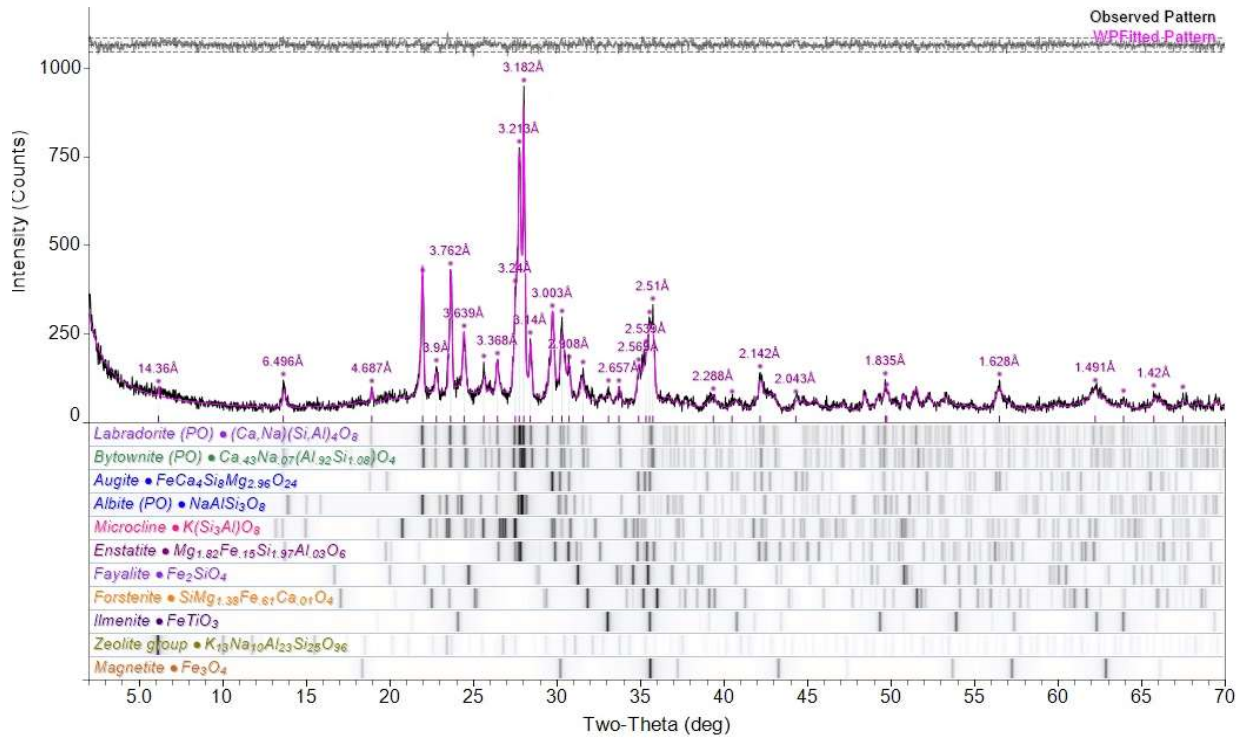


Figure S2.3. XRD pattern of the merged Iceland sediments. Quantitative results are listed in table

2.

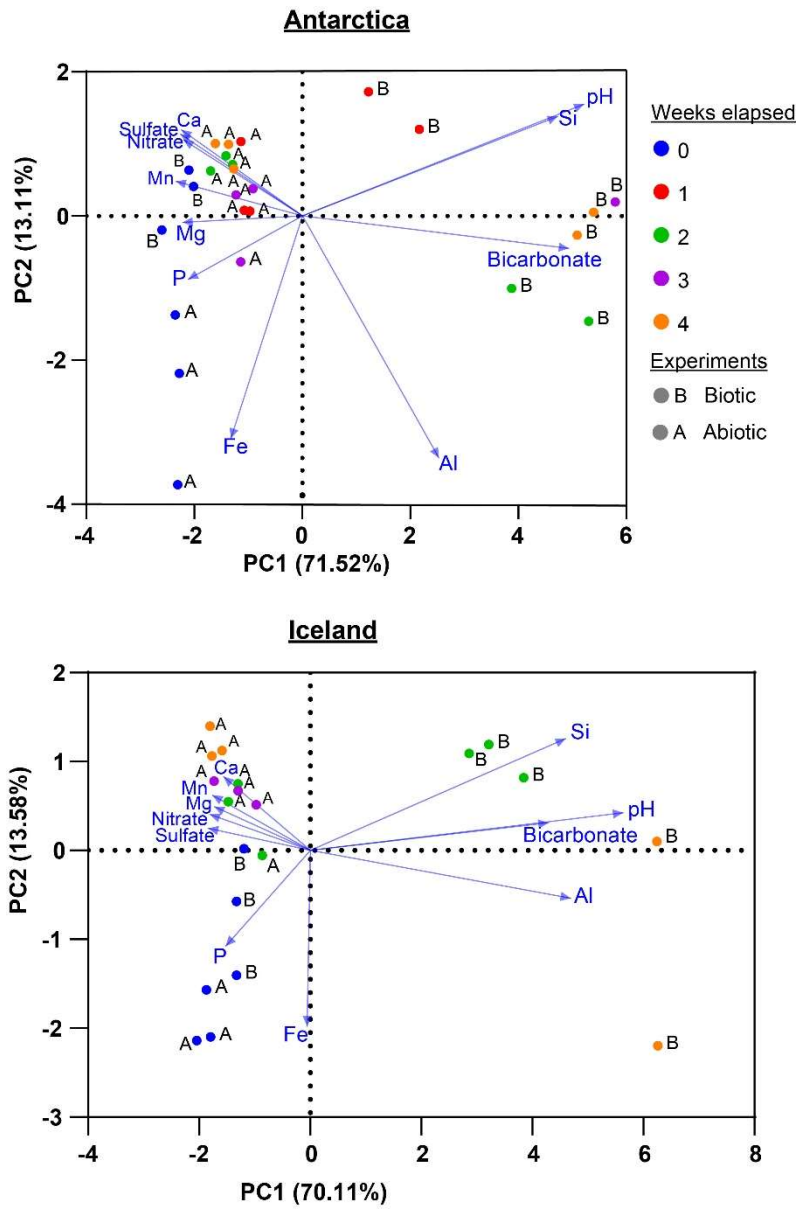


Figure S2.4. PCA biplots of the Antarctic and Icelandic experiments. Variables used are given as loadings. Color coding of the PC scores refer to the duration of the experiments (A: Abiotic, B: Biotic). Percentiles given in brackets in axis titles denote the proportion of variance of each PC.

Supplementary Tables for Chapter 2

Table S2.1. Leachate chemistry of 12°C Antarctic and Icelandic bioweathering and chemical weathering experiments. All units are in $\mu\text{mol/kg}$. BDL: Below detection limit.

ANTARCTICA			Units: $\mu\text{mol/kg}$								
Week	Replicate	Experiment	Al	Ca	Fe	K	Mg	Mn	Na	P	Si
0	a	Bioweathering	0.00	26.23	0.87	47.34	27.63	0.69	1880.05	13.38	19.22
0	b	Bioweathering	0.79	26.49	1.22	49.85	34.21	0.70	1983.93	13.67	18.93
0	c	Bioweathering	0.25	27.52	0.98	20.95	29.33	0.66	1955.81	13.06	22.17
1	a	Bioweathering	0.99	22.01	0.56	55.29	14.60	0.31	1975.63	2.91	59.83
1	b	Bioweathering	0.49	21.07	0.47	46.36	19.61	0.28	1933.88	BDL	47.77
1	c	Bioweathering	0.42	21.99	0.53	28.83	18.11	0.33	1885.51	1.95	48.30
2	a	Bioweathering	3.58	15.06	0.68	BDL	15.26	0.14	1994.77	2.07	57.46
2	b	Bioweathering	2.78	12.10	0.45	22.46	11.92	0.06	1995.95	BDL	60.70
2	c	Bioweathering	4.81	9.66	0.33	33.91	9.29	0.06	1891.94	2.47	76.34
3	a	Bioweathering	1.93	8.89	0.53	17.79	4.50	0.05	1816.82	2.84	110.68
3	b	Bioweathering	1.83	9.14	0.53	BDL	BDL	0.07	1906.14	2.61	143.78
3	c	Bioweathering	2.67	10.40	0.93	12.56	5.34	0.09	1851.62	3.60	109.60
4	a	Bioweathering	1.55	13.27	0.66	BDL	14.28	0.14	2022.82	3.08	103.66
4	b	Bioweathering	2.34	9.16	0.68	12.61	9.88	0.05	1899.48	3.17	99.97
4	c	Bioweathering	2.61	9.67	1.02	BDL	9.30	0.05	2253.60	2.53	109.37
0	a	Chemical weathering	1.66	28.08	1.90	55.37	31.86	0.55	1862.36	12.63	20.09
0	b	Chemical weathering	3.13	31.36	2.09	74.96	33.97	0.57	1925.35	10.70	24.90
0	c	Chemical weathering	3.70	26.56	3.05	32.08	29.89	0.60	1874.25	12.74	23.33
1	a	Chemical weathering	1.86	29.68	0.98	71.43	24.78	0.55	1923.68	10.03	40.36
1	b	Chemical weathering	0.60	30.59	0.84	28.17	23.54	0.59	1901.94	9.49	39.87
1	c	Chemical weathering	1.03	28.18	1.45	63.49	26.09	0.52	1950.16	9.46	42.87
2	a	Chemical weathering	0.98	31.96	0.88	50.74	34.83	0.60	1975.28	8.22	51.61
2	b	Chemical weathering	0.86	31.76	0.80	50.37	30.76	0.63	1956.28	8.95	46.50
2	c	Chemical weathering	1.13	31.19	0.77	52.47	33.04	0.60	1951.38	9.01	47.40
3	a	Chemical weathering	1.22	27.55	1.13	29.36	26.26	0.46	1972.97	8.77	69.76
3	b	Chemical weathering	1.05	29.72	1.33	44.70	25.79	0.50	2013.66	9.22	62.96
3	c	Chemical weathering	2.06	28.57	1.54	75.44	34.05	0.53	1949.22	7.95	56.57
4	a	Chemical weathering	0.98	35.69	0.73	38.45	36.41	0.57	2078.16	8.86	63.24
4	b	Chemical weathering	0.89	30.81	0.75	44.06	34.37	0.52	1991.08	8.28	63.01
4	c	Chemical weathering	1.06	29.42	1.13	23.75	25.61	0.51	1847.12	7.52	60.22
ICELAND			Units: $\mu\text{mol/kg}$								
Week	Replicate	Experiment	Al	Ca	Fe	K	Mg	Mn	Na	P	Si
0	a	Bioweathering	0.00	8.11	0.68	61.08	14.97	1.83	1934.23	10.68	15.24
0	b	Bioweathering	0.51	8.45	0.26	54.69	13.34	1.79	1832.02	10.30	17.14
0	c	Bioweathering	0.42	6.93	0.95	48.55	12.40	1.82	1904.19	12.04	16.43
2	a	Bioweathering	0.37	5.05	0.29	43.54	7.59	1.12	1912.81	0.00	165.82

2	b	Bioweathering	0.44	3.85	0.23	53.06	8.53	1.14	1905.56	0.00	128.26
2	c	Bioweathering	0.64	5.14	0.26	51.86	6.15	0.97	1885.60	0.00	145.22
3	a	Bioweathering	2.23	BDL	0.82	23.41	5.59	0.72	2007.97	0.45	177.21
3	b	Bioweathering	2.78	BDL	0.29	32.06	6.18	0.60	1838.12	2.14	173.41
3	c	Bioweathering	2.09	BDL	0.51	33.91	6.23	0.69	2027.88	3.50	240.76
4	a	Bioweathering	4.64	4.61	1.75	18.82	4.84	0.68	1930.34	2.90	225.07
4	b	Bioweathering	4.41	4.42	0.28	31.31	6.29	0.60	1911.28	3.59	210.60
4	c	Bioweathering	3.41	BDL	0.16	26.76	3.38	0.57	1793.16	2.40	216.92
6	a	Bioweathering	4.92	BDL	0.23	BDL	BDL	0.42	1748.97	3.04	195.13
6	b	Bioweathering	5.26	3.25	0.38	12.85	BDL	0.52	1829.21	5.41	271.80
6	c	Bioweathering	4.45	2.60	0.24	BDL	5.74	0.47	1657.35	4.73	198.59
0	a	Chemical weathering	0.17	8.44	1.10	54.71	13.68	1.90	1871.93	12.64	15.49
0	b	Chemical weathering	0.20	7.97	1.43	46.48	15.78	1.87	1777.97	12.96	0.00
0	c	Chemical weathering	0.00	9.17	1.44	46.30	13.88	1.93	1879.32	13.46	0.00
2	a	Chemical weathering	0.54	11.53	0.68	51.77	15.74	2.41	2184.46	7.76	93.27
2	b	Chemical weathering	0.00	9.52	0.88	47.92	14.18	2.05	1952.48	10.34	117.15
2	c	Chemical weathering	0.24	11.14	0.64	47.37	17.76	2.34	1924.96	7.83	82.60
3	a	Chemical weathering	0.20	10.09	0.65	40.47	12.96	2.21	1904.59	7.34	113.28
3	b	Chemical weathering	0.23	10.63	0.50	47.92	13.42	2.25	2010.76	7.61	96.97
3	c	Chemical weathering	0.00	10.90	0.48	43.23	17.10	2.24	1912.36	9.33	105.99
4	a	Chemical weathering	0.40	11.35	0.26	53.48	17.34	2.17	1949.66	9.11	114.80
4	b	Chemical weathering	0.00	10.71	0.32	65.89	17.08	2.21	1943.75	7.96	108.14
4	c	Chemical weathering	0.55	11.95	0.17	54.44	17.45	2.29	1829.87	7.83	100.35

Table S2.1. (Continued)

ANTARCTICA					
Week	Replicate	Experiment	Bicarbonate	Nitrate	Sulfate
0	a	Bioweathering	1100.89	1995.27	35.59
0	b	Bioweathering	780.80	1984.05	34.48
0	c	Bioweathering	1125.29	1993.04	33.22
1	a	Bioweathering	1230.99	1599.10	22.05
1	b	Bioweathering	1774.15	1734.88	31.33
1	c	Bioweathering	663.44	1774.60	30.22
2	a	Bioweathering	1766.01	1091.52	8.78
2	b	Bioweathering	1574.12	1259.65	14.55
2	c	Bioweathering	2008.32	925.48	4.06
3	a	Bioweathering	2312.42	728.30	5.90
3	b	Bioweathering	2377.47	636.29	5.30
3	c	Bioweathering	2388.85	422.40	BDL
4	a	Bioweathering	2554.73	74.12	4.27
4	b	Bioweathering	1844.07	763.41	5.48
4	c	Bioweathering	2211.60	BDL	5.87
0	a	Chemical weathering	800.05	1926.32	35.17

0	b	Chemical weathering	582.13	1930.20	32.81
0	c	Chemical weathering	923.64	1944.92	34.81
1	a	Chemical weathering	821.46	1971.28	35.87
1	b	Chemical weathering	705.72	1991.88	35.62
1	c	Chemical weathering	648.81	1962.26	33.19
2	a	Chemical weathering	1146.43	2060.84	40.61
2	b	Chemical weathering	1388.73	2021.71	35.32
2	c	Chemical weathering	647.18	2041.84	33.53
3	a	Chemical weathering	1076.50	2222.60	41.61
3	b	Chemical weathering	652.06	2083.70	37.41
3	c	Chemical weathering	1406.62	2060.01	40.91
4	a	Chemical weathering	948.03	2096.46	36.31
4	b	Chemical weathering	663.44	2096.95	35.89
4	c	Chemical weathering	980.55	2476.18	43.72

ICELAND

Week	Replicate	Experiment	Bicarbonate	Nitrate	Sulfate
0	a	Bioweathering	842.86	1768.80	32.55
0	b	Bioweathering	498.10	1815.56	32.75
0	c	Bioweathering	410.29	1873.50	34.57
2	a	Bioweathering	1036.38	1322.80	17.47
2	b	Bioweathering	1311.21	1457.61	23.03
2	c	Bioweathering	798.95	838.69	9.23
3	a	Bioweathering	2057.64	818.75	3.19
3	b	Bioweathering	1509.60	943.78	7.76
3	c	Bioweathering	1683.61	892.31	6.02
4	a	Bioweathering	1538.88	492.69	0.39
4	b	Bioweathering	1771.42	371.12	2.12
4	c	Bioweathering	2272.30	616.49	2.33
6	a	Bioweathering	1711.25	240.28	0.84
6	b	Bioweathering	1956.81	249.72	0.91
6	c	Bioweathering	1768.17	221.11	0.81
0	a	Chemical weathering	80.16	1795.54	33.71
0	b	Chemical weathering	512.74	1828.74	33.75
0	c	Chemical weathering	356.62	1799.17	33.56
2	a	Chemical weathering	1008.73	1879.73	34.19
2	b	Chemical weathering	984.34	1898.63	33.66
2	c	Chemical weathering	1503.10	1932.92	34.30
3	a	Chemical weathering	896.52	1882.84	34.03
3	b	Chemical weathering	415.16	1872.15	33.93
3	c	Chemical weathering	405.41	1907.69	34.27
4	a	Chemical weathering	317.59	1843.93	32.85
4	b	Chemical weathering	421.67	1875.18	33.34
4	c	Chemical weathering	374.51	1901.85	35.04

Table S2.2. Chlorophyll-a and pH measurements during 12°C biotic and abiotic weathering experiments and culture growth controls. NA: No analysis.

Week	Replicate	Experiment	ANTARCTICA		ICELAND	
			pH	Chlorophyll-a (µg/ml)	pH	Chlorophyll-a (µg/ml)
0	0a	Bioweathering	6.71	1.21	6.67	3.07
0	0b	Bioweathering	6.62	1.03	6.77	2.46
0	0c	Bioweathering	6.74	1.50	6.71	2.63
1	1a	Bioweathering	7.92	2.79		
1	1b	Bioweathering	7.97	2.55		NA
1	1c	Bioweathering	7.86	2.67		
2	2a	Bioweathering	7.73	2.79	7.55	8.94
2	2b	Bioweathering	7.71	3.75	7.40	5.30
2	2c	Bioweathering	7.79	3.70	7.54	4.81
3	3a	Bioweathering	7.99	5.79	7.75	9.92
3	3b	Bioweathering	8.00	3.07	7.64	3.84
3	3c	Bioweathering	8.04	6.15	7.68	2.95
4	4a	Bioweathering	7.88	3.88	7.71	13.52
4	4b	Bioweathering	7.85	4.46	7.70	5.50
4	4c	Bioweathering	7.98	1.71	7.78	4.78
0	0a	Chemical weathering	6.57		6.69	
0	0b	Chemical weathering	6.63		6.74	
0	0c	Chemical weathering	6.58		6.64	
1	1a	Chemical weathering	7.27			
1	1b	Chemical weathering	7.34		NA	
1	1c	Chemical weathering	7.33			
2	2a	Chemical weathering	7.12		6.70	
2	2b	Chemical weathering	6.86	NA	6.97	NA
2	2c	Chemical weathering	6.74		6.84	
3	3a	Chemical weathering	6.84		6.72	
3	3b	Chemical weathering	6.96		6.86	
3	3c	Chemical weathering	6.88		6.92	
4	4a	Chemical weathering	6.90		6.71	
4	4b	Chemical weathering	6.90		6.85	
4	4c	Chemical weathering	6.94		6.85	
0	0a	Culture growth	7.05	2.31	6.68	3.68
0	0b	Culture growth	7.14	3.26	7.12	3.51
0	0c	Culture growth	7.17	2.22	6.96	2.77
1	1a	Culture growth	7.90	0.94	7.08	3.32
1	1b	Culture growth	8.03	1.96	7.06	2.81
1	1c	Culture growth	8.11	1.45	7.37	1.83
2	2a	Culture growth	7.76	2.37	7.26	4.00

2	2b	Culture growth	7.75	1.99	7.38	NA
2	2c	Culture growth	7.80	1.22	7.36	NA
3	3a	Culture growth	7.89	2.81	7.30	2.60
3	3b	Culture growth	8.10	3.37	7.56	NA
3	3c	Culture growth	8.01	3.09	7.74	NA
4	4a	Culture growth	7.84	3.63	7.60	1.25
4	4b	Culture growth	7.85	2.60	7.54	NA
4	4c	Culture growth	7.97	3.66	7.43	NA
5	5a	Culture growth	7.85	2.15	7.63	2.48
5	5b	Culture growth	8.07	1.02	7.72	NA
5	5c	Culture growth	7.99	3.91	7.64	NA
6	6a	Culture growth	8.16	1.54	8.30	2.92
6	6b	Culture growth	8.11	NA	8.51	NA
6	6c	Culture growth	8.20	NA	8.46	NA

Table S2.3. Unpaired t-test results on Antarctic and Icelandic 12°C bioweathering experiments. Discoveries (in red) highlight the significant differences of means within each variable between comparable chemical and biological weathering timepoints. SE: Standard error. NA: No analyses.

Weeks elapsed	Variables	Antarctica t-test results									
		Discovery	P value	Bioweathering	Mean Chemical weathering	Difference	SE of difference	t ratio	df	q value	
WEEK 4	Al	Yes	0.0209	2.17	0.98	1.19	0.32	3.70	4	0.0088	
	Ca	Yes	0.0008	10.70	31.97	-21.27	2.30	9.25	4	0.0006	
	Fe	No	0.6585	0.79	0.87	-0.08	0.17	0.48	4	0.2375	
	K	Yes	0.0133	4.20	35.42	-31.22	7.37	4.24	4	0.0067	
	Mg	Yes	0.0046	11.15	32.13	-20.98	3.67	5.72	4	0.0026	
	Mn	Yes	0.0002	0.08	0.53	-0.45	0.04	12.85	4	0.0003	
	Na	No	0.5229	2059.00	1972.00	86.51	123.70	0.70	4	0.2031	
	P	Yes	0.0003	2.93	8.22	-5.29	0.44	12.13	4	0.0003	
	Si	Yes	0.0001	104.30	62.16	42.18	2.90	14.54	4	0.0003	
	Bicarbonate	Yes	0.0042	2203.00	864.00	1339.00	228.60	5.86	4	0.0026	
	Nitrate	Yes	0.0021	279.20	2223.00	-1944.00	274.00	7.10	4	0.0015	
	Sulfate	Yes	0.0002	5.21	38.64	-33.43	2.59	12.92	4	0.0003	
pH	Yes	0.0000	7.90	6.91	0.99	0.04	23.86	4	0.0001		
WEEK 3	Al	No	0.1625	2.14	1.44	0.70	0.41	1.71	4	0.0703	
	Ca	Yes	0.0000	9.48	28.61	-19.14	0.78	24.48	4	0.0001	
	Fe	No	0.0198	0.66	1.33	-0.67	0.18	3.76	4	0.0100	
	K	No	0.0524	10.12	49.83	-39.72	14.54	2.73	4	0.0244	
	Mg	Yes	0.0013	3.28	28.70	-25.42	3.15	8.07	4	0.0011	

	Mn	Yes	0.0001	0.07	0.50	-0.43	0.02	18.29	4	0.0001
	Na	No	0.0199	1858.00	1979.00	-120.40	32.09	3.75	4	0.0100
	P	Yes	0.0003	3.02	8.65	-5.63	0.48	11.80	4	0.0003
	Si	Yes	0.0079	121.40	63.10	58.26	11.85	4.92	4	0.0048
	Bicarbonate	Yes	0.0039	2360.00	1045.00	1315.00	219.70	5.98	4	0.0030
	Nitrate	Yes	0.0001	595.70	2122.00	-1526.00	103.80	14.70	4	0.0002
	Sulfate	Yes	0.0001	3.73	39.98	-36.24	2.28	15.89	4	0.0001
	pH	Yes	0.0000	8.01	6.89	1.12	0.04	29.05	4	0.0001
WEEK 2	Al	Yes	0.0101	3.72	0.99	2.73	0.60	4.59	4	0.0068
	Ca	Yes	0.0003	12.27	31.64	-19.36	1.58	12.27	4	0.0007
	Fe	No	0.0376	0.49	0.82	-0.33	0.11	3.06	4	0.0207
	K	No	0.0315	18.79	51.19	-32.40	9.98	3.25	4	0.0191
	Mg	Yes	0.0006	12.16	32.88	-20.72	2.09	9.91	4	0.0007
	Mn	Yes	0.0001	0.09	0.61	-0.52	0.03	18.38	4	0.0003
	Na	No	0.9980	1961.00	1961.00	-0.09	35.24	0.00	4	0.4320
	P	Yes	0.0009	1.51	8.73	-7.21	0.81	8.95	4	0.0009
	Si	No	0.0538	64.83	48.50	16.33	6.04	2.71	4	0.0251
	Bicarbonate	No	0.0456	1783.00	1061.00	722.00	251.90	2.87	4	0.0230
	Nitrate	Yes	0.0006	1092.00	2041.00	-949.20	97.13	9.77	4	0.0007
	Sulfate	Yes	0.0018	9.13	36.49	-27.36	3.70	7.39	4	0.0014
pH	Yes	0.0019	7.74	6.91	0.84	0.11	7.30	4	0.0014	
WEEK 1	Al	No	0.2668	0.63	1.16	-0.53	0.41	1.29	4	0.2021
	Ca	Yes	0.0005	21.69	29.48	-7.79	0.77	10.15	4	0.0013
	Fe	No	0.0377	0.52	1.09	-0.57	0.19	3.06	4	0.0429
	K	No	0.5192	43.49	54.36	-10.87	15.40	0.71	4	0.3631
	Mg	No	0.0113	17.44	24.80	-7.36	1.66	4.44	4	0.0147
	Mn	Yes	0.0006	0.31	0.55	-0.25	0.02	9.89	4	0.0013
	Na	No	0.8387	1932.00	1925.00	6.41	29.54	0.22	4	0.5446
	P	Yes	0.0008	1.62	9.66	-8.04	0.88	9.18	4	0.0014
	Si	No	0.0539	51.97	41.03	10.93	4.04	2.70	4	0.0544
	Bicarbonate	No	0.2002	1223.00	725.30	497.50	324.70	1.53	4	0.1654
	Nitrate	No	0.0072	1703.00	1975.00	-272.30	53.85	5.06	4	0.0109
	Sulfate	No	0.0825	27.87	34.89	-7.03	3.05	2.31	4	0.0750
pH	Yes	0.0001	7.92	7.31	0.60	0.04	15.64	4	0.0004	
WEEK 0	Al	No	0.0189	0.35	2.83	-2.48	0.65	3.82	4	0.0767
	Ca	No	0.2616	26.75	28.67	-1.92	1.47	1.31	4	0.3435
	Fe	No	0.0234	1.02	2.35	-1.32	0.37	3.57	4	0.0767
	K	No	0.3939	39.38	54.14	-14.76	15.46	0.95	4	0.4702
	Mg	No	0.5452	30.39	31.91	-1.52	2.30	0.66	4	0.5965
	Mn	No	0.0043	0.68	0.57	0.11	0.02	5.83	4	0.0282
	Na	No	0.2234	1940.00	1887.00	52.61	36.55	1.44	4	0.3259
	P	No	0.1209	13.37	12.02	1.35	0.69	1.97	4	0.2646
	Si	No	0.2031	20.11	22.77	-2.67	1.75	1.52	4	0.3259
	Bicarbonate	No	0.1925	1002.00	768.60	233.70	149.30	1.57	4	0.3259
	Nitrate	No	0.0010	1991.00	1934.00	56.97	6.62	8.60	4	0.0132
	Sulfate	No	0.8762	34.43	34.26	0.17	1.00	0.17	4	0.8849
pH	No	0.0757	6.69	6.59	0.10	0.04	2.38	4	0.1987	

Table S2.3. (Continued)

Weeks elapsed	Variables	Iceland t-test results								
		Discovery	P value	Mean Bioweathering	Mean Chemical weathering	Difference	SE of difference	t ratio	df	q value
WEEK 4	Al	Yes	0.0007	0.32	4.15	-3.84	0.41	9.32	4	0.0002
	Ca	Yes	0.0058	11.34	3.01	8.33	1.55	5.38	4	0.0011
	Fe	No	0.4024	0.25	0.73	-0.48	0.51	0.94	4	0.0677
	K	Yes	0.0039	57.94	25.63	32.31	5.41	5.98	4	0.0008
	Mg	Yes	0.0001	17.29	4.84	12.45	0.85	14.70	4	0.0000
	Mn	Yes	0.0000	2.22	0.62	1.61	0.05	33.34	4	0.0000
	Na	No	0.6376	1908.00	1878.00	29.50	57.97	0.51	4	0.0991
	P	Yes	0.0006	8.30	2.96	5.34	0.53	10.01	4	0.0002
	Si	Yes	0.0001	107.80	217.50	-109.80	5.91	18.56	4	0.0000
	Bicarbonate	Yes	0.0024	371.30	1861.00	-1490.00	218.50	6.82	4	0.0005
	Nitrate	Yes	0.0000	1874.00	493.40	1380.00	72.78	18.96	4	0.0000
	Sulfate	Yes	0.0000	33.74	1.61	32.13	0.90	35.52	4	0.0000
pH	Yes	0.0001	6.80	7.73	-0.93	0.05	17.48	4	0.0000	
WEEK 3	Al	Yes	0.0006	0.14	2.37	-2.22	0.22	9.99	4	0.0004
	Ca	Yes	0.0000	10.54	0.00	10.54	0.24	44.26	4	0.0000
	Fe	No	0.9846	0.54	0.54	0.00	0.16	0.02	4	0.3060
	K	Yes	0.0225	43.87	29.79	14.08	3.90	3.61	4	0.0083
	Mg	Yes	0.0031	14.49	6.00	8.49	1.33	6.41	4	0.0018
	Mn	Yes	0.0000	2.23	0.67	1.56	0.04	41.13	4	0.0000
	Na	No	0.8347	1943.00	1958.00	-15.42	69.23	0.22	4	0.2810
	P	Yes	0.0049	8.09	2.03	6.06	1.08	5.61	4	0.0025
	Si	Yes	0.0148	105.40	197.10	-91.71	22.35	4.10	4	0.0060
	Bicarbonate	Yes	0.0068	572.40	1750.00	-1178.00	228.90	5.15	4	0.0030
	Nitrate	Yes	0.0000	1888.00	884.90	1003.00	37.78	26.54	4	0.0000
	Sulfate	Yes	0.0000	34.08	5.66	28.42	1.34	21.28	4	0.0000
pH	Yes	0.0002	6.83	7.69	-0.86	0.07	12.71	4	0.0002	
WEEK 2	Al	No	0.2731	0.26	0.48	-0.22	0.18	1.27	4	0.1755
	Ca	Yes	0.0012	10.73	4.68	6.05	0.74	8.15	4	0.0029
	Fe	Yes	0.0034	0.73	0.26	0.47	0.08	6.21	4	0.0040
	K	No	0.8943	49.02	49.49	-0.47	3.30	0.14	4	0.4864
	Mg	Yes	0.0024	15.89	7.42	8.47	1.25	6.80	4	0.0035
	Mn	Yes	0.0006	2.27	1.08	1.19	0.12	9.71	4	0.0022
	Na	No	0.2226	2021.00	1901.00	119.30	82.70	1.44	4	0.1574
	P	Yes	0.0005	8.64	0.00	8.64	0.85	10.19	4	0.0022
	Si	No	0.0308	97.67	146.40	-48.76	14.91	3.27	4	0.0242
	Bicarbonate	No	0.6313	1165.00	1049.00	116.50	224.70	0.52	4	0.3719
	Nitrate	No	0.0209	1904.00	1206.00	697.40	188.60	3.70	4	0.0184
	Sulfate	No	0.0121	34.05	16.58	17.47	4.01	4.35	4	0.0122
pH	Yes	0.0020	6.84	7.50	-0.66	0.09	7.19	4	0.0035	
WEEK 1	Al									
	Ca									
	Fe									

	K	Mg	Mn	Na	P	Si	Bicarbonate	Nitrate	Sulfate	pH
					NA					
WEEK 0	Al	No	0.3315	0.12	0.31	-0.19	0.17	1.10	4	0.5109
	Ca	No	0.2945	8.53	7.83	0.70	0.58	1.21	4	0.5109
	Fe	No	0.0392	1.32	0.63	0.69	0.23	3.02	4	0.1717
	K	No	0.2859	49.16	54.77	-5.61	4.56	1.23	4	0.5109
	Mg	No	0.4326	14.45	13.57	0.88	1.01	0.87	4	0.5680
	Mn	No	0.0147	1.90	1.81	0.09	0.02	4.11	4	0.1674
	Na	No	0.3502	1843.00	1890.00	-47.07	44.54	1.06	4	0.5109
	P	No	0.0255	13.02	11.01	2.01	0.58	3.47	4	0.1674
	Si	No	0.0992	5.16	16.27	-11.11	5.19	2.14	4	0.3257
	Bicarbonate	No	0.2176	316.50	583.80	-267.20	182.80	1.46	4	0.5109
	Nitrate	No	0.7386	1808.00	1819.00	-11.47	32.06	0.36	4	0.7459
	Sulfate	No	0.5844	33.67	33.29	0.38	0.65	0.59	4	0.6394
	pH	No	0.5505	6.69	6.72	-0.03	0.04	0.65	4	0.6394

Table S2.4. Two-way ANOVA and Tukey's pairwise comparison outputs for 12°C Antarctica and Iceland solute chemistry variables. Below $p < 0.05$ threshold results in red highlights the significant differences of means within each variable between comparable chemical and biological weathering timepoints. NA: No analyses. ns: Not significant. Significance intervals: $p < 0.0001$ ‘****’ $p < 0.001$ ‘***’ $p < 0.01$ ‘**’ $p < 0.05$ ‘*’.

VARIABLES	Pairwise comparisons	ANOVA Antarctica Results					
		Mean Difference	95% confidence interval of difference	Below threshold ($p < 0.05$)?	Summary	Adjusted P Value	Weeks elapsed
Al	Biotic Week 0 vs. Abiotic Week 0	-2.483	-7.645 to 2.679	No	ns	0.1948	0
	Biotic Week 1 vs. Abiotic Week 1	-0.53	-2.737 to 1.677	No	ns	0.5522	1
	Biotic Week 2 vs. Abiotic Week 2	2.733	-2.337 to 7.804	No	ns	0.1593	2
	Biotic Week 3 vs. Abiotic Week 3	0.7	0.212 to 1.188	Yes	*	0.0243	3
	Biotic Week 4 vs. Abiotic Week 4	1.19	-1.891 to 4.271	No	ns	0.2817	4
Ca	Biotic Week 0 vs. Abiotic Week 0	-1.92	-18.58 to 14.74	No	ns	0.933	0
	Biotic Week 1 vs. Abiotic Week 1	-7.793	-17.32 to 1.738	No	ns	0.0736	1
	Biotic Week 2 vs. Abiotic Week 2	-19.36	-32.67 to -6.057	Yes	*	0.0236	2

	Biotic Week 3 vs. Abiotic Week 3	-19.14	-26.41 to -11.86	Yes	**	0.0091	3
	Biotic Week 4 vs. Abiotic Week 4	-21.27	-29.12 to -13.42	Yes	**	0.0086	4
Fe	Biotic Week 0 vs. Abiotic Week 0	-1.323	-5.046 to 2.399	No	ns	0.3213	0
	Biotic Week 1 vs. Abiotic Week 1	-0.57	-2.308 to 1.168	No	ns	0.3633	1
	Biotic Week 2 vs. Abiotic Week 2	-0.33	-1.023 to 0.363	No	ns	0.1981	2
	Biotic Week 3 vs. Abiotic Week 3	-0.67	-1.314 to -0.0262	Yes	*	0.0463	3
	Biotic Week 4 vs. Abiotic Week 4	-0.08333	-0.215 to 0.049	No	ns	0.1194	4
K	Biotic Week 0 vs. Abiotic Week 0	-14.76	-66.74 to 37.23	No	ns	0.4466	0
	Biotic Week 1 vs. Abiotic Week 1	-10.87	-164.1 to 142.3	No	ns	0.994	1
	Biotic Week 2 vs. Abiotic Week 2	-32.4	-127.0 to 62.17	No	ns	0.3402	2
	Biotic Week 3 vs. Abiotic Week 3	-39.72	-188.3 to 108.9	No	ns	0.4839	3
	Biotic Week 4 vs. Abiotic Week 4	-31.22	-73.22 to 10.79	No	ns	0.0882	4
Mg	Biotic Week 0 vs. Abiotic Week 0	-1.517	-15.13 to 12.10	No	ns	0.9416	0
	Biotic Week 1 vs. Abiotic Week 1	-7.363	-25.48 to 10.75	No	ns	0.2591	1
	Biotic Week 2 vs. Abiotic Week 2	-20.72	-35.86 to -5.585	Yes	*	0.0268	2
	Biotic Week 3 vs. Abiotic Week 3	-25.42	-45.36 to -5.483	Yes	*	0.031	3
	Biotic Week 4 vs. Abiotic Week 4	-20.98	-45.03 to 3.076	No	ns	0.065	4
Mn	Biotic Week 0 vs. Abiotic Week 0	0.11	-0.139 to 0.359	No	ns	0.2255	0
	Biotic Week 1 vs. Abiotic Week 1	-0.2467	-0.591 to 0.098	No	ns	0.0945	1
	Biotic Week 2 vs. Abiotic Week 2	-0.5233	-0.848 to -0.199	Yes	*	0.0191	2
	Biotic Week 3 vs. Abiotic Week 3	-0.4267	-0.514 to -0.339	Yes	***	0.0002	3
	Biotic Week 4 vs. Abiotic Week 4	-0.4533	-0.572 to -0.334	Yes	**	0.0021	4
Na	Biotic Week 0 vs. Abiotic Week 0	52.61	-132.2 to 237.4	No	ns	0.4449	0
	Biotic Week 1 vs. Abiotic Week 1	6.413	-349.8 to 362.6	No	ns	>0.9999	1
	Biotic Week 2 vs. Abiotic Week 2	-0.09333	-299.3 to 299.1	No	ns	>0.9999	2
	Biotic Week 3 vs. Abiotic Week 3	-120.4	-299.4 to 58.59	No	ns	0.1063	3
	Biotic Week 4 vs. Abiotic Week 4	86.51	-1500 to 1673	No	ns	0.9989	4
P	Biotic Week 0 vs. Abiotic Week 0	1.347	-6.778 to 9.472	No	ns	0.7835	0
	Biotic Week 1 vs. Abiotic Week 1	-8.04	-15.30 to -0.78	Yes	*	0.041	1
	Biotic Week 2 vs. Abiotic Week 2	-7.213	-15.88 to 1.451	No	ns	0.0711	2
	Biotic Week 3 vs. Abiotic Week 3	-5.63	-12.25 to 0.994	No	ns	0.0683	3
	Biotic Week 4 vs. Abiotic Week 4	-5.293	-7.725 to -2.861	Yes	*	0.012	4
Si	Biotic Week 0 vs. Abiotic Week 0	-2.667	-19.03 to 13.70	No	ns	0.7928	0
	Biotic Week 1 vs. Abiotic Week 1	10.93	-31.89 to 53.75	No	ns	0.5127	1
	Biotic Week 2 vs. Abiotic Week 2	16.33	-50.46 to 83.12	No	ns	0.5406	2
	Biotic Week 3 vs. Abiotic Week 3	58.26	-58.61 to 175.1	No	ns	0.183	3
	Biotic Week 4 vs. Abiotic Week 4	42.18	6.288 to 78.07	Yes	*	0.0365	4
Bicarbonate	Biotic Week 0 vs. Abiotic Week 0	233.7	-98.47 to 565.9	No	ns	0.0977	0
	Biotic Week 1 vs. Abiotic Week 1	497.5	-2544 to 3539	No	ns	0.7907	1
	Biotic Week 2 vs. Abiotic Week 2	722	-2675 to 4119	No	ns	0.6317	2
	Biotic Week 3 vs. Abiotic Week 3	1315	-843.7 to 3473	No	ns	0.1277	3
	Biotic Week 4 vs. Abiotic Week 4	1339	9.449 to 2669	Yes	*	0.0493	4
Nitrate	Biotic Week 0 vs. Abiotic Week 0	56.97	-4.501 to 118.4	No	ns	0.0579	0

	Biotic Week 1 vs. Abiotic Week 1	-272.3	-804.8 to 260.2	No	ns	0.175	1
	Biotic Week 2 vs. Abiotic Week 2	-949.2	-1966 to 67.67	No	ns	0.0571	2
	Biotic Week 3 vs. Abiotic Week 3	-1526	-2093 to -960.3	Yes	**	0.0087	3
	Biotic Week 4 vs. Abiotic Week 4	-1944	-5231 to 1343	No	ns	0.1347	4
Sulfate	Biotic Week 0 vs. Abiotic Week 0	0.1667	-9.229 to 9.563	No	ns	>0.9999	0
	Biotic Week 1 vs. Abiotic Week 1	-7.027	-40.85 to 26.79	No	ns	0.6466	1
	Biotic Week 2 vs. Abiotic Week 2	-27.36	-60.63 to 5.921	No	ns	0.0728	2
	Biotic Week 3 vs. Abiotic Week 3	-36.24	-61.52 to -10.97	Yes	*	0.0243	3
	Biotic Week 4 vs. Abiotic Week 4	-33.43	-55.78 to -11.09	Yes	*	0.0223	4
pH	Biotic Week 0 vs. Abiotic Week 0	0.09667	-0.434 to 0.628	No	ns	0.7292	0
	Biotic Week 1 vs. Abiotic Week 1	0.6033	0.236 to 0.971	Yes	*	0.0184	1
	Biotic Week 2 vs. Abiotic Week 2	0.8367	-0.422 to 2.095	No	ns	0.1086	2
	Biotic Week 3 vs. Abiotic Week 3	1.117	0.736 to 1.497	Yes	**	0.007	3
	Biotic Week 4 vs. Abiotic Week 4	0.99	0.728 to 1.252	Yes	**	0.0022	4

Table S2.4. (Continued)

VARIABLES	Pairwise comparisons	ANOVA Iceland Results					
		Mean Difference	95% confidence interval of difference	Below threshold (p<0.05)?	Summary	Adjusted P Value	Weeks elapsed
Al	Biotic Week 0 vs. Abiotic Week 0	0.1867	-1.482 to 1.855	No	ns	0.9295	0
	Biotic Week 1 vs. Abiotic Week 1			NA			
	Biotic Week 2 vs. Abiotic Week 2	0.2233	-1.592 to 2.038	No	ns	0.9017	2
	Biotic Week 3 vs. Abiotic Week 3	2.223	0.7102 to 3.736	Yes	*	0.0233	3
	Biotic Week 4 vs. Abiotic Week 4	3.837	-0.685 to 8.358	No	ns	0.0685	4
Ca	Biotic Week 0 vs. Abiotic Week 0	-0.6967	-8.125 to 6.731	No	ns	0.9648	0
	Biotic Week 1 vs. Abiotic Week 1						
	Biotic Week 2 vs. Abiotic Week 2	-6.05	-8.216 to -3.884	Yes	**	0.0077	2
	Biotic Week 3 vs. Abiotic Week 3	-10.54	-12.73 to -8.35	Yes	***	0.0004	3
	Biotic Week 4 vs. Abiotic Week 4	-8.327	-25.06 to 8.406	No	ns	0.1829	4
Fe	Biotic Week 0 vs. Abiotic Week 0	-0.6933	-2.897 to 1.510	No	ns	0.3827	0
	Biotic Week 1 vs. Abiotic Week 1			NA			
	Biotic Week 2 vs. Abiotic Week 2	-0.4733	-1.288 to 0.341	No	ns	0.1387	2
	Biotic Week 3 vs. Abiotic Week 3	-0.003333	-1.025 to 1.019	No	ns	>0.9999	3
	Biotic Week 4 vs. Abiotic Week 4	0.48	-4.173 to 5.133	No	ns	0.9481	4
K	Biotic Week 0 vs. Abiotic Week 0	5.61	-10.62 to 21.84	No	ns	0.3331	0
	Biotic Week 1 vs. Abiotic Week 1			NA			
	Biotic Week 2 vs. Abiotic Week 2	0.4667	-39.63 to 40.56	No	ns	>0.9999	2
	Biotic Week 3 vs. Abiotic Week 3	-14.08	-36.24 to 8.076	No	ns	0.1179	3
	Biotic Week 4 vs. Abiotic Week 4	-32.31	-53.62 to -10.99	Yes	*	0.0219	4
Mg	Biotic Week 0 vs. Abiotic Week 0	-0.8767	-11.18 to 9.425	No	ns	0.977	0

	Biotic Week 1 vs. Abiotic Week 1			NA			
	Biotic Week 2 vs. Abiotic Week 2	-8.47	-24.39 to 7.448	No	ns	0.1626	2
	Biotic Week 3 vs. Abiotic Week 3	-8.493	-19.45 to 2.459	No	ns	0.0813	3
	Biotic Week 4 vs. Abiotic Week 4	-12.45	-21.18 to -3.728	Yes	*	0.0248	4
Mn	Biotic Week 0 vs. Abiotic Week 0	-0.08667	-0.197 to 0.024	No	ns	0.0799	0
	Biotic Week 1 vs. Abiotic Week 1			NA			
	Biotic Week 2 vs. Abiotic Week 2	-1.19	-2.497 to 0.1172	No	ns	0.0599	2
	Biotic Week 3 vs. Abiotic Week 3	-1.563	-1.993 to -1.133	Yes	**	0.003	3
	Biotic Week 4 vs. Abiotic Week 4	-1.607	-2.219 to -0.993	Yes	**	0.0088	4
Na	Biotic Week 0 vs. Abiotic Week 0	47.07	-57.53 to 151.7	No	ns	0.2175	0
	Biotic Week 1 vs. Abiotic Week 1			NA			
	Biotic Week 2 vs. Abiotic Week 2	-119.3	-821.3 to 582.7	No	ns	0.7573	2
	Biotic Week 3 vs. Abiotic Week 3	15.42	-851.4 to 882.3	No	ns	>0.9999	3
	Biotic Week 4 vs. Abiotic Week 4	-29.5	-77.73 to 18.73	No	ns	0.1265	4
P	Biotic Week 0 vs. Abiotic Week 0	-2.013	-5.320 to 1.293	No	ns	0.1275	0
	Biotic Week 1 vs. Abiotic Week 1			NA			
	Biotic Week 2 vs. Abiotic Week 2	-8.643	-16.46 to -0.826	Yes	*	0.0411	2
	Biotic Week 3 vs. Abiotic Week 3	-6.063	-9.990 to -2.137	Yes	*	0.0211	3
	Biotic Week 4 vs. Abiotic Week 4	-5.337	-10.25 to -0.425	Yes	*	0.0426	4
Si	Biotic Week 0 vs. Abiotic Week 0	11.11	-41.24 to 63.45	No	ns	0.6237	0
	Biotic Week 1 vs. Abiotic Week 1			NA			
	Biotic Week 2 vs. Abiotic Week 2	48.76	-126.7 to 224.2	No	ns	0.4544	2
	Biotic Week 3 vs. Abiotic Week 3	91.71	-109.4 to 292.8	No	ns	0.2126	3
	Biotic Week 4 vs. Abiotic Week 4	109.8	72.17 to 147.4	Yes	**	0.0069	4
Bicarbonate	Biotic Week 0 vs. Abiotic Week 0	267.2	-2022 to 2557	No	ns	0.9179	0
	Biotic Week 1 vs. Abiotic Week 1			NA			
	Biotic Week 2 vs. Abiotic Week 2	-116.5	-2938 to 2705	No	ns	0.9996	2
	Biotic Week 3 vs. Abiotic Week 3	1178	683.1 to 1673	Yes	*	0.0104	3
	Biotic Week 4 vs. Abiotic Week 4	1490	-421.3 to 3401	No	ns	0.0805	4
Nitrate	Biotic Week 0 vs. Abiotic Week 0	11.47	-280.3 to 303.3	No	ns	0.9997	0
	Biotic Week 1 vs. Abiotic Week 1			NA			
	Biotic Week 2 vs. Abiotic Week 2	-697.4	-2551 to 1156	No	ns	0.2919	2
	Biotic Week 3 vs. Abiotic Week 3	-1003	-1368 to -636.9	Yes	**	0.008	3
	Biotic Week 4 vs. Abiotic Week 4	-1380	-1977 to -783.5	Yes	*	0.0108	4
Sulfate	Biotic Week 0 vs. Abiotic Week 0	-0.3833	-6.815 to 6.049	No	ns	0.9962	0
	Biotic Week 1 vs. Abiotic Week 1			NA			
	Biotic Week 2 vs. Abiotic Week 2	-17.47	-56.03 to 21.08	No	ns	0.215	2
	Biotic Week 3 vs. Abiotic Week 3	-28.42	-40.86 to -15.98	Yes	*	0.011	3
	Biotic Week 4 vs. Abiotic Week 4	-32.13	-36.37 to -27.89	Yes	****	<0.0001	4
pH	Biotic Week 0 vs. Abiotic Week 0	0.02667	-0.2132 to 0.267	No	ns	0.931	0
	Biotic Week 1 vs. Abiotic Week 1			NA			
	Biotic Week 2 vs. Abiotic Week 2	0.66	-0.4720 to 1.792	No	ns	0.138	2
	Biotic Week 3 vs. Abiotic Week 3	0.8567	0.05649 to 1.657	Yes	*	0.0438	3

Biotic Week 4 vs. Abiotic Week 4	0.9267	0.5275 to 1.326	Yes	*	0.0108	4
----------------------------------	--------	-----------------	-----	---	--------	---

Table S2.5. Two-way ANOVA and Šídák's pairwise comparison outputs for 12°C Antarctica and Iceland pH and Chlorophyll-a measurements. Below $p < 0.05$ threshold results in red highlights the significant differences of means within each variable between comparable biological weathering and culture growth control timepoints. ns: Not significant. Significance intervals: $p < 0.0001$

‘****’ $p < 0.001$ ‘***’ $p < 0.01$ ‘**’ $p < 0.05$ ‘*’.

VARIABLES	Pairwise comparisons	ANOVA Antarctica Results					
		Mean Difference	95% confidence interval of difference	Below threshold ($p < 0.05$)?	Summary	Adjusted P Value	Weeks elapsed
pH	Bioweathering Week 0 vs. Culture Week 0	-0.43	-2.254 to 1.394	No	ns	>0.9999	0
	Bioweathering Week 1 vs. Culture Week 1	-0.09667	-1.921 to 1.728	No	ns	>0.9999	1
	Bioweathering Week 2 vs. Culture Week 2	-0.02667	-1.851 to 1.798	No	ns	>0.9999	2
	Bioweathering Week 3 vs. Culture Week 3	0.01	-1.814 to 1.834	No	ns	>0.9999	3
	Bioweathering Week 4 vs. Culture Week 4	0.01667	-1.808 to 1.841	No	ns	>0.9999	4
Chlorophyll-a	Bioweathering Week 0 vs. Culture Week 0	-1.35	-3.174 to 0.474	No	ns	0.5054	0
	Bioweathering Week 1 vs. Culture Week 1	1.22	-0.604 to 3.044	No	ns	0.7387	1
	Bioweathering Week 2 vs. Culture Week 2	1.553	-0.271 to 3.378	No	ns	0.2135	2
	Bioweathering Week 3 vs. Culture Week 3	1.913	0.089 to 3.738	Yes	*	0.0297	3
	Bioweathering Week 4 vs. Culture Week 4	0.05333	-1.771 to 1.878	No	ns	>0.9999	4

Table S2.5. (Continued)

VARIABLES	Pairwise comparisons	ANOVA Iceland Results					
		Mean Difference	95% confidence interval of difference	Below threshold ($p < 0.05$)?	Summary	Adjusted P Value	Weeks elapsed

pH	Bioweathering Week 0 vs. Culture Week 0	-0.2033	-4.578 to 4.171	No	ns	>0.9999	0
	Bioweathering Week 1 vs. Culture Week 1						
	Bioweathering Week 2 vs. Culture Week 2	0.1633	-4.211 to 4.538	No	ns	>0.9999	2
	Bioweathering Week 3 vs. Culture Week 3	0.1567	-4.218 to 4.531	No	ns	>0.9999	3
	Bioweathering Week 4 vs. Culture Week 4	0.2067	-4.168 to 4.581	No	ns	>0.9999	4
Chlorophyll-a	Bioweathering Week 0 vs. Culture Week 0	-0.6	-4.975 to 3.775	No	ns	>0.9999	0
	Bioweathering Week 1 vs. Culture Week 1						
	Bioweathering Week 2 vs. Culture Week 2	2.35	-3.836 to 8.536	No	ns	0.9709	2
	Bioweathering Week 3 vs. Culture Week 3	2.97	-3.216 to 9.156	No	ns	0.8705	3
	Bioweathering Week 4 vs. Culture Week 4	6.683	0.4968 to 12.87	Yes	*	0.0247	4

Table S2.6. EDS results matching the numbered locations on SEM images. Semi-quantitative concentrations are given in wt%.

Spectrum	C	N	O	P	Si	Al	Fe	Ca	Mg	K	Ti	Na
1	5.8	0.0	49.4	0.0	3.8	1.5	2.2	35.2	0.9	0.7	0.4	0.0
2	9.4	0.0	47.8	0.0	14.5	5.5	14.0	2.4	2.9	2.1	1.1	0.3
3	0.0	0.0	19.9	0.0	19.2	5.8	37.0	8.5	1.4	1.8	6.1	0.2
4	9.4	0.0	46.7	0.0	15.3	5.8	10.2	5.1	2.2	1.1	2.7	1.6
5	66.5	0.0	23.7	0.0	4.1	2.4	0.2	0.7	0.4	1.5	0.5	0.0
6	15.2	0.0	39.5	0.0	22.3	7.2	8.8	0.8	1.4	2.1	1.1	1.7
7	12.1	0.0	46.3	0.0	17.5	13.1	2.9	0.5	0.6	6.8	0.0	0.2
8	11.1	0.0	27.0	0.0	28.8	12.5	15.5	2.2	0.7	2.3	0.0	0.0

9	14.7	0.0	28.6	0.0	24.7	9.9	16.6	3.0	0.5	1.4	2.2	0.3
10	10.3	0.0	27.2	0.0	27.6	11.6	17.0	3.6	1.0	0.7	0.9	0.0
11	32.6	3.7	35.1	0.0	13.8	3.9	4.6	2.1	0.8	0.0	0.7	2.8
12	11.4	0.0	37.4	0.8	16.6	6.4	22.5	3.3	0.0	0.0	1.5	0.0
13	12.6	0.0	36.1	0.5	14.9	6.1	20.8	3.1	0.4	0.7	1.2	3.6
14	15.5	0.0	43.6	0.0	18.1	7.7	6.2	3.7	0.6	0.8	0.5	3.5
15	17.7	3.3	39.1	0.0	11.9	4.2	17.6	1.9	0.5	0.6	0.0	3.2
16	16.8	1.7	40.0	0.0	11.8	4.1	19.5	1.6	0.5	0.5	0.0	3.5
17	12.5	4.3	40.5	0.0	11.7	4.0	21.3	1.6	0.5	0.0	0.0	3.6
18	12.5	0.0	41.3	0.0	20.0	7.7	9.3	3.0	0.8	0.9	1.2	3.4
19	4.4	0.0	38.2	0.0	1.3	1.6	41.0	0.0	2.4	0.0	0.0	0.0
20	15.2	5.7	46.4	0.0	13.7	1.3	5.2	6.2	5.1	0.0	0.0	1.0
21	11.3	0.0	35.1	0.0	16.3	2.5	21.9	2.1	6.2	0.0	3.1	1.5
22	19.5	3.7	43.3	0.0	16.5	2.4	6.8	0.7	4.8	0.9	0.0	1.4
23	34.0	3.2	37.1	0.0	8.9	2.5	7.6	1.4	3.0	0.6	0.0	1.7
24	4.2	2.6	41.0	0.0	14.6	0.0	21.8	0.4	15.5	0.0	0.0	0.0
25	5.6	2.7	36.1	2.8	13.2	0.0	22.3	5.4	11.8	0.0	0.0	0.0
26	5.7	2.1	34.1	0.0	16.1	0.0	26.7	0.0	15.2	0.0	0.0	0.0
27	9.0	3.2	41.2	0.0	16.1	2.4	16.3	1.4	8.7	0.0	0.0	1.6
28	11.5	5.9	45.3	7.4	4.9	0.0	5.3	15.5	3.7	0.0	0.0	0.5
29	19.3	2.4	32.8	6.0	7.8	0.4	11.2	13.0	5.8	0.4	0.0	0.8
30	28.5	5.9	34.4	0.0	9.4	0.8	11.4	28.5	8.5	0.0	0.0	1.0
31	5.2	1.6	35.5	0.0	15.1	0.0	27.1	0.0	15.5	0.0	0.0	0.0

SUPPLEMENTARY MATERIALS FOR CHAPTER 3

Supplementary Tables for Chapter 3

Table S3.1. Chemical composition of the initial Icelandic and Antarctic muds.

Reactor	SiO ₂ %	Al ₂ O ₃ %	Fe ₂ O ₃ %	CaO %	MgO %	Na ₂ O %	K ₂ O %	Cr ₂ O ₃ %	TiO ₂ %	MnO %	P ₂ O ₅ %
Iceland	52.9	15.6	11.8	7.0	3.2	3.9	1.3	0.0	2.4	0.2	0.5
Antarctica	56.4	15.0	8.6	6.6	4.9	2.5	2.2	0.0	1.2	0.1	0.3

Reactor	SrO %	BaO %	LOI %	Ba ppm	Ce ppm	Cr ppm	Cs ppm	Dy ppm	Er ppm	Eu ppm	Ga ppm
Iceland	0.0	0.0	1.1	315.0	90.3	60.0	0.4	9.7	5.2	3.5	26.7
Antarctica	0.0	0.1	2.0	482.0	89.0	120.0	2.5	5.9	3.1	1.4	18.4

Reactor	Gd ppm	Hf ppm	Ho ppm	La ppm	Lu ppm	Nb ppm	Nd ppm	Pr ppm	Rb ppm	Sm ppm	Sn ppm
Iceland											
Antarctica											

Iceland	10.6	10.3	1.8	42.1	0.6	53.0	50.3	12.2	27.8	12.1	5.0
Antarctica	6.8	13.0	1.2	45.3	0.5	26.7	37.5	10.3	83.3	7.2	13.0

	Sr	Ta	Tb	Th	Tm	U	V	W	Y	Yb	Zr
Reactor	ppm	ppm	ppm	ppm	ppm	ppm	ppm	ppm	ppm	ppm	ppm
Iceland	386.0	3.2	1.7	4.1	0.7	1.3	200.0	1.0	49.5	4.4	421.0
Antarctica	305.0	1.7	1.1	11.3	0.5	2.4	143.0	7.0	30.7	3.2	546.0

Table S3.2. pH measurements during 4 weeks of 4°C experiments.

REACTOR	EXPERIMENT	Week	Replicate	pH			pH
				1	2	3	Average
Iceland	Bioweathering	0	1	6.53	6.54	6.56	6.54
Iceland	Bioweathering	0	2	6.24	6.25	6.32	6.27
Iceland	Bioweathering	0	3	6.3	6.32	6.34	6.32
Iceland	Chemical weathering	0	1	6.36	6.39	6.39	6.38
Iceland	Chemical weathering	0	2	6.34	6.32	6.33	6.33
Iceland	Chemical weathering	0	3	6.33	6.36	6.36	6.35
Iceland	Culture growth	0	1	6.7	6.67	6.67	6.68
Iceland	Culture growth	0	2	6.8	6.76	6.8	6.79
Iceland	Culture growth	0	3	6.91	6.91	6.9	6.91
Iceland	Bioweathering	1	1	6.85	6.98	6.98	6.94
Iceland	Bioweathering	1	2	6.82	6.84	6.86	6.84
Iceland	Bioweathering	1	3	6.64	6.68	6.7	6.67
Iceland	Chemical weathering	1	1	6.56	6.52	6.55	6.54
Iceland	Chemical weathering	1	2	6.55	6.58	6.59	6.57
Iceland	Chemical weathering	1	3	6.54	6.57	6.59	6.57
Iceland	Culture growth	1	1	6.64	6.69	6.73	6.69
Iceland	Culture growth	1	2	6.79	6.8	6.81	6.80
Iceland	Culture growth	1	3	6.78	6.8	6.83	6.80

Iceland	Bioweathering	2	1	7.54	7.5	7.51	7.52
Iceland	Bioweathering	2	2	7.17	7.17	7.19	7.18
Iceland	Bioweathering	2	3	6.96	6.98	6.99	6.98
Iceland	Chemical weathering	2	1	6.63	6.65	6.67	6.65
Iceland	Chemical weathering	2	2	6.72	6.7	6.71	6.71
Iceland	Chemical weathering	2	3	6.93	6.91	6.9	6.91
Iceland	Culture growth	2	1	7.03	7.05	7.05	7.04
Iceland	Culture growth	2	2	6.99	7.02	7.03	7.01
Iceland	Culture growth	2	3	7.27	7.27	7.25	7.26
Iceland	Bioweathering	3	1	7.07	7.09	7.11	7.09
Iceland	Bioweathering	3	2	7.48	7.44	7.42	7.45
Iceland	Bioweathering	3	3	7.08	7.09	7.1	7.09
Iceland	Chemical weathering	3	1	6.71	6.73	6.74	6.73
Iceland	Chemical weathering	3	2	6.84	6.83	6.83	6.83
Iceland	Chemical weathering	3	3	6.89	6.89	6.9	6.89
Iceland	Culture growth	3	1	7.11	7.13	7.14	7.13
Iceland	Culture growth	3	2	7.29	7.28	7.28	7.28
Iceland	Culture growth	3	3	7.19	7.17	7.17	7.18
Iceland	Bioweathering	4	1	7.38	7.4	7.41	7.40
Iceland	Bioweathering	4	2	7.69	7.68	7.67	7.68
Iceland	Bioweathering	4	3	7.52	7.52	7.51	7.52
Iceland	Chemical weathering	4	1	6.71	6.73	6.74	6.73
Iceland	Chemical weathering	4	2	6.82	6.82	6.83	6.82
Iceland	Chemical weathering	4	3	6.84	6.83	6.86	6.84
Iceland	Culture growth	4	1	7.01	7.03	7.04	7.03
Iceland	Culture growth	4	2	7.11	7.13	7.15	7.13
Iceland	Culture growth	4	3	7.24	7.25	7.26	7.25
Antarctica	Bioweathering	0	1	7.06	7.03	7.03	7.04
Antarctica	Bioweathering	0	2	7.06	7.06	7.05	7.06
Antarctica	Bioweathering	0	3	6.98	6.96	7.01	6.98
Antarctica	Chemical weathering	0	1	6.88	6.86	6.85	6.86
Antarctica	Chemical weathering	0	2	6.89	6.87	6.86	6.87
Antarctica	Chemical weathering	0	3	6.72	6.7	6.68	6.70
Antarctica	Culture growth	0	1	6.89	6.86	6.83	6.86
Antarctica	Culture growth	0	2	6.91	6.85	6.86	6.87
Antarctica	Culture growth	0	3	6.88	6.87	6.86	6.87
Antarctica	Bioweathering	1	1	7.12	7.08	7.07	7.09
Antarctica	Bioweathering	1	2	7.47	7.11	7.06	7.21
Antarctica	Bioweathering	1	3	6.96	6.95	6.95	6.95
Antarctica	Chemical weathering	1	1	6.92	6.94	6.94	6.93
Antarctica	Chemical weathering	1	2	6.88	6.87	6.9	6.88
Antarctica	Chemical weathering	1	3	6.94	6.93	6.93	6.93
Antarctica	Culture growth	1	1	6.99	7	7	7.00
Antarctica	Culture growth	1	2	7.13	7.17	7.18	7.16
Antarctica	Culture growth	1	3	7.25	7.25	7.23	7.24

Antarctica	Bioweathering	2	1	6.87	6.9	6.9	6.89
Antarctica	Bioweathering	2	2	6.93	6.92	6.91	6.92
Antarctica	Bioweathering	2	3	6.9	6.89	6.88	6.89
Antarctica	Chemical weathering	2	1	6.68	6.69	6.7	6.69
Antarctica	Chemical weathering	2	2	6.63	6.65	6.66	6.65
Antarctica	Chemical weathering	2	3	6.58	6.6	6.6	6.59
Antarctica	Culture growth	2	1	6.99	6.99	7	6.99
Antarctica	Culture growth	2	2	7.04	7.05	7.06	7.05
Antarctica	Culture growth	2	3	7.06	7.06	7.07	7.06
Antarctica	Bioweathering	3	1	7.21	7.22	7.22	7.22
Antarctica	Bioweathering	3	2	7.09	7.06	7.06	7.07
Antarctica	Bioweathering	3	3	7.11	7.1	7.08	7.10
Antarctica	Chemical weathering	3	1	6.72	6.74	6.75	6.74
Antarctica	Chemical weathering	3	2	6.78	6.8	6.78	6.79
Antarctica	Chemical weathering	3	3	6.77	6.77	6.78	6.77
Antarctica	Culture growth	3	1	7.19	7.21	7.22	7.21
Antarctica	Culture growth	3	2	7.15	7.15	7.21	7.17
Antarctica	Culture growth	3	3	7.32	7.32	7.31	7.32
Antarctica	Bioweathering	4	1	7.56	7.55	7.53	7.55
Antarctica	Bioweathering	4	2	7.41	7.4	7.39	7.40
Antarctica	Bioweathering	4	3	7.37	7.38	7.38	7.38
Antarctica	Chemical weathering	4	1	6.99	6.96	6.95	6.97
Antarctica	Chemical weathering	4	2	6.9	6.92	6.93	6.92
Antarctica	Chemical weathering	4	3	6.92	6.61	6.9	6.81
Antarctica	Culture growth	4	1	7.62	7.63	7.65	7.63
Antarctica	Culture growth	4	2	7.75	7.75	7.74	7.75
Antarctica	Culture growth	4	3	7.58	7.56	7.56	7.57

Table S3.3. Chlorophyll-a measurements during 4 weeks of 4°C experiments. Final calculated units are in µg/ml.

Chlorophyll-a UV-VIS measurements								
FIELD	REACTOR	Week	A 663 nm			A 750 nm		
			1	2	3	1	2	3
Iceland	BW	0	0.101	0.101	0.101	0.004	0.004	0.004
Iceland	BW	0	0.151	0.151	0.151	0.006	0.005	0.005
Iceland	BW	0	0.274	0.274	0.274	0.004	0.004	0.004
Iceland	CW	0	0.020	0.020	0.020	0.018	0.018	0.019
Iceland	CW	0	0.042	0.042	0.042	0.037	0.036	0.037
Iceland	CW	0	0.001	0.001	0.001	0.001	0.001	0.000

Iceland	Cg	0	0.201	0.201	0.201	0.007	0.007	0.007
Iceland	Cg	0	0.309	0.309	0.309	0.008	0.009	0.008
Iceland	Cg	0	0.330	0.330	0.330	0.008	0.010	0.010
Iceland	BW	1	0.080	0.080	0.080	0.004	0.004	0.004
Iceland	BW	1	0.113	0.113	0.113	0.006	0.006	0.006
Iceland	BW	1	0.173	0.173	0.173	0.006	0.006	0.006
Iceland	CW	1	0.008	0.008	0.008	0.007	0.007	0.007
Iceland	CW	1	0.003	0.003	0.003	0.003	0.003	0.003
Iceland	CW	1	0.008	0.008	0.008	0.007	0.007	0.007
Iceland	Cg	1	0.107	0.107	0.107	0.004	0.004	0.003
Iceland	Cg	1	0.102	0.102	0.102	0.004	0.004	0.004
Iceland	Cg	1	0.090	0.091	0.091	0.004	0.004	0.004
Iceland	BW	2	0.160	0.160	0.160	0.003	0.001	0.004
Iceland	BW	2	0.130	0.131	0.131	0.002	0.002	0.002
Iceland	BW	2	0.335	0.335	0.335	0.003	0.004	0.004
Iceland	CW	2	0.008	0.009	0.009	0.007	0.007	0.007
Iceland	CW	2	0.005	0.005	0.005	0.005	0.005	0.005
Iceland	CW	2	0.002	0.002	0.002	0.001	0.001	0.001
Iceland	Cg	2	0.137	0.131	0.131	0.004	0.004	0.004
Iceland	Cg	2	0.136	0.136	0.136	0.003	0.002	0.002
Iceland	Cg	2	0.059	0.059	0.059	0.002	0.002	0.003
Iceland	BW	3	0.131	0.131	0.131	0.012	0.013	0.013
Iceland	BW	3	0.159	0.159	0.159	0.005	0.005	0.005
Iceland	BW	3	0.167	0.166	0.167	0.004	0.005	0.005
Iceland	CW	3	0.000	0.000	0.000	0.000	0.000	0.000
Iceland	CW	3	0.001	0.001	0.001	0.001	0.001	0.001
Iceland	CW	3	0.002	0.002	0.002	0.002	0.002	0.002
Iceland	Cg	3	0.142	0.142	0.142	0.004	0.004	0.004
Iceland	Cg	3	0.096	0.096	0.096	0.002	0.002	0.002
Iceland	Cg	3	0.035	0.034	0.034	0.003	0.004	0.004
Iceland	BW	4	0.154	0.184	0.154	0.004	0.003	0.003
Iceland	BW	4	0.485	0.483	0.483	0.008	0.007	0.007
Iceland	BW	4	0.072	0.072	0.072	0.003	0.003	0.003
Iceland	CW	4	0.029	0.028	0.028	0.026	0.025	0.027
Iceland	CW	4	0.009	0.009	0.010	0.009	0.008	0.008
Iceland	CW	4	0.041	0.041	0.041	0.036	0.036	0.035
Iceland	Cg	4	0.074	0.074	0.074	0.002	0.003	0.003
Iceland	Cg	4	0.046	0.046	0.046	0.003	0.003	0.003
Iceland	Cg	4	0.054	0.053	0.053	0.003	0.003	0.003
Antarctica	BW	0	0.049	0.050	0.050	0.001	0.001	0.001
Antarctica	BW	0	0.058	0.058	0.058	0.001	0.001	0.000
Antarctica	BW	0	0.057	0.057	0.057	0.001	0.001	0.001
Antarctica	CW	0	0.008	0.008	0.007	0.007	0.007	0.007
Antarctica	CW	0	0.023	0.023	0.024	0.020	0.020	0.020
Antarctica	CW	0	0.016	0.016	0.016	0.013	0.013	0.013

Antarctica	Cg	0	0.050	0.049	0.049	0.000	0.000	0.000
Antarctica	Cg	0	0.055	0.055	0.056	0.000	0.000	0.000
Antarctica	Cg	0	0.045	0.045	0.044	0.000	0.000	0.000
Antarctica	BW	1	0.036	0.035	0.035	0.000	0.000	0.000
Antarctica	BW	1	0.105	0.104	0.104	0.001	0.001	0.001
Antarctica	BW	1	0.073	0.073	0.072	0.001	0.001	0.000
Antarctica	CW	1	0.011	0.011	0.012	0.009	0.009	0.009
Antarctica	CW	1	0.010	0.011	0.011	0.008	0.008	0.008
Antarctica	CW	1	0.042	0.041	0.041	0.034	0.034	0.035
Antarctica	Cg	1	0.134	0.133	0.133	0.003	0.003	0.003
Antarctica	Cg	1	0.054	0.053	0.053	0.000	0.000	0.000
Antarctica	Cg	1	0.036	0.036	0.035	0.000	0.000	0.000
Antarctica	BW	2	0.133	0.134	0.134	0.001	0.001	0.001
Antarctica	BW	2	0.149	0.150	0.150	0.001	0.001	0.001
Antarctica	BW	2	0.085	0.085	0.086	0.002	0.002	0.002
Antarctica	CW	2	0.016	0.015	0.015	0.014	0.014	0.014
Antarctica	CW	2	0.011	0.010	0.011	0.010	0.010	0.010
Antarctica	CW	2	0.014	0.013	0.013	0.013	0.013	0.013
Antarctica	Cg	2	0.023	0.024	0.024	0.000	0.000	0.000
Antarctica	Cg	2	0.041	0.041	0.041	0.000	0.000	0.000
Antarctica	Cg	2	0.054	0.054	0.054	0.000	0.000	0.000
Antarctica	BW	3	0.107	0.108	0.107	0.000	0.000	0.000
Antarctica	BW	3	0.068	0.068	0.069	0.001	0.001	0.001
Antarctica	BW	3	0.045	0.044	0.045	0.001	0.001	0.001
Antarctica	CW	3	0.009	0.009	0.009	0.007	0.007	0.007
Antarctica	CW	3	0.011	0.011	0.011	0.010	0.010	0.010
Antarctica	CW	3	0.030	0.031	0.031	0.026	0.025	0.025
Antarctica	Cg	3	0.184	0.184	0.185	0.001	0.001	0.001
Antarctica	Cg	3	0.088	0.088	0.088	0.000	0.001	0.001
Antarctica	Cg	3	0.068	0.068	0.068	0.000	0.000	0.000
Antarctica	BW	4	0.230	0.230	0.230	0.002	0.002	0.002
Antarctica	BW	4	0.419	0.418	0.418	0.003	0.004	0.003
Antarctica	BW	4	0.220	0.220	0.220	0.003	0.003	0.002
Antarctica	CW	4	0.004	0.004	0.004	0.003	0.004	0.004
Antarctica	CW	4	0.016	0.017	0.017	0.015	0.014	0.014
Antarctica	CW	4	0.010	0.010	0.011	0.009	0.009	0.009
Antarctica	Cg	4	0.119	0.119	0.119	0.002	0.001	0.001
Antarctica	Cg	4	0.115	0.155	0.115	0.002	0.002	0.002
Antarctica	Cg	4	0.084	0.084	0.084	0.001	0.001	0.001

*Corrected values: Chl-a values of bioweathering reactors corrected for absorbances measured in chemical weatherin reactors.

BW: Bioweathering; CW: Chemical weathering; Cg: Culture growth

Table S3.3. (Continued)

FIELD	REACTOR	Week	Calculated Values								
			A 663 nm - A 750 nm			Calculated			Corrected values*		
			1	2	3	1	2	3	1	2	3
Iceland	BW	0	0.097	0.097	0.097	1.232	1.232	1.232	1.207	1.207	1.219
Iceland	BW	0	0.145	0.146	0.146	1.842	1.854	1.854	1.778	1.778	1.791
Iceland	BW	0	0.270	0.270	0.270	3.429	3.429	3.429	3.429	3.429	3.416
Iceland	CW	0	0.002	0.002	0.001	0.025	0.025	0.013			
Iceland	CW	0	0.005	0.006	0.005	0.064	0.076	0.064			
Iceland	CW	0	0.000	0.000	0.001	0.000	0.000	0.013			
Iceland	Cg	0	0.194	0.194	0.194	2.464	2.464	2.464			
Iceland	Cg	0	0.301	0.300	0.301	3.823	3.810	3.823			
Iceland	Cg	0	0.322	0.320	0.320	4.089	4.064	4.064			
Iceland	BW	1	0.076	0.076	0.076	0.965	0.965	0.965	0.953	0.953	0.953
Iceland	BW	1	0.107	0.107	0.107	1.359	1.359	1.359	1.359	1.359	1.359
Iceland	BW	1	0.167	0.167	0.167	2.121	2.121	2.121	2.108	2.108	2.108
Iceland	CW	1	0.001	0.001	0.001	0.013	0.013	0.013			
Iceland	CW	1	0.000	0.000	0.000	0.000	0.000	0.000			
Iceland	CW	1	0.001	0.001	0.001	0.013	0.013	0.013			
Iceland	Cg	1	0.103	0.103	0.104	1.308	1.308	1.321			
Iceland	Cg	1	0.098	0.098	0.098	1.245	1.245	1.245			
Iceland	Cg	1	0.086	0.087	0.087	1.092	1.105	1.105			
Iceland	BW	2	0.157	0.159	0.156	1.994	2.019	1.981	1.981	1.994	1.956
Iceland	BW	2	0.128	0.129	0.129	1.626	1.638	1.638	1.626	1.638	1.638
Iceland	BW	2	0.332	0.331	0.331	4.216	4.204	4.204	4.204	4.191	4.191
Iceland	CW	2	0.001	0.002	0.002	0.013	0.025	0.025			
Iceland	CW	2	0.000	0.000	0.000	0.000	0.000	0.000			
Iceland	CW	2	0.001	0.001	0.001	0.013	0.013	0.013			
Iceland	Cg	2	0.133	0.127	0.127	1.689	1.613	1.613			
Iceland	Cg	2	0.133	0.134	0.134	1.689	1.702	1.702			
Iceland	Cg	2	0.057	0.057	0.056	0.724	0.724	0.711			
Iceland	BW	3	0.119	0.118	0.118	1.511	1.499	1.499	1.511	1.499	1.499
Iceland	BW	3	0.154	0.154	0.154	1.956	1.956	1.956	1.956	1.956	1.956
Iceland	BW	3	0.163	0.161	0.162	2.070	2.045	2.057	2.070	2.045	2.057
Iceland	CW	3	0.000	0.000	0.000	0.000	0.000	0.000			
Iceland	CW	3	0.000	0.000	0.000	0.000	0.000	0.000			
Iceland	CW	3	0.000	0.000	0.000	0.000	0.000	0.000			
Iceland	Cg	3	0.138	0.138	0.138	1.753	1.753	1.753			
Iceland	Cg	3	0.094	0.094	0.094	1.194	1.194	1.194			
Iceland	Cg	3	0.032	0.030	0.030	0.406	0.381	0.381			
Iceland	BW	4	0.150	0.181	0.151	1.905	2.299	1.918	1.867	2.261	1.905
Iceland	BW	4	0.477	0.476	0.476	6.058	6.045	6.045	6.058	6.033	6.020
Iceland	BW	4	0.069	0.069	0.069	0.876	0.876	0.876	0.813	0.813	0.800

Iceland	CW	4	0.003	0.003	0.001	0.038	0.038	0.013			
Iceland	CW	4	0.000	0.001	0.002	0.000	0.013	0.025			
Iceland	CW	4	0.005	0.005	0.006	0.064	0.064	0.076			
Iceland	Cg	4	0.072	0.071	0.071	0.914	0.902	0.902			
Iceland	Cg	4	0.043	0.043	0.043	0.546	0.546	0.546			
Iceland	Cg	4	0.051	0.050	0.050	0.648	0.635	0.635			
Antarctica	BW	0	0.048	0.049	0.049	0.610	0.622	0.622	0.597	0.610	0.622
Antarctica	BW	0	0.057	0.057	0.058	0.724	0.724	0.737	0.686	0.686	0.686
Antarctica	BW	0	0.056	0.056	0.056	0.711	0.711	0.711	0.673	0.673	0.673
Antarctica	CW	0	0.001	0.001	0.000	0.013	0.013	0.000			
Antarctica	CW	0	0.003	0.003	0.004	0.038	0.038	0.051			
Antarctica	CW	0	0.003	0.003	0.003	0.038	0.038	0.038			
Antarctica	Cg	0	0.050	0.049	0.049	0.635	0.622	0.622			
Antarctica	Cg	0	0.055	0.055	0.056	0.699	0.699	0.711			
Antarctica	Cg	0	0.045	0.045	0.044	0.572	0.572	0.559			
Antarctica	BW	1	0.036	0.035	0.035	0.457	0.445	0.445	0.432	0.419	0.406
Antarctica	BW	1	0.104	0.103	0.103	1.321	1.308	1.308	1.295	1.270	1.270
Antarctica	BW	1	0.072	0.072	0.072	0.914	0.914	0.914	0.813	0.826	0.838
Antarctica	CW	1	0.002	0.002	0.003	0.025	0.025	0.038			
Antarctica	CW	1	0.002	0.003	0.003	0.025	0.038	0.038			
Antarctica	CW	1	0.008	0.007	0.006	0.102	0.089	0.076			
Antarctica	Cg	1	0.131	0.130	0.130	1.664	1.651	1.651			
Antarctica	Cg	1	0.054	0.053	0.053	0.686	0.673	0.673			
Antarctica	Cg	1	0.036	0.036	0.035	0.457	0.457	0.445			
Antarctica	BW	2	0.132	0.133	0.133	1.676	1.689	1.689	1.651	1.676	1.676
Antarctica	BW	2	0.148	0.149	0.149	1.880	1.892	1.892	1.867	1.892	1.880
Antarctica	BW	2	0.083	0.083	0.084	1.054	1.054	1.067	1.041	1.054	1.067
Antarctica	CW	2	0.002	0.001	0.001	0.025	0.013	0.013			
Antarctica	CW	2	0.001	0.000	0.001	0.013	0.000	0.013			
Antarctica	CW	2	0.001	0.000	0.000	0.013	0.000	0.000			
Antarctica	Cg	2	0.023	0.024	0.024	0.292	0.305	0.305			
Antarctica	Cg	2	0.041	0.041	0.041	0.521	0.521	0.521			
Antarctica	Cg	2	0.054	0.054	0.054	0.686	0.686	0.686			
Antarctica	BW	3	0.107	0.108	0.107	1.359	1.372	1.359	1.334	1.346	1.334
Antarctica	BW	3	0.067	0.067	0.068	0.851	0.851	0.864	0.838	0.838	0.851
Antarctica	BW	3	0.044	0.043	0.044	0.559	0.546	0.559	0.508	0.470	0.483
Antarctica	CW	3	0.002	0.002	0.002	0.025	0.025	0.025			
Antarctica	CW	3	0.001	0.001	0.001	0.013	0.013	0.013			
Antarctica	CW	3	0.004	0.006	0.006	0.051	0.076	0.076			
Antarctica	Cg	3	0.183	0.183	0.184	2.324	2.324	2.337			
Antarctica	Cg	3	0.088	0.087	0.087	1.118	1.105	1.105			
Antarctica	Cg	3	0.068	0.068	0.068	0.864	0.864	0.864			
Antarctica	BW	4	0.228	0.228	0.228	2.896	2.896	2.896	2.883	2.896	2.896
Antarctica	BW	4	0.416	0.414	0.415	5.283	5.258	5.271	5.271	5.220	5.232
Antarctica	BW	4	0.217	0.217	0.218	2.756	2.756	2.769	2.743	2.743	2.743

Antarctica	CW	4	0.001	0.000	0.000	0.013	0.000	0.000
Antarctica	CW	4	0.001	0.003	0.003	0.013	0.038	0.038
Antarctica	CW	4	0.001	0.001	0.002	0.013	0.013	0.025
Antarctica	Cg	4	0.117	0.118	0.118	1.486	1.499	1.499
Antarctica	Cg	4	0.113	0.153	0.113	1.435	1.943	1.435
Antarctica	Cg	4	0.083	0.083	0.083	1.054	1.054	1.054

*Corrected values: Chl-a values of bioweathering reactors corrected

for absorbances measured in chemical weathering reactors.

BW: Bioweathering; CW: Chemical weathering; Cg: Culture growth

Table S3.4. Major anion measurements during 4 weeks of 4°C experiments. Units are in $\mu\text{mol}/\text{kg}$.

REACTOR	EXPERIMENT	Week	Replicate	Cl- ($\mu\text{mol}/\text{kg}$)	NO3- ($\mu\text{mol}/\text{kg}$)	PO4 3- ($\mu\text{mol}/\text{kg}$)	SO4 2- ($\mu\text{mol}/\text{kg}$)	HCO3- ($\mu\text{mol}/\text{kg}$)
Iceland	Bioweathering	0	1	145.47	1946.61	6.98	32.71	235.30
Iceland	Bioweathering	0	2	155.57	1964.93	6.47	33.21	206.29
Iceland	Bioweathering	0	3	175.90	1946.73	4.29	30.99	206.97
Iceland	Chemical weathering	0	1	149.46	1933.42	5.31	30.54	214.42
Iceland	Chemical weathering	0	2	140.92	1935.76	6.64	31.36	210.35
Iceland	Chemical weathering	0	3	146.64	1935.64	7.46	32.21	204.93
Iceland	Bioweathering	1	1	154.40	1949.38	BDL	30.64	230.00
Iceland	Bioweathering	1	2	152.57	1937.87	0.00	31.05	227.97
Iceland	Bioweathering	1	3	156.57	1980.37	0.00	32.42	227.29
Iceland	Chemical weathering	1	1	161.23	1940.41	5.47	34.21	269.30
Iceland	Chemical weathering	1	2	135.31	2014.71	BDL	33.44	215.78
Iceland	Chemical weathering	1	3	135.43	2021.80	5.30	34.95	384.49
Iceland	Bioweathering	2	1	133.82	1999.21	0.00	32.20	269.98
Iceland	Bioweathering	2	2	132.63	1977.87	0.00	35.35	300.35
Iceland	Bioweathering	2	3	132.55	1975.34	0.00	32.94	257.48
Iceland	Chemical weathering	2	1	131.59	1950.03	BDL	32.64	258.96
Iceland	Chemical weathering	2	2	128.45	1920.00	BDL	32.07	295.92
Iceland	Chemical weathering	2	3	137.50	1921.47	BDL	32.47	230.13
Iceland	Bioweathering	3	1	136.17	2024.10	0.00	33.07	286.31
Iceland	Bioweathering	3	2	137.61	1949.13	0.00	33.28	489.58
Iceland	Bioweathering	3	3	147.53	1955.61	0.00	33.91	316.61
Iceland	Chemical weathering	3	1	158.04	2051.69	BDL	34.57	253.04
Iceland	Chemical weathering	3	2	151.08	1997.79	BDL	33.00	269.30
Iceland	Chemical weathering	3	3	158.33	2063.48	BDL	34.29	269.30
Iceland	Bioweathering	4	1	125.83	1618.15	0.00	25.32	ND
Iceland	Bioweathering	4	2	130.93	1695.43	0.00	27.74	550.93
Iceland	Bioweathering	4	3	137.54	1790.15	0.00	31.58	238.26
Iceland	Chemical weathering	4	1	133.24	1802.72	BDL	30.62	223.23
Iceland	Chemical weathering	4	2	132.03	1823.20	0.00	30.86	269.30
Iceland	Chemical weathering	4	3	134.68	1765.95	BDL	30.58	273.74

Antarctica	Bioweathering	0	1	163.24	2072.04	14.02	36.12	246.57
Antarctica	Bioweathering	0	2	157.94	2075.93	14.92	35.54	49.77
Antarctica	Bioweathering	0	3	162.63	2049.16	14.11	35.36	301.09
Antarctica	Chemical weathering	0	1	150.61	1978.98	14.80	34.76	67.51
Antarctica	Chemical weathering	0	2	149.91	1970.06	12.28	34.85	324.74
Antarctica	Chemical weathering	0	3	146.73	1954.60	14.76	35.45	252.05
Antarctica	Bioweathering	1	1	151.96	2020.45	10.90	34.93	281.13
Antarctica	Bioweathering	1	2	163.04	2028.48	7.49	35.67	100.59
Antarctica	Bioweathering	1	3	155.88	2053.27	8.26	38.57	260.43
Antarctica	Chemical weathering	1	1	158.20	2112.13	12.91	37.11	258.96
Antarctica	Chemical weathering	1	2	155.57	2070.41	12.19	36.38	254.52
Antarctica	Chemical weathering	1	3	156.43	2068.10	13.06	35.84	271.52
Antarctica	Bioweathering	2	1	145.22	2059.44	0.00	32.26	281.87
Antarctica	Bioweathering	2	2	149.02	2093.28	0.00	37.52	283.35
Antarctica	Bioweathering	2	3	153.95	2155.64	0.00	34.48	390.38
Antarctica	Chemical weathering	2	1	144.13	2021.73	4.42	34.15	241.95
Antarctica	Chemical weathering	2	2	147.49	2040.26	BDL	33.02	461.49
Antarctica	Chemical weathering	2	3	191.16	2044.20	4.18	33.87	352.83
Antarctica	Bioweathering	3	1	156.69	2147.95	0.00	33.97	295.18
Antarctica	Bioweathering	3	2	160.98	2247.21	0.00	35.11	284.83
Antarctica	Bioweathering	3	3	162.14	2206.18	0.00	7.31	278.91
Antarctica	Chemical weathering	3	1	158.98	2279.12	4.22	6.71	286.92
Antarctica	Chemical weathering	3	2	153.26	2184.12	BDL	35.53	284.83
Antarctica	Chemical weathering	3	3	152.23	2207.50	4.46	36.25	265.61
Antarctica	Bioweathering	4	1	164.27	2124.68	0.00	32.34	417.95
Antarctica	Bioweathering	4	2	165.67	2220.26	0.00	7.78	417.47
Antarctica	Bioweathering	4	3	155.36	2073.16	0.00	32.10	648.51
Antarctica	Chemical weathering	4	1	160.50	2336.89	BDL	7.66	232.35
Antarctica	Chemical weathering	4	2	159.29	2289.99	8.09	37.05	213.87
Antarctica	Chemical weathering	4	3	146.77	2100.03	4.27	35.60	ND

Table S3.5. Total anion and cation measurements during 4 weeks of 4°C experiments. Units are in $\mu\text{mol}/\text{kg}$.

FIELD	REACTOR	Week	Al $\mu\text{mol}/\text{kg}$	Ca $\mu\text{mol}/\text{kg}$	Fe $\mu\text{mol}/\text{kg}$	K $\mu\text{mol}/\text{kg}$	Mg $\mu\text{mol}/\text{kg}$	Si $\mu\text{mol}/\text{kg}$	Na $\mu\text{mol}/\text{kg}$
Iceland	BW	0	3.70	37.26	2.12	271.30	32.21	10.11	1998.88
Iceland	BW	0	2.28	19.59	1.01	177.91	20.41	9.33	1962.68
Iceland	BW	0	2.42	18.93	1.04	133.04	19.73	9.69	1929.81
Iceland	CW	0	2.58	22.92	1.00	110.10	28.99	9.23	1900.62
Iceland	CW	0	2.85	20.46	1.34	101.35	24.91	9.61	1897.63
Iceland	CW	0	3.19	23.49	1.34	85.85	28.34	9.55	1866.30
Iceland	BW	1	2.81	11.71	0.61	71.81	10.47	34.42	1954.37
Iceland	BW	1	2.84	18.68	0.41	68.37	24.29	31.36	1960.80
Iceland	BW	1	2.47	13.50	0.29	71.05	12.29	35.18	1974.29
Iceland	CW	1	2.21	17.09	0.41	68.25	15.17	34.14	1949.60

Iceland	CW	1	2.37	41.68	0.76	70.51	31.34	33.68	1902.84
Iceland	CW	1	2.61	34.86	0.82	70.65	43.69	36.11	1918.06
Iceland	BW	2	2.67	13.87	0.48	57.72	15.63	43.28	1956.09
Iceland	BW	2	3.28	12.96	0.49	49.18	11.49	49.35	1953.93
Iceland	BW	2	2.59	14.31	0.74	57.92	22.30	59.66	2022.12
Iceland	CW	2	2.35	15.54	0.63	56.21	13.05	44.78	1933.56
Iceland	CW	2	2.28	18.53	0.42	53.92	17.68	42.79	1899.23
Iceland	CW	2	2.61	18.16	0.63	51.38	17.43	51.07	1916.86
Iceland	BW	3	2.85	9.37	0.52	45.63	10.08	85.07	2013.35
Iceland	BW	3	2.18	11.62	0.32	36.55	8.50	57.93	1955.13
Iceland	BW	3	2.34	10.63	0.47	44.58	7.63	73.60	2033.56
Iceland	CW	3	2.10	17.33	0.57	50.29	14.21	61.91	1972.14
Iceland	CW	3	1.93	42.10	0.58	55.54	42.06	61.14	1922.06
Iceland	CW	3	2.14	21.25	0.61	52.58	16.65	55.31	1918.60
Iceland	BW	4	2.54	8.98	0.39	28.67	6.46	62.51	1970.84
Iceland	BW	4	2.82	12.57	0.61	43.70	9.57	73.53	2003.69
Iceland	BW	4	2.09	15.29	0.48	31.28	17.36	72.12	1947.79
Iceland	CW	4	2.99	20.81	0.97	59.08	15.61	67.77	1955.47
Iceland	CW	4	2.41	18.36	0.70	47.21	14.86	64.13	1984.71
Iceland	CW	4	2.01	21.75	0.72	48.79	23.40	63.49	1963.57
Antarctica	BW	0	3.60	23.16	2.07	47.13	23.70	7.22	1675.46
Antarctica	BW	0	13.74	24.24	2.36	40.06	25.67	8.96	1676.95
Antarctica	BW	0	14.62	23.14	2.20	49.58	24.33	5.95	1649.03
Antarctica	CW	0	14.99	23.26	2.15	34.22	24.83	4.84	1632.59
Antarctica	CW	0	14.16	25.37	2.25	50.91	26.36	5.48	1651.03
Antarctica	CW	0	14.31	23.10	2.35	50.34	25.62	5.45	1638.96
Antarctica	BW	1	14.30	27.26	2.05	47.49	28.96	22.32	1612.51
Antarctica	BW	1	17.62	27.72	1.69	41.07	26.37	23.64	1644.39
Antarctica	BW	1	12.80	27.16	1.86	41.01	25.81	26.89	1704.78
Antarctica	CW	1	13.01	41.74	2.22	45.83	51.58	28.36	1664.98
Antarctica	CW	1	11.70	28.56	2.72	40.41	28.26	28.91	1669.41
Antarctica	CW	1	11.06	28.30	2.42	48.46	28.19	26.69	1635.73
Antarctica	BW	2	11.18	25.77	1.47	36.80	24.74	34.72	1693.41
Antarctica	BW	2	11.33	23.33	2.64	43.99	23.52	32.04	1664.90
Antarctica	BW	2	11.83	26.08	1.63	39.75	24.34	33.90	1709.51
Antarctica	CW	2	11.77	28.67	2.35	49.05	27.52	34.39	1712.90
Antarctica	CW	2	12.03	30.49	2.28	44.52	27.37	34.25	1673.33
Antarctica	CW	2	12.56	29.00	2.39	42.08	28.96	34.01	1665.15
Antarctica	BW	3	13.04	16.18	1.48	32.99	16.51	35.87	1644.96
Antarctica	BW	3	13.48	23.44	1.32	49.28	26.20	40.45	1739.88
Antarctica	BW	3	10.85	18.17	1.28	31.49	17.28	38.18	1656.36
Antarctica	CW	3	11.49	32.47	2.04	47.45	35.44	36.52	1668.58
Antarctica	CW	3	9.90	28.87	2.46	41.29	27.92	40.39	1736.43
Antarctica	CW	3	11.33	28.61	2.22	39.09	27.75	37.54	1714.58
Antarctica	BW	4	11.02	14.86	1.12	29.63	16.53	44.25	1718.99

Antarctica	BW	4	11.11	24.52	1.14	29.33	28.03	43.12	1724.98
Antarctica	BW	4	11.01	23.67	1.16	32.17	30.35	38.94	1686.81
Antarctica	CW	4	9.51	31.39	2.17	34.89	30.90	51.53	1746.66
Antarctica	CW	4	8.83	29.11	1.99	39.33	29.30	41.75	1733.70
Antarctica	CW	4	9.39	31.22	1.74	42.15	30.72	56.41	1752.70

BW: Bioweathering; CW: Chemical weathering

Table S3.5. (Continued)

FIELD	REACTOR	Week	Mn μmol/kg	Mo μmol/kg	Ni μmol/kg	P μmol/kg	S μmol/kg	Sr μmol/kg	B μmol/kg	Cu μmol/kg
Iceland	BW	0	1.76	0.18	0.06	18.22	42.16	0.11	4.75	0.28
Iceland	BW	0	1.82	0.14	BDL	18.28	41.46	0.04	4.70	BDL
Iceland	BW	0	1.73	0.18	BDL	18.22	42.54	0.03	5.57	BDL
Iceland	CW	0	1.82	0.17	BDL	17.48	42.58	BDL	4.15	BDL
Iceland	CW	0	1.73	0.17	BDL	17.68	40.03	0.06	2.15	BDL
Iceland	CW	0	1.81	0.17	0.05	17.67	39.50	0.05	4.56	BDL
Iceland	BW	1	1.27	0.13	BDL	13.80	41.59	BDL	8.28	BDL
Iceland	BW	1	1.21	0.16	0.06	9.23	39.80	BDL	8.12	BDL
Iceland	BW	1	1.17	0.18	BDL	8.60	41.36	BDL	5.56	BDL
Iceland	CW	1	1.76	0.15	0.06	13.53	43.06	0.03	12.89	BDL
Iceland	CW	1	1.79	0.17	BDL	14.53	41.35	0.07	6.54	BDL
Iceland	CW	1	1.91	0.15	0.09	14.68	40.20	0.07	10.93	BDL
Iceland	BW	2	0.99	0.16	0.08	BDL	39.96	0.04	12.68	0.31
Iceland	BW	2	1.07	0.15	0.10	BDL	41.04	BDL	12.28	0.36
Iceland	BW	2	0.83	0.23	1.10	4.14	39.27	0.03	16.47	0.32
Iceland	CW	2	1.75	0.18	0.06	13.50	40.35	0.03	12.15	0.27
Iceland	CW	2	1.93	0.18	0.10	14.46	40.83	0.05	7.03	BDL
Iceland	CW	2	1.71	0.21	0.06	13.85	40.30	0.04	8.46	BDL
Iceland	BW	3	0.82	0.17	0.11	3.64	38.46	BDL	12.53	0.41
Iceland	BW	3	1.10	0.21	0.05	0.36	38.87	0.04	11.71	BDL
Iceland	BW	3	0.93	0.17	0.10	1.80	40.66	BDL	16.35	0.29
Iceland	CW	3	1.84	0.19	0.06	12.37	40.52	0.04	16.82	0.27
Iceland	CW	3	1.85	0.15	0.09	13.50	41.35	0.05	19.55	0.32
Iceland	CW	3	1.96	0.17	0.08	14.35	41.92	BDL	11.92	BDL
Iceland	BW	4	0.65	0.18	BDL	3.95	39.72	BDL	11.06	BDL
Iceland	BW	4	0.65	0.21	0.09	9.25	43.86	0.04	13.79	0.32
Iceland	BW	4	0.99	0.15	0.05	1.36	42.79	BDL	20.07	BDL
Iceland	CW	4	2.10	0.17	BDL	14.38	42.97	0.03	21.98	BDL
Iceland	CW	4	2.01	0.15	0.05	14.37	40.82	0.05	9.92	BDL
Iceland	CW	4	1.91	0.15	0.06	13.48	40.60	0.04	13.05	BDL
Antarctica	BW	0	0.66	0.17	0.14	13.22	37.72	0.07	BDL	0.45
Antarctica	BW	0	0.72	0.18	0.13	17.58	39.51	0.06	4.93	0.41
Antarctica	BW	0	0.68	0.14	0.14	17.28	38.49	0.06	3.31	0.44

Antarctica	CW	0	0.70	0.14	0.14	16.34	36.62	0.06	5.09	0.37
Antarctica	CW	0	0.71	0.16	0.13	15.10	35.52	BDL	2.65	0.38
Antarctica	CW	0	0.72	0.15	0.15	13.54	38.06	BDL	4.13	0.37
Antarctica	BW	1	0.71	0.15	0.21	7.71	35.60	0.07	2.95	0.47
Antarctica	BW	1	0.68	0.14	0.11	6.41	34.65	0.10	10.24	0.45
Antarctica	BW	1	0.68	0.17	0.17	9.83	35.98	0.07	8.18	0.34
Antarctica	CW	1	0.70	0.14	0.15	12.16	37.09	0.09	7.92	0.46
Antarctica	CW	1	0.73	0.15	0.20	9.73	36.12	0.07	7.11	0.60
Antarctica	CW	1	0.70	0.18	0.16	11.82	36.01	0.09	15.72	0.38
Antarctica	BW	2	0.55	0.16	0.17	7.83	35.92	0.07	10.86	0.44
Antarctica	BW	2	0.48	0.17	0.12	4.63	36.45	0.05	16.99	0.37
Antarctica	BW	2	0.59	0.17	0.15	3.20	36.17	0.07	10.19	0.44
Antarctica	CW	2	0.69	0.14	0.14	11.00	37.46	0.08	13.46	0.41
Antarctica	CW	2	0.70	0.19	0.19	13.59	38.87	0.08	10.82	0.34
Antarctica	CW	2	0.69	0.16	0.15	13.07	39.62	0.08	8.36	0.51
Antarctica	BW	3	0.23	0.16	0.15	BDL	32.02	0.06	8.77	0.35
Antarctica	BW	3	0.36	0.17	0.19	4.67	37.33	0.07	13.68	0.46
Antarctica	BW	3	0.34	0.17	0.13	0.92	36.19	BDL	20.19	0.41
Antarctica	CW	3	0.64	0.15	0.18	10.45	39.02	0.07	8.88	0.51
Antarctica	CW	3	0.69	0.18	0.15	9.10	38.72	0.08	15.63	0.46
Antarctica	CW	3	0.69	0.16	0.18	10.51	38.46	0.06	19.79	0.44
Antarctica	BW	4	0.20	0.18	0.18	1.37	31.40	BDL	33.02	0.46
Antarctica	BW	4	0.34	0.17	0.14	BDL	35.11	BDL	36.17	0.47
Antarctica	BW	4	0.30	0.15	0.11	BDL	31.65	0.07	24.50	0.36
Antarctica	CW	4	0.75	0.22	0.19	7.78	39.48	0.09	10.91	0.48
Antarctica	CW	4	0.73	0.16	0.16	8.85	38.29	0.09	11.07	0.38
Antarctica	CW	4	0.76	0.20	0.12	8.36	39.13	0.09	17.20	0.45

BW: Bioweathering; CW: Chemical weathering

Table S3.6. pH measurements at the start and end of variable weathering solute experiments.

FIELD	REACTOR	Week	Temperature (°C)	Solute Concentration	pH
Antarctica	Bioweathering	0	4	0.1X	6.83
Antarctica	Bioweathering	0	4	0.1X	6.8
Antarctica	Bioweathering	0	4	0.1X	6.75
Antarctica	Bioweathering	4	4	0.1X	7.29
Antarctica	Bioweathering	4	4	0.1X	7.32
Antarctica	Bioweathering	4	4	0.1X	7.3
Antarctica	Chemical Weathering	0	4	0.1x	6.863333
Antarctica	Chemical Weathering	0	4	0.1x	6.873333
Antarctica	Chemical Weathering	0	4	0.1x	6.7
Antarctica	Chemical Weathering	4	4	0.1x	6.966667
Antarctica	Chemical Weathering	4	4	0.1x	6.916667

Antarctica	Chemical Weathering	4	4	0.1x	6.81
Antarctica	Bioweathering	0	4	0.001X	6.77
Antarctica	Bioweathering	0	4	0.001X	6.73
Antarctica	Bioweathering	0	4	0.001X	6.71
Antarctica	Bioweathering	4	4	0.001X	7.44
Antarctica	Bioweathering	4	4	0.001X	7.37
Antarctica	Bioweathering	4	4	0.001X	7.53
Antarctica	Chemical Weathering	0	4	0.001X	7
Antarctica	Chemical Weathering	0	4	0.001X	7
Antarctica	Chemical Weathering	0	4	0.001X	6.86
Antarctica	Chemical Weathering	4	4	0.001X	6.86
Antarctica	Chemical Weathering	4	4	0.001X	7.02
Antarctica	Chemical Weathering	4	4	0.001X	6.95
Antarctica	Bioweathering	0	12	0.1X	6.83
Antarctica	Bioweathering	0	12	0.1X	6.8
Antarctica	Bioweathering	0	12	0.1X	6.75
Antarctica	Bioweathering	4	12	0.1X	7.92
Antarctica	Bioweathering	4	12	0.1X	7.96
Antarctica	Bioweathering	4	12	0.1X	7.98
Antarctica	Chemical Weathering	0	12	0.1x	6.573333
Antarctica	Chemical Weathering	0	12	0.1x	6.633333
Antarctica	Chemical Weathering	0	12	0.1x	6.58
Antarctica	Chemical Weathering	4	12	0.1x	6.9
Antarctica	Chemical Weathering	4	12	0.1x	6.903333
Antarctica	Chemical Weathering	4	12	0.1x	6.936667
Antarctica	Bioweathering	0	12	0.001X	6.77
Antarctica	Bioweathering	0	12	0.001X	6.73
Antarctica	Bioweathering	0	12	0.001X	6.71
Antarctica	Bioweathering	4	12	0.001X	7.75
Antarctica	Bioweathering	4	12	0.001X	7.52
Antarctica	Bioweathering	4	12	0.001X	7.58
Antarctica	Chemical Weathering	0	12	0.001X	7
Antarctica	Chemical Weathering	0	12	0.001X	7
Antarctica	Chemical Weathering	0	12	0.001X	6.86
Antarctica	Chemical Weathering	4	12	0.001X	6.88
Antarctica	Chemical Weathering	4	12	0.001X	6.93
Antarctica	Chemical Weathering	4	12	0.001X	6.91
Iceland	Bioweathering	0	4	0.1X	6.58
Iceland	Bioweathering	0	4	0.1X	6.67
Iceland	Bioweathering	0	4	0.1X	7.01
Iceland	Bioweathering	4	4	0.1X	7.37
Iceland	Bioweathering	4	4	0.1X	7.34
Iceland	Bioweathering	4	4	0.1X	7.4
Iceland	Chemical Weathering	0	4	0.1x	6.38
Iceland	Chemical Weathering	0	4	0.1x	6.33

Iceland	Chemical Weathering	0	4	0.1x	6.35
Iceland	Chemical Weathering	4	4	0.1x	6.726667
Iceland	Chemical Weathering	4	4	0.1x	6.823333
Iceland	Chemical Weathering	4	4	0.1x	6.843333
Iceland	Bioweathering	0	4	0.001X	6.9
Iceland	Bioweathering	0	4	0.001X	6.85
Iceland	Bioweathering	0	4	0.001X	6.82
Iceland	Bioweathering	4	4	0.001X	7.61
Iceland	Bioweathering	4	4	0.001X	7.66
Iceland	Bioweathering	4	4	0.001X	7.68
Iceland	Chemical Weathering	0	4	0.001X	6.98
Iceland	Chemical Weathering	0	4	0.001X	7.06
Iceland	Chemical Weathering	0	4	0.001X	6.76
Iceland	Chemical Weathering	4	4	0.001X	7.06
Iceland	Chemical Weathering	4	4	0.001X	7.09
Iceland	Chemical Weathering	4	4	0.001X	7.12
Iceland	Bioweathering	0	12	0.1X	6.58
Iceland	Bioweathering	0	12	0.1X	6.67
Iceland	Bioweathering	0	12	0.1X	7.01
Iceland	Bioweathering	4	12	0.1X	7.56
Iceland	Bioweathering	4	12	0.1X	7.76
Iceland	Bioweathering	4	12	0.1X	7.82
Iceland	Chemical Weathering	0	12	0.1x	6.69
Iceland	Chemical Weathering	0	12	0.1x	6.74
Iceland	Chemical Weathering	0	12	0.1x	6.64
Iceland	Chemical Weathering	4	12	0.1x	6.71
Iceland	Chemical Weathering	4	12	0.1x	6.85
Iceland	Chemical Weathering	4	12	0.1x	6.853333
Iceland	Bioweathering	0	12	0.001X	6.9
Iceland	Bioweathering	0	12	0.001X	6.85
Iceland	Bioweathering	0	12	0.001X	6.82
Iceland	Bioweathering	4	12	0.001X	7.75
Iceland	Bioweathering	4	12	0.001X	7.65
Iceland	Bioweathering	4	12	0.001X	7.58
Iceland	Chemical Weathering	0	12	0.001X	6.98
Iceland	Chemical Weathering	0	12	0.001X	7.06
Iceland	Chemical Weathering	0	12	0.001X	6.76
Iceland	Chemical Weathering	4	12	0.001X	6.89
Iceland	Chemical Weathering	4	12	0.001X	6.95
Iceland	Chemical Weathering	4	12	0.001X	7.15
	Culture Growth	0	4	0.1X	6.52
	Culture Growth	0	4	0.1X	6.63
	Culture Growth	0	4	0.1X	6.73
	Culture Growth	4	4	0.1X	7.15
	Culture Growth	4	4	0.1X	7.17

Culture Growth	4	4	0.1X	7.16
Culture Growth	0	4	0.001X	6.68
Culture Growth	0	4	0.001X	6.62
Culture Growth	0	4	0.001X	6.41
Culture Growth	4	4	0.001X	7.17
Culture Growth	4	4	0.001X	7.12
Culture Growth	4	4	0.001X	7.18
Culture Growth	0	12	0.1X	6.52
Culture Growth	0	12	0.1X	6.63
Culture Growth	0	12	0.1X	6.73
Culture Growth	4	12	0.1X	7.93
Culture Growth	4	12	0.1X	8
Culture Growth	4	12	0.1X	ND
Culture Growth	0	12	0.001X	6.68
Culture Growth	0	12	0.001X	6.62
Culture Growth	0	12	0.001X	6.41
Culture Growth	4	12	0.001X	7.31
Culture Growth	4	12	0.001X	7.35
Culture Growth	4	12	0.001X	7.23

Table S3.7. Total anion and cation measurements at the start and end of variable weathering solute experiments. Concentration units are in $\mu\text{mol/kg}$.

FIELD	REACTOR	Week	Temperature (°C)	Solute Concentration	Al	B	Ca	Fe	K
Antarctica	BW	0	12	0.1X	0.00	10.33	26.89	0.89	78.11
Antarctica	BW	0	12	0.1X	0.61	10.86	27.96	0.93	78.50
Antarctica	BW	0	12	0.1X	0.75	10.92	26.78	0.94	70.63
Antarctica	BW	4	12	0.1X	3.23	22.65	16.30	0.90	27.81
Antarctica	BW	4	12	0.1X	2.84	88.94	14.33	0.83	37.64
Antarctica	BW	4	12	0.1X	2.96	88.85	16.79	0.77	35.74
Antarctica	BW	0	12	0.001X	0.51	6.00	4.20	0.17	90.23
Antarctica	BW	0	12	0.001X	0.00	6.09	3.80	0.14	100.81
Antarctica	BW	0	12	0.001X	0.00	5.83	3.94	0.16	102.12
Antarctica	BW	4	12	0.001X	2.55	60.30	4.34	1.23	21.14
Antarctica	BW	4	12	0.001X	2.36	40.42	4.84	1.07	0.11
Antarctica	BW	4	12	0.001X	2.10	33.17	4.96	0.89	22.43
Antarctica	BW	0	4	0.1X	0.00	10.33	26.89	0.89	78.11
Antarctica	BW	0	4	0.1X	0.61	10.86	27.96	0.93	78.50
Antarctica	BW	0	4	0.1X	0.75	10.92	26.78	0.94	70.63
Antarctica	BW	4	4	0.1X	1.68	96.46	35.77	0.90	57.31
Antarctica	BW	4	4	0.1X	0.93	40.25	36.61	0.50	56.35
Antarctica	BW	4	4	0.1X	1.62	54.45	34.40	0.83	61.30
Antarctica	BW	0	4	0.001X	0.51	6.00	4.20	0.17	90.23
Antarctica	BW	0	4	0.001X	0.00	6.09	3.80	0.14	100.81
Antarctica	BW	0	4	0.001X	0.00	5.83	3.94	0.16	102.12

Antarctica	BW	4	4	0.001X	2.50	51.27	11.00	1.21	28.65
Antarctica	BW	4	4	0.001X	2.41	43.35	3.76	0.91	24.59
Antarctica	BW	4	4	0.001X	1.41	32.36	4.21	0.70	20.18
Antarctica	CW	0	12	0.1X	1.66	0.00	28.08	1.90	55.37
Antarctica	CW	0	12	0.1X	3.13	7.27	31.36	2.09	74.96
Antarctica	CW	0	12	0.1X	3.70	0.00	26.56	3.05	32.08
Antarctica	CW	4	12	0.1X	0.98	37.10	35.69	0.73	38.45
Antarctica	CW	4	12	0.1X	0.89	55.50	30.81	0.75	44.06
Antarctica	CW	4	12	0.1X	1.06	17.73	29.42	1.13	23.75
Antarctica	CW	0	12	0.001X	0.51	4.91	0.00	0.24	0.11
Antarctica	CW	0	12	0.001X	1.34	4.72	0.65	1.18	0.11
Antarctica	CW	0	12	0.001X	0.81	4.21	0.00	0.49	0.11
Antarctica	CW	4	12	0.001X	2.14	5.57	3.13	1.25	0.11
Antarctica	CW	4	12	0.001X	2.08	5.40	3.20	1.15	0.11
Antarctica	CW	4	12	0.001X	1.38	5.92	3.63	0.73	0.11
Antarctica	CW	0	4	0.1X	14.99	5.09	23.26	2.15	34.22
Antarctica	CW	0	4	0.1X	14.16	2.65	25.37	2.25	50.91
Antarctica	CW	0	4	0.1X	14.31	4.13	23.10	2.35	50.34
Antarctica	CW	4	4	0.1X	9.51	10.91	31.39	2.17	34.89
Antarctica	CW	4	4	0.1X	8.83	11.07	29.11	1.99	39.33
Antarctica	CW	4	4	0.1X	9.39	17.20	31.22	1.74	42.15
Antarctica	CW	0	4	0.001X	0.51	4.91	0.00	0.24	0.11
Antarctica	CW	0	4	0.001X	1.34	4.72	0.65	1.18	0.11
Antarctica	CW	0	4	0.001X	0.81	4.21	0.00	0.49	0.11
Antarctica	CW	4	4	0.001X	1.99	5.17	2.02	1.20	0.11
Antarctica	CW	4	4	0.001X	2.42	5.55	3.60	1.48	0.11
Antarctica	CW	4	4	0.001X	1.84	5.05	4.05	4.29	0.11
Iceland	BW	0	12	0.1X	0.54	10.21	26.18	1.11	72.06
Iceland	BW	0	12	0.1X	0.00	9.80	25.07	1.02	64.00
Iceland	BW	0	12	0.1X	0.78	9.31	24.02	1.14	80.75
Iceland	BW	4	12	0.1X	2.27	65.02	13.58	0.58	26.84
Iceland	BW	4	12	0.1X	3.41	46.06	24.87	1.02	29.67
Iceland	BW	4	12	0.1X	1.46	46.51	12.89	0.67	35.58
Iceland	BW	0	12	0.001X	0.00	5.03	2.96	0.13	95.90
Iceland	BW	0	12	0.001X	0.00	4.90	3.93	0.13	102.70
Iceland	BW	0	12	0.001X	0.00	5.47	1.94	0.08	92.58
Iceland	BW	4	12	0.001X	0.71	33.76	2.33	0.20	0.11
Iceland	BW	4	12	0.001X	0.98	36.87	3.25	0.31	0.11
Iceland	BW	4	12	0.001X	1.00	42.08	3.01	0.38	0.11
Iceland	BW	0	4	0.1X	0.54	10.21	26.18	1.11	72.06
Iceland	BW	0	4	0.1X	0.00	9.80	25.07	1.02	64.00
Iceland	BW	0	4	0.1X	0.78	9.31	24.02	1.14	80.75
Iceland	BW	4	4	0.1X	0.51	53.42	20.82	0.45	52.23
Iceland	BW	4	4	0.1X	34.22	33.25	20.65	0.49	43.20
Iceland	BW	4	4	0.1X	0.51	19.24	23.79	0.40	55.46
Iceland	BW	0	4	0.001X	0.00	5.03	2.96	0.13	95.90
Iceland	BW	0	4	0.001X	0.00	4.90	3.93	0.13	102.70
Iceland	BW	0	4	0.001X	0.00	5.47	1.94	0.08	92.58
Iceland	BW	4	4	0.001X	0.70	36.32	1.55	0.18	0.11

Iceland	BW	4	4	0.001X	0.80	62.04	2.03	0.19	0.11
Iceland	BW	4	4	0.001X	0.71	49.47	1.59	0.21	0.11
Iceland	CW	0	12	0.1X	0.17	5.76	8.44	1.10	54.71
Iceland	CW	0	12	0.1X	0.20	3.77	7.97	1.43	46.48
Iceland	CW	0	12	0.1X	0.00	2.24	9.17	1.44	46.30
Iceland	CW	4	12	0.1X	0.40	68.48	11.35	0.26	53.48
Iceland	CW	4	12	0.1X	0.00	51.86	10.71	0.32	65.89
Iceland	CW	4	12	0.1X	0.55	32.81	11.95	0.17	54.44
Iceland	CW	0	12	0.001X	0.49	4.49	0.00	0.20	0.11
Iceland	CW	0	12	0.001X	0.53	3.69	0.64	0.47	0.11
Iceland	CW	0	12	0.001X	0.00	3.54	0.54	0.11	0.11
Iceland	CW	4	12	0.001X	0.00	4.78	0.00	0.25	0.11
Iceland	CW	4	12	0.001X	0.69	4.83	1.21	0.36	0.11
Iceland	CW	4	12	0.001X	0.60	9.71	0.54	0.50	0.11
Iceland	CW	0	4	0.1X	2.58	4.15	22.92	1.00	110.10
Iceland	CW	0	4	0.1X	2.85	2.15	20.46	1.34	101.35
Iceland	CW	0	4	0.1X	3.19	4.56	23.49	1.34	85.85
Iceland	CW	4	4	0.1X	2.99	21.98	20.81	0.97	59.08
Iceland	CW	4	4	0.1X	2.41	9.92	18.36	0.70	47.21
Iceland	CW	4	4	0.1X	2.01	13.05	21.75	0.72	48.79
Iceland	CW	0	4	0.001X	0.49	4.49	0.00	0.20	0.11
Iceland	CW	0	4	0.001X	0.53	3.69	0.64	0.47	0.11
Iceland	CW	0	4	0.001X	0.00	3.54	0.54	0.11	0.11
Iceland	CW	4	4	0.001X	0.75	6.08	0.71	0.17	0.11
Iceland	CW	4	4	0.001X	0.63	4.83	1.20	0.31	0.11
Iceland	CW	4	4	0.001X	0.00	5.01	1.09	0.37	0.11
	Cg	0	12	0.1X	0.00	10.13	24.44	1.11	89.75
	Cg	0	12	0.1X	0.00	10.18	25.50	0.67	89.96
	Cg	0	12	0.1X	0.00	9.34	26.16	0.74	88.90
	Cg	4	12	0.1X	1.30	46.34	11.34	0.19	35.24
	Cg	4	12	0.1X	0.75	43.61	11.06	0.34	19.71
	Cg	4	12	0.1X	0.79	25.65	11.29	0.22	0.11
	Cg	0	12	0.001X	0.00	4.46	4.28	0.10	121.16
	Cg	0	12	0.001X	0.00	4.43	2.90	0.06	125.34
	Cg	0	12	0.001X	0.00	4.96	3.44	0.10	128.33
	Cg	4	12	0.001X	0.00	34.85	5.03	0.66	58.32
	Cg	4	12	0.001X	0.00	44.40	3.65	0.12	55.32
	Cg	4	12	0.001X	0.00	29.00	3.96	0.13	46.95
	Cg	0	4	0.1X	0.00	10.13	24.44	1.11	89.75
	Cg	0	4	0.1X	0.00	10.18	25.50	0.67	89.96
	Cg	0	4	0.1X	0.00	9.34	26.16	0.74	88.90
	Cg	4	4	0.1X	0.00	29.11	28.56	0.51	87.39
	Cg	4	4	0.1X	0.00	56.15	28.52	2.26	80.58
	Cg	4	4	0.1X	0.00	57.62	29.87	1.07	70.03
	Cg	0	4	0.001X	0.00	4.46	4.28	0.10	121.16
	Cg	0	4	0.001X	0.00	4.43	2.90	0.06	125.34
	Cg	0	4	0.001X	0.00	4.96	3.44	0.10	128.33
	Cg	4	4	0.001X	0.00	40.11	1.93	0.12	55.25
	Cg	4	4	0.001X	0.00	45.83	1.78	0.09	40.13

Cg	4	4	0.001X	0.00	23.32	2.39	0.08	33.72
----	---	---	--------	------	-------	------	------	-------

BW: Bioweathering; CW: Chemical weathering; Cg: Culture growth
Concentration units are in $\mu\text{mol/kg}$

Table S3.7. (Continued)

FIELD	REACTOR	Week	Temperature (°C)	Solute Concentration	Mg	Mn	Na	P	Si
Antarctica	BW	0	12	0.1X	37.60	1.04	2383.26	31.93	10.88
Antarctica	BW	0	12	0.1X	34.90	0.89	2428.96	32.15	11.37
Antarctica	BW	0	12	0.1X	35.12	0.99	2413.76	34.99	11.34
Antarctica	BW	4	12	0.1X	14.46	0.18	2550.89	3.97	136.27
Antarctica	BW	4	12	0.1X	12.83	0.15	2535.30	2.74	145.19
Antarctica	BW	4	12	0.1X	13.90	0.16	2559.77	2.48	159.98
Antarctica	BW	0	12	0.001X	4.47	0.15	203.99	15.25	8.05
Antarctica	BW	0	12	0.001X	4.87	0.22	162.96	17.62	6.81
Antarctica	BW	0	12	0.001X	5.53	0.23	185.49	16.64	7.47
Antarctica	BW	4	12	0.001X	5.07	0.15	362.22	3.88	98.74
Antarctica	BW	4	12	0.001X	5.08	0.13	341.60	6.16	104.70
Antarctica	BW	4	12	0.001X	5.94	0.15	336.06	1.24	99.92
Antarctica	BW	0	4	0.1X	37.60	1.04	2383.26	31.93	10.88
Antarctica	BW	0	4	0.1X	34.90	0.89	2428.96	32.15	11.37
Antarctica	BW	0	4	0.1X	35.12	0.99	2413.76	34.99	11.34
Antarctica	BW	4	4	0.1X	35.73	0.75	2623.87	15.31	117.21
Antarctica	BW	4	4	0.1X	38.18	0.85	2615.16	18.17	99.99
Antarctica	BW	4	4	0.1X	35.14	0.73	2589.06	16.40	97.68
Antarctica	BW	0	4	0.001X	4.47	0.15	203.99	15.25	8.05
Antarctica	BW	0	4	0.001X	4.87	0.22	162.96	17.62	6.81
Antarctica	BW	0	4	0.001X	5.53	0.23	185.49	16.64	7.47
Antarctica	BW	4	4	0.001X	11.05	0.19	362.45	4.72	86.81
Antarctica	BW	4	4	0.001X	4.64	0.10	369.56	6.19	82.19
Antarctica	BW	4	4	0.001X	5.01	0.12	319.72	6.87	65.55
Antarctica	CW	0	12	0.1X	26.16	0.55	1862.36	12.78	20.09
Antarctica	CW	0	12	0.1X	29.63	0.57	1925.35	11.11	24.90
Antarctica	CW	0	12	0.1X	27.96	0.60	1874.25	14.25	23.33
Antarctica	CW	4	12	0.1X	30.66	0.57	2078.16	7.23	63.24
Antarctica	CW	4	12	0.1X	28.62	0.52	1991.08	9.48	63.01
Antarctica	CW	4	12	0.1X	27.45	0.51	1847.12	5.47	60.22
Antarctica	CW	0	12	0.001X	0.37	0.00	93.85	0.00	8.20
Antarctica	CW	0	12	0.001X	0.51	0.02	85.06	2.95	8.93
Antarctica	CW	0	12	0.001X	0.74	0.01	89.82	0.33	8.32
Antarctica	CW	4	12	0.001X	3.49	0.08	166.18	1.20	11.15
Antarctica	CW	4	12	0.001X	4.13	0.09	172.29	2.07	12.41
Antarctica	CW	4	12	0.001X	3.38	0.07	189.56	2.67	7.73
Antarctica	CW	0	4	0.1X	24.83	0.70	1632.59	16.34	4.84
Antarctica	CW	0	4	0.1X	26.36	0.71	1651.03	15.10	5.48
Antarctica	CW	0	4	0.1X	25.62	0.72	1638.96	13.54	5.45
Antarctica	CW	4	4	0.1X	30.90	0.75	1746.66	7.78	51.53

Antarctica	CW	4	4	0.1X	29.30	0.73	1733.70	8.85	41.75
Antarctica	CW	4	4	0.1X	30.72	0.76	1752.70	8.36	56.41
Antarctica	CW	0	4	0.001X	0.37	0.00	93.85	0.00	8.20
Antarctica	CW	0	4	0.001X	0.51	0.02	85.06	2.95	8.93
Antarctica	CW	0	4	0.001X	0.74	0.01	89.82	0.33	8.32
Antarctica	CW	4	4	0.001X	2.66	0.06	162.64	0.00	11.95
Antarctica	CW	4	4	0.001X	4.00	0.08	166.05	0.85	11.91
Antarctica	CW	4	4	0.001X	2.91	0.11	160.91	3.66	9.97
Iceland	BW	0	12	0.1X	32.36	1.86	2328.84	36.48	13.36
Iceland	BW	0	12	0.1X	34.90	1.79	2369.76	41.36	13.02
Iceland	BW	0	12	0.1X	33.41	1.82	2386.46	37.23	13.43
Iceland	BW	4	12	0.1X	9.99	0.71	3005.52	1.89	204.62
Iceland	BW	4	12	0.1X	13.06	0.65	2604.54	2.76	169.27
Iceland	BW	4	12	0.1X	9.96	0.78	2656.83	5.13	174.11
Iceland	BW	0	12	0.001X	4.76	0.41	213.14	22.16	9.99
Iceland	BW	0	12	0.001X	5.26	0.44	196.54	21.85	8.99
Iceland	BW	0	12	0.001X	3.06	0.32	175.94	16.18	9.05
Iceland	BW	4	12	0.001X	1.96	0.34	394.60	9.24	123.30
Iceland	BW	4	12	0.001X	2.39	0.43	393.04	13.64	122.19
Iceland	BW	4	12	0.001X	1.93	0.32	393.46	15.78	129.08
Iceland	BW	0	4	0.1X	32.36	1.86	2328.84	36.48	13.36
Iceland	BW	0	4	0.1X	34.90	1.79	2369.76	41.36	13.02
Iceland	BW	0	4	0.1X	33.41	1.82	2386.46	37.23	13.43
Iceland	BW	4	4	0.1X	20.41	2.13	2673.84	19.42	107.65
Iceland	BW	4	4	0.1X	20.49	2.15	2597.74	15.83	98.52
Iceland	BW	4	4	0.1X	24.54	2.48	2749.94	17.93	99.19
Iceland	BW	0	4	0.001X	4.76	0.41	213.14	22.16	9.99
Iceland	BW	0	4	0.001X	5.26	0.44	196.54	21.85	8.99
Iceland	BW	0	4	0.001X	3.06	0.32	175.94	16.18	9.05
Iceland	BW	4	4	0.001X	1.75	0.23	412.04	17.33	106.85
Iceland	BW	4	4	0.001X	2.05	0.34	421.68	21.78	106.80
Iceland	BW	4	4	0.001X	1.60	0.22	394.94	15.61	102.60
Iceland	CW	0	12	0.1X	15.28	1.90	1871.93	17.54	15.49
Iceland	CW	0	12	0.1X	14.90	1.87	1777.97	15.91	0.00
Iceland	CW	0	12	0.1X	16.04	1.93	1879.32	19.07	0.00
Iceland	CW	4	12	0.1X	15.21	2.17	1949.66	11.38	114.80
Iceland	CW	4	12	0.1X	15.36	2.21	1943.75	9.46	108.14
Iceland	CW	4	12	0.1X	17.69	2.29	1829.87	10.72	100.35
Iceland	CW	0	12	0.001X	0.00	0.00	85.94	0.67	10.21
Iceland	CW	0	12	0.001X	0.00	0.01	83.54	2.68	10.72
Iceland	CW	0	12	0.001X	0.00	0.00	87.77	2.75	10.92
Iceland	CW	4	12	0.001X	0.46	0.07	201.37	9.54	8.83
Iceland	CW	4	12	0.001X	0.37	0.05	229.04	10.32	15.64
Iceland	CW	4	12	0.001X	0.39	0.07	203.39	6.88	15.16
Iceland	CW	0	4	0.1X	28.99	1.82	1900.62	17.48	9.23
Iceland	CW	0	4	0.1X	24.91	1.73	1897.63	17.68	9.61
Iceland	CW	0	4	0.1X	28.34	1.81	1866.30	17.67	9.55
Iceland	CW	4	4	0.1X	15.61	2.10	1955.47	14.38	67.77
Iceland	CW	4	4	0.1X	14.86	2.01	1984.71	14.37	64.13

Iceland	CW	4	4	0.1X	23.40	1.91	1963.57	13.48	63.49
Iceland	CW	0	4	0.001X	0.00	0.00	85.94	0.67	10.21
Iceland	CW	0	4	0.001X	0.00	0.01	83.54	2.68	10.72
Iceland	CW	0	4	0.001X	0.00	0.00	87.77	2.75	10.92
Iceland	CW	4	4	0.001X	0.42	0.07	292.94	4.79	12.21
Iceland	CW	4	4	0.001X	0.53	0.05	193.10	7.99	12.20
Iceland	CW	4	4	0.001X	0.43	0.05	206.64	8.20	13.94
	Cg	0	12	0.1X	37.20	1.29	2414.59	35.01	8.53
	Cg	0	12	0.1X	40.47	1.37	2338.92	31.10	7.92
	Cg	0	12	0.1X	37.24	1.39	2372.00	32.05	8.12
	Cg	4	12	0.1X	16.79	0.34	2506.28	0.93	42.77
	Cg	4	12	0.1X	16.02	0.41	2529.03	3.20	52.47
	Cg	4	12	0.1X	15.09	0.44	2526.05	2.64	36.55
	Cg	0	12	0.001X	7.18	0.47	158.17	20.16	4.09
	Cg	0	12	0.001X	7.23	0.45	137.75	15.49	3.66
	Cg	0	12	0.001X	7.23	0.47	147.72	21.95	4.27
	Cg	4	12	0.001X	5.52	0.51	205.88	1.57	11.79
	Cg	4	12	0.001X	4.16	0.35	244.35	5.11	16.83
	Cg	4	12	0.001X	5.02	0.41	215.39	8.26	7.62
	Cg	0	4	0.1X	37.20	1.29	2414.59	35.01	8.53
	Cg	0	4	0.1X	40.47	1.37	2338.92	31.10	7.92
	Cg	0	4	0.1X	37.24	1.39	2372.00	32.05	8.12
	Cg	4	4	0.1X	41.12	2.12	2502.10	24.88	14.24
	Cg	4	4	0.1X	39.29	1.89	2555.36	23.71	20.41
	Cg	4	4	0.1X	41.78	1.97	2485.19	24.83	26.32
	Cg	0	4	0.001X	7.18	0.47	158.17	20.16	4.09
	Cg	0	4	0.001X	7.23	0.45	137.75	15.49	3.66
	Cg	0	4	0.001X	7.23	0.47	147.72	21.95	4.27
	Cg	4	4	0.001X	3.46	0.21	199.11	12.26	9.85
	Cg	4	4	0.001X	2.34	0.09	192.06	9.00	11.22
	Cg	4	4	0.001X	2.60	0.13	194.58	8.94	8.15

BW: Bioweathering; CW: Chemical weathering; Cg: Culture growth

Concentration units are in $\mu\text{mol/kg}$

Table S3.7. Major anion measurements at the start and end of variable weathering solute experiments. Concentration units are in $\mu\text{mol/kg}$. Refer to Table S2.1 for values for 12°C 0.1X chemical weathering reactors.

FIELD	REACTOR	Week	Temperature (°C)	Solute Concentration	F-	Cl-	NO ₂ -	NO ₃ -	PO ₄ ³⁻	SO ₄ ²⁻	HCO ₃ ⁻
Iceland	BW	0	4	0.1X	12.63	151.19	BDL	1834.05	10.11	32.90	467.77
Iceland	BW	0	4	0.1X	12.63	152.31	6.09	1778.57	1.26	32.06	424.58
Iceland	BW	0	4	0.1X	BDL	155.70	6.09	1790.83	BDL	30.81	475.77
Iceland	BW	4	4	0.1X	BDL	122.98	BDL	1760.51	BDL	26.23	513.50
Iceland	BW	4	4	0.1X	BDL	136.52	BDL	1874.05	BDL	27.07	509.14

Iceland	BW	4	4	0.1X	BDL	133.13	BDL	1837.27	BDL	27.07	303.82
Iceland	BW	0	12	0.1X	12.63	151.19	BDL	1834.05	10.11	32.90	467.77
Iceland	BW	0	12	0.1X	12.63	152.31	6.09	1778.57	1.26	32.06	424.58
Iceland	BW	0	12	0.1X	BDL	155.70	6.09	1790.83	BDL	30.81	475.77
Iceland	BW	4	12	0.1X	23.16	117.34	BDL	930.89	BDL	7.50	1252.75
Iceland	BW	4	12	0.1X	23.16	141.03	BDL	1145.07	BDL	9.58	1149.98
Iceland	BW	4	12	0.1X	BDL	128.62	BDL	1129.59	BDL	9.99	1133.99
Iceland	BW	0	4	0.001X	BDL	107.18	3.48	10.97	BDL	3.75	478.97
Iceland	BW	0	4	0.001X	12.63	110.57	24.35	80.64	5.90	6.25	482.97
Iceland	BW	0	4	0.001X	BDL	107.18	16.52	58.06	1.26	5.00	304.62
Iceland	BW	4	4	0.001X	33.41	19.09	6.74	79.22	11.35	4.63	579.74
Iceland	BW	4	4	0.001X	31.33	17.23	8.37	53.01	12.28	5.09	532.55
Iceland	BW	4	4	0.001X	31.40	15.53	5.30	59.64	9.49	5.04	630.93
Iceland	BW	0	12	0.001X	BDL	107.18	3.48	10.97	BDL	3.75	478.97
Iceland	BW	0	12	0.001X	12.63	110.57	24.35	80.64	5.90	6.25	482.97
Iceland	BW	0	12	0.001X	BDL	107.18	16.52	58.06	1.26	5.00	304.62
Iceland	BW	4	12	0.001X	25.27	16.92	BDL	BDL	BDL	BDL	584.54
Iceland	BW	4	12	0.001X	23.16	18.05	BDL	29.68	BDL	BDL	559.31
Iceland	BW	4	12	0.001X	23.16	21.44	BDL	24.51	BDL	BDL	620.53
Iceland	CW	0	4	0.001X	12.63	13.54	BDL	BDL	BDL	3.75	311.81
Iceland	CW	0	4	0.001X	14.74	11.28	BDL	BDL	BDL	2.91	305.42
Iceland	CW	0	4	0.001X	12.63	12.41	BDL	BDL	BDL	3.33	438.18
Iceland	CW	4	4	0.001X	25.27	14.67	BDL	BDL	BDL	3.33	484.57
Iceland	CW	4	4	0.001X	25.27	14.67	BDL	BDL	BDL	3.75	480.57
Iceland	CW	4	4	0.001X	25.27	13.54	BDL	BDL	BDL	3.33	485.37
Iceland	CW	0	12	0.001X	12.63	13.54	BDL	BDL	BDL	3.75	311.81
Iceland	CW	0	12	0.001X	14.74	11.28	BDL	BDL	BDL	2.91	305.42
Iceland	CW	0	12	0.001X	12.63	12.41	BDL	BDL	BDL	3.33	438.18
Iceland	CW	4	12	0.001X	31.58	14.67	BDL	BDL	2.11	3.33	482.97
Iceland	CW	4	12	0.001X	29.48	15.80	BDL	BDL	BDL	3.33	550.95
Iceland	CW	4	12	0.001X	27.37	14.67	BDL	BDL	BDL	3.33	317.41
Antarctica	BW	0	4	0.1X	BDL	169.24	24.35	2036.61	13.06	36.23	312.61
Antarctica	BW	0	4	0.1X	12.63	157.96	21.74	1903.08	10.95	34.56	445.38
Antarctica	BW	0	4	0.1X	BDL	174.88	17.39	2090.80	12.21	36.64	301.42
Antarctica	BW	4	4	0.1X	22.86	129.00	BDL	1749.19	5.76	27.90	569.34
Antarctica	BW	4	4	0.1X	23.37	139.87	BDL	1954.22	6.57	30.79	586.94
Antarctica	BW	4	4	0.1X	24.45	144.32	BDL	1962.81	6.44	31.20	305.42
Antarctica	BW	0	12	0.1X	BDL	169.24	24.35	2036.61	13.06	36.23	312.61
Antarctica	BW	0	12	0.1X	12.63	157.96	21.74	1903.08	10.95	34.56	445.38
Antarctica	BW	0	12	0.1X	BDL	174.88	17.39	2090.80	12.21	36.64	301.42
Antarctica	BW	4	12	0.1X	27.47	115.81	BDL	854.07	BDL	12.62	1340.33
Antarctica	BW	4	12	0.1X	26.05	122.14	BDL	1035.91	BDL	11.60	1210.77
Antarctica	BW	4	12	0.1X	27.34	133.76	BDL	1162.60	BDL	13.52	1098.80
Antarctica	BW	0	4	0.001X	BDL	111.70	7.83	48.38	BDL	5.41	432.58
Antarctica	BW	0	4	0.001X	BDL	117.34	15.65	62.58	1.26	5.83	427.78

Antarctica	BW	0	4	0.001X	BDL	116.21	24.35	78.06	2.53	5.83	311.81
Antarctica	BW	4	4	0.001X	24.41	18.64	BDL	80.82	BDL	6.49	569.34
Antarctica	BW	4	4	0.001X	26.80	19.32	BDL	83.49	BDL	5.35	568.54
Antarctica	BW	4	4	0.001X	24.02	20.22	BDL	66.97	BDL	3.23	562.15
Antarctica	BW	0	12	0.001X	BDL	111.70	7.83	48.38	BDL	5.41	432.58
Antarctica	BW	0	12	0.001X	BDL	117.34	15.65	62.58	1.26	5.83	427.78
Antarctica	BW	0	12	0.001X	BDL	116.21	24.35	78.06	2.53	5.83	311.81
Antarctica	BW	4	12	0.001X	29.19	15.53	BDL	26.27	BDL	12.79	656.52
Antarctica	BW	4	12	0.001X	26.81	24.82	BDL	33.14	BDL	5.95	662.92
Antarctica	BW	4	12	0.001X	29.20	18.27	BDL	23.57	BDL	5.77	537.35
Antarctica	CW	0	4	0.001X	BDL	9.94	BDL	26.59	BDL	BDL	394.99
Antarctica	CW	0	4	0.001X	BDL	37.41	BDL	12.47	BDL	BDL	458.31
Antarctica	CW	0	4	0.001X	BDL	10.49	BDL	12.81	BDL	BDL	263.39
Antarctica	CW	4	4	0.001X	18.95	13.54	BDL	BDL	BDL	4.16	474.97
Antarctica	CW	4	4	0.001X	18.95	14.67	BDL	BDL	BDL	4.16	482.97
Antarctica	CW	4	4	0.001X	18.95	13.54	BDL	BDL	BDL	3.75	482.17
Antarctica	CW	0	12	0.001X	BDL	9.94	BDL	26.59	BDL	BDL	394.99
Antarctica	CW	0	12	0.001X	BDL	37.41	BDL	12.47	BDL	BDL	458.31
Antarctica	CW	0	12	0.001X	BDL	10.49	BDL	12.81	BDL	BDL	263.39
Antarctica	CW	4	12	0.001X	26.13	11.17	BDL	22.00	BDL	BDL	406.32
Antarctica	CW	4	12	0.001X	18.95	16.92	BDL	BDL	BDL	4.16	300.62
Antarctica	CW	4	12	0.001X	21.05	24.82	BDL	BDL	BDL	4.58	467.77
Cg	0	4	0.1X	BDL	170.37	22.61	2061.13	14.32	36.64	311.81	
Cg	0	4	0.1X	BDL	157.96	18.26	1917.27	12.64	33.73	311.01	
Cg	0	4	0.1X	BDL	179.39	24.35	2159.18	13.06	38.31	270.23	
Cg	4	4	0.1X	BDL	129.61	BDL	1747.48	13.13	23.85	563.74	
Cg	4	4	0.1X	BDL	135.66	BDL	1771.65	11.19	34.30	558.15	
Cg	4	4	0.1X	BDL	131.62	BDL	1787.71	10.18	29.06	494.60	
Cg	0	12	0.1X	BDL	170.37	22.61	2061.13	14.32	36.64	311.81	
Cg	0	12	0.1X	BDL	157.96	18.26	1917.27	12.64	33.73	311.01	
Cg	0	12	0.1X	BDL	179.39	24.35	2159.18	13.06	38.31	270.23	
Cg	4	12	0.1X	BDL	119.21	BDL	BDL	BDL	BDL	1233.16	
Cg	4	12	0.1X	BDL	122.49	BDL	600.28	BDL	BDL	1583.46	
Cg	4	12	0.1X	BDL	136.70	BDL	575.45	BDL	3.40	1485.89	
Cg	0	4	0.001X	BDL	119.59	13.04	60.00	2.11	5.00	300.62	
Cg	0	4	0.001X	BDL	111.70	24.35	76.77	4.63	5.00	441.38	
Cg	0	4	0.001X	BDL	125.24	26.95	85.80	4.21	5.83	343.01	
Cg	4	4	0.001X	BDL	15.11	6.30	64.07	15.03	3.92	269.21	
Cg	4	4	0.001X	BDL	16.88	8.74	69.04	5.12	6.03	425.53	
Cg	4	4	0.001X	BDL	17.83	BDL	73.62	4.60	5.36	426.26	
Cg	0	12	0.001X	BDL	119.59	13.04	60.00	2.11	5.00	300.62	
Cg	0	12	0.001X	BDL	111.70	24.35	76.77	4.63	5.00	441.38	
Cg	0	12	0.001X	BDL	125.24	26.95	85.80	4.21	5.83	343.01	
Cg	4	12	0.001X	BDL	18.11	BDL	52.85	BDL	5.37	522.23	
Cg	4	12	0.001X	BDL	21.31	BDL	66.81	BDL	4.50	458.97	

Cg	4	12	0.001X	BDL	18.16	BDL	75.11	BDL	7.30	600.75
----	---	----	--------	-----	-------	-----	-------	-----	------	--------

BW: Bioweathering; CW: Chemical weathering; Cg: Culture growth

Refer to table S2.1 for 12°C 0.1x chemical weathering values

Concentration units are in $\mu\text{mol/kg}$
